Title
Low Velocity Impacts of Variable Tip Radius on Carbon/ Epoxy Plates /

Author
Delaney, Mac P.

Publication Date
2013

Peer reviewed|Thesis/dissertation

UNIVERSITY OF CALIFORNIA, SAN DIEGO

Low Velocity Impacts of Variable Tip Radius on Carbon/Epoxy Plates

A Thesis submitted in partial satisfaction of the requirements

for the degree of Master of Science

in

Structural Engineering

by

Mac P. Delaney

Committee in Charge:

Professor Hyonny Kim, Chair
Professor Jurijs Bazilevs
Professor Petr Krysl

2013

The Thesis of Mac Delaney is approved, and it is acceptable in quality and form for Publication on microfilm and electronically:

Chair

University of California, San Diego

2013

TABLE OF CONTENTS

LIST OF ABBREVIATIONS

BVID – Barely visible impact damage

CFRP – Carbon Fiber Reinforced Polymer

FRP - Fiber Reinforced Polymer

FTE – Failure threshold energy

FTF- Failure threshold force

LIST OF FIGURES

LIST OF TABLES

ACKNOWLEDGEMENTS

I would like to thank Professor Hyonny Kim for giving me the opportunity to work on this research. His patience and guidance have given me skills that I will use far beyond the field of aerospace structures. He is a truly dedicated professor and has been a pleasure to work for.

I would also like to thank all the other students in the lab that have each given me much needed assistance over the course of this project, including Sarah Fung for the hundreds of impact tests that she helped me perform. I would like to thank all of the other professors I have had in my undergraduate and graduate careers for the knowledge and inspiration that they have given me.

I would also like to thank my parents, my sister, and my brother, each of you has been a unique inspiration, and I would not have gotten to where I am today without you. Thank you.

ABSTRACT OF THE THESIS

Low Velocity Impacts of Variable Tip Radius on Carbon/Epoxy Plates

by

Mac P. Delaney

Master of Science in Structural Engineering

University of California, San Diego, 2012

Professor Hyonny Kim, Chair

With a growing use of composite materials in aircraft structures, there is a greater need to understand the response of these materials to low velocity impacts. Low velocity impacts from tool drops or ground equipment collisions can be of varying bluntness and can leave little or no visible evidence of damage. Therefore, a need exists to investigate the initiation of internal damage and the relationship between this internal damage and the external visible damage with respect to the bluntness of the impactor.

A pendulum impactor was used to impact 76.2 x 127 mm carbon/epoxy panels that were 8, 16, and 24 plies thick. The panels were impacted by hardened steel tips with radii of 12.7 to 76.2 mm.

The experimental results show that the failure threshold energies for each panel thickness and tip radius combination occur at a distinct and consistent energy. This threshold increases with impactor bluntness, and this effect is greater for the 8 ply panel than it is for the 16 or 24 ply panels. To describe the visibility of impact damage, the area of delamination was compared to the depth of the dents resulting from the impacts. For the sharper impact tips, there is a clear relationship between the delamination area and the depth of the dents. However, these relationships are dependent on the radius of the impact tip, and for the blunter impact tips no strong correlation could be determined between the delamination area and the depth of the dents.

CHAPTER 1: INTRODUCTION

1.1 Motivation

In recent decades composite materials have seen an increasing role in the civilian and military aerospace industry. Fiber-reinforced polymers (FRPs) have high stiffness and strength to weight ratios, as well as favorable fatigue and corrosion properties [1]. Since weight savings is of such high importance in aerospace structures, recent designs have replaced much of their metal structures with composite materials. For example, the Boeing 787 Dreamliner relies on FRPs for 50% of its structural weight, while in 1980 the comparable MD-80 only used composites in 5% of its structural weight [2].

A major concern with these materials that has prevented even faster utilization is their vulnerability to impact damage. The through-thickness strength in FRPs is significantly lower than the in-plane properties, thereby making them susceptible to damage during transverse impact events such as tool drops, runway kickup, or vehicle collisions [3]. These impacts are particularly dangerous because they often leave either non-visible or barely visible impact damage, yet can result in reductions in residual strength of up to 50% [4]. In contrast, metal components more readily exhibit evidence of the occurrence of a damaging impact event in the form of highly visible dents or cracks. In fiber reinforced composites, the initial forms of damage due to impacts include delamination and back face fiber breakage. These modes of damage are typically internal and thus not directly detectable by visually inspecting the exterior of the site of the impact.

The threat of impact damage on aircraft structures and the limited visibility of the resulting damage increase the importance of self-reporting the occurrence of impact events. Unfortunately, many events will not be witnessed, and those that are may go unreported because of a fear of the repercussions or a belief that no damage has occurred. Due to the modes by which FRPs sustain damage, a section that seems pristine on the surface may have significant internal damage that can potentially lead to structural failure. For composite materials to continue expanding their role in the aerospace and other fields, their behavior under impact loading still requires more extensive investigation.

1.2 Previous Work

Because of the vulnerability of composite materials to being damaged by impact loads, extensive experimental and analytical research has been performed on this subject. Analytical work has attempted to create models that predict the delamination threshold loads or the depth of surface dents from impacts. In addition, numerous experimental investigations have tested composite structures under impact loads in attempts to further understand the material behavior. A review of some of the relevant work is provided here.

Analytical models have made use of the Hertzian contact law or variations of it to attempt to describe the relationship between the contact force and the indentation of a composite material subjected to low velocity impacts. This law was originally developed for the contact between two isotropic spheres, but has served as a base for models describing composite plates impacted by rigid spheres. Equation (1) describes the contact of an elastic sphere onto a semi-infinite elastic half space.

$$F = k\alpha^n \tag{1}$$

In this relationship *F* is the contact force, α is the indentation depth of the sphere into the half space, *n* is a power index determined experimentally, and *k* is the contact stiffness of a semi-infinite solid given by:

$$k = \frac{4}{3}\left(\frac{R^{1/2}}{\frac{1-\nu_s^2}{E_s} + \frac{1-\nu_t^2}{E_t}}\right) \tag{2}$$

In equation (2), the subscript *s* refers to the impacting sphere and *t* refers to the target panel, *R* is the radius of the impacting sphere, *E* refers to the modulus of elasticity, and ν is Poisson's ratio. Sun [5] developed a modified version of this contact law for composite laminates, where he defined the contact rigidity using the modulus of elasticity of the composite in the transverse direction, E_z:

$$k = \frac{4}{3}\left(\frac{R^{1/2}}{\frac{1-\nu_s^2}{E_s} + \frac{1}{E_z}}\right) \tag{3}$$

The dependence on the radius of the impactor in these relationships is important because it indicates that higher forces will be required for blunter impact tips to create the same level of indentation. These higher forces caused by the blunter tips can exceed damage threshold levels for the material while leaving less visual evidence that damage has occurred. Wu and Shyu [6] experimentally determined that for impacts on thin composite plates, this relationship breaks down as the impact tip radius increases from a 12.7 mm diameter tip to a 25.0 mm diameter tip. So with blunter tips, the force would still correlate with the parameters in equations 1-3, but not to the same degree as with sharper impact tips.

Willis [7] showed that 1.5 could be used as a value for *n* in equation (1), and this value is often used for describing impacts on composite plates. Yang and Sun [8] investigated the fact that the force-indentation relationship was different during the unloading process measured through static indentation tests. The unloading force was described as:

$$F = F_m \left(\frac{\alpha - \alpha_o}{\alpha_m - \alpha_o} \right)^{2.5} \quad (4)$$

In equation (4) α_m is the maximum indentation, F_m is the maximum force, and α_o is the residual, or permanent, indentation.

The initial form of damage from low-velocity impacts on FRPs is typically cracking or delamination. Tests by Sjöblom and Hartness [9] showed matrix cracking from impacts as low as 1.0 J. This type of damage is difficult to detect, and does not significantly reduce the stiffness of the laminate. However, matrix cracks do serve as flaws that allow delamination and fiber breakage to initiate [10]. Adsit and Waszczak [4] showed through residual strength tests that delamination can significantly reduce the compressive strength and stiffness of the material. The tensile strength and stiffness is not greatly reduced until fiber breakage has occurred, which is usually only initiated at impact energy levels much greater than those that cause delamination. Zhang [11] and

Davies and Zhang [12] pointed out that delamination is a result of transverse shear stresses, which are at a maximum roughly halfway through the thickness of the laminate. Fiber failure, however, is a result of high tensile forces on the back face due to bending. Zhang also found that the threshold for delamination was chiefly dependent on the thickness, t, of the laminate, and in his experiments, the critical force thresholds could be predicted using the equation:

$$F_{crit} = 680t^{1.5} \tag{5}$$

The relationship in equation (5) does not take into account the radius of the impact tip, which was 6.35 mm in the experiments of Davies and Zhang. For larger impact radii, equation (5) would not be valid without having to redefine parameters (e.g., 680).

Some studies have looked at the effect of the impact tip radius on low-velocity impacts. In a study on impacts using tip radii of 12.7 to 152.4 mm, Whisler and Kim [13] found that increasing the tip radius also increased the damage initiation threshold in glass/epoxy composites. It was found that for a given panel thickness and impact energy level, the peak force was the same regardless of tip radius, but the blunter tips created a greater contact area and therefore a lower average contact pressure. This indicated that a blunter tip was less likely to cause surface dents than a sharper one because the contact force was less concentrated. Siow and Shim [1] investigated impacts on woven fiber composites with tip radii of 6.3 and 21 mm, and also found that increasing the radius of the impactor increases the damage initiation threshold. Yang and Cantwell [14] reached similar conclusions while looking at impacts from 4.6, 12, 14.4, and 19.2 mm diameter tips. They noted that the effect of the increased tip radius was more significant for thinner laminates. Adsit and Waszczak [4] tested composite panels with tip radii of 6.3 and 25.4 mm. They found that the sharper impactor created more fiber damage which reduced tensile and compressive strength, while a blunter impactor created more delamination and less fiber damage, which only significantly reduced the compressive strength. In their study, the area of the dents were recorded rather than the depth, which was found to be difficult to record. Quantifying the dents in this way can be subjective, and in some cases the visible damage could not be recorded because the boundaries of the dents were questionable. Their study did prove that impacts causing internal but not visible damage can result in a dramatic reduction in strength.

Attempts have been made to use the depths of surface dents as a metric to indicate internal damage. Wardle and Lagace [15] concluded that no useful correlation existed between the dent depth and internal damage of impacted graphite/epoxy plate and shell structures since dent depth and the internal damage extent was not distinct enough to describe a clear relationship. Their study also found that some impacts created significant internal damage with no measurable surface dents, and others created visible dents without any internal damage. In contrast, other investigations found clear relationships between internal and visible damage. Anderson and Madenci [16] found that significant internal damage was indicated by a threshold dent depth for foam and honeycomb core composite sandwich panels. In another study, Sun and Dicken [17] found that the extent of internal damage could be predicted by the depth of the surface dent in ARALL (aramid-aluminum) laminates. Both the sandwich and ARALL composites possess properties that could have caused the damage to be more visual than in thin composite plates. The core in the sandwich panels and the aluminum in the ARALL sustain dents more readily than the fiber reinforced polymer portions of these materials, and this could be why relationships between dent depth and internal damage were more clearly visible than in thin monolithic FRP panels.

1.3 Objectives

This investigation will explore the damage initiation of carbon/epoxy composite panels subjected to low-velocity impacts in relation to the radius of the impacting tip and the thickness of the panel. The relationship between visible damage (i.e. surface dents and cracks) and internal damage will also be investigated, as this is of particular interest in composite aircraft structures. In this research, visible damage will be quantified as the depths of the dents created on the surface of the panels as well as the span over which these dents exist. The depths of the initial and residual surface dents and the span of the dents will be related to the radius of the impact tip, the thickness of the panel, the peak contact force, and the extent of the internal damage.

CHAPTER 2: EXPERIMENTAL SETUP

2.1 Pendulum Impact System

For this investigation a series of impact tests were carried out using a pendulum impact system (Figure 1). This system consisted of a stack of 50.8 mm diameter stainless steel masses, totaling up to 5.08 to 5.85 kg (depending on each tip's geometry), mounted on the end of a stiff, lightweight fiberglass rod. The swinging radius of the mass center is 1.42 m. The impacting face of the mass consisted of a hemispherical tip mounted onto a dynamic force-measuring load cell. A US Digital A-2 absolute encoder wheel with 3600 discrete steps was incorporated into the pendulum system so that the angle of the arm could be determined with 0.1 degree resolution. This enabled the desired potential energy to be set via exact placement of the pendulum arm prior to the impact test. Just before the pendulum came into contact with the panel, the arm passed through a laser photogate system so that the velocity of the pendulum head could be determined. The kinetic energy of the pendulum could then be calculated, allowing for a more accurate measure of the impact energy and a validation of the predicted energy prior to the test.

The panels were confined between two 12.7 mm thick A36 steel plates (shown in Figure 1), each with a 76.2 x 127 mm window in accordance with ASTM D7136 standard [18]. The composite panels tested were 152 x 305 mm (visible in Figure 1), and consisted of three impact sites per panel. It should be noted that these panels were painted white (as shown in Figure 1) by an airline company's maintenance technicians using aircraft exterior paint. In order to allow these panels to slide into the fixture, the front plate was only bolted on the top and bottom with 7.9 mm bolts (5/16 in.). To avoid damage that could potentially be created by the sharp corners at the boundary of the window, 3.2 mm thick silicone rubber strips were added to the edges. Aluminum shims were placed between the two steel plates so that the rubber strips would be compressed 1 mm every time. A drawing of the specimen-holding fixture setup is shown in Figure 2.

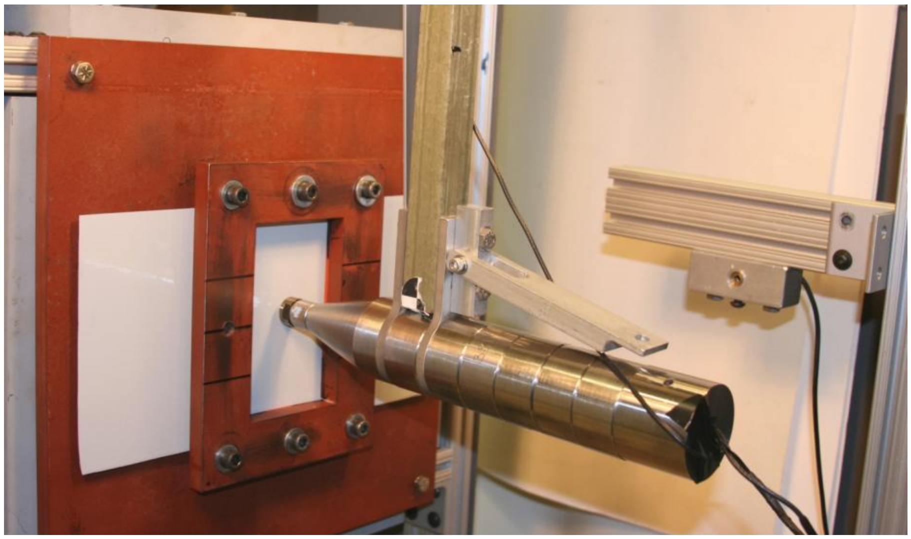

Figure 1. Pendulum Impact System

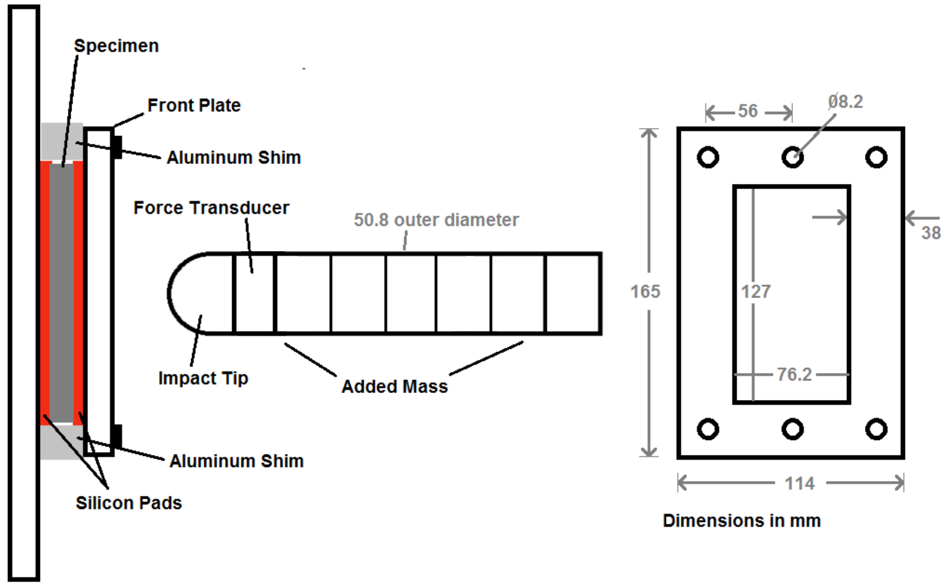

Figure 2. Test Setup Drawing. Side view (left) and front view (right)

Four interchangeable impact tips made of hardened steel were used in this investigation. The tips had radii of 12.7, 25.4, 50.8, and 76.2 mm (Figure 3). These tips had masses of 23.5, 462.2, 262.3, and 168.4 grams respectively. The 12.7 mm radius tip was mounted to a DYTRAN 1050V6 force transducer which had a mass of 34.2 grams, and the other three tips were mounted to a DYTRAN 1060V5 force transducer which had a mass of 461.3 grams. This was due to the different size of the 12.7 mm radius tip in comparison to the other three (see Figure 3). Because the mass of the impact tip was not negligible compared to the mass of the entire pendulum head, the force measured by the transducer had to be corrected to accurately know the force at the face of the impact. This is primarily a function of the mass of the tip which sits between the load cell and target panel. This dynamic correction is further described in Appendix I. The force transducer's output was in volts and needed to be converted to units of force. The conversion factors given by the manufacturer were 4.58 kN/V and 20.8 kN/V for the 1050V6 and 1060V5 sensors respectively.

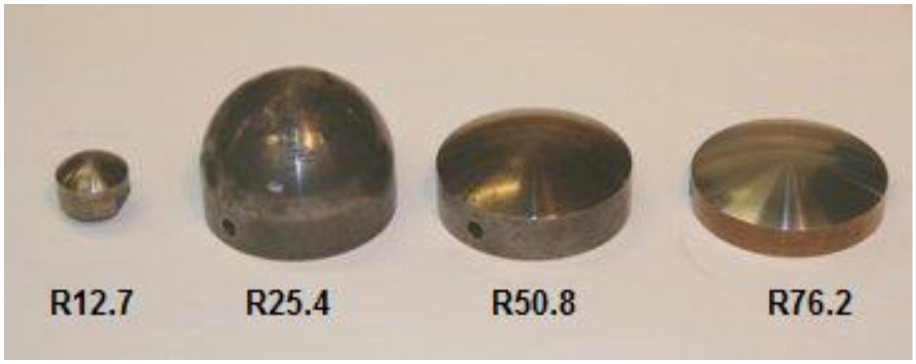

Figure 3. Impact tips of radii 12.7, 25.4, 50.8 and 76.2 mm from left to right

2.2 Test Specimens

The material used for these experiments was Toray T800/3900-2 Carbon/Epoxy prepreg tape. Panels were layed up quasi-isotropically in the orientation $[(0/45/90/-45)_n]_S$, where n ranged from 1 to 3, to make panels 8, 16, and 24 plies thick. The panels also included a 0.05 mm thick ply of plain weave glass/epoxy and aerospace grade paint on the impact side of the panel. These additions were included to make the panels more representative of aircraft laminates. The laminates were originally fabricated as 305 x 305 mm specimens and cut in half to make two 152 x 305 mm panels. The 8, 16, and 24 ply panels were measured to be 1.7, 3.3 and 4.9 mm respectively. From these measurements it can be calculated that each ply is 0.2 mm thick and the combined layer of glass fiber and paint on the impact side of the panels is 0.1 mm thick.

2.3 Experimental Procedure

Before each impact test, the desired potential energy of the impact would be used to calculate the angle the pendulum arm would need to be set to (see Appendix II). The arm would be attached to a pneumatic release mechanism, and raised to the appropriate angle. As a safety precaution, the arm was also attached to a tether until just before impact, in case the release was accidentally triggered.

Before releasing the pendulum, the tip would be marked with Dry Erase ink, and a sheet of paper was placed over the front of the panel. When the pendulum would strike the panel, the ink would transfer from the tip to the paper, leaving an imprint of the part of the tip that had come into contact with the panel. The paper was then digitally scanned and the contact area was determined via MATLAB image processing (see Appendix IV). In previous experiments, carbon paper was used to record the contact area, but this was found to be inconsistent and did not leave as clear of a mark as was desired. Several different types of ink were tested for this system including stamp ink, permanent ink, and roll on ink. Dry Erase ink was chosen because it transferred onto the paper very well, did not dry up (so it would transfer even after sitting for some time), and it did not splatter onto areas that the tip had not come into contact with. Figure 4 shows the contact sheet from a 53 J impact on a 16 ply panel, for an impact tip radius of 76.2 mm. The square in the lower left has a known area, and is used as a reference when calculating the contact area.

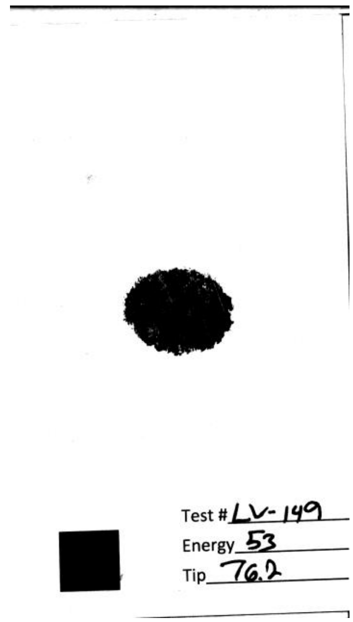

Figure 4. Contact area sheet of a 53 J impact from a 76.2 mm tip on a 16 ply panel

After each impact, the panels were examined to determine the extent of internal damage and the depth of any surface dents. The presence of delamination was detected by pulse-echo ultrasonic A-Scan using a hand-held 5 MHz sensor connected to an NDT Automation Pocket UT version V1.81. If delamination was detected the panels were set aside to be C-Scanned using through-transmission ultrasound (5 MHz transducers) to determine the area of the damage. This was done using an NDT Automation 36” Lab Ultrason C-Scan System, model UPKII-T36. The surface dents were measured using a Mitutoyo model ID-S1012E depth indicator, capable of measuring dent depths with a resolution of 0.01 mm. Depth measurements were taken at the center of the point of impact and at +/- 25.4 mm distance on either side of that point. The depth of the dent was then calculated as the average of the depths on either side of the impact minus the depth at the point of impact. The surface dents were measured immediately after the impacts, and then again 24 hours later to record the relaxed dent depth. If no surface dent or delamination was detected, the panel could be impacted again, up to a limit of 3 total impacts to prevent the onset of damage from repeated loads.

In order to keep track of all the steps involved in this test procedure, a checklist was implemented. This was referred to during testing, and can be found in Appendix III.

CHAPTER 3: RESULTS

For this experimental investigation, 152 impact tests were performed on 8, 16, and 24 ply carbon/epoxy panels using impact tip radii of 12.7, 25.4, 50.8, and 76.2 mm. The amount of tests performed for each condition is shown in Table 1. These totals do not include practice or calibration tests, or impacts that did not yield valid data.

Table 1. Number of tests for each panel thickness and impactor tip radius R (mm)

Panel Type	Thickness (mm)	R 12.7 mm	R 25.4 mm	R 50.8 mm	R 76.2 mm
8 plies	1.7	10	13	14	10
16 plies	3.3	13	13	12	12
24 plies	4.9	13	14	15	13

From these tests the main quantities sought were the damage initiation thresholds, the visibility (dent depth) of damage, and insight regarding the interaction between the impactor radius and the resulting damage level. Each test is given a unique test number. A complete record of each test and associated information is listed in Appendix IV.

3.1 Data Collection

For each impact, data were collected in several different forms. This section will summarize what type of data were collected and show typical outputs for a particular test.

Immediately after an impact, data files were saved containing outputs from the force transducer and laser photogate systems. The laser excites a photodiode sensor which is connected to a circuit that outputs a voltage of 2V when the beam was not blocked and 8V when it was blocked. By measuring the width of the pendulum arm and determining the time it took for the arm to pass through the laser, the velocity of the pendulum head just prior to impact could be calculated. As an example, Figure 5 shows a plot of the voltage vs. time for test LV-160. This test involved a R50.8 mm tip impacting a 4.9 mm thick 24 ply panel at 54 J of energy. Using these data, both the incoming and rebounding velocities could be determined.

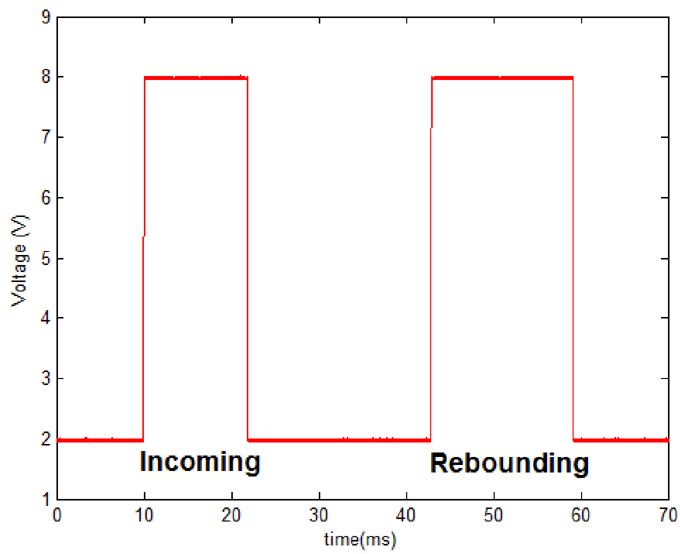

Figure 5. Incoming and rebounding laser voltage data for test LV-160; R50.8 mm tip impacting 24 ply panel at 54 J

Data for this impact from the force transducer are shown in Figure 6. In this figure the appropriate dynamic force correction factor (see Appendix 1) and voltage-to-kN conversion factor have been applied. The mark left by test LV-160 is shown in Figure 7 indicates a contact area of 158 mm^2.

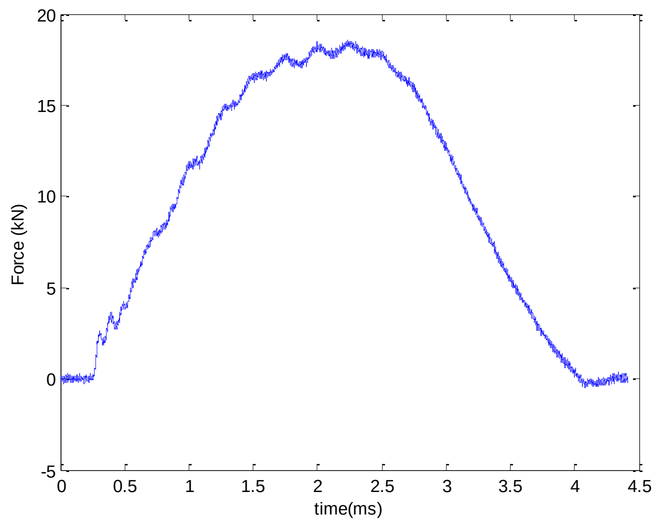

Figure 6. Force vs. time history for test LV-160; R50.8 mm tip impacting 24 ply panel at 54 J

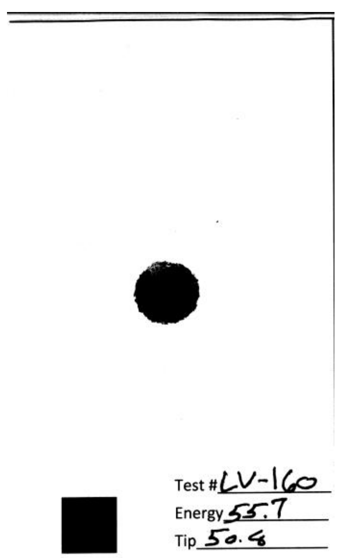

Figure 7. Contact mark left by test LV-160; R50.8 mm tip impacting 24 ply panel at 54 J

To determine the area of delamination damage, each panel was C-Scanned. Each panel had up to three impact areas, so multiple tests were C-Scanned simultaneously. The C-Scan map of tests LV-160 to LV-162 can be seen in Figure 8.

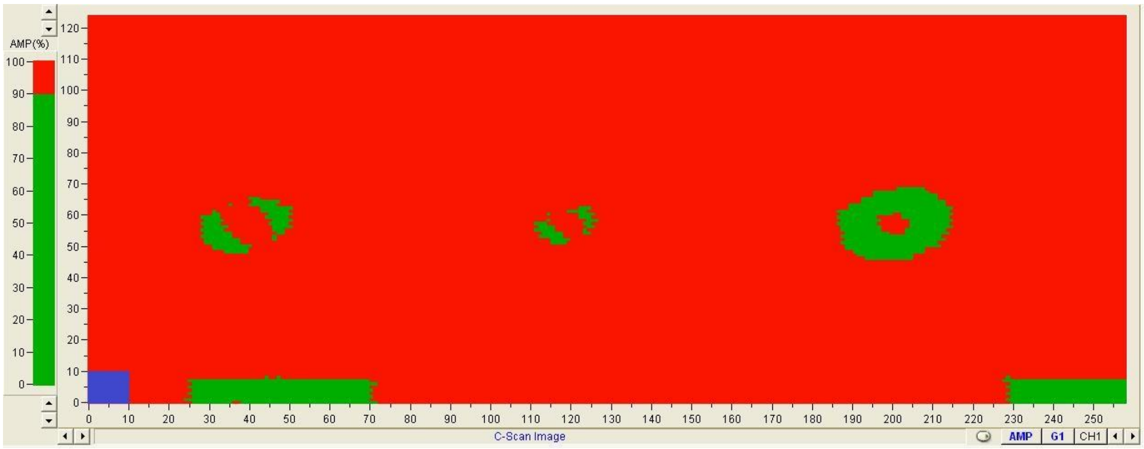

Figure 8. C-Scan map for tests LV-160 (left), LV-161 (center), and LV-162 (right)

Immediately after each impact, the panel was removed from the fixture so that the depth of the dent could be measured. The dent was then measured again no earlier than 24 hours after the impact so that the relaxed dent depth could also be measured. For test LV-160, the initial dent depth was measured to be 0.05 mm and the relaxed depth was 0.04 mm. In addition to the maximum depth of the dents, a profile was taken so that the span over which the dents existed could be measured. This was achieved by taking depth measurements every 1.58 mm (1/16 of an inch) along a path that passed through the dent. Figure 9 shows a plot of these measurements.

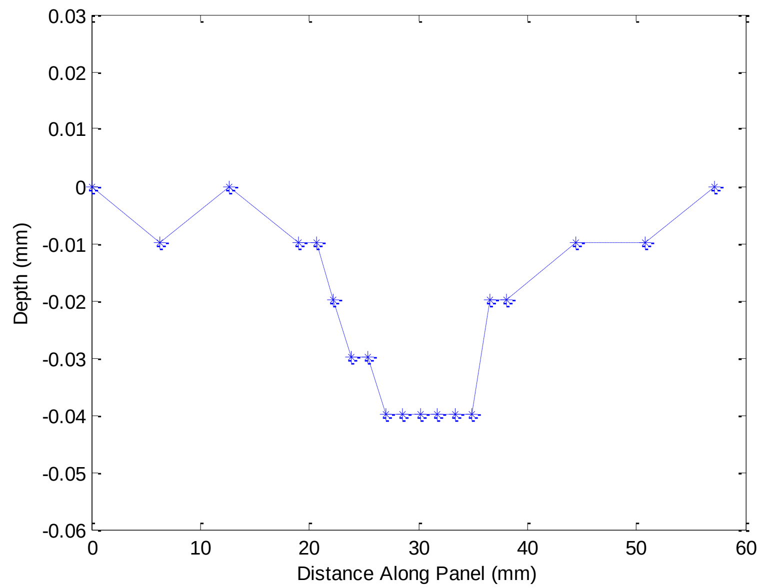

Figure 9. Dent profile for test LV-160

3.2 Failure Thresholds

3.2.1 Determining the Failure Thresholds

For each test the peak force and projectile kinetic energy were recorded, as well as whether any delamination or fiber breakage could be detected. The failure threshold force (FTF) was the minimum peak force at which an impact still initiated detectable damage (delamination or fiber breakage). Similarly, the failure threshold energy (FTE) was the minimum projectile kinetic energy at which an impact initiated damage (within detectable limit by ultrasonic A-Scan).

In order to objectively determine the failure threshold forces and energies, a binomial regression was applied to the data. To do this, each impact was given a value of

1 if it was damaged and 0 if it was undamaged. These values were plotted against the peak force or impact energy, and a binomial regression fit was run to determine the likelihood of damage existing. The failure threshold was then defined as the point at which damage has a 50% probability of occurring, as determined by the binomial regression. The reason that this regression was used to determine the failure thresholds was because some impacts had no damage above the failure threshold and others had developed damage below it. This was because the damage initiation was driven by flaws in the material, and each panel had unique flaws that caused the onset of damage to vary slightly. Although there is a fairly narrow range where the damage threshold exists, there is still some overlap in the data. Using the binomial regression, the data of damaging and non-damaging hits was used to determine probability of damage, and we have defined the threshold to be when this probability is 50%. In many cases there is no overlap between damaging and non-damaging hits. In this case the regression simply produces a straight line from the highest non-damaging hit to the lowest damaging hit. The binomial regressions for the FTEs can be seen in Figures 10-12. More information on how these plots were produced can be found in Appendix V.

These plots of the FTEs were useful during testing because they helped indicate what energy levels future tests should be run at in order to further refine the failure threshold. In terms of describing the behavior of the material however, the FTF is a more physically insightful parameter. This is because the contact force represents a direct local relationship between the impactor and the target, while the FTE masks information related to the projectile mass and velocity, and is known to be sensitive to panel geometry and boundary condition details. A direct relationship exists, however, between impact kinetic energy and peak contact force for each panel thickness. Thicker panels generated higher peak contact forces than thinner panels because of their increased stiffness. Figure 13 shows the impact energy vs. the peak contact force for all tests. Note the data for each panel thickness defines a different combined force vs. kinetic energy relationship, regardless of the tip radius.

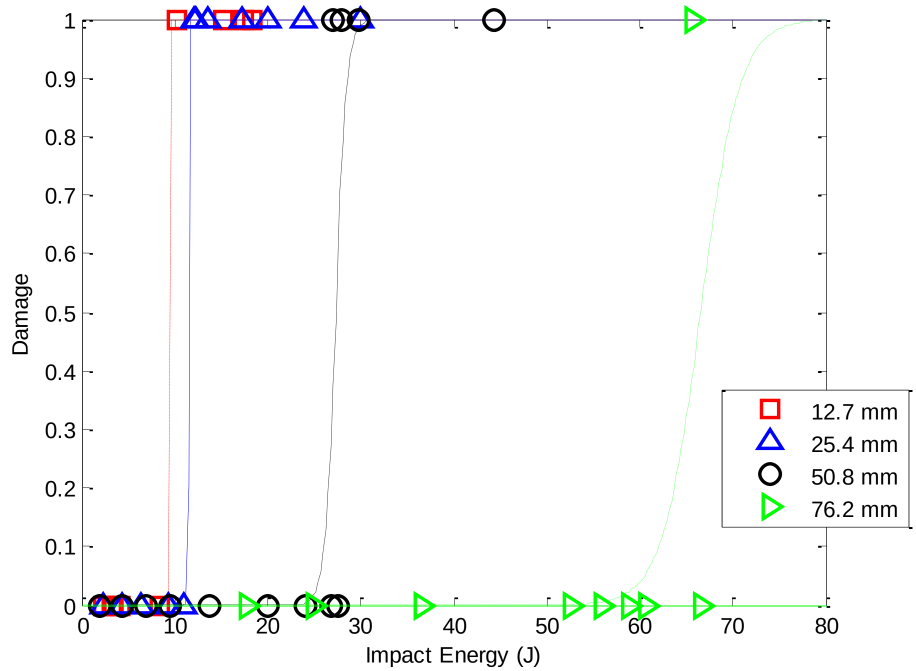

Figure 10. Binomial regressions for impact energies on 8 ply panels

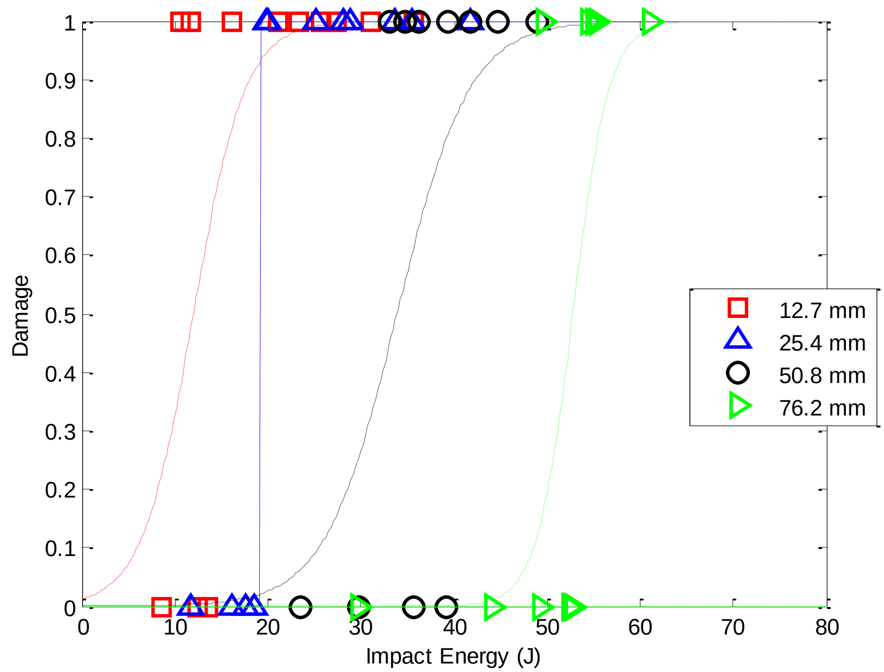

Figure 11. Binomial regressions for impact energies on 16 ply panels

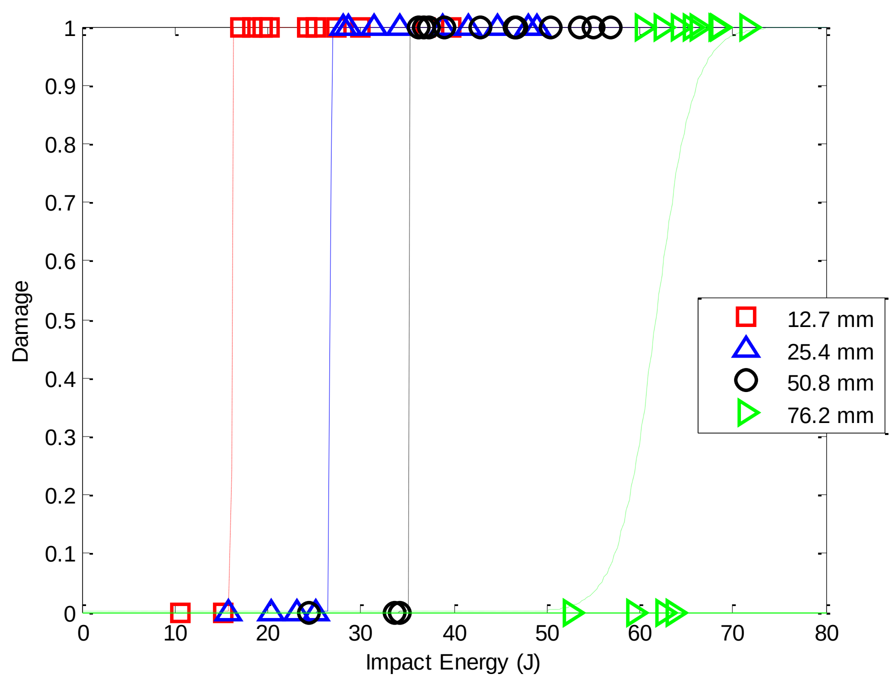

Figure 12. Binomial regressions for impact energies on 24 ply panels

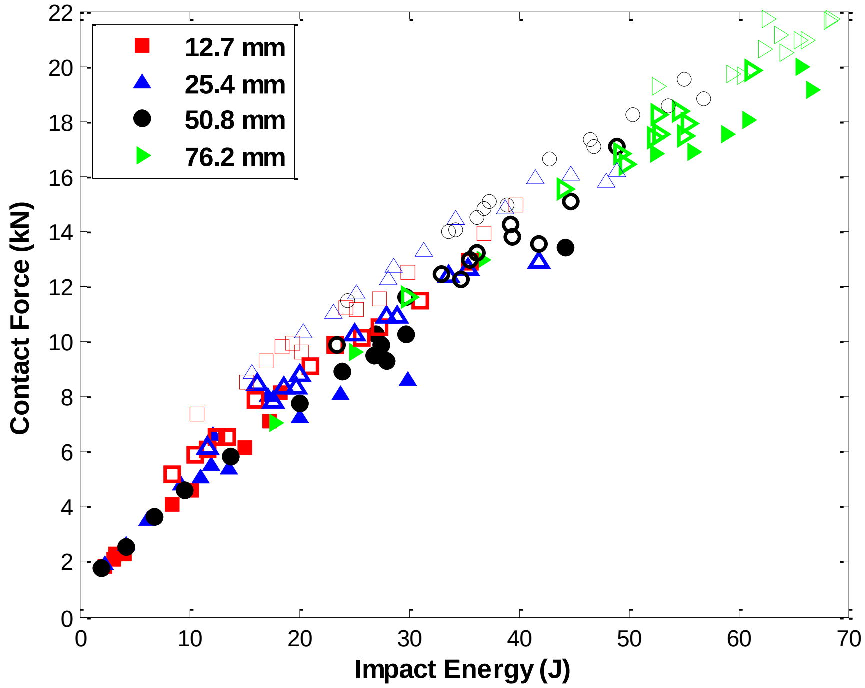

Figure 13. Impact energy vs. contact force for all tests. Solid markers are 8 ply tests, unfilled with thick borders are 16 ply tests, and unfilled with thin borders are 24 ply tests

Figures 14-16 show the binomial regression plots for the FTFs where the peak contact forces are those measured during each test. These FTF values are known to be intrinsic to the combination of panel thicknesses and impact tip radius, regardless of boundary condition [19, 10].

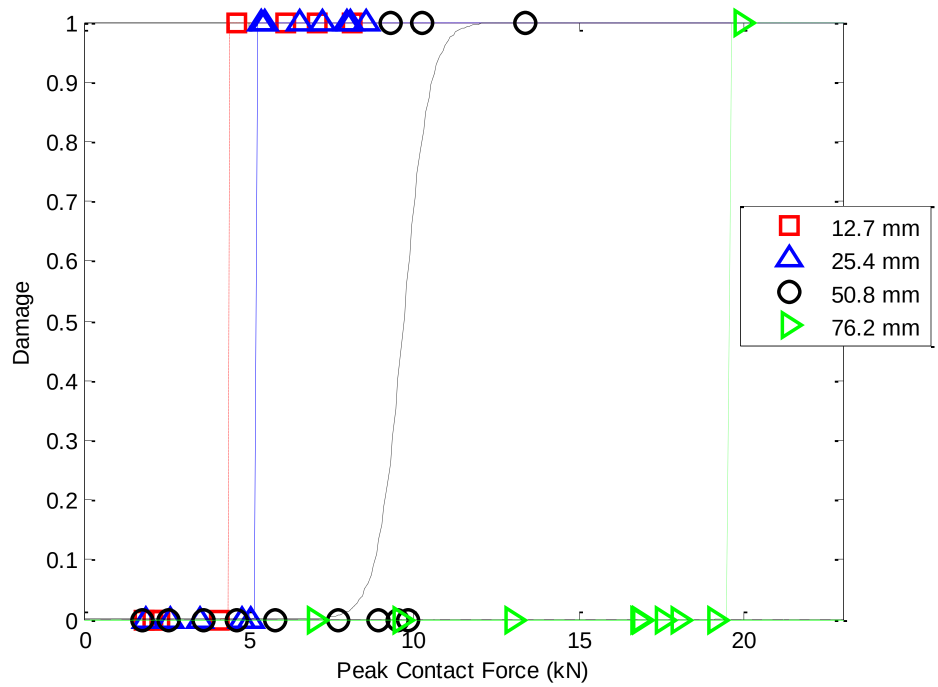

Figure 14. Binomial regressions for peak contact forces on 8 ply panels

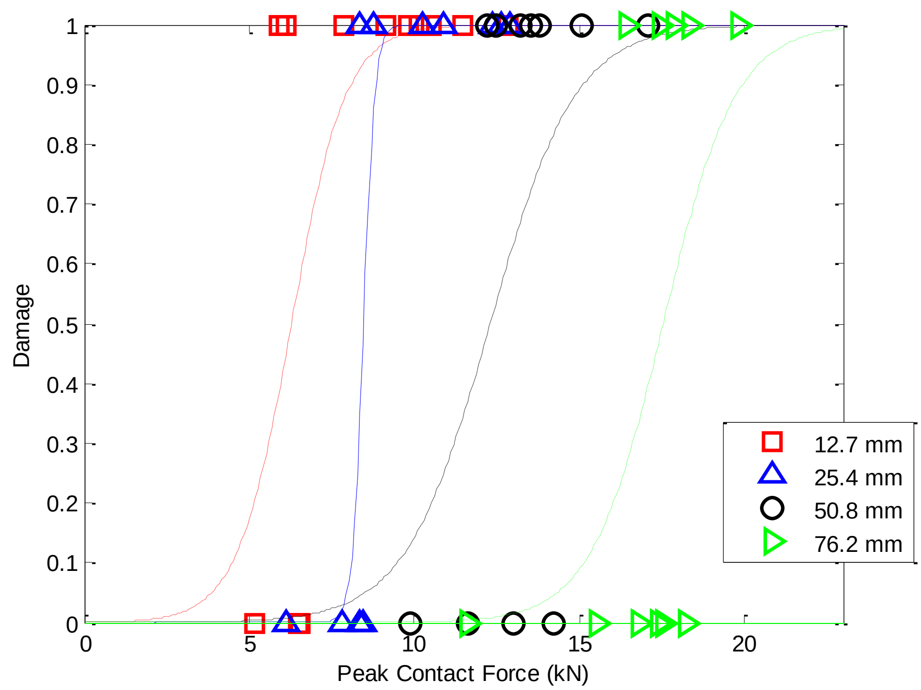

Figure 15. Binomial regressions for peak contact forces on 16 ply panels

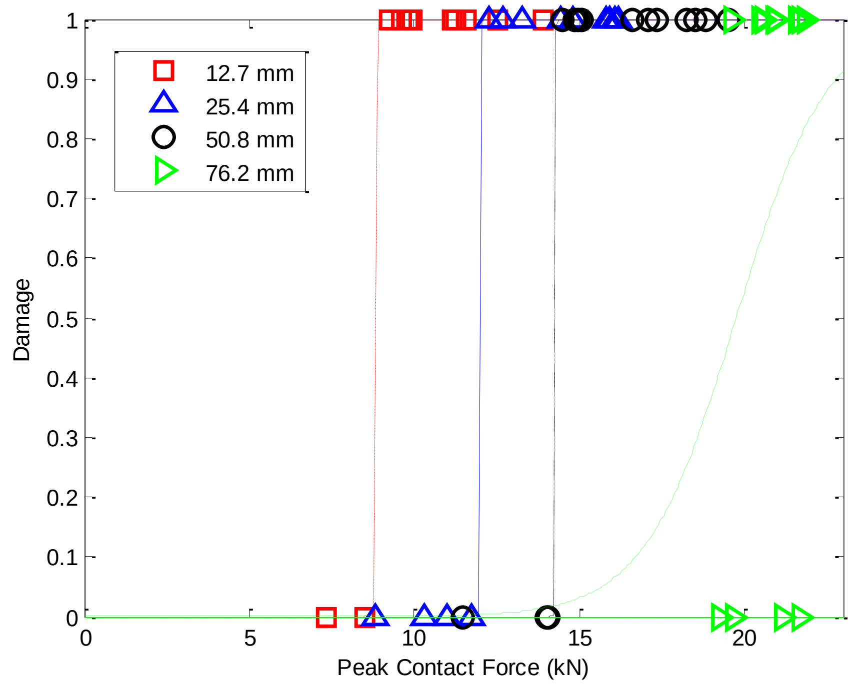

Figure 16. Binomial regressions for peak contact forces on 24 ply panels

3.2.2 Failure Threshold Forces and Energies

The failure threshold force and energy data determined from binomial regressions are plotted in Figures 17 and 18 and Tables 2 and 3. The FTE and FTF can be seen to increase with impact tip radius, with this effect being greater on the 8 ply panels than for the 16 and 24 ply panels. This observation was consistent with the findings of Yang and Cantwell [14]. For the 76.2 mm tip, the FTE for the 8 ply panel was actually greater than for the two thicker panels. The differences in damage initiation between the panel thicknesses were due to different combinations of flexural and shear stresses being imposed by the various radius impacts. The 24 ply panels experienced much lower flexural deformation during impact, so the force was mostly converted into transverse shear stresses, resulting in delamination damage. Fiber failure from flexural stress would require forces much higher than those that created delamination in this case. The 8 ply panels however, allowed for much more flexural deformation. This deformation created higher flexural stresses and prevented shear stress from building up.

Tables 2 and 3 show the failure thresholds for both delamination and fiber breakage. The entries marked as “NA” indicates that the particular failure mode did not occur. The difference between the threshold for delamination and fiber failure is dependent on the thickness of the panel as well as the radius of the tip. The 8 ply panels had the smallest difference between delamination and fiber failure thresholds, with a 7% average change from the delamination FTF to the fiber failure. However, the average difference in delamination and fiber failure threshold forces for the 16 ply panels was 15%, and while no fiber failure was created in the 24 ply panels, the difference is expected to be even greater. This supports the idea that as the panel stiffness increases, more of the impact force is converted into shear stress than flexural stress, and so the difference between the delamination and fiber failure thresholds will be greater.

The difference between the delamination and fiber failure thresholds decreases as the radius of the tip increases. For the 12.7, 25.4, 50.8, and 76.2 mm tips, the average changes between delamination FTF and fiber failure FTF were 54%, 21%, 3%, and 0% respectively. This is due to the combination of flexural and shear stresses from the impacts. The smaller tip radii have a smaller contact area, so the interlaminar shear stress around the border of the contact region will be higher, making delamination damage more likely. The larger impact tip radii have larger contact areas and therefore lower interlaminar shear stresses around the border of the contact region. Therefore, less shear stress will develop and damage is more likely to be caused from flexural stresses, making fiber failure more likely. The reason the difference between the delamination FTF and the fiber failure FTF decreases with tip radius is because more of the impact force is being converted into shear stress for the smaller tip radii, and more of the impact force is being converted into flexural stresses for the larger tip radii.

The difference in impact energy between the onset of delamination damage and fiber failure increases with panel thickness and decreases with impact tip radius. Due to these combined effects, the onset of fiber failure occurs at a lower impact energy than the onset of delamination damage in the 8 ply panels when impacted by a 76.2 mm tip. The onset of fiber failure occurs simultaneously with the onset of delamination damage in the 8 ply panels impacted by the 50.8 mm radius tips. In all other test conditions, delamination damage occurs at lower impact energy levels than fiber failure.

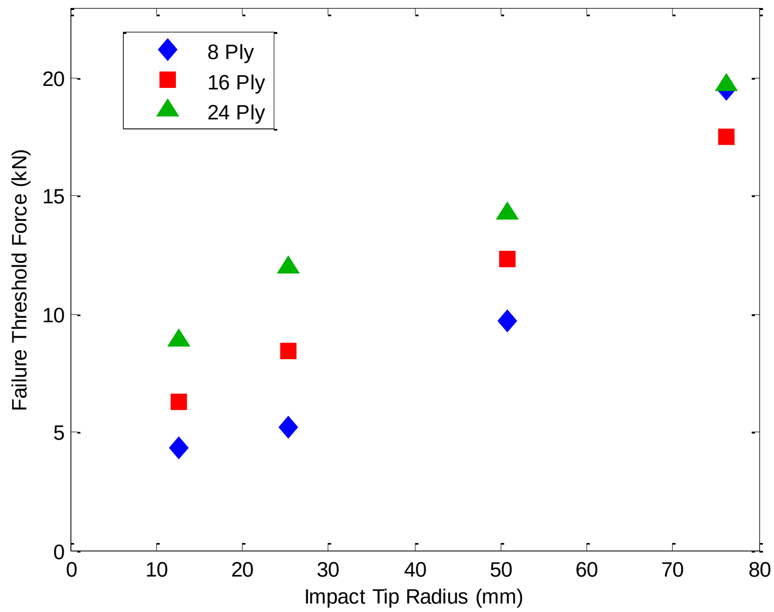

Figure 17. Failure Threshold Forces

Table 2. Delamination/fiber failure threshold forces (kN) for each panel thickness (T in number of plies) and impact tip radius (R in mm)

Panel Type	Thickness (mm)	FTF (kN) for Tip Radius (Fiber Failure Onset, kN)			
		R12.7	R25.4	R50.8	R76.2
8 Plies	1.7	4.4 (6.6)	5.2 (5.7)	9.7 (9.7)	NA (19.6)
16 Plies	3.3	6.3 (9.9)	8.5 (10.9)	12.3 (13.0)	17.6 (17.6)
24 Plies	4.9	8.9 (NA)	12 (NA)	14.3 (NA)	19.8 (NA)

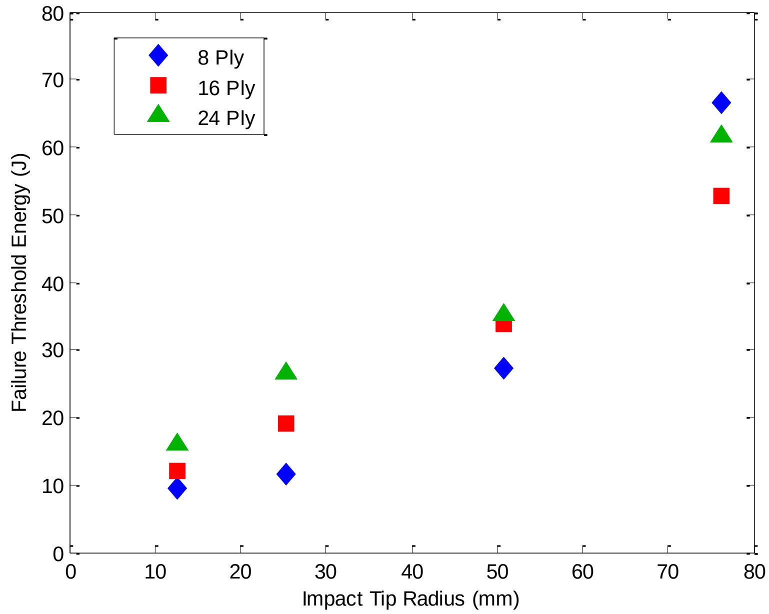

Figure 18. Failure Threshold Energies

Table 3. Delamination/fiber failure threshold energies (J) for each panel thickness (T in number of plies) and impact tip radius (R in mm)

Panel Type	Thickness (mm)	FTE (J) for Tip Radius (Fiber Failure Onset, J)			
		R12.7	R25.4	R50.8	R76.2
8 Plies	1.7	9.4 (16.3)	11.5 (12.2)	27.3 (27.3)	NA (66.6)
16 Plies	3.3	12.0 (22.2)	19.2 (28.5)	33.9 (36.2)	52.8 (52.9)
24 Plies	4.9	16.1 (NA)	26.6 (NA)	35.2 (NA)	61.7 (NA)

3.3 Damage Visibility

A common method of quantifying the visibility of damage is by using the depth of the dent left by the impact. Ideally, this depth which describes the surface deformations would correlate directly with the degree of internal damage. Figures 19-21 show that the dent depth correlates with peak force (i.e. higher peak forces where damage formation corresponds with larger dent depths) particularly for the initial dents and for smaller radius impactor tips.

Figure 22 shows that the delamination damage area has some correlation with peak force, meaning a relationship between dent depth and delamination area is implied. Again, this correlation is stronger for smaller-radius impactors and almost non-existent for the combination of largest-radius tip (76.2 mm) on thinnest panel (8 plies). Since there is a large range of scatter, and the relaxed dent depths often dropped to near zero, the lack of a visible dent does not necessarily guarantee that there is no internal damage present. This is supported by Wardle and Lagace [20], who concluded from their experiments that there was no clear relationship between dent depth and the internal damage. However, their experiments used a sharper impact tip (6.35 mm radius) and the impacts all had a peak contact forces below 3 kN. In the experiments presented here, blunter impact tips were used and contact forces were generated exceeding 20 kN.

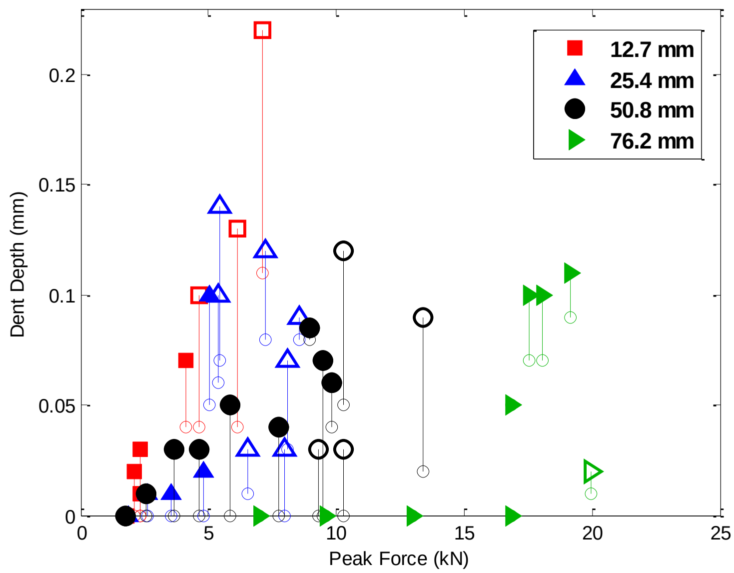

Figure 19. Dent depth vs. peak contact force for 8 ply panel. Filled in data points indicate non damaging impacts, and open points indicate damaging impacts. The tail below each data point indicates relaxation of the dent. Points without a tail had no relaxation

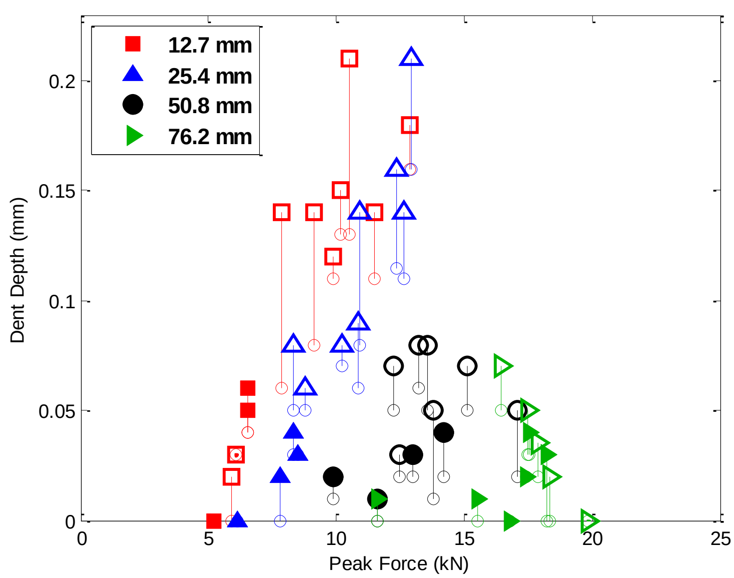

Figure 20. Dent depth vs. peak contact force for 16 ply panel. Filled in data points indicate non damaging impacts, and open points indicate damaging impacts. The tail below each data point indicates relaxation of the dent. Points without a tail had no relaxation

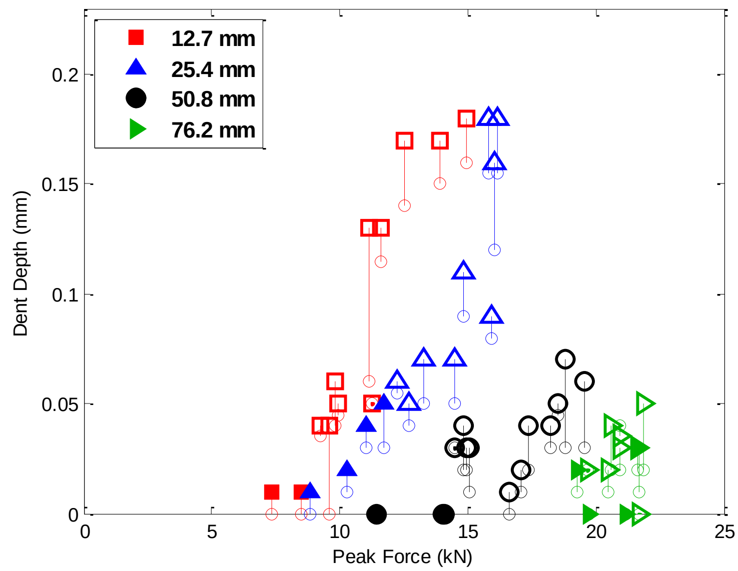

Figure 21. Dent depth vs. peak contact force for 24 ply panel. Filled in data points indicate non damaging impacts, and open points indicate damaging impacts. The tail below each data point indicates relaxation of the dent. Points without a tail had no relaxation

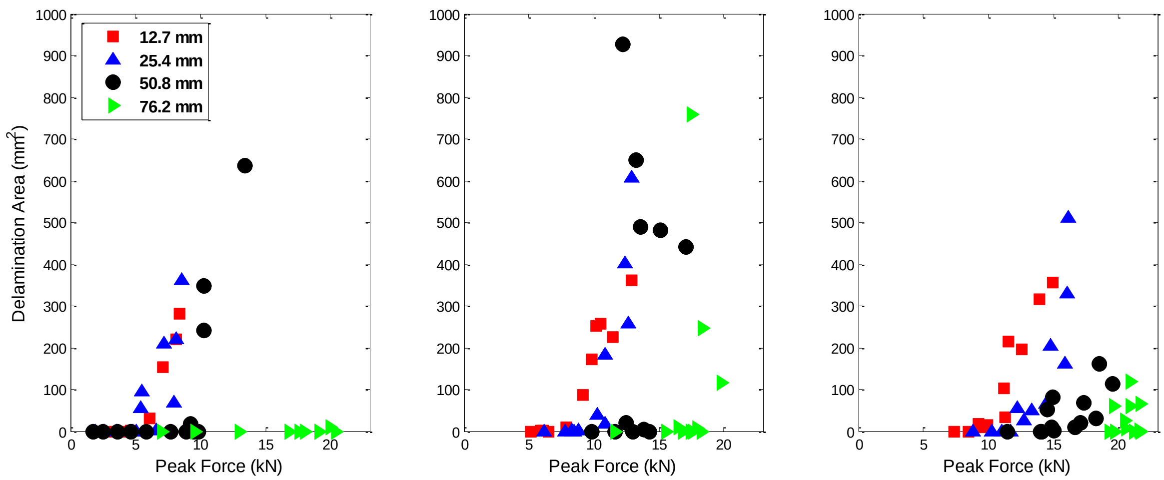

Figure 22. Damage area vs. peak contact force for 8 (left), 16 (middle), and 24 (right) ply panels

Although the results from the impact tests do indicate that there is a correlation between internal damage and indentation, the usefulness of this relationship is questionable. Previous work has found that the visible threshold depth for a dent on a composite structure may be between 0.25 mm and 2.5 mm [21]. In this research, the largest dents created were all less than 0.25 mm. The only impacts that created dents greater than 0.25mm in depth also created visible cracks and significant fiber breakage on the front face of the panel. When such cracking exists on the impact-side, there is no need to rely on dent depth visibility to detect the presence of damage since the crack is much more easily detectable. The test results indicate that for this range of impact tip radii, significant damage occurs from impacts that create dents much shallower than these visible thresholds.

Even though the dents created have been below the defined visual threshold for inspections, it does not mean that they are not identifiable. The visible thresholds of the dents refer to the detectability of the dents during an inspection of the aircraft. In other words, how easily the dents could be identified when the location of suspected damage is unknown. Based on observations from the experiments presented here, dents below 0.25 mm have been found to be readily observable. For impacts with the 12.7 mm tip, even dents as shallow as 0.02 mm could be seen with careful inspection in oblique lighting. However, the locations of the dents generated from these impacts are always known, so this level of visibility may only apply when an impact event is observed or when the area being inspected is relatively small. This emphasizes the necessity to report any observed impacts as soon as they occur. An unreported impact may cause a dent that will be missed during subsequent blind inspections (i.e., location of the impact is not known a. priori), but when the location of the impact is known these shallow dents are much more likely to be identified since the exact location of the impact can be targeted for focused inspection.

Another reason that observed impacts should be reported as soon as they occur is that the dents have a tendency to relax over time. Figures 19-21 show the initial measured dent for each impact and underneath each data point is a tail indicating the relaxed dent depth measured over 24 hours after the impact occurred. Almost all impacts exhibited a measurable relaxation, and some even relaxed to less than 50% of their initial depth. For 8 ply panels, complete dent relaxation was even observed to occur (see Figure 19) for several cases. In order to investigate this dent relaxation further, the depth was recorded as a function of time for the case of identical 37 J impacts applied to a 24 ply panel with 12.7, 25.4, and 50.8 mm radius tips. Figure 23 shows these depth measurements over time. Measurements were taken up to 24 after the impacts, and again after even more time had passed, but after 6 hours no further relaxation was measurable. This relaxation phenomena further emphasizes the need to report any observed impacts quickly. Potential damage from impacts will be more difficult to locate after significant time passes before they are reported, not only because it will be more difficult to remember the exact impact site, but also because the visibility of the damage will be less evident.

The amount that each dent relaxes relative to the initial depth generally decreases with increasing panel thickness and tip radius. Table 4 indicates the average percentage of relaxation from the initial dent depth for each tip radius and panel thickness. This can be explained by the reduction in interlaminar shear and bending stress as both the tip radius and panel thickness increase, which effectively reduces the peak strains and severity of damage that the impact event produces.

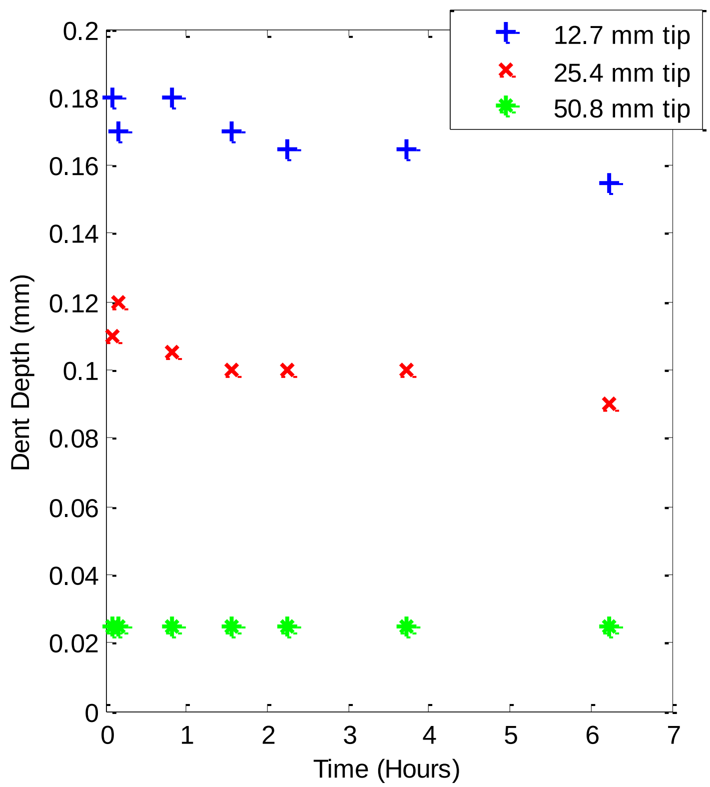

Figure 23. Dent relaxation over time for 37 J impacts on a 24 ply panel

Table 4. Average percent change from initial to relaxed dent depth for each panel thickness (T in number of plies) and impact tip radius (R in mm)

Panel Type	Thickness (mm)	Percent Dent Relaxation for Tip: R12.7	R25.4	R50.8	R76.2
8 Plies	1.7	65	34	29	3
16 Plies	3.3	29	14	15	12
24 Plies	4.9	38	15	13	7

After the tests were run it was apparent that the shape of the dents were different depending on the radius of the impacting tip. To account for this, the span of each dent was measured by taking measurements every 1.58 mm (1/16 of an inch) along a path on the impact-side surface of the panel passing through the impact site. In order to avoid subjectivity from determining the span of the dents, the span of the dent was defined as the distance between those points on either side of the maximum depth location where the depth reached 1/3 the total depth. Figure 24 shows an illustration of how the span of a dent would be measured. After close inspection it was concluded that this threshold depth defining the span most closely matched the span over which the dent can be visually perceived to exist since contours and changes at depths less than 1/3 the total tended to be more gradual and thus difficult to perceive.

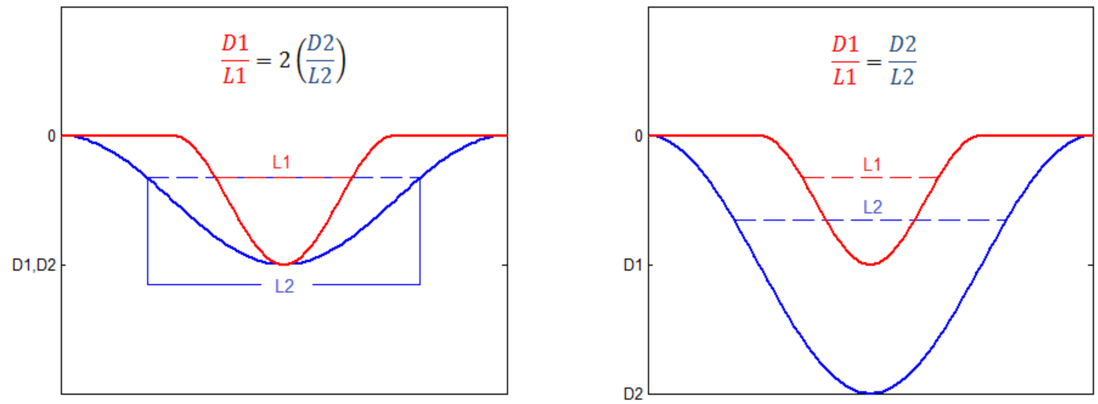

Figure 24. Illustration of dents with equal depth but different "visibility" (left) and equal "visibility" but different depth (right)

Visibility of the dent depends on a combination of both the depth and the span. A dent with a short span will have sharper boundaries and will be more visible than a dent of equal depth but existing over a larger span (resulting in more smoothly-defined, shallower boundaries). Since the visibility of the dents increases with depth and decreases with span, a more comprehensive metric for describing the visibility can be defined as the ratio of dent depth divided by the dent span. Figure 24 shows an illustration of dents with equal depth but different depth/length ratio and dents with different depths but the same depth/span ratio. When relating this value of "visibility" to the delamination area, the correlation becomes more strongly dependent on the tip radius than when comparing dent depth alone. Figure 25 shows the dent depth vs. the delamination area, and Figure 26 shows the visibility (depth/span ratio) vs. delamination area for the 8, 16, and 24 ply panels. Both of these relationships are dependent on the impact tip radius, with the smaller-radius tips exhibiting more dent visibility than larger-radius tips, for a given delamination area, particularly for the thicker panels.

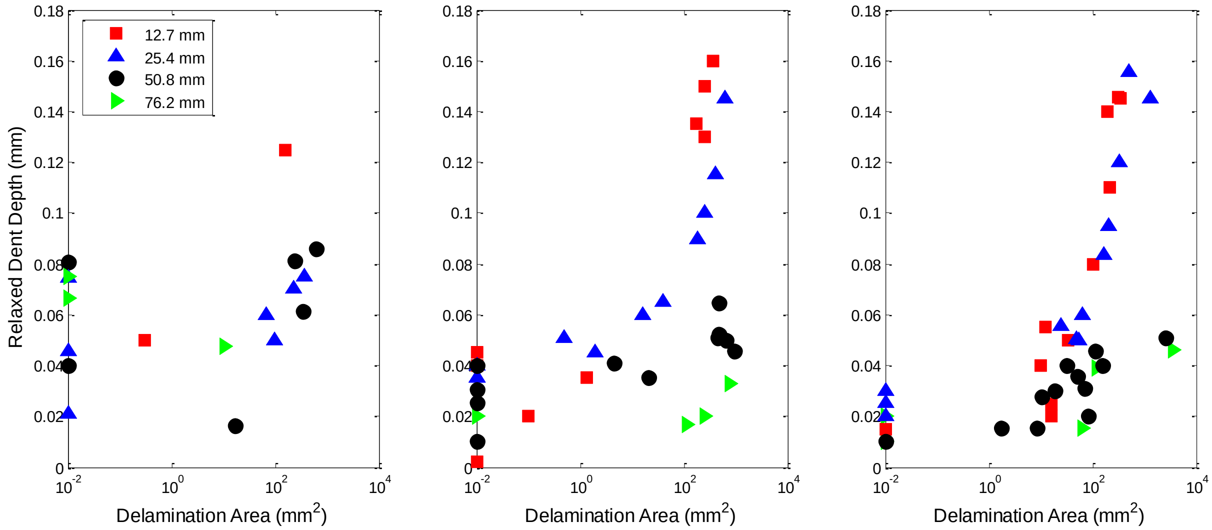

Figure 25. Damage area vs. relaxed dent depth for 8 (left), 16 (middle), and 24 (right) ply panels

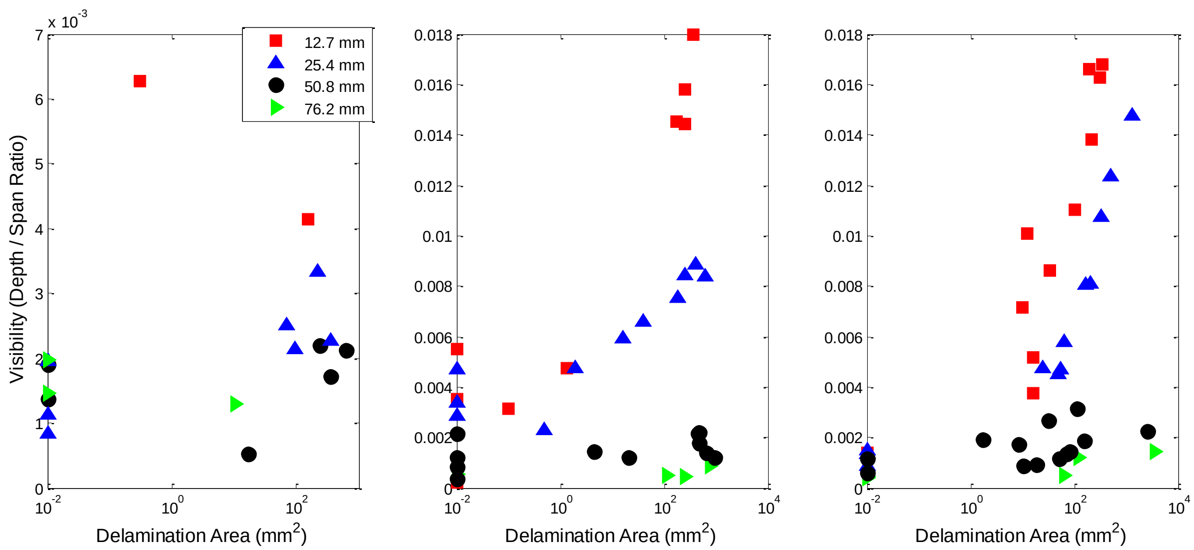

Figure 26. Damage area vs. dent visibility for 8 (left), 16 (middle), and 24 (right) ply panels

Even if the dent from an impact could be located, determining the extent of damage from the characteristics of the dent remains a challenge. Figure 26 indicates that dents can have equal visibility but drastically different delamination areas based on the radius of the impactor. Figure 25 shows that looking at only the depth of the dent gives a weaker correlation with internal damage (i.e., there is more scatter range of delamination area for a given depth). Some low energy impacts from the 12.7 and 25.4 mm tips did not result in any internal damage, but created dents much more visible than impacts from the 50.8 and 76.2 mm tips that caused significant internal damage. As the radius of the impact tip increases, the visual evidence of damage decreases. Because of the strong dependence of the radius of the impactor on the visual and internal damage, determining internal damage level from visual damage could only be accurately accomplished if the radius of the impactor was known. This would be very difficult to determine in the field where even in witnessed events such as tool drops the radius of the impact tip would be difficult to determine as the tool could land in many different orientations. Since the radius of the impact is most likely not known for impacts on structures in the field, it cannot be concluded what size and kind of internal damage a visible dent may indicate, or in the case of the dent not being visible, whether or not there exists internal damage at all.

3.4 Force History Data

Information regarding the nature of impact events has often been found by examining the force vs. time history. Appendix VI includes the force vs. time curves paired with the corresponding C-Scans for all impacts. They are organized by impact tip radius and panel thickness so that distinctive characteristics for each set of test parameters can be more easily identified.

The force vs. time histories can reveal the occurrence of damage in two possible ways. The first is for a sharp section of oscillations to occur in a distinct section of the curve. This is seen in the 8 and 16 ply panels but not 24 ply panels. These oscillations indicated both delamination and fiber failure forms of damage. Figure 27 shows this type of response for a non-damaging (12.5 J, 6.5 kN peak force) and a damaging (23.3 J, 9.9 kN peak force) impact with a 12.7 mm tip radius on a 16 ply panel.

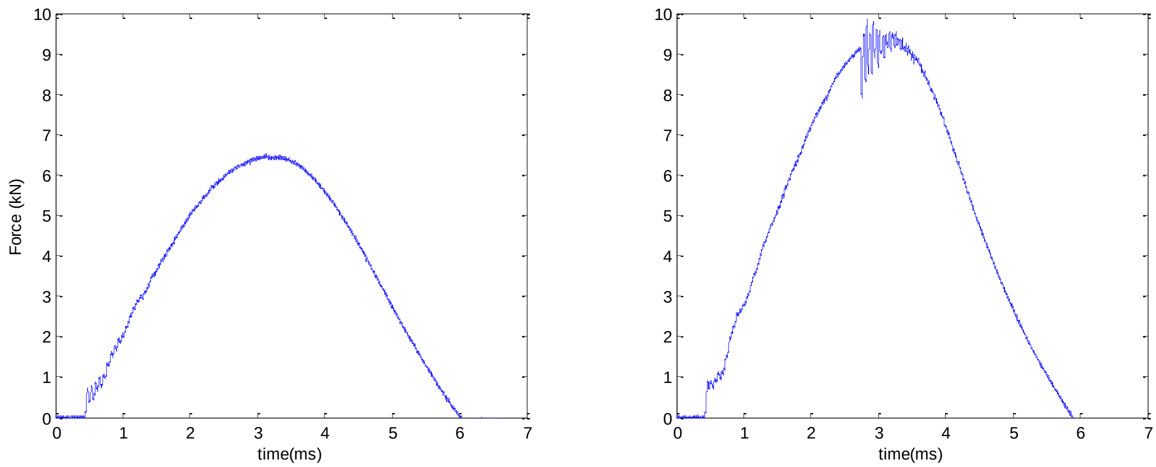

Figure 27. Force vs. time history for a non-damaging (12.5 J, 6.5 kN peak force) and a damaging (23.3 J, 9.9 kN peak force) impact with a 12.7 mm tip radius on a 16 ply panel

The second way force curves could indicate damage was by the overall shape of the curve becoming distorted. In most cases a dip in the up-loading portion of the curve near the peak force can be observed. In some cases it could be seen that after an initial drop in force the load would increase again. This type of damage indication was only seen in the 24 ply panels, which only exhibited damage in the form of delamination (no fiber failure was created in any 24 ply panel). Figure 28 shows an example force history curve exhibiting these features.

Both of these deviations from a simple "half-sine" like shaped force vs. time pulse indicate that damage has occurred, with the timing and force level of the onset of these deviations corresponding to the initiation of damage.

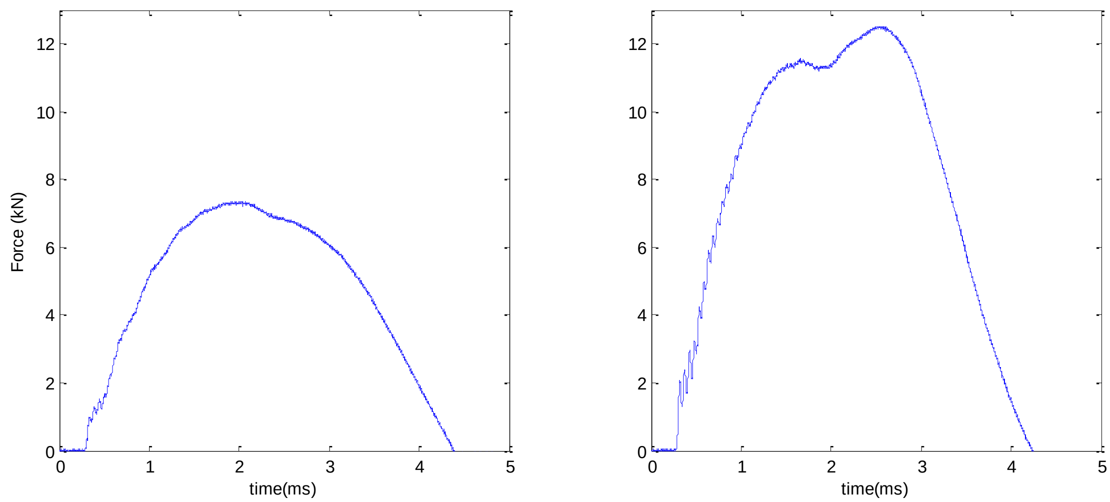

Figure 28. Force vs. time history for a non-damaging (10.7 J, 7.4 kN peak force) and a damaging (30.0 J, 12.5 kN peak force) impact with a 12.7 mm tip radius on a 24 ply panel

The impact tip radius had a unique effect on the force history curves. Although the overall shape of the curve remained somewhat consistent, the magnitude and pulse duration were dependent on the tip radius. Figures 29-31 show impacts that created similar levels of damage for each impact tip radius. The impacts plotted in the figures correspond to the lowest energy impacts at which the presence of damage became evident in the force vs. time history curves.

It can be seen from these figures that as the impact tip radius increases, the pulse time decreases and the peak force to create an initial level of damage increases. This decreasing critical force for smaller radius tips is due to the higher contact stresses and interlaminar shear stress developed by a smaller contact area for a given force level. It can also be seen that the differences between the curves for different tip radii become less distinct as the panel thickness increases.

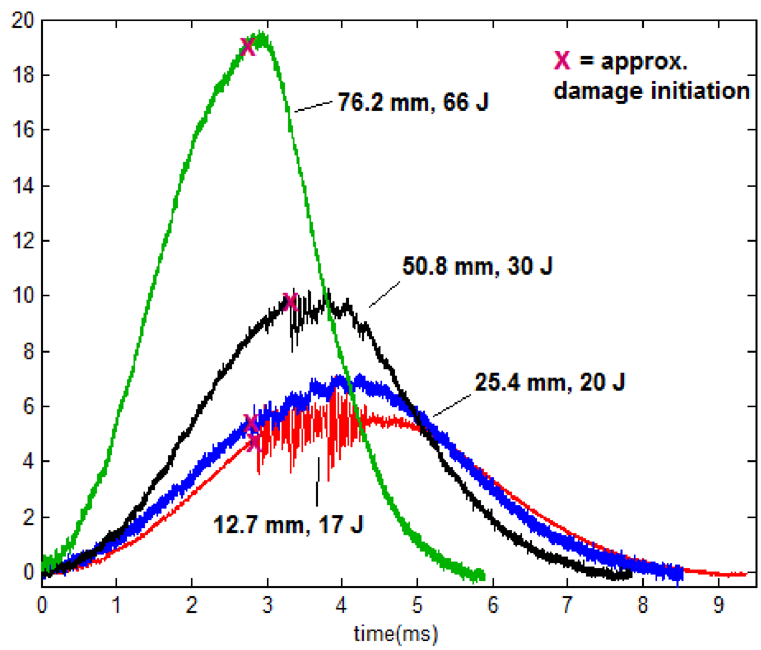

Figure 29. Damage indicating force pulses for 8 ply panels

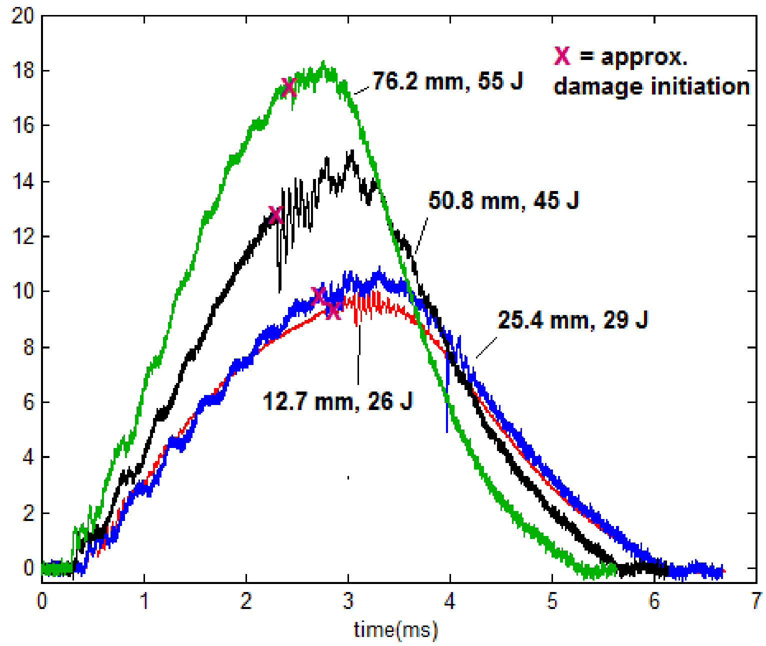

Figure 30. Damage indicating force pulses for 16 ply panels

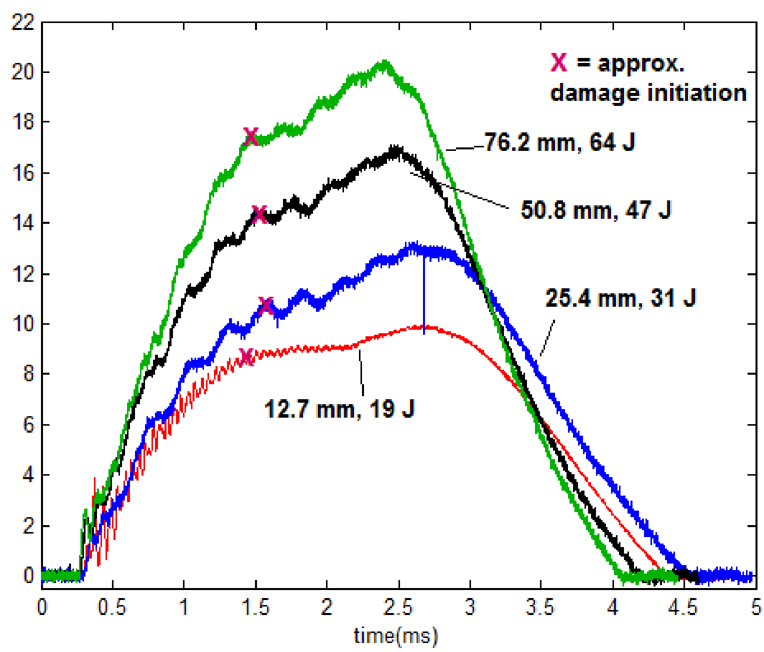

Figure 31. Damage indicating force pulses for 24 ply panels

The thickness of the panels had a large influence on the force curves as well. The pulse time decreased with an increasing thickness, since the thicker panel is stiffer and thus dynamically responds at a higher frequency. Also, the peak force level required to create a certain level of damage increased with higher thickness since increased thickness results in lower interlaminar shear stress for a given radius tip and force level. This was the same effect that the tip radius had (i.e., increasing force for larger radius). The panel thickness however, also influenced the overall shape of the force curve. Impacts onto the 8 ply panels produced a more sinusoidal shape than the thicker panels. As seen in Figure 29, even though significant damage was evident, the overall shape of the curve was mostly unaffected for thinner panels. For the 24 ply panels however, the onset of damage greatly influenced the shape of the force curve. Figure 31 shows the typical shape of the force pulse from damaging impacts on 24 ply panels. The rate of force increases departs from the sine-type profile at the onset of damage and “flattens” out. This different force behavior for the panel thicknesses was most likely due to the ability of the thicker panels to develop alternate load paths, namely as planes of delamination are formed. With the 8 and 16 ply panels, the force curve peaks once damage has occurred and the onset of damage was indicated by the onset of distinct sharp oscillations in the curve. For the 24 ply panels however, the force continues to rise even after damage has occurred as new load paths develop, giving the pulse a distorted shape but no section of sharp oscillations as seen in the thinner panels.

The difference between the 24 ply panels and the thinner panels may be a result of a difference in failure mode. In the 8 and 16 ply panels, damage was only evident in the force vs. time histories when fiber breakage had occurred. There was no indication of damage in the force vs. time curves if only delamination had occurred. In the 24 ply panels, no fiber breakage was initiated for the range of impact energies investigated, and delamination was the only significant form of damage. For these panels, low levels of delamination were not detectable from the force vs. time histories, and there was only an indication of damage after larger amounts of delamination had occurred.

3.6 Contact Pressure

The peak contact force was not dependent on the radius of the impact tip for impacts of the same energy on the same panel type. Figure 13 shows that a given energy level will correspond to a peak force independently of the tip radius. However, a blunter impact tip will create a larger contact area and require higher forces to produce damage. The kinetic energy vs. contact area can be seen in Figure 32.

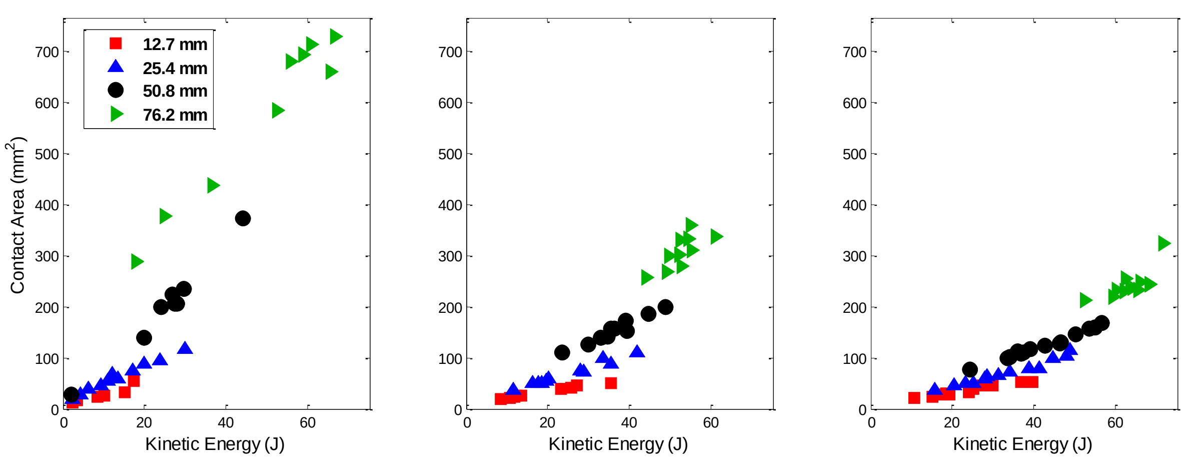

Figure 32. Kinetic energy vs. contact area for 8 (left), 16 (middle), and 24 (right) ply panels

The plots indicate that while the peak force may be the same for different tip radii, the contact area is strongly dependent on both the tip radius and panel thickness, and thus average contact pressure (calculated as peak force over contact area) will be different for varying radius impactors. It should be noted that the distribution of contact pressure throughout the entire contact region during an impact is not evenly distributed. It will typically be at a maximum in the center and greatly decrease at the boundaries. However, observing the average contact force can still offer some insight. Figure 33 shows the kinetic energy vs. the average contact pressure.

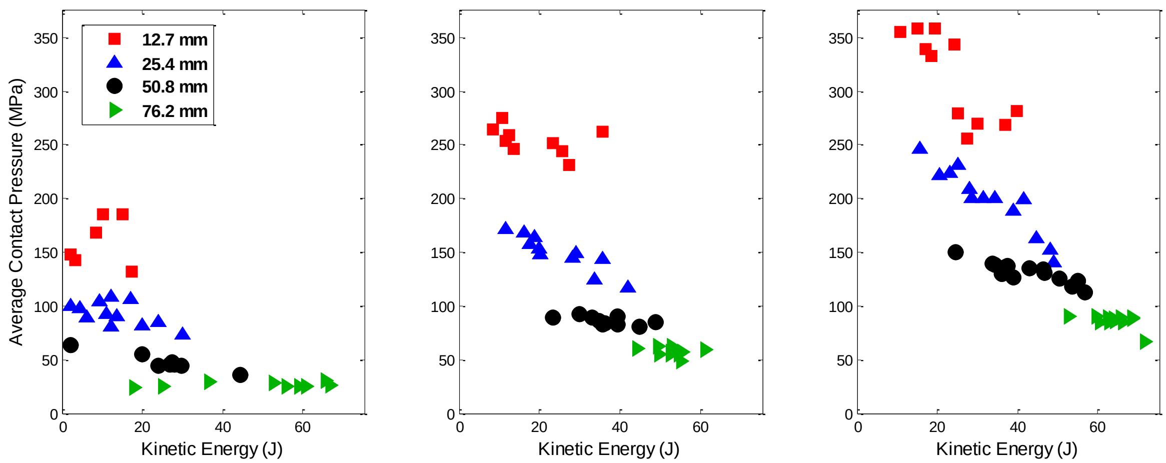

Figure 33. Kinetic energy vs. average contact pressure for 8 (left), 16 (middle), and 24 (right) ply panels

An overall observation is that the average contact pressure increases for decreasing tip radius (smaller contact area), and also increases for thicker panels due to their higher stiffness (higher force). For the 76.2 mm radius tip, the contact pressure remains essentially constant for each panel type, despite the increasing peak force (see Figure 13). The other impact tip radii actually show a decrease in contact pressure as kinetic energy increased. This indicates that the contact area increases with kinetic energy at a greater rate than the peak contact force does. It should be noted, however, that this decreasing contact pressure trend is dependent on the boundary conditions. For example, if the dimensions of the panel were much smaller, the global stiffness of the panel would be higher and the total deflection of the panel would be less. This smaller deflection would result in smaller contact areas and the average contact pressure could potentially increase with kinetic energy. The important observation from Figures 32 and 33 are that the contact area and average contact pressure are dependent on the impact tip radius. For a given kinetic energy, sharper radius tips will create much higher average contact pressures than blunter tips. Finally, from viewpoint of visibility, if the contact pressure is high enough, the panel surface could form a local indentation due to direct contact pressures, thereby leaving more visible dents. As indicated by Figure 33, this could more likely happen for smaller radius tips impacting thicker panels.

3.5 Microscopy

In order to further investigate the damage morphology within the panels, a few select specimens were sectioned for microscope inspection. This was done by cutting through the impact site in the zero degree direction. This section of panel was then mounted in epoxy (see Figure 34) and then polished using five levels of sand paper with a progressively finer grit, the final level being 14,000 grit.

Figure 34. Panel section prepared for microscopy mounted in epoxy

Figure 35 shows the cross section of a 16 ply panel damaged from a 12.7 mm radius tip impact. The figure also shows the corresponding C-Scan map indicating the cross section from the microscope image. The 31 J impact created 225 mm^2 of delamination damage and a small amount of backside fiber failure. The residual surface dent measured for this impact was 0.11 mm. This image shows that the surface dent is more evident on the impact side, with the permanent deformation propagating through the first plies and gradually decreasing as it reaches the back face. This clearly shows that such surface dents were not simply a result of the layer of paint on the front surface (see uppermost white layer in Figure 35) being compressed, and shows that the composite plies are in fact being permanently deformed by the impacts. Delamination can be identified in the panel at the mid-plane between the center two 45 degree plies, and between the 5^{th} and 6^{th} plies from the bottom, which are 0 and 45 degree plies respectively.

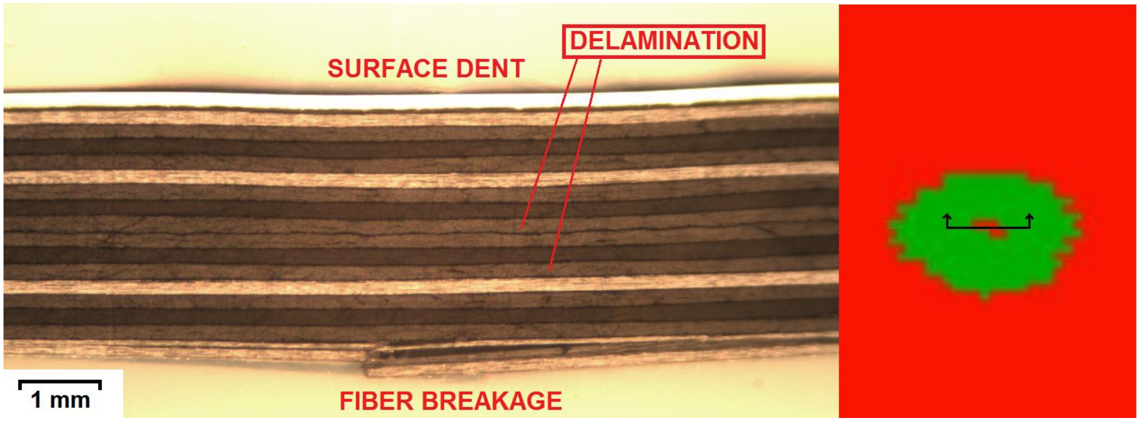

Figure 35. Microscope image and C-Scan map of test LV-021, 16 ply panel impacted with 31 J by a 12.7 mm tip

Figure 36 shows an image of this same section with increased magnification. Matrix cracks in the 8^{th} and 9^{th} plies are indicated in the figure, these can be seen on either side of the center of the impact in Figure 35 as well. These matrix cracks are at a 45 degree angle relative to the impact, indicating that they are a result of transverse shear stresses. The cracks are also at the center of the laminate, where the shear stress is the highest. These matrix cracks do not typically result in significant losses in residual strength, but they do serve as flaws that allow delamination to initiate [9].

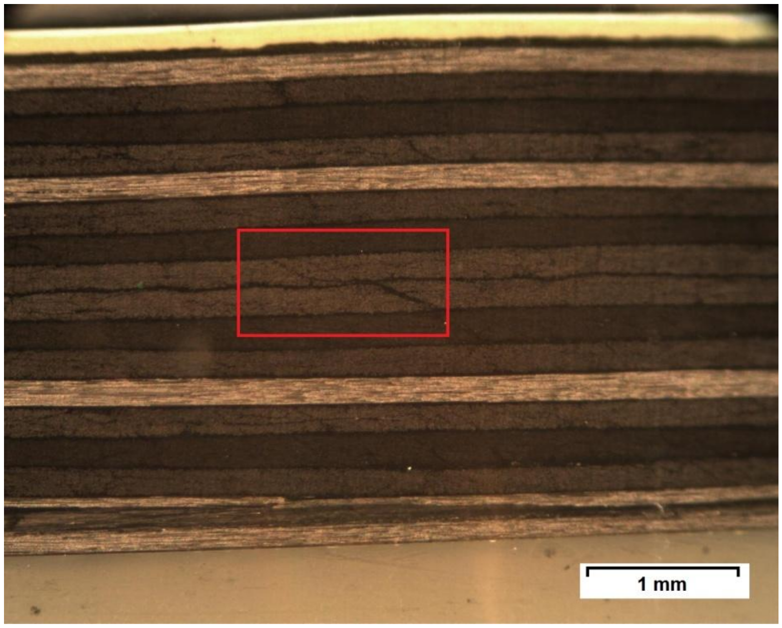

Figure 36. Microscope image of test LV-021 with increased magnification

Figure 37 shows a 16 ply panel damaged with a 76.2 mm radius tip by a 55 J impact, which created 248 mm^2 of delamination and back side fiber breakage. In this image there is no obvious indication of a dent, and no measurable residual dent was detected. Furthermore, unlike the 12.7 mm impact shown in Figure 35, the delamination planes are not clearly visible for the larger-radius impactor.

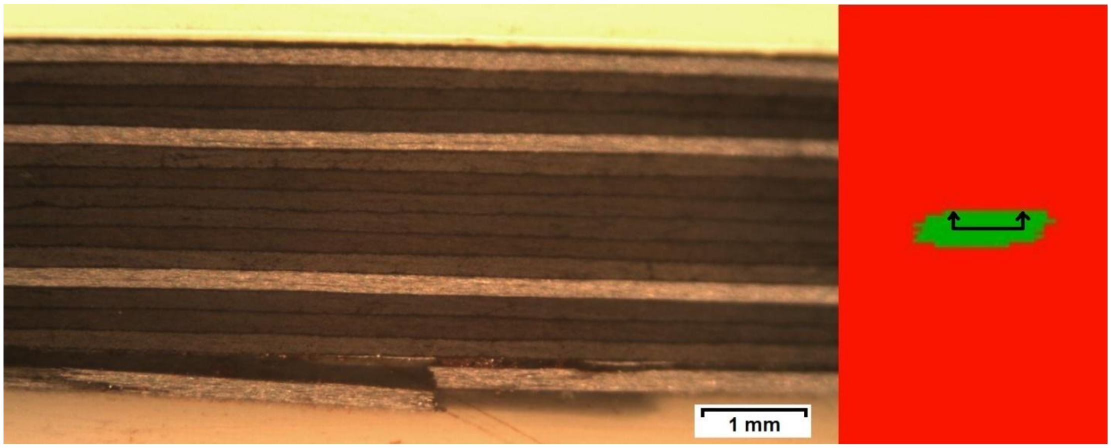

Figure 37. Microscope image of test LV-113, 16 ply panel impacted with 55 J by a 76.2 mm tip

Figure 38 shows the same panel as in Figure 37 with increased magnification. This image shows that a large amount of matrix cracking (see faint vertical lines) has occurred in the 2nd, 3rd, and 4th plies from the bottom (a small portion of the cracks are indicated in the figure, there are many more cracks along these plies, although they can be difficult to see). Unlike the cracks shown in Figure 34, these cracks are parallel to the direction of the impact and are on the back portion of the laminate rather than at the center, which indicates that they were caused by tensile bending stresses.

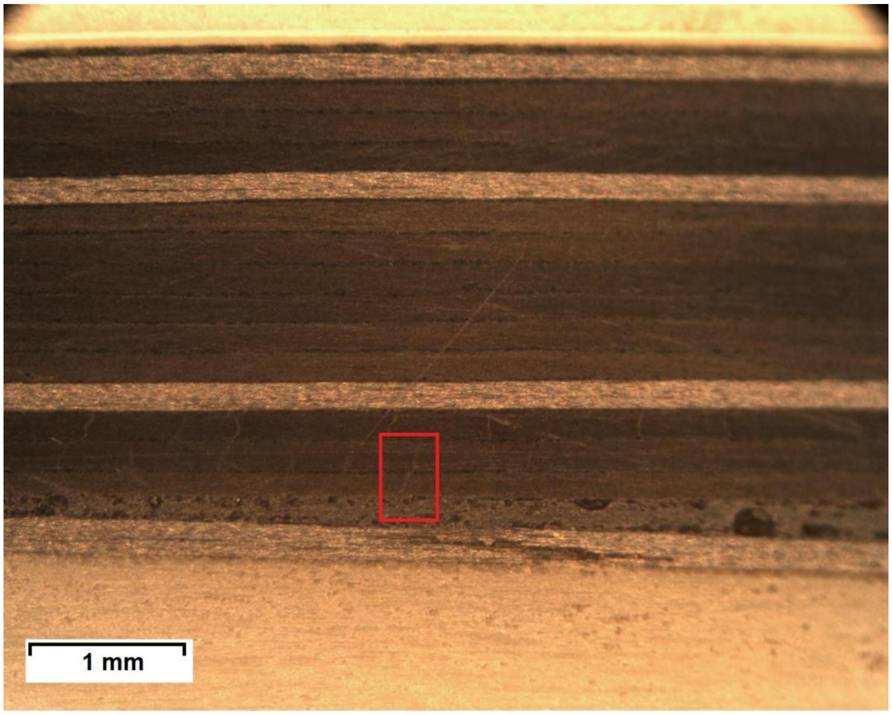

Figure 38. Microscope image of test LV-113 with increased magnification

The matrix cracks in the microscope images are direct evidence that damage is being created by different mechanisms for impact tips of different radius. The sharper 12.7 mm tip impacts result in a smaller contact area, and create higher interlaminar shear stresses around the border of the contact region (i.e., in shear plug mode). The blunter 76.2 mm radius tip has a larger contact area and lower shear stress around the periphery. In order to initiate damage with the 76.2 mm tip, comparatively high contact forces and flexural stresses had to be developed, which required more energy than for failure resulting from the shear stress from the 12.7 mm radius tip.

CHAPTER 4: DISCUSSION AND CONCLUSIONS

The failure modes of unidirectional carbon/epoxy composite panels subjected to low velocity impacts are complex and often leave little or no visible evidence of the existence damage, particularly for contact with large radius objects. Due to the increased use of composites in the aerospace industry, a more comprehensive understanding of the response of composite materials subject to a broader variety of impact loading is necessary. Experimental data were collected in order to investigate the damage initiation in composite panels subjected to low velocity impacts. Of major interest is the relationship between the development of externally visible damage and the extent of internal damage and how damage is affected by impactor radius. In these experiments, carbon/epoxy panels of 8, 16, and 24 ply thicknesses (1.7 mm to 4.9 mm) were impacted with steel tips having radii of 12.7, 25.4, 50.8, and 76.2 mm.

For a given impact energy, peak contact force is not dependent on the radius of the impact tip, but mainly on the panel stiffness which is affected by the thickness, layup, and boundary conditions. However, the contact area and average contact pressure are strongly dependent on the tip radius. Thus, for a given energy and panel thickness, a larger-radius impact tip will produce the same peak force but a larger contact area than a smaller impact tip. A blunter tip distributes the contact force over a larger area, thereby developing lower interlaminar shear stress around the periphery of this contact area, and thus resulting in higher failure threshold with increasing tip radius. This effect is greater in the 8 ply panels than in the 16 or 24 ply panels. This is because the impact force excites a combination of flexural and shear deformation, and also due to the reduced stiffness of the thinner panel. The thicker panels are stiffer and thus undergo much less flexural deformation. Thus, the impact generates higher contact forces that in turn produce high interlaminar shear stresses which induce delamination. However, the more compliant 8 ply panels undergo larger amounts of flexural deformations and thus lower contact force develops, resulting in reduced shear stress but increased flexural stress. Failure of a composite panel in bending is typically in the form of back face fiber breakage, usually just the backside adjacent one or two plies fail. For the 8 ply panels, fiber failure actually preceded delamination when impacted by the 50.8 or 76.2 mm tips (for the 12.7 and 25.4 mm tips delamination was still the initial form of failure). The failure thresholds of thinner panels, where bending failure response is dominant, are therefore more strongly affected by the tip radius geometry since the thinner panels are able to more closely conform to the tip's radius, thereby controlling the peak local bending stress. This relationship weakens as the panel flexural stiffness (panel thickness) increases. For the 76.2 mm tip, the FTE is actually higher in the 8 ply panels than in the 16 or 24 ply panels.

Since visual inspection is the cheapest and most efficient method of inspecting an aircraft, a relationship between the presence of internal damage and the formation of visually-detectable evidence of this damage's presence, is desirable. Results show that for the 12.7 and 25.4 mm radius tips, relationships can be drawn between the dent depth and the delamination area. However, the usefulness of these relationships is questionable since the correlation between delamination area and dent depth is very dependent on the impact tip radius, a parameter which is not always known except in a lab environment. Therefore, unless the radius of the impact tip is known, it will not be possible to relate the dent depth to an accurate estimate the internal damage size, particularly delamination. Even if the impact event is witnessed, determining the impacting radius can be difficult since an object could potentially impact the structure in many different orientations. For the larger radius impact tips (50.8 mm and 76.2 mm), no such relationship between dent depth and delamination can be observed over the range of energies tested and for the modes of damage produced (namely delamination and some small backside fiber failure). If a relationship does exist at higher energies, it would only be evident at impact energies that far exceed the FTE.

Surface dents can be further described by measuring the span of the dents. A dent with a larger span will have more gradual boundaries and will therefore be less visible than a dent of equal depth but shorter span. A metric of visibility was defined as the depth of the dent divided by the span. However, relating this quantity to the delamination size produces similar results as when relating to the raw dent depth alone. The correlations for the sharper impact tips are still dependent on the tip radius, and no strong correlation emerges from the blunter impact tips.

When an impact event such as a tool drop is witnessed, it is important to report the event as soon as possible based on two factors that were observed in this experiment. The first is that none of the dents created exceeded the depth that would be considered detectable during a visual inspection, but many of them were still easily detected when closely examined. This is because when the location of an impact is known and that area is closely inspected, even very shallow dents (e.g., less than 0.05 mm) can be found. This is particularly important for very large structures where small depth dents (less than 0.25 mm) would normally not be visible. Therefore, if an impact is reported quickly, or if its location is marked/tagged, it is much more likely that the exact location of the impact is identified and the inspection and repair will be much more efficient. The second reason it is important to report witnessed impacts quickly is that the dents were observed to relax over time. Almost all dents exhibited some degree of relaxation, and time dependent studies indicate that it only takes six hours for the dents to relax to their final state. Not only will it be harder to remember exactly where an impact occurred when the event is not reported quickly, but the visual evidence of the impact will actually reduce as time passes. For this material system, the dents relaxed to their final state after six hours.

Future work could consider residual strength testing to further determine what type of performance reduction would result from these types of impacts. Residual strength has been related to the extent and type of damage in the past, but it has been shown here that damage from different tip radii is induced by two separate mechanisms (shear or bending stresses) which are affected by the impactor tip geometry. Therefore, a direct comparison between the residual strength and the impact characteristics measured in these experiments (i.e., damage visibility, peak force, contact pressure, etc.) would be useful, especially with regards to the radius of the impact tip. Different layup orientations could also be considered. The layups used in this experiment were quasi-isotropic and had even distributions of 0, 90 and +/-45 degree plies, and were not tailored to any specific aerospace structure. However, interlaminar shear stresses are dependent on the layup orientation, and different layups could affect the damage initiation thresholds as well as the damage visibility.

REFERENCES

[1] Y. P. Siow and V. P. W. Shim, "An Experimental Study of Low Velocity Impact Damage in Woven Fiber Composites," *Journal of Composite Materials,* vol. 32, no. 12, 1998.

[2] R. McAdam, T. O'Hare and S. Moffett, "Collaborative Knowledge Sharing in Composite New Product Development: An Aerospace Study," *Technovation,* vol. 28, no. 5, pp. 245-256, 2008.

[3] D. S. Cairns and P. A. Lagace, "Thick Composite Plates Subjected to Lateral Loading," *ASME Journal of Applied Mechanics,* vol. 54, pp. 611-615, 1987.

[4] N. R. Adsit and J. P. Waszczak, "Effect of Near-Visual Damage on the Properties of Graphite/Epoxy," *Composite Materials: Testing and Design, Fifth Conference,* American Society for Testing and Materials, New Orleans, March 1978.

[5] C. T. Sun, "An Analytical Method for Evaluation of Impact Damage Energy of Laminated Composites," *Composite Materials: Testing and Design (Fourth Conference),* American Society for Testing and Materials. pp. 427-440, May 1976.

[6] E. Wu and K. Shyu, "Response of Composite Laminates to Contact Loads and Relationship to Low-Velocity Impact," *Journal of Composite Materials,* vol. 27, no. 15, 1993.

[7] J. Willis, "Hertzian Contact of Anisotrpotic Bodies," *Journal of Mechanics and Physics of Solids,* vol. 14, pp. 163-176, 1966.

[8] S. H. Yang and C. T. Sun, "Indentation Law for Composite Laminates," *AM. Soc. Test. Mater,* 1981.

[9] P. Sjöblom and T. Hartness, "On Low-Velocity Impact Testing of Composite Materials," *Journal of Composite Materials,* vol. 22, pp. 30-52, 1988.

[10] G. Schoeppner and S. Arbrate, "Delamination Threshold Loads For Low Velocity Impact on Composite Laminates.," *Composites Part A: Applied Science and Manufacturing,* vol. 31, pp. 903-915, 2000.

[11] X. Zhang, "Impact damage in composite aircraft structures- experimental testing and numerical simulation," *Proceedings of the Institute of Mechanical Engineers*, Part G: Journal of Aerospace Engineering, vo. 212, pp. 245-259, April 1998.

[12] G. Davies and X. Zhang, "Impact Damage Prediction in Carbon Composite Structures," *International Journal of Impact Engineering*, Vol. 16, pp. 149-70, 1995.

[13] D. Whisler and H. Kim, "Effect of impactor radius on low-velocity impact damage of glass/epoxy composites," *Journal of Composite Materials,* p. DOI 10.117/0021998312436991, 2012.

[14] F. J. Yang and W. J. Cantwell, "Impact Damage Initiation in Composite Materials," *Composites Science and Technology,* vol. 70, no. 2, pp. 336-342, 2010.

[15] B. L. Wardle and P. A. Lagace, "On the Use of Dent Depth as an Impact Damage Metric for Thin Composite Structures," *Journal of Reinforced Plastics and Composites,* vol. 16, no. 12, 1997.

[16] T. Anderson and E. Madenci, "Experimental Investigation of Low-Velocity Impact Characteristics of Sandwich Composites," *Composite Structures,* vol. 50, no. 3, pp. 239-247, 2000.

[17] C. T. Sun, A. Dicken and H. F. Wu, "Characterization of Impact Damage in ARALL Laminates," *Composites Science and Technology,* vol. 49, no. 2, pp. 139-144, 1993.

[18] ASTM Standard, D7136, "Standard Test method for Measuring the Damage Resistance of a Fiber-Reinforced Polymer-Matrix Composite to a Drop-Weight Impact Event", ASTM International 2005.

[19] W. C. Jackson and C. J. Poe, "The use of impact force as a scale parameter for the impact response of composite laminates," *NASA Technical Memorandum 104189 AVSCOM Technical Report 92-B-001,* January 1992.

[20] B. Wardle and P. Lagace, "On the Use of Dent Depth as an Impact Damage Metric for Thin Composite Structures," *Journal of Reinforced Plastics and Composites,* vol. 16, no. 12, 1997.

[21] "Military Handbook 17 - MIL-HDBK-17-3F: Composite Materials Handbook, Volume 3 - Polymer Matrix Composites Materials Usage, Design, and Analysis, Chapter 7," U.S. Department of Defense. June 2002, Chapter 7

[22] K. F. Ryan, "Dynamic Response of Graphite/Epoxy Plates Subjected to Impact Loading.," *TELAC Report M.S Thesis, Massachusetts Institute of Technology,* Vols. 89-13, 1990.

APPENDICES

Appendix I. Impact Force Correction

During an impact event using the pendulum a transducer is used to measure the force data, the raw data from this transducer however is not the actual force seen at the point of impact. This is because of the hardened steel tip that experiences the impact before the force transducer. Because this mass is between the site of the impact and the force transducer, the force measured by the transducer will be less than the force at the point of impact. Two methods were used to determine the difference between the force measured and the actual force at the tip of the pendulum.

In the first method, used by Ryan [22], the mass of the pendulum is split halfway through the force transducer to create two free body diagrams (see Figure 39). The equation of motion for both bodies together can be written:

$$F = (m_1 + m_2)a \tag{A1}$$

Where F is the force at the tip, m_1 is the mass of the tip and half the mass of the force transducer, m_2 is the total pendulum mass minus m_1, and a is the acceleration. The equation of motion for just the back end of the pendulum can be written as:

$$F_T = (m_2)a \tag{A2}$$

Where F_T is the force measured by the transducer. Assuming that both sections have the same acceleration, equations (A1) and (A2) can be used to find the force at the tip in terms of the force in the transducer by solving for *a* and equating them:

$$F = \frac{m_1 + m_2}{m_2} F_t \qquad (A3)$$

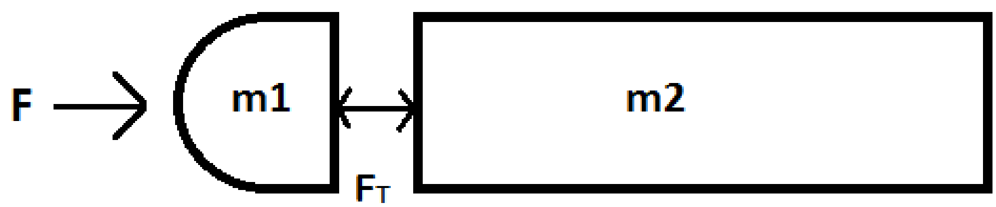

Figure 39. Pendulum Free Body Diagram

For the second method the pendulum is split through the force transducer to make a free body diagram in the same way as the first method. In this model however, the stiffness of the force transducer is used to model the pendulum as a spring-mass system (see Figure 40).

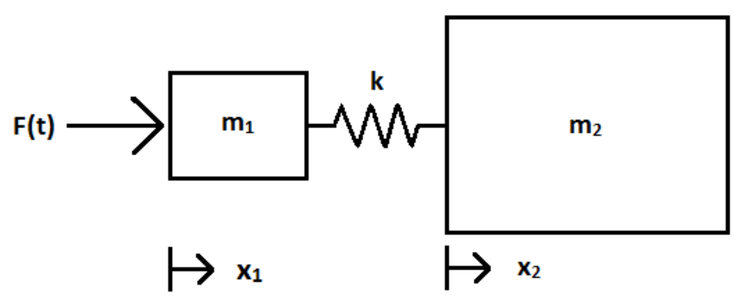

Figure 40. Pendulum as spring-mass system

The equations of motion for the two masses x_1 and x_2 are written as:

$$m_1\ddot{x}_1 + (x_1 - x_2)k = F(t) \qquad (A4)$$

$$m_2\ddot{x}_2 + (x_2 - x_1)k = 0 \qquad (A5)$$

In these equations $\ddot{x}$ is the acceleration and x is the displacement of each mass, $F(t)$ is the force pulse applied at the tip, and k is the stiffness of the force transducer given by the manufacturer. Equations (A4) and (A5) can be solved to get the total displacement of the spring: $(x_1$-$x_2)$. (See Appendix Ia for solution method.) The force in the transducer can then be found using the spring-mass relation $F=kx$. This will be the force that the transducer should measure based on the impulse force applied to the system, so the relationship between the force at the tip to the force in the transducer can be determined.

Table 5 shows the mass and force correction factors determined from each method for each impact tip. The difference between the two methods is very small, only about 0.3% for each tip. Because the vibration method takes into account more dynamic behavior of the system, the correction factors determined using that method were used when determining the force for the tests.

Table 5. Force correction factors determined using constant acceleration and vibration analysis

Tip Radius (mm)	Tip Mass (g)	Constant Acceleration Factor	Vibration Factor
12.7	23.5	1.008	1.005
25.4	462.2	1.134	1.131
50.8	262.3	1.096	1.092
76.2	168.4	1.077	1.074

Appendix Ia. Solving Force Correction Vibration Equations with MATLAB:

Equations (A4) and (A5) can be solved using the built in differential equation solvers in MATLAB.

$$m_1\ddot{x}_1 + (x_1 - x_2)k = F(t) \qquad (A4)$$

$$m_2\ddot{x}_2 + (x_2 - x_1)k = 0 \qquad (A5)$$

These solvers can only solve first order differential equations however, so the equations are manipulated to reduce the order. To do this, new variables are introduced, y_1 and y_2, such that:

$$y_1 = \dot{x}_1 \qquad (A6)$$

$$y_2 = \dot{x}_2 \qquad (A7)$$

Using these new variables equations (A4) and (A5) can be re-written as:

$$m_1\dot{y}_1 + (x_1 - x_2)k = F(t) \qquad (A8)$$

$$m_2\dot{y}_2 + (x_2 - x_1)k = 0 \qquad (A9)$$

Now equations (A6) through (A9) give a system of four first order linear differential equations with four unknowns instead of two second order differential equations with two unknowns.

The force pulse, *F(t)*, can be approximated as a half sine wave.

$$F(t) = A sin(\omega t) \qquad (A10)$$

Where A is the maximum amplitude and ω is the period of the pulse, or pi divided by the duration of the force pulse.

MATLAB has several solvers for ordinary differential equations, but in order to use them the differential equations need to be called as a “function handle”. This means that the equations need to be stored as a separate function. Here is an example of how create a function with equations (A6)-(A9) above:

For this example k = 9 x 10^9 N/m, m1 = 0.5 kg, m2 = 5.5 kg, peak force = 4 kN, and the force pulse is 0.0005 seconds.

```
function xprime = Vib_ode(t,x)
% Since the states are passed in as a single vector, let
% x(1) = x1
% x(2) = x2
% x(3) = y1
% x(4) = y2

k=9e9;
m1=0.5;
m2=5;
w=pi/0.0005;
F=4e3*sin(w*t);

xprime(1) = x(3);

xprime(2) = x(4);

xprime(3) = ((k*(x(2)-x(1)))+F)/m1;

xprime(4) = (k*(x(1)-x(2)))/m2;

xprime = xprime(:);% This ensures that the vector returned is a column
vector
end
```

Now the four equations are stored as a function, and can be called by a MATLAB solver such as ode45. Below is a script that solves the equations using the MATLAB solver ode45 and calculates what the force in the force transducer will be (using $F=k((x_1-x_2))$ relative to the impulse force.

```
t0=0;
tf=0.0005
k=9e9;
w=pi/0.0005;
x0 = [0 0 0 0];
[t,s] = ode45(@Vib_ode,[t0,tf],x0);
x1=s(:,1);
x2=s(:,2);
fc=k*(x1-x2);              %calculated force in transducer
fp=4e3*sin(w*t);           %force pulse approximated as a sine wave
Fa=max(fp)/max(fc);
fprintf('F_tip = %4.4f x F_gauge\n\n', Fa)
```

The output of this code reads:

```
F_tip = 1.0462 x F_gauge
```

This indicates that the force at the tip of the impactor is 4.62% greater than the force measured by the transducer. A plot can be made showing the original force pulse (approximated by a sine wave), and the force in the transducer as calculated above.

```
figure
hold on
plot(t,fc,'r-')
plot(t,fp,'b-')
title('Force Analysis')
xlabel('time (s)')
ylabel('Force (N)')
legend('Force Pulse', 'Force in Transducer')
```

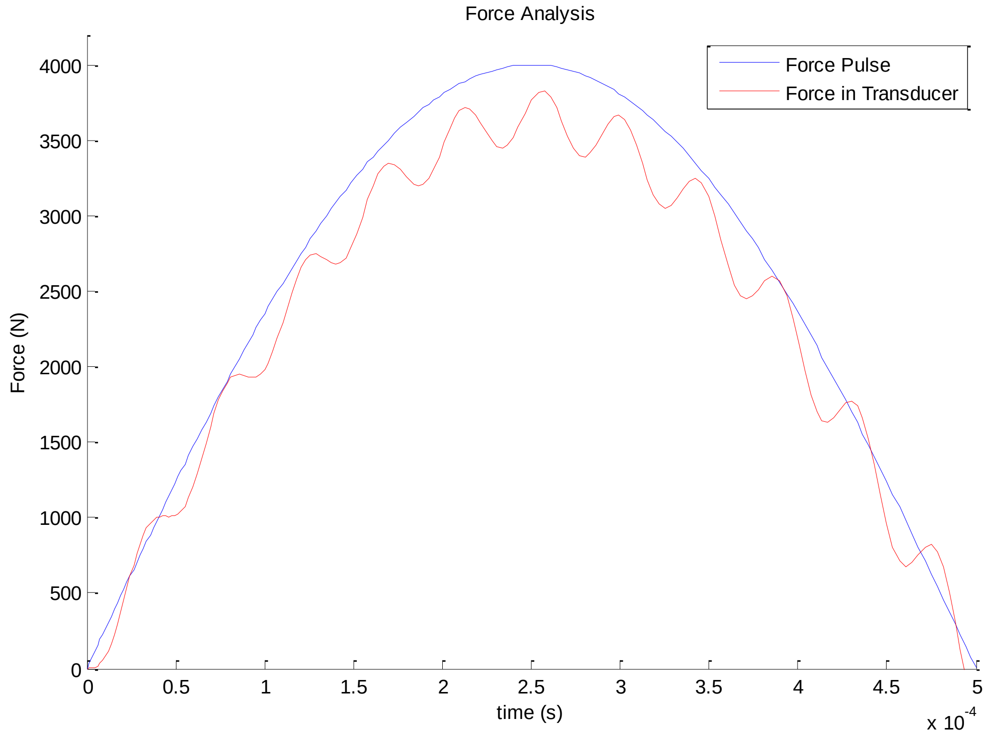

Figure 41. Force pulse at impact site and in the transducer

Appendix II. Potential Energy Calculations

In order to calculate the height of the pendulum required for a desired potential energy, an energy balance model is used (see Figure 42).

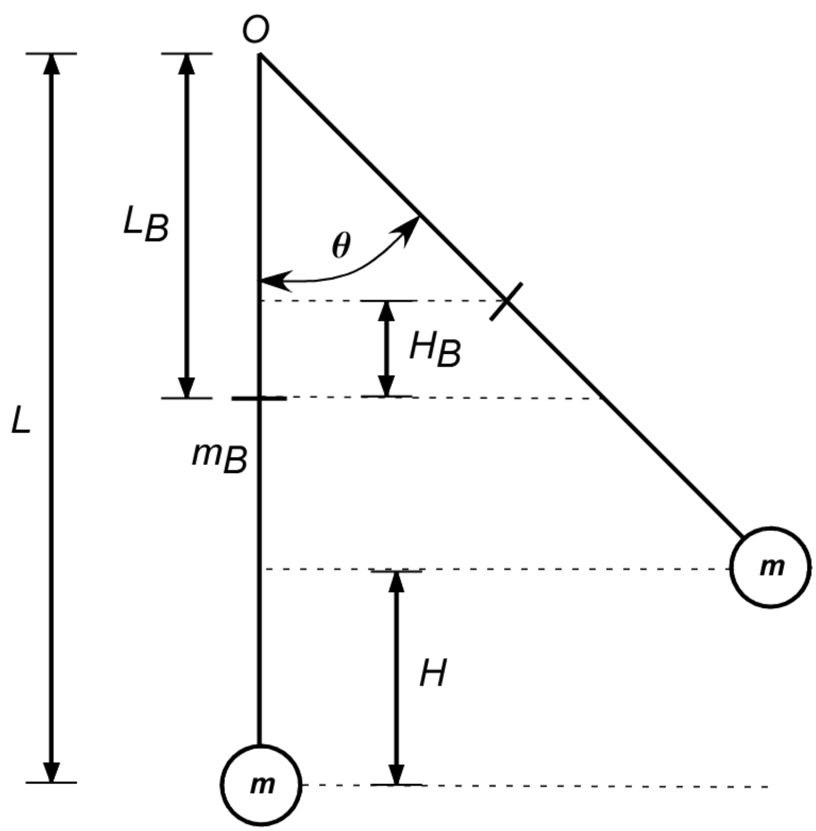

Figure 42. Pendulum energy balance model

In order to analyze the energy of the pendulum system, it will be broken down into two components. The first part is the concentrated mass, m, which is a distance L away from the pivot point O. The second part is the fiberglass bar that has a mass of m_B, which acts through the centroid of the bar a distance L_B away from point O. When the arm is rotated by an angle of θ, the change in height of the mass is:

$$H = L(1 - cos\theta) \qquad (A11)$$

And the change in height of the centroid of the bar is:

$$H_B = L_B(1 - cos\theta) \qquad (A12)$$

The potential energy is:

$$PE = mgH + m_B g H_B \qquad (A13)$$

Substituting equations A11 and A12 into A13 and simplifying the result:

$$PE = mgL(1 - cos\theta) + m_B L_B(1 - cos\theta) \qquad (A14)$$

$$PE = g((1 - cos\theta)(m_B L_B + mL) \qquad (A15)$$

The kinetic energy of a heavy mass on the end of a rotating bar is:

$$KE = \frac{1}{2} J_B \dot{\theta}^2 + \frac{1}{2} m v^2 \qquad (A16)$$

Where J_B is the rotational inertia:

$$J_B = \frac{1}{3} m_B L_B^2 \qquad (A17)$$

Substituting A17 into A16 and simplifying gives:

$$KE = \left(\frac{1}{6} m_b L_b^2 + \frac{1}{2} m L^2\right) \dot{\theta}^2 \qquad (A18)$$

Assuming that all of the potential energy is converted into kinetic energy, KE=PE, equations A15 can be set equal to A18:

$$\left(\frac{1}{6}m_b L_b^2 + \frac{1}{2}mL^2\right)\dot{\theta}^2 = g((1 - cos\theta)(m_B L_B + mL) \qquad (A19)$$

Solving this equation for velocity gives:

$$v = L\sqrt{g(\frac{(1 - cos\theta)(m_B L_B + mL)}{\left(\frac{1}{6}m_b L_b^2 + \frac{1}{2}mL^2\right)}} \qquad (A20)$$

In order to facilitate calculating the height for each test, a MATLAB function was created to incorporate these calculations. The inputs are the initial step (the angle that the encoder wheel reads when the pendulum is touching the panel), the desired potential energy, and either the impact tip or mass of the head of the pendulum. The encoder wheel measures the angle of the pendulum arm in tenths of a degree so the output is a four digit integer (for example, 145 degrees = 1450). Since the pendulum can only be set to the nearest tenth of a degree, the MATLAB function calculates the exact angle of the arm for the desired potential energy, and then calculates and reports the energy at the angles rounded up and down to the nearest tenth of a degree.

```
function Potential_Energy2
%%% -- ENTER TEST DATA --
STEP=input('Initial STEP = ');
PE=input('Potential Energy = ');
tip=input('Tip Radius = ');
if tip==50.8
    MASS=4.813; %R50.8mm
elseif tip==152.4
    MASS=4.849; %R152.4mm
elseif tip==101.6
    MASS=4.841;  %R101.6mm
elseif tip==12.7
```

```
    MASS=4.240; %R12.7mm
elseif tip==25.4
    MASS=5.013; %R=25.4mm
else
    MASS=input('Pendulum Mass = ');
end
%%% -- CONSTANT DATA --
MBAR=0.838;%Mass of the fiberglass bar
L=1.4224;%dist from pivot to mass CG
G=9.80665;

%%% -- CALCULATIONS --
LB=0.70485; %dist. from pivot to bar CG
THETA=acosd(1-PE/(G*(MBAR*LB+MASS*L)));

VEL=L*sqrt((G*(1-
cosd(THETA))*(MBAR*LB+MASS*L))/(((1/6)*MBAR*LB^2)+(0.5*MASS*L^2)));
KE=(1/6)*MBAR*LB^2*(VEL/L)^2+0.5*MASS*VEL^2;

HGT=STEP-(10*THETA);
LOW_H=ceil(HGT);%LOW ENERGY HEIGHT
LOW_T=(STEP-LOW_H)/10;
LOW_STEP=STEP-(10*LOW_T);
LOW_V=L*sqrt((G*(1-
cosd(LOW_T))*(MBAR*LB+MASS*L))/(((1/6)*MBAR*LB^2)+(0.5*MASS*L^2)));
LOW_E=(1/6)*MBAR*LB^2*(LOW_V/L)^2+0.5*MASS*LOW_V^2;

HI_H=floor(HGT);%HIGH ENERGY HEIGHT
HI_T=(STEP-HI_H)/10;
HI_STEP=STEP-(10*HI_T);
HI_V=L*sqrt((G*(1-
cosd(HI_T))*(MBAR*LB+MASS*L))/(((1/6)*MBAR*LB^2)+(0.5*MASS*L^2)));
HI_E=(1/6)*MBAR*LB^2*(HI_V/L)^2+0.5*MASS*HI_V^2;
HEIGHT=L*(1-cosd(THETA));
fprintf('\nENERGY= %4.4fJ  vel= %4.4fm/s\n',PE,VEL)
fprintf('STEP= %4.4g for high energy of %4.4fJ\n',HI_STEP,HI_E)
fprintf('STEP= %4.4g for low  energy of %4.4fJ\n',LOW_STEP,LOW_E)
fprintf('HEIGHT= %4.4f m\n\n',HEIGHT)
```

As an example, if we input 2600 as the initial step, 15 J as the potential energy, and 12.7 mm as the impact tip radius, the output of the function would read:

```
ENERGY= 15.0000J  vel= 2.6387m/s

STEP= 2202 for high energy of 15.0468J

STEP= 2203 for low  energy of 14.9743J

HEIGHT= 0.3286 m
```

Appendix III. Testing Checklist

Pre-test

-Tighten pendulum head and bolts on fixture

-Set voltage scale, time capture range, and trigger value on picoscope

-Test that force gauge and laser are capturing properly

-Make sure all cables are properly connected

-Make sure pendulum is secured at a low angle to the safety restraint before working in test area

Test Procedure

1. Insert specimen into test fixture, mark corners to specify impact zone, write test number on upper left corner
2. Record test specifications:
    - Date, target ID, target hit #, tip radius, pendulum height, potential energy
3. Turn on airflow for pneumatic release mechanism
4. Attach pendulum to release mechanism
5. Set up contact sheet and mark pendulum tip with dry erase
6. Set desired pendulum angle with crank based on target potential energy level
7. Set capture mode on picoscope and confirm "capturing" status in lower right corner
8. Clear any obstructions in path of pendulum
9. Impact panel by pressing "open" button, **make sure to catch the pendulum carefully after impact to prevent multiple strikes.**
10. Save test data
11. Secure pendulum with safety restraint before entering impact area
12. Measure indentation depth
13. A-scan impacted area to detect damage
14. If there is no damage and the panel has been hit less than three times on this impact zone then return to step 2.
15. If there is damage or the specimen has been impacted three times, move on to the next impact zone of the specimen. If this was the last impact zone then remove the specimen for C-scanning.

Appendix IV. Data Summary Table

IVa. Data Organized by Test Number

Test No. (LV-XXX)	Date	Target ID	Plies	Target Hit # (1, 2, 3)	Tip Radius (mm)	Pend. Height(m)	Potential Energy, mgh (J)	Pendulum Head Veloc. In(m/s)	System total mass (kg)	Actual KE, (J)	Peak Force (kN)	Dent Depth (δ1,mm)	Dent Depth (δ2,mm)	Vis-ible Dmg. (Y/N)	A-Scan Damage (Y/N)	Fiber Break	Contact Area (mm^2)	Average Contact Pressure (N/mm^2)	Delami nation Area (mm^2)	Dent Length (mm)
LV-001	5/9/2011	TC-8-21A		1	25.4		3.50		5.851					N		N				
LV-002	5/9/2011	TC-8-21A	8	2	25.4		9.50		5.851					Y		N				
LV-003	5/9/2011	TC-8-21A	8	3	25.4		16.00		5.851		7.576			Y	Y	N				
LV-004	5/9/2011	TC-8-21B	8	1	25.4		20.00		5.851		9.104			Y	Y	N				
LV-005	5/9/2011	TC-8-21C	8	1	25.4		18.00		5.851		8.080			Y	Y	N				
LV-006	5/27/2011	TC-8-21D	8	1	12.7		4.00		5.078					Y	N	N			0	
LV-007	5/27/2011	TC-8-21E	8	1	12.7		1.50		5.078					N	N	N			0	
LV-008	6/20/2011	TC-8-21E	8	2	12.7		2.75		5.078					N	N	N			0	
LV-009	6/23/2011	TC-8-21E	8	3	12.7	0.0725	3.50	1.325	5.078	4.171	2.312	0.03	0.00	Y	N	N			0	
LV-010	6/23/2011	TC-8-21F	8	1	12.7	0.062	3.00	1.227	5.078	3.210	2.081	0.02	0.00	Y	N	N			0	
LV-011	6/27/2011	TC-8-22A	8	1	50.8	0.074	4.00	1.332	5.651	4.333	2.554	0.01	0.00	N	N	N			0	
LV-012	6/27/2011	TC-8-22A	8	2	50.8	0.1202	6.50	1.681	5.651	6.896	3.632	0.03	0.00	N	N	N			0	
LV-013	6/27/2011	TC-8-22A	8	3	50.8	0.1664	9.00	1.975	5.651	9.521	4.631	0.03	0.00	N	N	N			0	
LV-014	6/29/2011	TC-8-22B	8	1	50.8	0.2524	15.00	2.378	5.651	13.802	5.820	0.05	0.00	N	N	N			0	
LV-015	6/29/2011	TC-8-22B	8	2	50.8	0.5069	30.00	3.304	5.651	26.856	9.499	0.07	0.00	N	N	N			0	29.21
LV-016	7/20/2011	TC-8-22C	8	1	12.7	0.2019	10.00	2.182	5.078	10.259	4.627	0.10	0.04	Y	Y	N	24.947	185.4878	0.2967	7.9772
LV-017	7/20/2011	TC-8-22D	8	1	12.7	0.121	6.00	1.639	5.078	5.789	3.399		0.03	Y	N	N	19.845	171.2673	0	0
LV-018	7/27/2011	TC-8-22E	8	1	12.7	0.1619	9.00	1.982	5.078	8.459	4.101	0.07	0.04	Y	N	N	24.449	167.7526	0	0
LV-019	7/27/2011	TC-8-22F	8	1	12.7	0.3031	15.00	2.651	5.078	15.143	6.121	0.13	0.04	Y	Y	N	33.023	185.3551	31.302	0
LV-020	9/15/2011	TC-16-42A	16	1	12.7	0.3286	15.00	2.732	5.078	16.084	7.848	0.14	0.06	Y	Y	N			9.0336	0
LV-021	9/15/2011	TC-16-42B	16	1	12.7	0.6571	30.00	3.798	5.078	31.076	11.484	0.14	0.11	Y	Y	Y			225.42	0
LV-022	9/15/2011	TC-16-42C	16	1	12.7	0.4381	20.00	3.131	5.078	21.116	9.122	0.14	0.08	Y	Y	Y			86.835	0
LV-023	10/21/2011	TC-16-42D	16	1	50.8	0.9752	50.00	4.476	5.651	48.897	17.089	0.05	0.02	Y	Y	Y	200.55	85.2091	442.17	23.758
LV-024	10/21/2011	TC-16-42E	16	1	50.8	0.5851	30.00	3.495	5.651	29.817	11.624	0.01	0.00	N	N	N	126.39	91.9761	0	47.72
LV-025	5/9/2011	TC-8-21A		1.004	30.05		25.39		5.160					N		N				

Notes:

Test No. (LV-XXX)	Date	Target ID	Plies	Target Hit # (1, 2, 3)	Tip Radius (mm)	Pend. Height(m)	Potential Energy, mgh (J)	Pendulum Head Veloc. In(m/s)	System total mass (kg)	Actual KE, (J)	Peak Force (kN)	Dent Depth (δ1,mm)	Dent Depth (δ2,mm)	Vis-ible Dmg. (Y/N)	A-Scan Damage (Y/N)	Fiber Break	Contact Area (mm^2)	Average Contact Pressure (N/mm^2)	Delami nation Area (mm^2)	Dent Length (mm)
LV-026	10/25/2011	TC-8-44A	8	1	50.8	0.8777	45.00	4.260	5.651	44.288	13.386	0.09	0.02	Y	Y	Y	373.74	35.81547	635.93	40.451
LV-027	10/28/2011	TC-8-44B	8	1	50.8	0.5851	30.00	3.491	5.651	29.739	10.278	0.03	0.00	Y	Y	Y	234.58	43.8149	348.9	35.656
LV-028	10/28/2011	TC-8-44C	8	1	50.8	0.3901	20.00	2.864	5.651	20.018	7.731	0.04	0.00	N	Y	N	139.97	55.2299	0	42.457
LV-029	10/28/2011	TC-16-43A	16	1	152.4	1.3075	67.50	5.181	5.687	65.529	23.118	0.01	0.00	N	N	N	750.27	30.81286	0	0
LV-030	10/28/2011	TC-16-43B	16	1	152.4	1.7434	90.00	5.667	5.687	78.384	27.350	0.01	0.00	N	Y	N	949.01	28.81941	635.22	0
LV-031	11/10/2011	TC-8-44D	8	1	101.6	0.776	40.00	4.020	5.679	39.677	14.312	0.05	0.00	N	N	N	814.21	17.5775	0	0
LV-032	11/10/2011	TC-8-44E	8	1	101.6	1.164	60.00	4.948	5.679	60.096	19.896	0.04	0.01	N	N	N	1038	19.16828	0	0
LV-033	11/16/2011	TC-16-43D	16	1	12.7	0.219	10.00	2.223	5.078	10.645	5.900	0.02	0.00	Y	N	N	21.47	274.7889	0.0877	6.3659
LV-034	11/22/2011	TC-16-43E	16	1	101.6	1.537	78.00	5.664	5.679			0.02	0.00	N	N	N	547.58		0	0
LV-035	11/28/2011	TC-16-44F	16	1	101.6	1.843	95.00	6.148	5.679	92.800	27.072	0.00	0.00	N	N	N	565.03	47.91303	0	0
LV-036	1/26/2012	TC-24-36A	24	1	12.7	0.5257	24.00	3.421	5.078	25.214	11.167	0.13	0.06	Y	Y	N	40.049	278.8302	101.57	7.2422
LV-037	1/30/2012	TC-24-36B	24	1	12.7	0.3607	14.00	2.656	5.078	15.201	8.499	0.01	0.00	Y	N	N	23.748	357.8599	0	10.78
LV-038	1/31/2012	TC-24-36C	24	1	12.7	0.4162	19.00	3.060	5.078	20.170	9.611	0.04	0.00	Y	Y	N			10.191	5.5721
LV-039	2/8/2012	TC-8-43A	8	1	152.4	0.3874	30.00		5.687			0.00	NA	N	N	N			0	0
LV-040	2/9/2012	TC-8-43A	8	2	101.6	0.485	25.00	3.221	5.679	25.469	10.189	0.02	NA	N	N	N	498.59	20.43453	0	0
LV-041	2/9/2012	TC-8-43A	8	3	101.6	0.679	35.00	3.805	5.679	35.536	13.364	0.04	0.00	N	N	N	660.19	20.24248	0	0
LV-042	2/9/2012	TC-8-43B	8	1	101.6	0.873	45.00	4.300	5.679	45.393	15.844	0.05	NA	N	N	N	805.47	19.67027	0	0
LV-043	2/15/2012	TC-24-36D	24	1	50.8	1.1702	60.00	4.812	5.651	56.835	18.834	0.07	0.03	N	Y	N	167.31	112.5709	2582.5	22.796
LV-044	2/15/2012	TC-24-36E	24	1	50.8	0.878	45.00	4.179	5.651	42.870	16.612	0.01	0.00	N	Y	N	123.39	134.6293	8.4488	8.87
LV-045	2/15/2012	TC-24-36F	24	1	50.8	0.683	35.00	3.701	5.651	33.625	13.999	0.00	0.00	N	N	N	100.19	139.7334	0	8.4773
LV-046	2/16/2012	TC-8-43B	8	2	101.6	1.164	60	4.966	5.679	60.528	19.217	0.03	0.00	N	N	N			0	0
LV-047	4/2/2012	TC-8-43D	8	1	25.4	0.319	17	2.603	5.851	17.213	7.993	0.03	0.00	Y	Y	Y	75.07	106.4713	68.838	23.88
LV-048	4/4/2012	TC-8-43E	8	1	25.4	0.225	12	2.196	5.851	12.251	6.562	0.03	0.01	Y	Y	N	60.483	108.4878	0.6303	0
LV-049	4/4/2012	TC-8-43F	8	1	25.4	0.169	9	1.918	5.851	9.342	4.788	0.02	0.00	Y	N	N	46.19	103.6556	0	25.313
LV-050	4/4/2012	TC-8-44F	8	1	25.4	0.113	6	1.537	5.851	6.281	3.520	0.01	0.00	N	N	N	39.619	88.85496	0	40.374

Notes:

LV-030 had to be hand released, contact with the arm of the person releasing it caused energy to only reach 79J instead of 90J

LV-039 violated test conditions, contact area reached the boundary of the impact tip, indicating that the 152.8 mm tip cannot be used for the 8 ply panels

Test No. (LV-XXX)	Date	Target ID	Plies	Target Hit # (1, 2, 3)	Tip Radius (mm)	Pend. Height(m)	Potential Energy, mgh (J)	Pendulum Head Veloc. In(m/s)	System total mass (kg)	Actual KE, (J)	Peak Force (kN)	Dent Depth (δ1,mm)	Dent Depth (δ2,mm)	Vis-ible Dmg. (Y/N)	A-Scan Damage (Y/N)	Fiber Break	Contact Area (mm^2)	Average Contact Pressure (N/mm^2)	Delami nation Area (mm^2)	Dent Length (mm)
LV-051	4/6/2012	TC-16-44A	16	1	25.4	0.301	16	2.526	5.851	16.214	8.470	0.03	0.03	Y	N	N	50.439	167.9174	0	10.511
LV-052	4/6/2012	TC-16-44B	16	1	25.4	0.47	25	3.147	5.851	25.161	10.234	0.08	0.07	Y	Y	N			39.006	9.882
LV-053	4/6/2012	TC-16-44C	16	1	25.4	0.376	20	2.812	5.851	20.092	8.780	0.06	0.05	Y	Y	N	59.547	147.4492	1.8908	9.5509
LV-054	4/6/2012	TC-24-37A	24	1	25.4	0.545	29	3.355	5.851	28.599	12.716	0.05	0.04	Y	Y	N	63.362	200.6824	25.21	11.651
LV-055	4/6/2012	TC-24-37B	24	1	25.4	0.657	35	3.673	5.851	34.270	14.466	0.07	0.05	Y	Y	N	72.301	200.0741	64.356	10.366
LV-056	4/18/2012	TC-24-37D	24	1	12.7	0.219	10	2.227	5.078	10.685	7.358	0.01	0.00	N	N	N	20.719	355.1102	0	0
LV-057	4/18/2012	TC-24-37D	24	2	12.7	0.394	18	2.924	5.078	18.424	9.829	0.06	0.04	Y	Y	N	29.529	332.8615	12.325	5.4415
LV-058	4/18/2012	TC-24-37E	24	1	12.7	0.657	30	3.729	5.078	29.962	12.526	0.17	0.14	Y	Y	N	46.539	269.1575	196.36	8.4375
LV-059	4/18/2012	TC-24-37F	24	1	12.7	0.876	40	4.295	5.078	39.737	14.953	0.18	0.16	Y	Y	N	53.193	281.1092	354.97	8.6588
LV-060	4/19/2012	TC-16-44D	16	1	12.7	0.175	8	1.990	5.078	8.530	5.191	0.00	0.00	N	N	N	19.634	264.4141	0	9.5726
LV-061	4/19/2012	TC-16-44E	16	1	12.7	0.285	13	2.501	5.078	13.477	6.558	0.05	0.04	Y	N	N	26.656	246.0384	0	7.2602
LV-062	4/19/2012	TC-16-44F	16	1	12.7	0.263	12	2.409	5.078	12.502	6.514	0.06	0.04	Y	N	N	25.202	258.4843	0	12.817
LV-063	4/19/2012	TC-24-37C	24	1	50.8	0.741	38	3.884	5.651	36.823	14.850	0.04	0.02	Y	Y	N	108.9	136.3676	10.504	31.218
LV-064	4/19/2012	TC-16-43C	16	1	50.8	0.663	34	3.680	5.651	33.051	12.459	0.03	0.02	N	Y	N	139.67	89.20292	20.658	29.322
LV-065	4/25/2012	TC-24-38A	24	1	25.4	0.3757	20	2.836	5.851	20.442	10.307	0.02	0.01	Y	N	N	46.499	221.6585	0	23.336
LV-066	4/25/2012	TC-24-38B	24	1	25.4	0.582	31	3.517	5.851	31.425	13.295	0.07	0.05	Y	Y	N	66.229	200.7504	48.88	11.262
LV-067	4/25/2012	TC-24-38C	24	1	25.4	0.845	45	4.197	5.851	44.760	16.068	0.16	0.12	Y	Y	N	98.863	162.5226	328.5	11.144
LV-068	5/2/2012	TC-16-45A	16	1	25.4	0.207	11	2.141	5.851	11.643	6.147	0.00	0.00	N	N	N	35.953	170.9769	0	0
LV-069	5/2/2012	TC-16-45A	16	2	25.4	0.338	18	2.705	5.851	18.594	8.336	0.04	0.03	Y	N	N	50.826	164.0063	0	8.509
LV-070	5/2/2012	TC-16-45B	16	1	25.4	0.319	17	2.636	5.851	17.661	7.826	0.02	0.00	Y	N	N	49.692	157.4794	0	12.321
LV-071	5/2/2012	TC-16-45C	16	1	25.4	0.657	35	3.736	5.851	35.471	12.637	0.14	0.11	Y	Y	Y	88.246	143.2049	256.41	11.848
LV-072	5/4/2012	TC-8-48A	8	1	76.2	0.357	18	2.732	5.557	17.872	7.016	0.00	0.00	N	N	N	289.34	24.24651	0	0
LV-073	5/4/2012	TC-8-48A	8	2	76.2	0.596	30	3.521	5.557	29.670	9.626	NA	NA	Y	Y	N	202.02	47.64839		0
LV-074	5/4/2012	TC-16-45D	16	1	76.2	0.596	30	3.532	5.557	29.861	11.626	0.01	0.00	N	N	N	NA		0	0
LV-075	5/4/2012	TC-16-45D	16	2	76.2	0.894	45	4.294	5.557	44.139	15.551	0.01	0.00	N	N	N	256.75	60.56853	0	0

Notes:

LV-073 Panel broke so that fiber failure was visible on front and back faces, tip boundary condition was also violated so test was invalid

Test No. (LV-XXX)	Date	Target ID	Plies	Target Hit # (1, 2, 3)	Tip Radius (mm)	Pend. Height(m)	Potential Energy, mgh (J)	Pendulum Head Veloc. In(m/s)	System total mass (kg)	Actual KE, (J)	Peak Force (kN)	Dent Depth (δ1,mm)	Dent Depth (δ2,mm)	Vis-ible Dmg. (Y/N)	A-Scan Damage (Y/N)	Fiber Break	Contact Area (mm^2)	Average Contact Pressure (N/mm^2)	Delami nation Area (mm^2)	Dent Length (mm)
LV-076	5/16/2012	TC-8-48B	8	1	76.2	0.497	25	3.235	5.557	25.046	9.602	0.00	0.00	N	N	N	377.3	25.44836	0	0
LV-077	5/16/2012	TC-16-45E	16	1	76.2	0.993	50	4.535	5.557	49.226	16.803	0.00	0.00	N	N	N	267.98	62.69971	0	36.068
LV-078	5/16/2012	TC-16-45F	16	1	76.2	1.231	62	5.055	5.557	61.163	19.840	0.00	0.00	N	Y	Y	337.66	58.7558	117.01	33.836
LV-079	5/16/2012	TC-24-38D	24	1	76.2	1.39	70	5.349	5.557	68.494	21.699	0.00	0.00	N	Y	N	244.4	88.78663	64.068	30.547
LV-080	5/16/2012	TC-24-38E	24	1	76.2	1.192	60	4.984	5.557	59.458	19.702	0.00	0.00	N	N	N	219.39	89.80317	0	48.768
LV-081	5/16/2012	TC-24-38F	24	1	76.2	1.291	65	5.161	5.557	63.770	21.161	0.00	0.00	N	N	N	239.7	88.2824	0	0
LV-082	5/23/2012	TC-24-39A	24	1	25.4	0.2979	15	2.487	5.851	15.718	8.840	0.01	0.00	N	N	N	35.908	246.1937	0	0
LV-083	5/23/2012	TC-24-39A	24	2	25.4	0.4767	24	3.151	5.851	25.225	11.737	0.05	0.03	Y	N	N	50.728	231.3682	0	22.304
LV-084	5/23/2012	TC-24-39B	24	1	25.4	0.7944	40	4.042	5.851	41.509	15.905	0.09	0.08	Y	Y	N	80.044	198.701	161.74	10.408
LV-085	5/23/2012	TC-24-39C	24	1	25.4	0.4369	22	3.018	5.851	23.136	11.013	0.04	0.03	Y	N	N	49.233	223.686	0	16.731
LV-086	5/23/2012	TC-24-39D	24	1	50.8	0.4876	25	3.167	5.651	24.479	11.455	0.00	0.00	N	N	N	76.22	150.2881	0	0
LV-087	5/23/2012	TC-24-39D	24	2	50.8	0.6826	35	3.746	5.651	34.256	14.057	0.00	0.00	N	N	N	101.32	138.7405	0	16.415
LV-088	5/23/2012	TC-24-39E	24	1	50.8	0.9361	48	4.378	5.651	46.793	17.074	0.02	0.01	N	Y	N	130.53	130.8049	18.841	31.877
LV-089	6/20/2012	TC-8-48D	8	1	12.7	0.0438	2	1.025	5.078	2.263	1.831	0.00	0.00	N	N	N	12.41	147.5378	0	0
LV-090	6/20/2012	TC-8-48D	8	2	12.7	0.0657	3	1.252	5.078	3.376	2.315	0.01	0.00	N	N	N	16.251	142.4633	0	0
LV-091	6/20/2012	TC-8-48D	8	3	12.7	0.438	20	3.103	5.078	20.745	8.397	0.86	NA	Y	Y	Y	179.5	46.78258	282.14	9.3792
LV-092	6/20/2012	TC-8-48B	8	2	76.2	0.695	35	3.796	5.557	36.620	12.986	0.00	0.00	N	N	N	437.18	29.70405	0	0
LV-093	6/20/2012	TC-8-48B	8	3	76.2	0.993	50	4.548	5.557	52.558	16.849	0.00	0.00	N	N	N	585.11	28.79602	0	0
LV-094	6/20/2012	TC-8-48E	8	1	76.2	1.192	60	4.992	5.557	63.310	19.476	0.00	0.00	N	Y	N	NA	NA	NA	0
LV-095	6/20/2012	TC-8-48C	8	1	25.4	0.0397	2	0.947	5.851	2.277	1.897	0.00	0.00	N	N	N	18.953	100.1045	0	0
LV-096	6/20/2012	TC-8-48C	8	2	25.4	0.437	22	3.065	5.851	23.864	8.099	0.07	0.03	Y	Y	Y	95.196	85.07491	221.33	21.202
LV-097	6/21/2012	TC-8-48F	8	1	25.4	0.079	4	1.331	5.851	4.321	2.610	0.01	0.00	N	N	N	26.804	97.36871	0	0
LV-098	6/21/2012	TC-8-48F	8	2	25.4	0.576	29	3.504	5.851	29.962	8.582	0.09	0.08	Y	Y	Y	117.83	72.8347	361.02	33.06
LV-099	6/21/2012	TC-8-43B	8	3	76.2	1.291	65	5.188	5.557	65.686	19.959	0.02	0.01	N	Y	Y	661.15	30.18863	10.509	36.915
LV-100	6/21/2012	TC-8-43C	8	1	50.8	0.039	2	0.908	5.655	2.012	1.774	0.00	0.00	N	N	N	28.162	63.00644	0	0

Notes:

LV-091 Punch through failure

LV-094 Exceeded tip boundary condition, invalid test

Test No. (LV-XXX)	Date	Target ID	Plies	Target Hit # (1, 2, 3)	Tip Radius (mm)	Pend. Height(m)	Potential Energy, mgh (J)	Pendulum Head Veloc. In(m/s)	System total mass (kg)	Actual KE, (J)	Peak Force (kN)	Dent Depth (δ1,mm)	Dent Depth (δ2,mm)	Vis-ible Dmg. (Y/N)	A-Scan Damage (Y/N)	Fiber Break	Contact Area (mm^2)	Average Contact Pressure (N/mm^2)	Delami nation Area (mm^2)	Dent Length (mm)
LV-101	6/21/2012	TC-8-43C	8	2	50.8	0.546	28	3.384	5.651	27.953	9.275	0.03	0.00	N	Y	Y	205.92	45.04082	17.052	30.827
LV-102	6/28/2012	TC-24-39F	24	1	50.8	0.975	50	4.406	5.651	46.478	17.345	0.04	0.02	N	Y	N	129.08	134.3717	69.179	23.47
LV-103	6/28/2012	TC-24-40A	24	1	50.8	1.053	54	4.587	5.651	50.374	18.242	0.04	0.03	Y	Y	N	145.59	125.3008	31.455	14.859
LV-104	6/28/2012	TC-24-40B	24	1	50.8	1.151	59	4.796	5.651	55.054	19.553	0.06	0.03	Y	Y	N	158.54	123.3308	114.65	14.419
LV-105	6/28/2012	TC-24-40C	24	1	50.8	0.78	40	3.951	5.651	37.373	15.055	0.03	0.01	N	N	N	109.9	136.988	1.6901	8.1219
LV-106	6/28/2012	TC-16-46A	16	1	50.8	0.488	25	3.129	5.651	23.432	9.874	0.02	0.01	N	N	N	110.36	89.46969	0	29.131
LV-107	6/28/2012	TC-16-46B	16	1	50.8	0.741	38	3.856	5.651	35.601	12.993	0.03	0.02	N	N	Y	157.47	82.50784	0	11.648
LV-108	6/28/2012	TC-16-46C	16	1	50.8	0.819	42	4.047	5.651	39.213	14.228	0.04	0.02	N	N	Y	172.63	82.41558	0	25.124
LV-109	6/28/2012	TC-24-40D	24	1	76.2	1.092	55	4.687	5.557	52.586	19.272	0.02	0.01	N	N	N	212.46	90.71017	0	22.781
LV-110	6/28/2012	TC-24-40E	24	1	76.2	1.311	66	5.114	5.557	62.607	21.697	0.03	0.01	N	N	N	254.92	85.11137	0	0
LV-111	6/28/2012	TC-24-40F	24	1	76.2	1.489	75	5.471	5.557	71.647	21.842	0.05	0.02	N	N	N	325.21	67.16196	3556.1	31.868
LV-112	6/28/2012	TC-16-46D	16	1	76.2	1.092	55	4.687	5.557	52.586	18.234	0.03	0.00	Y	N	Y	330.1	55.23617	0	0
LV-113	6/28/2012	TC-16-46E	16	1	76.2	1.152	58	4.773	5.557	54.525	18.375	0.02	0.00	Y	N	Y	333.52	55.09503	247.63	42.418
LV-114	6/29/2012	TC-8-45A	8	1	76.2	1.197	60		5.557			NA	NA	Y	Y	Y	NA	#VALUE!	NA	0
LV-115	6/29/2012	TC-8-45D	8	1	50.8	0.5656	29		5.651			NA	NA	Y	Y	Y	NA	#VALUE!	NA	0
LV-116	6/29/2012	TC-16-46F	16	1	25.4	0.536	27	3.323	5.851	28.063	10.874	0.09	0.06	Y	Y	N	75.108	144.7763	16.457	10.096
LV-117	7/2/2012	TC-16-47A	16	1	25.4	0.556	28	3.374	5.851	28.929	10.891	0.14	0.08	Y		Y	73.353	148.4731	182.04	11.978
LV-118	7/2/2012	TC-16-47B	16	1	25.4	0.377	19	2.789	5.851	19.760	8.326	0.08	0.05	Y		N	54.313	153.3012	0.4892	22.458
LV-119	7/2/2012	TC-8-46A	8	1	25.4	0.209	10.5	2.079	5.851	10.978	5.043	0.10	0.05	Y	N	N	54.754	92.10502	0	38.301
LV-120	7/2/2012	TC-8-46B	8	1	25.4	0.2284	11.5	2.180	5.851	12.074	5.471	0.14	0.07	Y	Y	Y	67.641	80.88497	94.911	23.416
LV-121	7/3/2012	TC-24-41A	24	1	25.4	0.735	37	3.907	5.851	38.791	14.810	0.11	0.09	Y	Y	N	78.7	188.1795	205.16	11.694
LV-122	7/3/2012	TC-24-41B	24	1	12.7	0.81	37	4.140	5.078	36.928	13.896	0.17	0.15	Y	Y	N	51.775	268.3868	314.67	8.9633
LV-123	7/6/2012	TC-8-46C	8	1	12.7	0.372	17	2.842	5.078	17.403	7.086	0.22	0.11	Y	Y	Y	53.511	132.4128	152.94	30.208
LV-124	7/6/2012	TC-8-46D	8	1	12.7	0.394	18	2.918	5.078	18.340	8.154	0.71	0.25	Y	Y	Y	160	50.95966	221.28	0
LV-125	7/6/2012	TC-16-47C	16	1	12.7	0.504	23	3.292	5.078	23.344	9.855	0.12	0.11	Y	Y	Y	39.215	251.2935	171.91	9.2832

LV-114 Tip boundary condition violated, invalid test

LV-115 Tip boundary condition violated, invalid test

LV-124 Crack on front face visible

Test No. (LV-XXX)	Date	Target ID	Plies	Target Hit # (1, 2, 3)	Tip Radius (mm)	Pend. Height(m)	Potential Energy, mgh (J)	Pendulum Head Veloc. In(m/s)	System total mass (kg)	Actual KE, (J)	Peak Force (kN)	Dent Depth (δ1,mm)	Dent Depth (δ2,mm)	Vis-ible Dmg. (Y/N)	A-Scan Damage (Y/N)	Fiber Break	Contact Area (mm^2)	Average Contact Pressure (N/mm^2)	Delami nation Area (mm^2)	Dent Length (mm)
LV-126	7/6/2012	TC-16-47D	16	1	12.7	0.591	27	3.560	5.078	27.298	10.497	0.21	0.13	Y	Y	Y	45.306	231.6874	257.44	10.398
LV-127	7/6/2012	TC-8-46E	8	1	50.8	0.536	27.5	3.325	5.651	26.982	10.259	0.12	0.05	Y	N	Y	224.97	45.60279	241.11	37.083
LV-128	7/6/2012	TC-8-46F	8	1	50.8	0.556	28.5	NA	5.651	NA	NA	NA	NA	NA	NA	NA	NA	NA	NA	0
LV-129	7/6/2012	TC-16-47E	16	1	50.8	0.839	43	4.139	5.651	41.815	13.556	0.08	0.05	Y	Y	Y			489.16	29.686
LV-130	7/6/2012	TC-16-47F	16	1	50.8	0.897	46	4.282	5.651	44.755	15.095	0.07	0.05	Y	Y	Y	186.68	80.86231	481.76	29.702
LV-131	7/10/2012	TC-24-41C	24	1	50.8	0.7216	37	3.848	5.651	36.143	14.489	0.03	0.03	N	Y	N	111.93	129.4389	52.941	30.632
LV-132	7/17/2012	TC-24-41D	24	1	25.4	0.914	46	4.347	5.851	48.009	15.817	0.18	0.15	Y	Y	N	103.7	152.5284	1301.1	9.8273
LV-133	7/17/2012	TC-24-41E	24	1	12.7	0.526	24	3.351	5.078	24.197	11.255	0.05	0.05	Y	Y	N	32.816	342.9791	34.104	5.8115
LV-134	7/17/2012	TC-24-41F	24	1	12.7	0.5914	27	3.565	5.078	27.385	11.579	0.13	0.12	Y	Y	N	45.3	255.6026	214.54	7.9666
LV-135	7/17/2012	TC-16-48A	16	1	25.4	0.6355	32	3.641	5.851	33.678	12.380	0.16	0.12	Y	Y	Y	99.328	124.632	401.26	13.002
LV-136	7/17/2012	TC-16-48B	16	1	25.4	0.794	40	4.057	5.851	41.826	12.908	0.21	0.16	Y	Y	Y	110.85	116.4418	607.6	17.328
LV-137	7/17/2012	TC-16-48C	16	1	76.2	1.132	57	4.794	5.557	55.024	17.486	0.05	0.03	N	Y	Y	358.92	48.71736	758.96	37.504
LV-138	7/17/2012	TC-8-47A	8	1	76.2	1.1519	58	4.834	5.557	55.942	16.864	0.05	0.05	N	N	N	682.08	24.72513	0	45.529
LV-139	7/17/2012	TC-8-47B	8	1	76.2	1.212	61	4.960	5.557	58.880	17.557	0.10	0.07	N	N	N	693.84	25.30355	0	0
LV-140	7/17/2012	TC-8-47D	8	1	76.2	1.251	63	5.040	5.557	60.807	18.035	0.10	0.07	N	N	N	714.45	25.24378	0	0
LV-141	7/17/2012	TC-8-47E	8	1	76.2	1.3704	69	5.278	5.557	66.680	19.149	0.11	0.09	N	N	N	730.29	26.22178	0	37.866
LV-142	7/23/2012	TC-16-48D	16	1	50.8	0.722	37	3.853	5.651	36.231	13.222	0.08	0.06	Y	Y	Y	157.92	83.72821	648.99	36.195
LV-143	7/23/2012	TC-16-48E	16	1	50.8	0.673	34.5	3.775	5.651	34.781	12.240	0.07	0.05	Y	Y	Y	142.36	85.98093	927.81	37.706
LV-144	7/23/2012	TC-16-48F	16	1	76.2	0.993	50	4.557	5.557	49.713	16.457	0.07	0.05	N	Y	N	300.2	54.81977	10.342	0
LV-145	7/27/2012	TC-24-42A	24	1	76.2	1.2115	61	5.023	5.557	60.384	19.650	0.02	0.02	N	Y	N	232.64	84.46392	60.098	0
LV-146	7/27/2012	TC-24-42B	24	1	76.2	1.291	65	5.183	5.557	64.296	20.460	0.02	0.01	N	N	N	236.6	86.47597	25.018	0
LV-147	7/27/2012	TC-24-42C	24	1	76.2	1.331	67	5.261	5.557	66.255	20.937	0.04	0.04	N	N	N	247.54	84.58118	117.89	32.735
LV-148	7/27/2012	TC-8-49A	8	1	76.2	1.43	72	5.452	5.557	71.151	20.361	0.09	0.08	N	N	N	687.96	29.59571	0	0
LV-149	7/30/2012	TC-16-49A	16	1	76.2	1.053	53	4.678	5.557	52.373	17.407	0.02	0.02	N	N	N	302.8	57.48598	0	0
LV-150	7/30/2012	TC-16-49B	16	1	76.2	1.112	56	4.809	5.557	55.361	17.893	0.04	0.02	N	N	Y	311.33	57.4703	6.6612	0

Notes:

LV-128 Invalid test, failure at edge of panel

LV-132 Contact sheet fell as pendulum was released, mark left on panel was carefully measured by hand to determine contact area

Test No. (LV-XXX)	Date	Target ID	Plies	Target Hit # (1, 2, 3)	Tip Radius (mm)	Pend. Height(m)	Potential Energy, mgh (J)	Pendulum Head Veloc. In(m/s)	System total mass (kg)	Actual KE, (J)	Peak Force (kN)	Dent Depth (δ1,mm)	Dent Depth (δ2,mm)	Vis-ible Dmg. (Y/N)	A-Scan Damage (Y/N)	Fiber Break	Contact Area (mm^2)	Average Contact Pressure (N/mm^2)	Delamination Area (mm^2)	Dent Length (mm)
LV-151	7/30/2012	TC-16-49C	16	1	76.2	1.065	53.6	4.694	5.557	52.743	17.555	0.04	0.03	N	N	N	280.15	62.66436	0	0
LV-152	7/30/2012	TC-8-49A	8	1	50.8	0.468	24	3.138	5.651	24.026	8.930	0.09	0.08	N	N	N	200.13	44.62201	0	0
LV-153	7/30/2012	TC-8-49C	8	1	50.8	0.536	27.5	3.359	5.651	27.545	9.844	0.06	0.04	N	N	N	205.29	47.95217	0	0
LV-154	7/30/2012	TC-16-49D	16	1	12.7	0.241	11	2.331	5.078	11.705	6.099	0.03	0.03	N	Y	N	24.057	253.5115	1.3277	7.422
LV-155	7/30/2012	TC-16-49E	16	1	12.7	0.548	25	3.455	5.078	25.717	10.141	0.15	0.13	Y	Y	Y	41.54	244.1309	252.48	8.2211
LV-156	7/30/2012	TC-16-49F	16	1	12.7	0.767	35	4.066	5.078	35.622	12.868	0.18	0.16	Y	Y	Y	49.145	261.837	362.33	8.9059
LV-157	8/7/2012	TC-24-42D	24	1	12.7	0.3614	16.5	2.809	5.078	17.002	9.267	0.04	0.04	Y	Y	N	27.292	339.538	16.493	5.3023
LV-158	8/7/2012	TC-24-42E	24	1	12.7	0.416	19	3.007	5.078	19.479	9.924	0.05	0.05	Y	Y	N	27.72	357.9929	15.973	4.8292
LV-159	8/7/2012	TC-24-42F	24	1	50.8	0.78	40	3.999	5.651	39.028	14.972	0.03	0.02	N	Y	N	117.99	126.8942	82.541	13.779
LV-160	8/7/2012	TC-24-43A	24	1	50.8	1.086	55.7	4.684	5.651	53.561	18.540	0.05	0.05	Y	Y	N	157.63	117.6153	160.18	21.273
LV-161	8/7/2012	TC-24-43B	24	1	25.4	0.526	26.5	3.325	5.851	28.082	12.252	0.06	0.06	Y	Y	N	58.706	208.7017	55.275	10.636
LV-162	8/7/2012	TC-24-43C	24	1	25.4	0.914	46	4.387	5.851	48.889	16.183	0.18	0.16	Y	Y	N	115.16	140.5242	509.36	12.603
LV-163	8/9/2012	TC-8-49D	8	1	25.4	0.263	14	2.310	5.851	13.556	5.399	0.10	0.06	Y	Y	Y	60.006	89.97464	54.385	0
LV-164	8/9/2012	TC-8-49F	8	1	25.4	0.3757	20	2.810	5.851	20.056	7.226	0.12	0.08	Y	Y	Y	88.638	81.52156	208.13	0
LV-165	8/9/2012	TC-8-49E	8	1	76.2	1.509	76	5.565	5.557	74.120	21.069	NA	NA	Y	Y	Y	NA	NA	1	0
LV-166	8/9/2012	TC-24-43D	24	1	76.2	1.25	63	5.105	5.557	62.386	20.588	0.04	0.02	N	Y	N	231.12	89.07541	6.9837	0
LV-167	8/9/2012	TC-24-43E	24	1	76.2	1.33	67	5.236	5.557	65.615	20.927	0.03	0.02	N	Y	N	233.94	89.45765	60.178	0
LV-168	8/9/2012	TC-24-43F	24	1	76.2	1.37	69	5.344	5.557	68.368	21.621	0.03	0.02	N	Y	N	244.29	88.50445	2.3031	0

Notes:

LV-165 Invalid test, failure at edge of panel

IVb. Data Organized by Panel Thickness and Tip Radius

8 Ply

Test No. (LV-XXX)	Target ID	Target Hit # (1, 2, 3)	Tip Radius (mm)	Actual KE, (J)	Peak Force (kN)	Dent Depth (δ1,mm)	Dent Depth (δ2,mm)	Vis-ible Dmg. (Y/N)	A-Scan Damage (Y/N)	Fiber Break	Contact Area (mm^2)	Average Contact Pressure (N/mm^2)	Delamination Area (mm^2)	Dent Length (mm)
LV-089	TC-8-48D	1	12.7	2.2627	1.8309	0	0	N	N	0	12.4097	147.5378	0	0
LV-010	TC-8-21F	1	12.7	3.2099	2.081	0.02	0	Y	N	0	C	C	0	0
LV-009	TC-8-21E	3	12.7	4.1711	2.312	0.03	0	Y	N	0	C	C	0	0
LV-090	TC-8-48D	2	12.7	3.3762	2.3151	0.01	0	N	N	0	16.2505	142.4633	0	0
LV-018	TC-8-22E	1	12.7	8.4586	4.1013	0.07	0.04	Y	N	0	24.4485	167.7526	0	0
LV-016	TC-8-22C	1	12.7	10.2594	4.6274	0.1	0.04	Y	Y	0	24.9472	185.4878	0.2967	7.977187
LV-019	TC-8-22F	1	12.7	15.1425	6.121	0.13	0.04	Y	Y	0	33.0231	185.3551	31.3019	0
LV-123	TC-8-46C	1	12.7	17.4025	7.0855	0.22	0.11	Y	Y	1	53.5107	132.4128	152.9412	30.20786
LV-124	TC-8-46D	1	12.7	18.3402	8.1535	0.71	0.25	Y	Y	1	C	C	221.2822	0
LV-095	TC-8-48C	1	25.4	2.2765	1.8973	0	0	N	N	0	18.9532	100.1045	0	0
LV-097	TC-8-48F	1	25.4	4.3213	2.6099	0.01	0	N	N	0	26.8043	97.36871	0	0
LV-050	TC-8-44F	1	25.4	6.2814	3.5203	0.01	0	N	N	0	39.6185	88.85495	0	40.37409
LV-049	TC-8-43F	1	25.4	9.3424	4.7878	0.02	0	Y	N	0	46.1895	103.6556	0	25.31256
LV-119	TC-8-46A	1	25.4	10.9775	5.0431	0.1	0.05	Y	N	0	54.7538	92.10502	0	38.30122
LV-048	TC-8-43E	1	25.4	12.2509	6.5617	0.03	0.01	Y	Y	0	60.4833	108.4878	0.6303	0
LV-163	TC-8-49D	1	25.4	13.5556	5.399	0.1	0.06	Y	Y	1	60.0058	89.97464	54.3847	0
LV-047	TC-8-43D	1	25.4	17.2128	7.9928	0.03	0	Y	Y	1	75.07	106.4713	68.8375	23.87961
LV-120	TC-8-46B	1	25.4	12.0742	5.4711	0.14	0.07	Y	Y	1	67.6405	80.88497	94.9108	23.41562
LV-164	TC-8-49F	1	25.4	20.0561	7.2259	0.12	0.08	Y	Y	1	88.6379	81.52156	208.133	0
LV-096	TC-8-48C	2	25.4	23.8642	8.0988	0.07	0.03	Y	Y	1	95.1961	85.07491	221.3324	21.20181
LV-098	TC-8-48F	2	25.4	29.9624	8.5822	0.09	0.08	Y	Y	1	117.8312	72.8347	361.0206	33.05958
LV-100	TC-8-43C	1	50.8	2.0123	1.7744	0	0	N	N	0	28.1622	63.00644	0	0
LV-011	TC-8-22A	1	50.8	4.3334	2.5538	0.01	0	N	N	0	C	C	0	0
LV-012	TC-8-22A	2	50.8	6.896	3.6323	0.03	0	N	N	0	C	C	0	0
LV-013	TC-8-22A	3	50.8	9.5208	4.6312	0.03	0	N	N	0	C	C	0	0

Test No. (LV-XXX)	Target ID	Target Hit # (1, 2, 3)	Tip Radius (mm)	Actual KE, (J)	Peak Force (kN)	Dent Depth (δ1,mm)	Dent Depth (δ2,mm)	Vis-ible Dmg. (Y/N)	A-Scan Damage (Y/N)	Fiber Break	Contact Area (mm^2)	Average Contact Pressure (N/mm^2)	Delamination Area (mm^2)	Dent Length (mm)
LV-014	TC-8-22B	1	50.8	13.8016	5.82	0.05	0	N	N	0	C	C	0	0
LV-028	TC-8-44C	1	50.8	20.0181	7.7307	0.04	0	N	Y	0	139.9731	55.2299	0	42.45725
LV-152	TC-8-49A	1	50.8	24.0263	8.9304	0.085	0.08	N	N	0	200.1344	44.62201	0	0
LV-015	TC-8-22B	2	50.8	26.8556	9.4985	0.07	0	N	N	0	C	C	0	29.21
LV-153	TC-8-49C	1	50.8	27.5452	9.8441	0.06	0.04	N	N	0	205.29	47.95217	0	0
LV-101	TC-8-43C	2	50.8	27.9533	9.2749	0.03	0	N	Y	1	205.9221	45.04082	17.0522	30.82673
LV-127	TC-8-46E	1	50.8	26.9821	10.2591	0.12	0.05	Y	N	1	224.9665	45.60279	241.1104	37.08321
LV-027	TC-8-44B	1	50.8	29.7394	10.2783	0.03	0	Y	Y	1	234.5846	43.8149	348.9015	35.65595
LV-026	TC-8-44A	1	50.8	44.2884	13.3855	0.09	0.02	Y	Y	1	373.7352	35.81547	635.932	40.45121
LV-072	TC-8-48A	1	76.2	17.8721	7.0155	0	0	N	N	0	289.3406	24.24651	0	0
LV-076	TC-8-48B	1	76.2	25.0457	9.6017	0	0	N	N	0	377.3014	25.44836	0	0
LV-092	TC-8-48B	2	76.2	36.6195	12.9861	0	0	N	N	0	437.1828	29.70405	0	0
LV-093	TC-8-48B	3	76.2	52.5579	16.8487	0	0	N	N	0	585.1052	28.79602	0	0
LV-138	TC-8-47A	1	76.2	55.942	16.8644	0.05	0.05	N	N	0	682.0752	24.72513	0	45.52877
LV-139	TC-8-47B	1	76.2	58.8802	17.5566	0.1	0.07	N	N	0	693.8395	25.30355	0	0
LV-140	TC-8-47D	1	76.2	60.807	18.0353	0.1	0.07	N	N	0	714.4453	25.24378	0	0
LV-141	TC-8-47E	1	76.2	66.6796	19.1494	0.11	0.09	N	N	0	730.2861	26.22178	0	37.8658
LV-099	TC-8-43B	3	76.2	65.6861	19.9593	0.02	0.01	N	Y	1	661.1529	30.18863	10.5089	36.91482

16 ply

Test No. (LV-XXX)	Target ID	Target Hit # (1, 2, 3)	Tip Radius (mm)	Actual KE, (J)	Peak Force (kN)	Dent Depth (δ1,mm)	Dent Depth (δ2,mm)	Vis-ible Dmg. (Y/N)	A-Scan Damage (Y/N)	Fiber Break	Contact Area (mm^2)	Average Contact Pressure (N/mm^2)	Delamination Area (mm^2)	Dent Length (mm)
LV-060	TC-16-44D	1	12.7	8.5298	5.1914	0	0	N	N	0	19.6336	264.4141	0	9.572625
LV-062	TC-16-44F	1	12.7	12.5023	6.5144	0.06	0.04	Y	N	0	25.2023	258.4843	0	12.8166
LV-061	TC-16-44E	1	12.7	13.477	6.5583	0.05	0.04	Y	N	0	26.6556	246.0384	0	7.260167
LV-033	TC-16-43D	1	12.7	10.645	5.8998	0.02	0	Y	N	0	21.4703	274.7889	0.0877	6.365875
LV-154	TC-16-49D	1	12.7	11.7049	6.0987	0.03	0.03	N	Y	0	24.0569	253.5115	1.3277	7.421998
LV-020	TC-16-42A	1	12.7	16.084	7.8482	0.14	0.06	Y	Y	0	C	C	9.0336	0
LV-022	TC-16-42C	1	12.7	21.1161	9.1215	0.14	0.08	Y	Y	0	C	C	86.8347	0
LV-125	TC-16-47C	1	12.7	23.3441	9.8545	0.12	0.11	Y	Y	1	39.2151	251.2935	171.9078	9.283203
LV-021	TC-16-42B	1	12.7	31.0763	11.484	0.14	0.11	Y	Y	1	C	C	225.4202	0
LV-155	TC-16-49E	1	12.7	25.7169	10.1411	0.15	0.13	Y	Y	1	41.5396	244.1309	252.4808	8.221133
LV-126	TC-16-47D	1	12.7	27.2978	10.4969	0.21	0.13	Y	Y	1	45.3063	231.6874	257.4356	10.39812
LV-156	TC-16-49F	1	12.7	35.6218	12.8679	0.18	0.16	Y	Y	1	49.1447	261.837	362.334	8.905875
LV-068	TC-16-45A	1	25.4	11.6429	6.1471	0	0	N	N	0	35.9528	170.9769	0	0
LV-070	TC-16-45B	1	25.4	17.6613	7.8255	0.02	0	Y	N	0	49.6922	157.4794	0	12.32057
LV-069	TC-16-45A	2	25.4	18.5936	8.3358	0.04	0.03	Y	N	0	50.8261	164.0063	0	8.509
LV-051	TC-16-44A	1	25.4	16.2142	8.4695	0.03	0.03	Y	N	0	50.4385	167.9174	0	10.51119
LV-118	TC-16-47B	1	25.4	19.76	8.3262	0.08	0.05	Y	0	0	54.3127	153.3012	0.4892	22.45769
LV-053	TC-16-44C	1	25.4	20.0919	8.7801	0.06	0.05	Y	Y	0	59.5466	147.4492	1.8908	9.55089
LV-116	TC-16-46F	1	25.4	28.0633	10.8738	0.09	0.06	Y	Y	0	75.1076	144.7763	16.4569	10.0965
LV-052	TC-16-44B	1	25.4	25.161	10.2342	0.08	0.07	Y	Y	0	C	C	39.0056	9.881957
LV-117	TC-16-47A	1	25.4	28.9286	10.8909	0.14	0.08	Y	0	1	73.3527	148.4731	182.0405	11.97769
LV-071	TC-16-45C	1	25.4	35.4708	12.6372	0.14	0.11	Y	Y	1	88.2456	143.2049	256.4139	11.8476
LV-135	TC-16-48A	1	25.4	33.6777	12.3795	0.16	0.115	Y	Y	1	99.3284	124.632	401.2558	13.00237
LV-136	TC-16-48B	1	25.4	41.8258	12.9078	0.21	0.16	Y	Y	1	110.8519	116.4418	607.6008	17.3284
LV-106	TC-16-46A	1	50.8	23.4319	9.874	0.02	0.01	N	N	0	110.3614	89.46969	0	29.13063

Test No. (LV-XXX)	Target ID	Target Hit # (1, 2, 3)	Tip Radius (mm)	Actual KE, (J)	Peak Force (kN)	Dent Depth (δ1,mm)	Dent Depth (δ2,mm)	Vis-ible Dmg. (Y/N)	A-Scan Damage (Y/N)	Fiber Break	Contact Area (mm^2)	Average Contact Pressure (N/mm^2)	Delamination Area (mm^2)	Dent Length (mm)	Profile Depth (mm)
LV-024	TC-16-42E	1	50.8	29.8174	11.6244	0.01	0	N	N	0	126.385	91.9761	0	47.72025	0.04
LV-107	TC-16-46B	1	50.8	35.6008	12.9927	0.03	0.02	N	N	0	157.4723	82.50784	0	11.64801	0.025278
LV-108	TC-16-46C	1	50.8	39.2127	14.2276	0.04	0.02	N	N	1	172.6324	82.41558	0	25.12373	0.030556
LV-025	TC-16-42F	1	50.8	39.391	13.8122	0.05	0.01	N	Y	0	153.3526	90.06825	4.5358	28.63438	0.041111
LV-064	TC-16-43C	1	50.8	33.0505	12.4594	0.03	0.02	N	Y	0	139.6748	89.20292	20.6583	29.32152	0.035278
LV-023	TC-16-42D	1	50.8	48.8965	17.089	0.05	0.02	Y	Y	1	200.5537	85.2091	442.1687	23.75807	0.051111
LV-130	TC-16-47F	1	50.8	44.7552	15.0954	0.07	0.05	Y	Y	1	186.6803	80.86231	481.7581	29.70176	0.052222
LV-129	TC-16-47E	1	50.8	41.8145	13.5562	0.08	0.05	Y	Y	1	C	C	489.1606	29.68585	0.064722
LV-142	TC-16-48D	1	50.8	36.2311	13.2222	0.08	0.06	Y	Y	1	157.9181	83.72821	648.9867	36.195	0.05
LV-143	TC-16-48E	1	50.8	34.7805	12.2404	0.07	0.05	Y	Y	1	142.3618	85.98093	927.8127	37.70639	0.045833
LV-074	TC-16-45D	1	76.2	29.861	11.626	0.01	0	N	N	0	NA	NA	0	0	0
LV-075	TC-16-45D	2	76.2	44.1387	15.5508	0.01	0	N	N	0	256.7472	60.56853	0	0	0
LV-077	TC-16-45E	1	76.2	49.2257	16.8025	0	0	N	N	0	267.9837	62.69971	0	36.068	0.02
LV-149	TC-16-49A	1	76.2	52.3733	17.4068	0.02	0.02	N	N	0	302.8008	57.48598	0	0	0
LV-151	TC-16-49C	1	76.2	52.7432	17.5552	0.04	0.03	N	N	0	280.1465	62.66436	0	0	0
LV-112	TC-16-46D	1	76.2	52.5862	18.2335	0.03	0	Y	N	1	330.1007	55.23617	0	0	0
LV-150	TC-16-49B	1	76.2	55.3607	17.8925	0.035	0.02	N	N	1	311.3347	57.4703	6.6612	0	0
LV-144	TC-16-48F	1	76.2	49.7128	16.4569	0.07	0.05	N	Y	0	300.2001	54.81977	10.3424	0	0
LV-078	TC-16-45F	1	76.2	61.1626	19.8395	0	0	N	Y	1	337.6603	58.7558	117.0092	33.83628	0.016667
LV-113	TC-16-46E	1	76.2	54.5245	18.3752	0.02	0	Y	N	1	333.5183	55.09503	247.6283	42.418	0.02
LV-137	TC-16-48C	1	76.2	55.024	17.4856	0.05	0.03	N	Y	1	358.9193	48.71736	758.9557	37.50376	0.032778

24 ply

Test No. (LV-XXX)	Target ID	Target Hit # (1, 2, 3)	Tip Radius (mm)	Actual KE, (J)	Peak Force (kN)	Dent Depth (δ1,mm)	Dent Depth (δ2,mm)	Vis-ible Dmg. (Y/N)	A-Scan Damage (Y/N)	Fiber Break	Contact Area (mm^2)	Average Contact Pressure (N/mm^2)	Delamination Area (mm^2)	Dent Length (mm)
LV-056	TC-24-37D	1	12.7	10.6854	7.3576	0.01	0	N	N	N	20.7192	355.1102	0	0
LV-037	TC-24-36B	1	12.7	15.2007	8.4986	0.01	0	Y	N	N	23.7484	357.8599	0	10.77992
LV-038	TC-24-36C	1	12.7	20.1697	9.6113	0.04	0	Y	Y	N	C	C	10.1906	5.572125
LV-057	TC-24-37D	2	12.7	18.4239	9.8292	0.06	0.04	Y	Y	N	29.5294	332.8615	12.3249	5.441496
LV-158	TC-24-42E	1	12.7	19.4786	9.9236	0.05	0.045	Y	Y	N	27.7201	357.9929	15.9733	4.829231
LV-157	TC-24-42D	1	12.7	17.0024	9.2665	0.04	0.035	Y	Y	N	27.2915	339.538	16.4933	5.30225
LV-133	TC-24-41E	1	12.7	24.1968	11.2551	0.05	0.05	Y	Y	N	32.8157	342.9791	34.1044	5.811487
LV-036	TC-24-36A	1	12.7	25.2138	11.1669	0.13	0.06	Y	Y	N	40.0491	278.8302	101.5742	7.242175
LV-058	TC-24-37E	1	12.7	29.9618	12.5264	0.17	0.14	Y	Y	N	46.5393	269.1575	196.3585	8.437509
LV-134	TC-24-41F	1	12.7	27.385	11.5788	0.13	0.115	Y	Y	N	45.3	255.6026	214.5406	7.966604
LV-122	TC-24-41B	1	12.7	36.9284	13.8957	0.17	0.15	Y	Y	N	51.7749	268.3868	314.6728	8.963252
LV-059	TC-24-37F	1	12.7	39.7374	14.9529	0.18	0.16	Y	Y	N	53.1925	281.1092	354.972	8.658833
LV-082	TC-24-39A	1	25.4	15.7184	8.8402	0.01	0	N	N	N	35.9075	246.1937	0	0
LV-065	TC-24-38A	1	25.4	20.4424	10.3069	0.02	0.01	Y	N	N	46.499	221.6585	0	23.33625
LV-085	TC-24-39C	1	25.4	23.1357	11.0128	0.04	0.03	Y	N	N	49.2333	223.686	0	16.73066
LV-083	TC-24-39A	2	25.4	25.2251	11.7368	0.05	0.03	Y	N	N	50.7278	231.3682	0	22.30438
LV-054	TC-24-37A	1	25.4	28.5988	12.7157	0.05	0.04	Y	Y	N	63.3623	200.6824	25.2101	11.65066
LV-066	TC-24-38B	1	25.4	31.4249	13.2954	0.07	0.05	Y	Y	N	66.2285	200.7504	48.8796	11.26237
LV-161	TC-24-43B	1	25.4	28.0822	12.252	0.06	0.055	Y	Y	N	58.7058	208.7017	55.2749	10.63625
LV-055	TC-24-37B	1	25.4	34.2697	14.4655	0.07	0.05	Y	Y	N	72.3007	200.0741	64.3557	10.36637
LV-084	TC-24-39B	1	25.4	41.509	15.9048	0.09	0.08	Y	Y	N	80.0439	198.701	161.7357	10.40784
LV-121	TC-24-41A	1	25.4	38.7913	14.8098	0.11	0.09	Y	Y	N	78.7004	188.1795	205.1553	11.69419
LV-067	TC-24-38C	1	25.4	44.7604	16.0675	0.16	0.12	Y	Y	N	98.8632	162.5226	328.5014	11.14425
LV-162	TC-24-43C	1	25.4	48.8889	16.1833	0.18	0.155	Y	Y	N	115.1638	140.5242	509.3611	12.60304
LV-132	TC-24-41D	1	25.4	48.0091	15.8172	0.18	0.155	Y	Y	N	103.7	152.5284	1301.058	9.827309
LV-086	TC-24-39D	1	50.8	24.4789	11.4549	0	0	N	N	N	76.2196	150.2881	0	0

Test No. (LV-XXX)	Target ID	Target Hit # (1, 2, 3)	Tip Radius (mm)	Actual KE, (J)	Peak Force (kN)	Dent Depth (δ1,mm)	Dent Depth (δ2,mm)	Vis-ible Dmg. (Y/N)	A-Scan Damage (Y/N)	Fiber Break	Contact Area (mm^2)	Average Contact Pressure (N/mm^2)	Delamination Area (mm^2)	Dent Length (mm)
LV-045	TC-24-36F	1	50.8	33.6249	13.9993	0	0	N	N	N	100.1858	139.7334	0	8.47725
LV-087	TC-24-39D	2	50.8	34.2556	14.0568	0	0	N	N	N	101.3172	138.7405	0	16.41475
LV-105	TC-24-40C	1	50.8	37.3733	15.0553	0.03	0.01	N	N	N	109.9023	136.988	1.6901	8.12192
LV-044	TC-24-36E	1	50.8	42.8704	16.6122	0.01	0	N	Y	N	123.3922	134.6293	8.4488	8.869993
LV-063	TC-24-37C	1	50.8	36.8229	14.8502	0.04	0.02	Y	Y	N	108.8983	136.3676	10.5042	31.21819
LV-088	TC-24-39E	1	50.8	46.7927	17.0737	0.02	0.01	N	Y	N	130.528	130.8049	18.8406	31.877
LV-103	TC-24-40A	1	50.8	50.3736	18.2423	0.04	0.03	Y	Y	N	145.5881	125.3008	31.4554	14.859
LV-131	TC-24-41C	1	50.8	36.1426	14.4887	0.03	0.03	N	Y	N	111.9347	129.4389	52.9412	30.6324
LV-102	TC-24-39F	1	50.8	46.4775	17.3449	0.04	0.02	N	Y	N	129.0815	134.3717	69.1787	23.47047
LV-159	TC-24-42F	1	50.8	39.028	14.9717	0.03	0.02	N	Y	N	117.9857	126.8942	82.5409	13.7795
LV-104	TC-24-40B	1	50.8	55.0544	19.5533	0.06	0.03	Y	Y	N	158.5435	123.3308	114.6479	14.41925
LV-160	TC-24-43A	1	50.8	53.5606	18.5399	0.05	0.045	Y	Y	N	157.6317	117.6153	160.1783	21.2725
LV-043	TC-24-36D	1	50.8	56.8346	18.8337	0.07	0.03	N	Y	N	167.3053	112.5709	2582.549	22.79555
LV-109	TC-24-40D	1	76.2	52.5862	19.2723	0.02	0.01	N	N	N	212.4602	90.71017	0	22.78063
LV-080	TC-24-38E	1	76.2	59.4579	19.7018	0	0	N	N	N	219.3887	89.80317	0	48.768
LV-081	TC-24-38F	1	76.2	63.77	21.161	0	0	N	N	N	239.6967	88.2824	0	0
LV-110	TC-24-40E	1	76.2	62.6073	21.6967	0.03	0.01	N	N	N	254.9213	85.11137	0	0
LV-168	TC-24-43F	1	76.2	68.3677	21.6207	0.03	0.02	N	Y	N	244.2894	88.50445	2.3031	0
LV-166	TC-24-43D	1	76.2	62.386	20.5875	0.04	0.02	N	Y	N	231.1244	89.07541	6.9837	0
LV-146	TC-24-42B	1	76.2	64.296	20.4603	0.02	0.01	N	N	N	236.601	86.47597	25.0175	0
LV-145	TC-24-42A	1	76.2	60.3844	19.65	0.02	0.02	N	Y	N	232.6437	84.46392	60.0978	0
LV-167	TC-24-43E	1	76.2	65.6151	20.9274	0.03	0.02	N	Y	N	233.9364	89.45765	60.1783	0
LV-079	TC-24-38D	1	76.2	68.4944	21.6994	0	0	N	Y	N	244.3994	88.78663	64.068	30.54668
LV-147	TC-24-42C	1	76.2	66.2547	20.9372	0.035	0.04	N	N	N	247.5397	84.58118	117.8896	32.73504
LV-111	TC-24-40F	1	76.2	71.6468	21.8415	0.05	0.02	N	N	N	325.2064	67.16196	3556.084	31.86827

Appendix V. Contact Area Plots

Square shown in each plot has dimension 12.33 x 12.33 mm. Contact area reported in Appendix IV.


Test # LV-024
Energy 30 J
Tip 50.8
Test # LV-025
Energy 40J
Tip 50.8
Test # LV-026
Energy
Tip 50.8mm
Test # LV-027
Energy 30 J
Tip 50.8
Test # LV-028
Energy 20 J
Tip 50.8mm
Test # LV-033
Energy
Tip

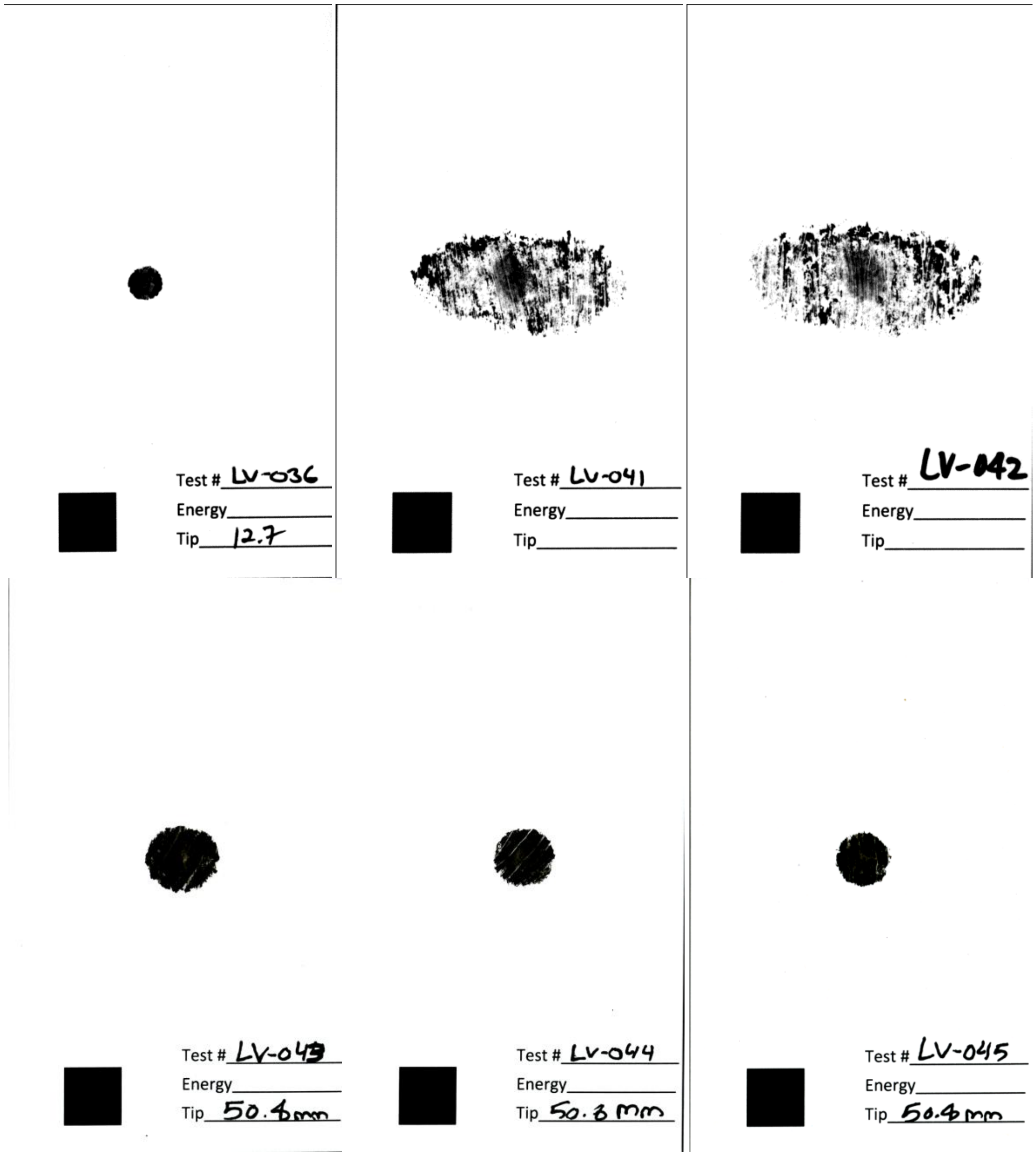

Test # LV-036
Energy
Tip 12.7
Test # LV-041
Energy
Tip
Test # LV-042
Energy
Tip
Test # LV-043
Energy
Tip 50.4mm
Test # LV-044
Energy
Tip
Test # LV-045
Energy
Tip 50.4mm

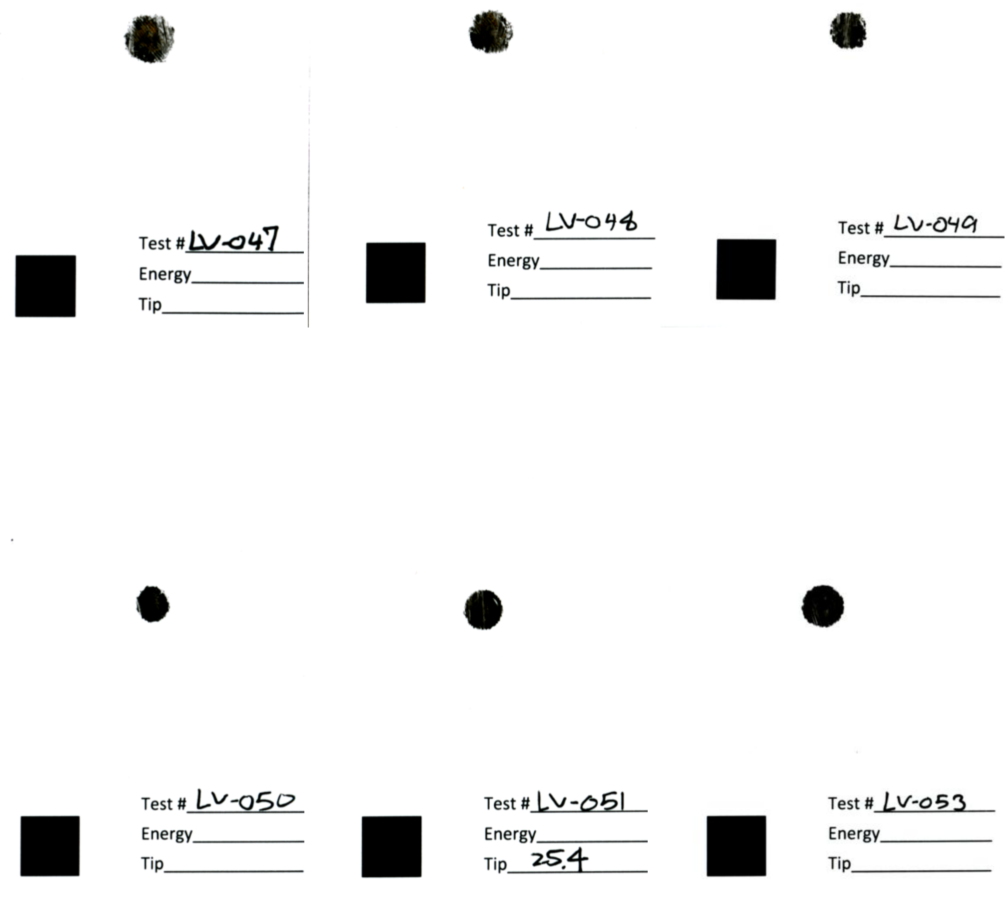
Test # LV-047
Energy
Tip
Test # LV-048
Energy
Tip
Test # LV-049
Energy
Tip
Test # LV-050
Energy
Tip
Test # LV-051
Energy
Tip 25.4
Test # LV-053
Energy
Tip

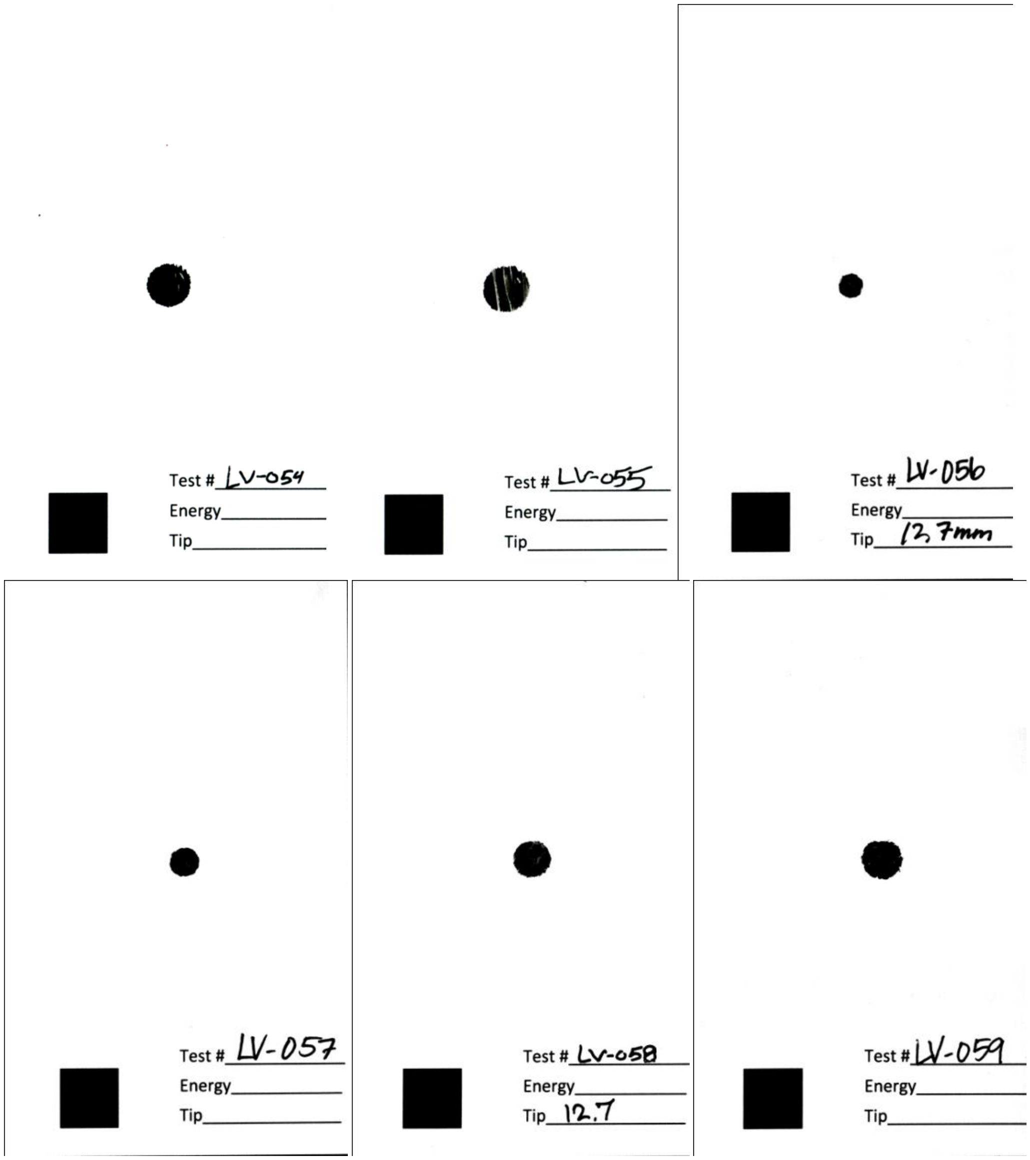
Test # LV-054
Energy
Tip
Test # LV-055
Energy
Tip
Test # LV-056
Energy
Tip 12.7mm
Test # LV-057
Energy
Tip
Test # LV-058
Energy
Tip 12.7
Test # LV-059
Energy
Tip

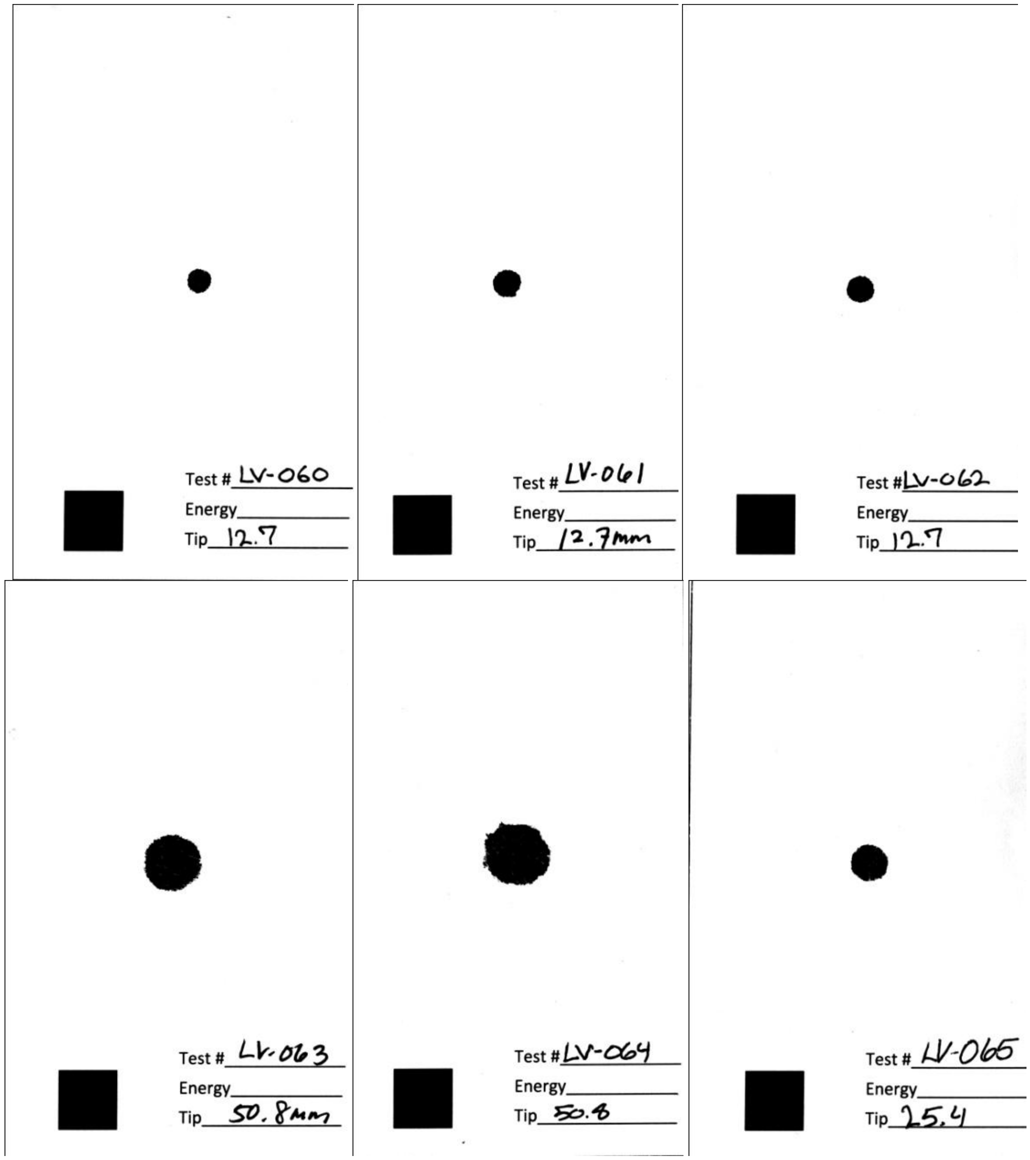

Test # LV-060
Energy
Tip 12.7
Test # LV-061
Energy
Tip 12.7mm
Test # LV-062
Energy
Tip 12.7
Test # LV-063
Energy
Tip 50.8mm
Test # LV-064
Energy
Tip 50.8
Test # LV-065
Energy
Tip 25.4

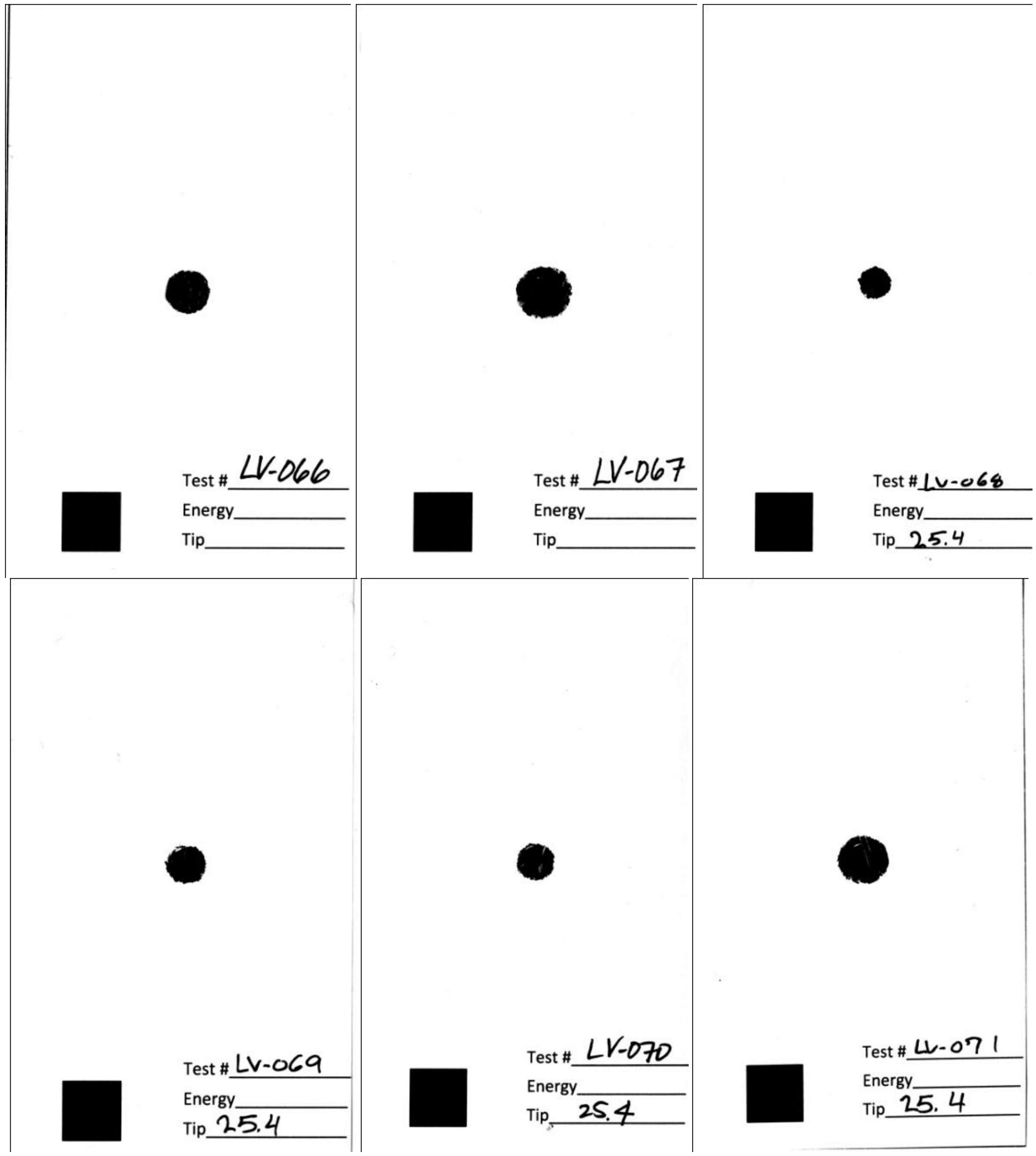
Test # LV-066
Energy
Tip
Test # LV-067
Energy
Tip
Test # LV-068
Energy
Tip 25.4
Test # LV-069
Energy
Tip 25.4
Test # LV-070
Energy
Tip 25.4
Test # LV-071
Energy
Tip 25.4

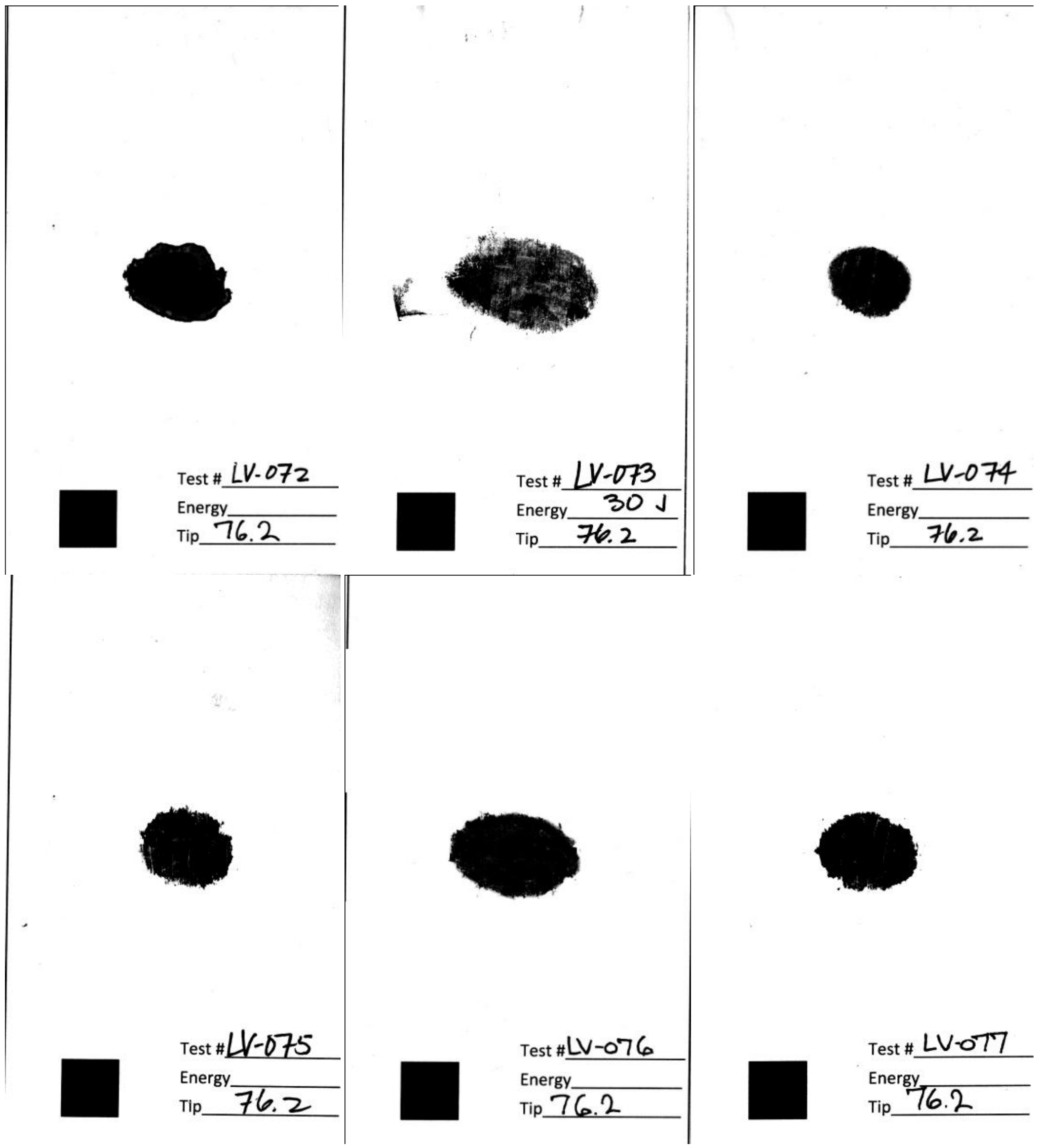
Test # LV-072
Energy
Tip 76.2
Test # LV-073
Energy 30 J
Tip 76.2
Test # LV-074
Energy
Tip 76.2
Test # LV-075
Energy
Tip 76.2
Test # LV-076
Energy
Tip 76.2
Test # LV-077
Energy
Tip 76.2

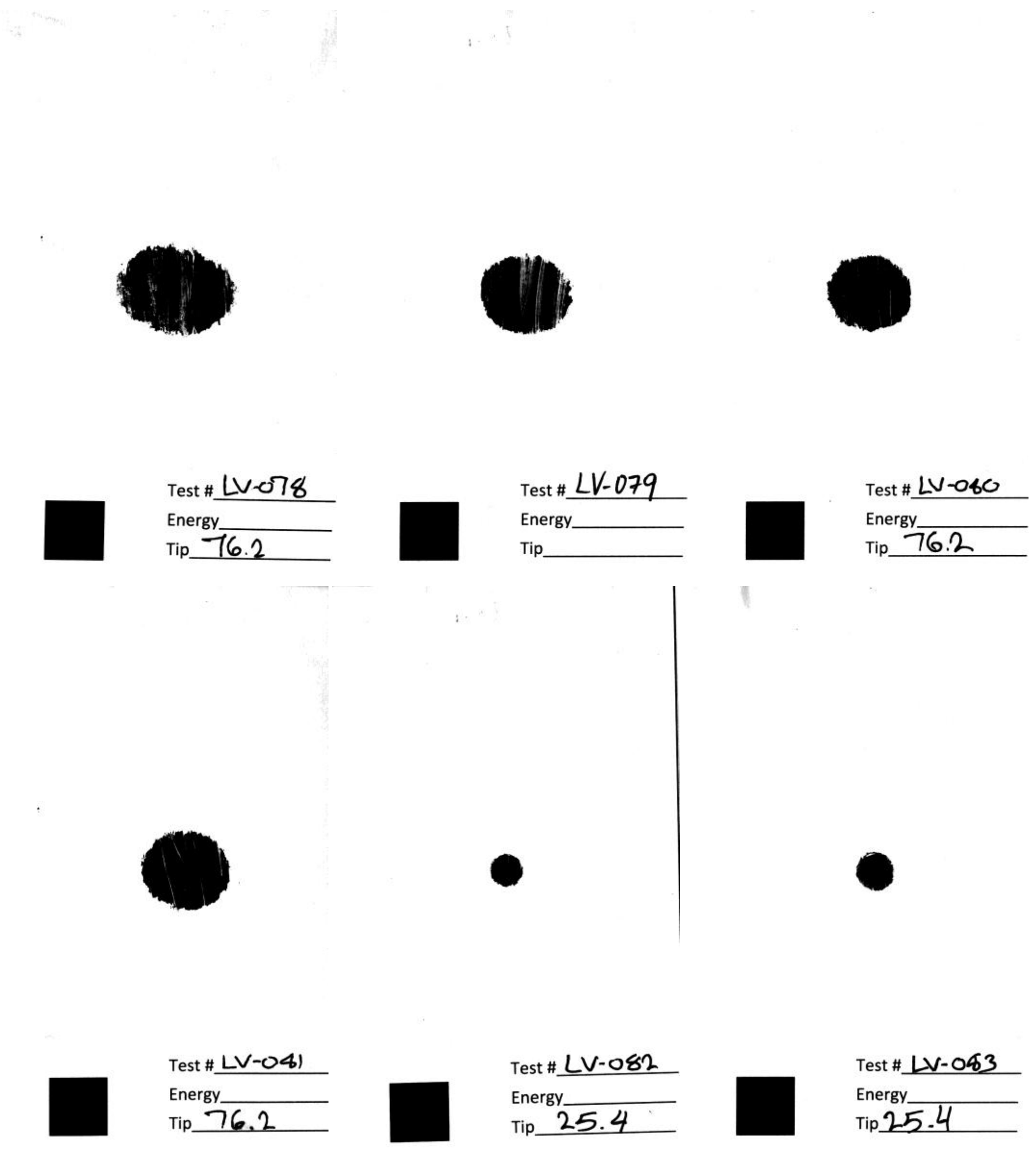
Test # LV-078
Energy
Tip 76.2
Test # LV-079
Energy
Tip
Test # LV-080
Energy
Tip 76.2
Test # LV-081
Energy
Tip 76.2
Test # LV-082
Energy
Tip 25.4
Test # LV-083
Energy
Tip 25.4

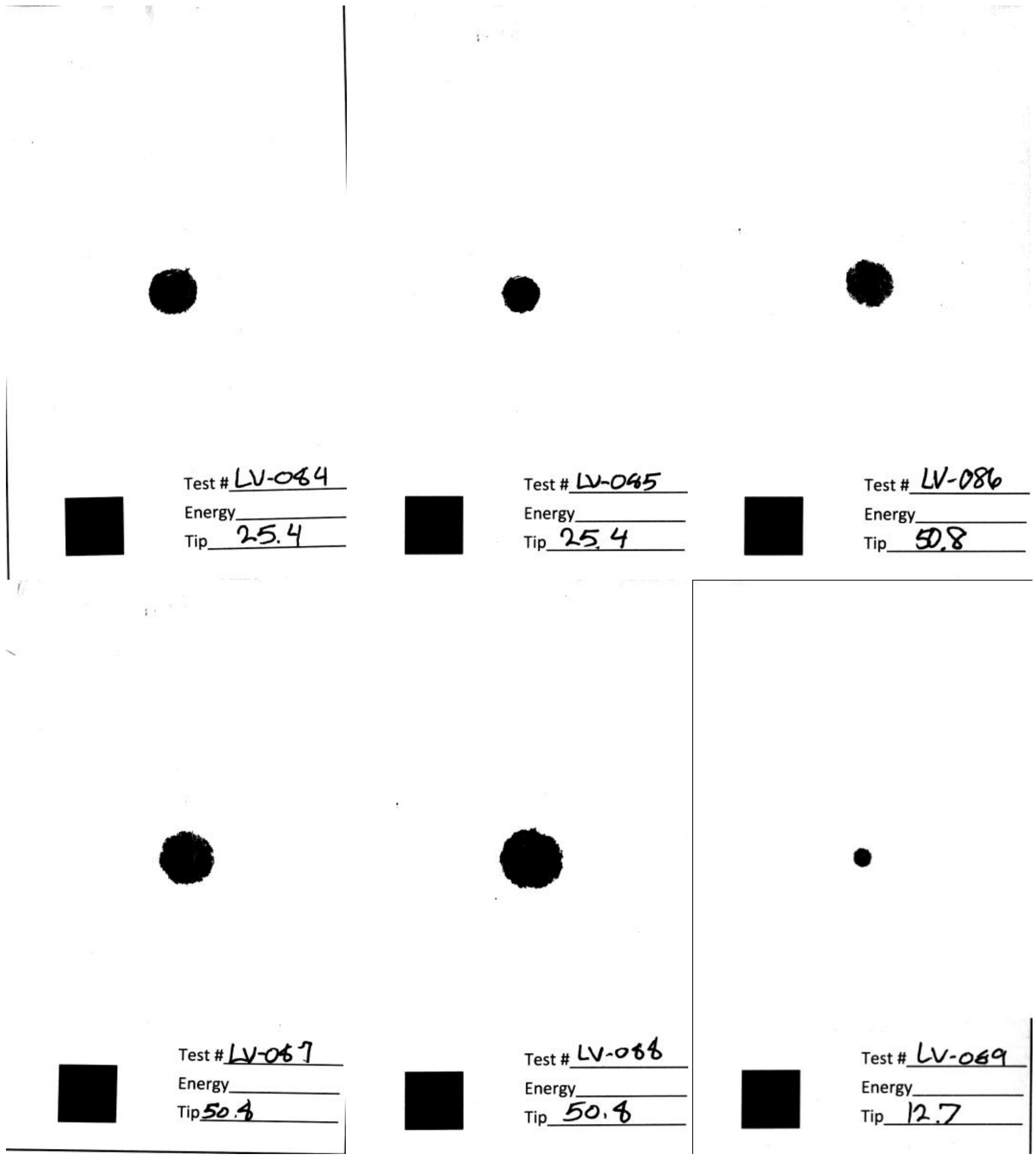
Test # LV-084
Energy
Tip 25.4
Test # LV-085
Energy
Tip 25.4
Test # LV-086
Energy
Tip 50.8
Test # LV-087
Energy
Tip 50.8
Test # LV-088
Energy
Tip 50.8
Test # LV-089
Energy
Tip 12.7

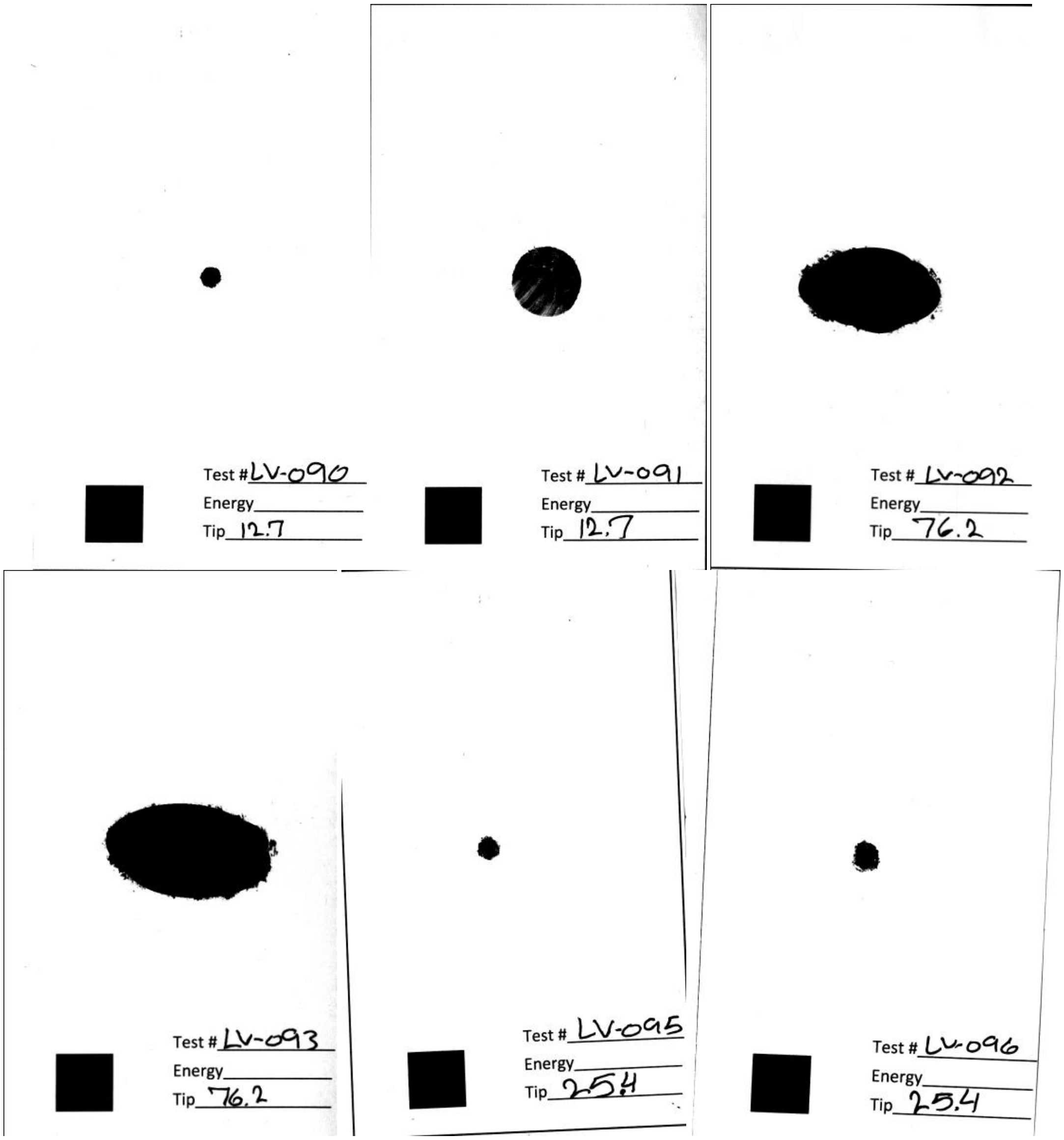
Test # LV-090
Energy
Tip 12.7
Test # LV-091
Energy
Tip 12.7
Test # LV-092
Energy
Tip 76.2
Test # LV-093
Energy
Tip 76.2
Test # LV-095
Energy
Tip 25.4
Test # LV-096
Energy
Tip 25.4

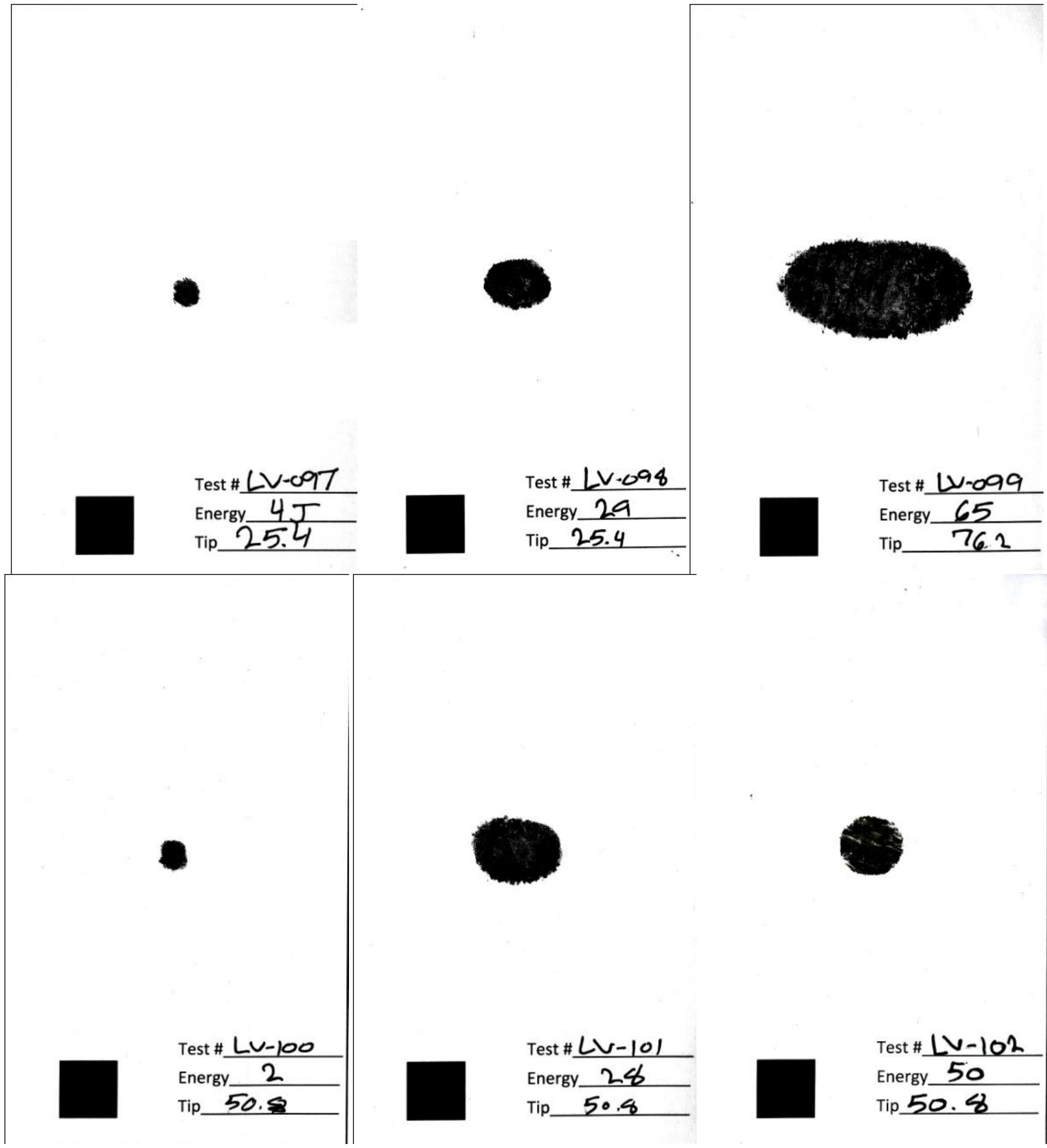
Test # LV-097
Energy 4J
Tip 25.4
Test # LV-098
Energy 29
Tip 25.4
Test # LV-099
Energy 65
Tip 76.2
Test # LV-100
Energy 2
Test # LV-101
Energy 26
Test # LV-102
Energy 50
Tip 50.8

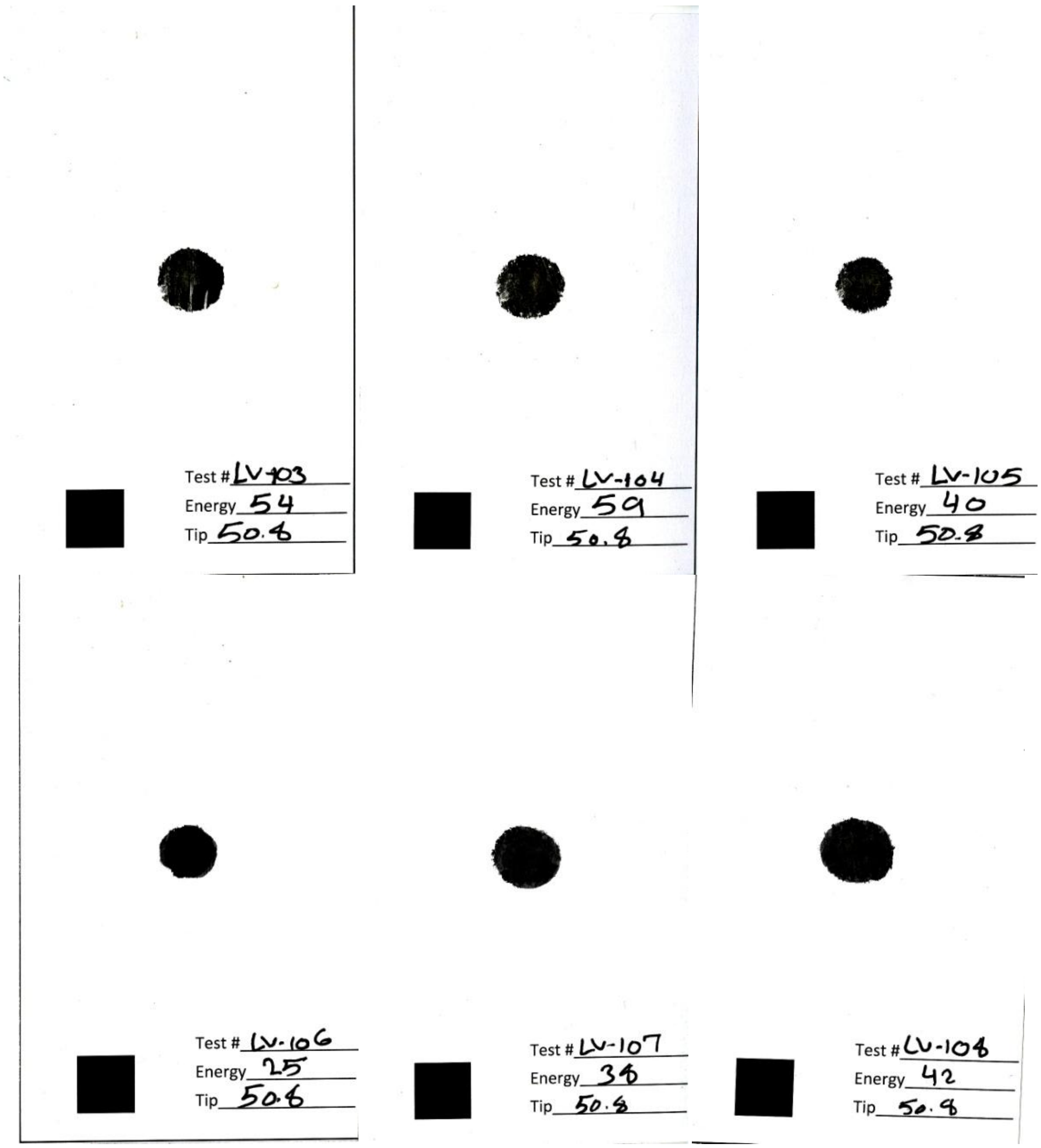
Test # LV-103
Energy 54
Tip 50.8
Test # LV-104
Energy 59
Tip 50.8
Test # LV-105
Energy 40
Tip 50.8
Test # LV-106
Energy 25
Tip 50.8
Test # LV-107
Energy 38
Tip 50.8
Test # LV-108
Energy 42
Tip 50.8

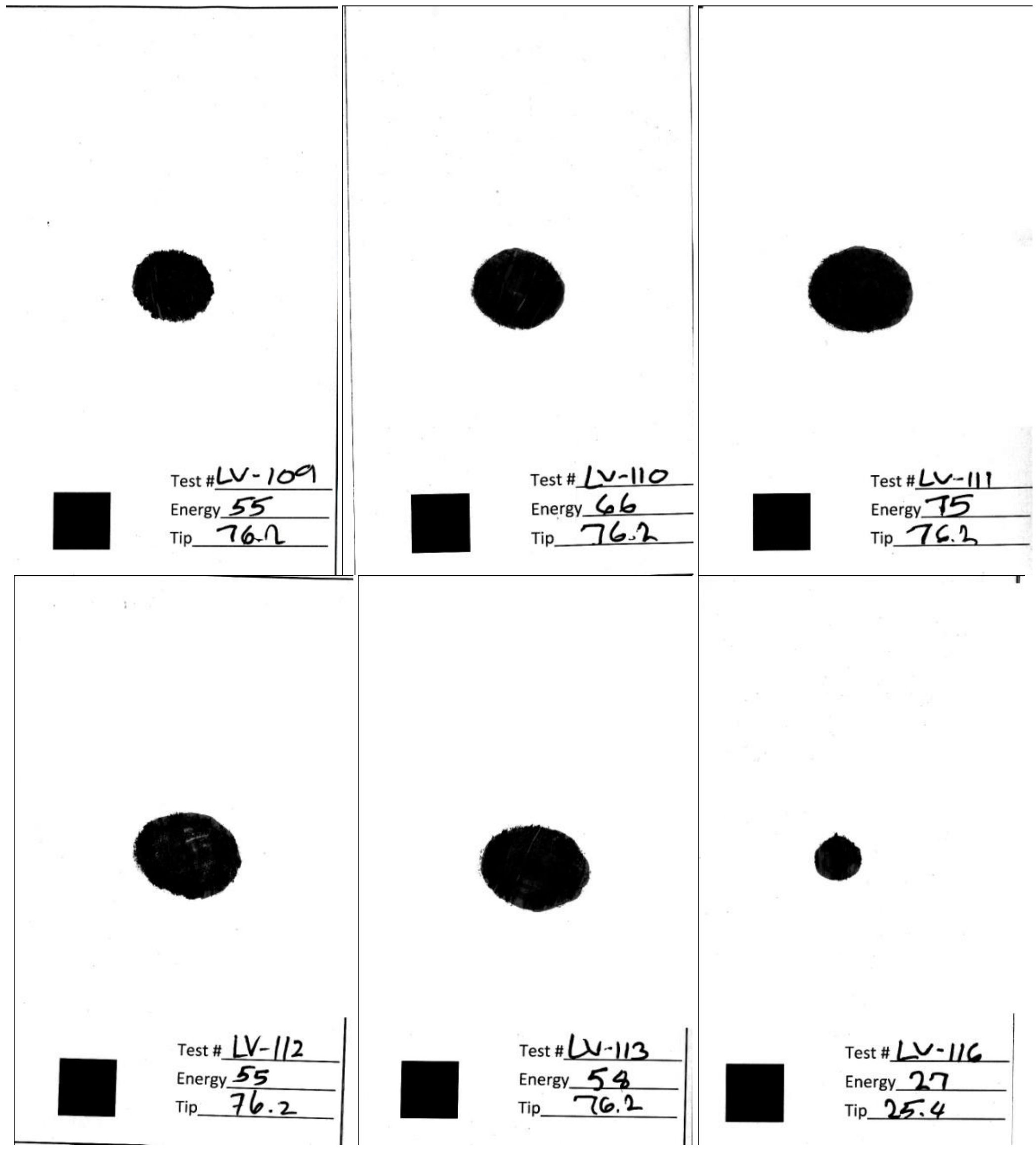
Test # LV-109
Energy 55
Tip 76.2
Test # LV-110
Energy 66
Tip 76.2
Test # LV-111
Energy 75
Tip 76.2
Test # LV-112
Energy 55
Tip 76.2
Test # LV-113
Energy 58
Tip 76.2
Test # LV-116
Energy 27
Tip 25.4

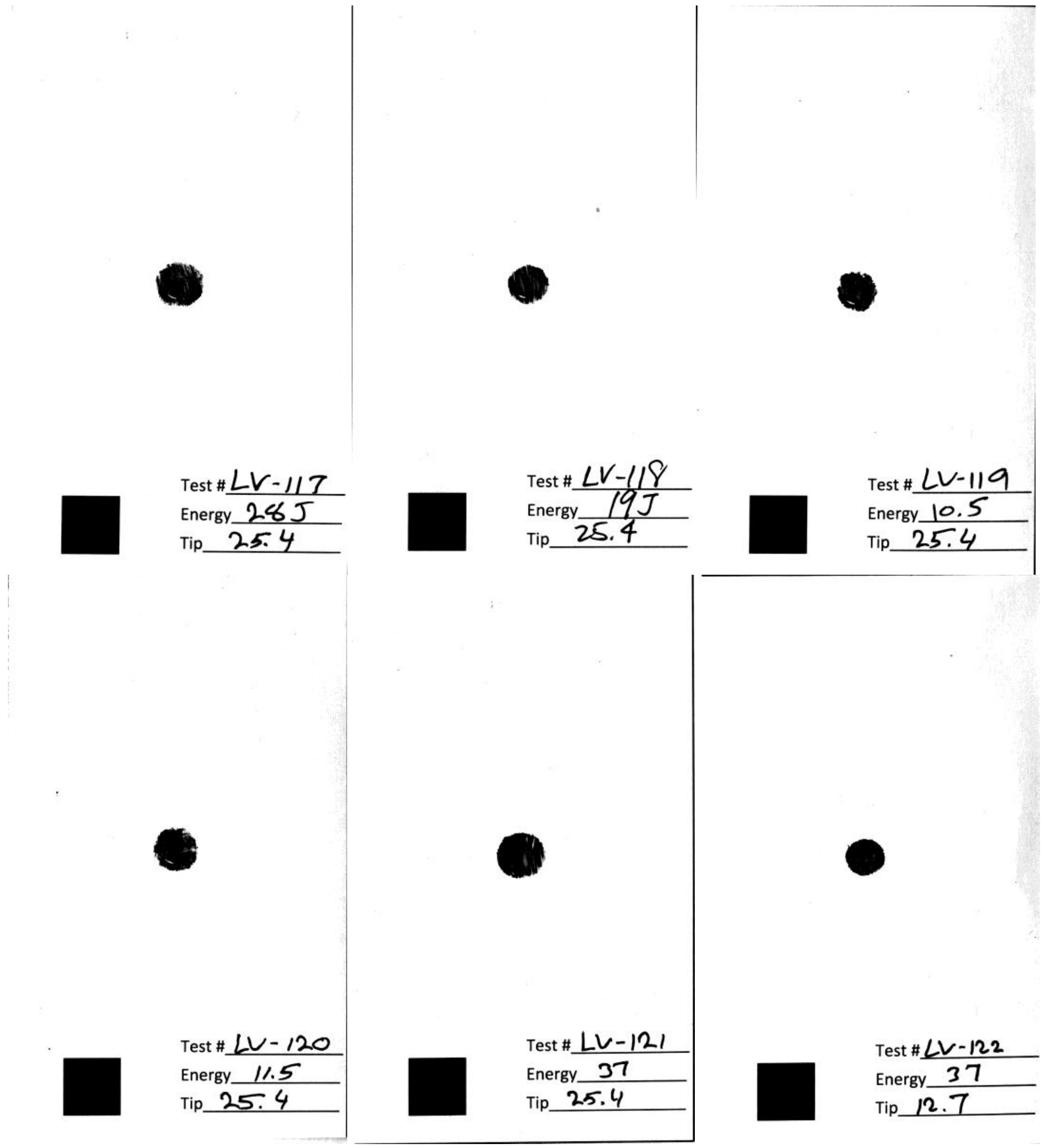
Test # LV-117
Energy 28J
Tip 25.4
Test # LV-118
Energy 19J
Tip 25.4
Test # LV-119
Energy 10.5
Tip 25.4
Test # LV-120
Energy 11.5
Tip 25.4
Test # LV-121
Energy 37
Tip 25.4
Test # LV-122
Energy 37
Tip 12.7

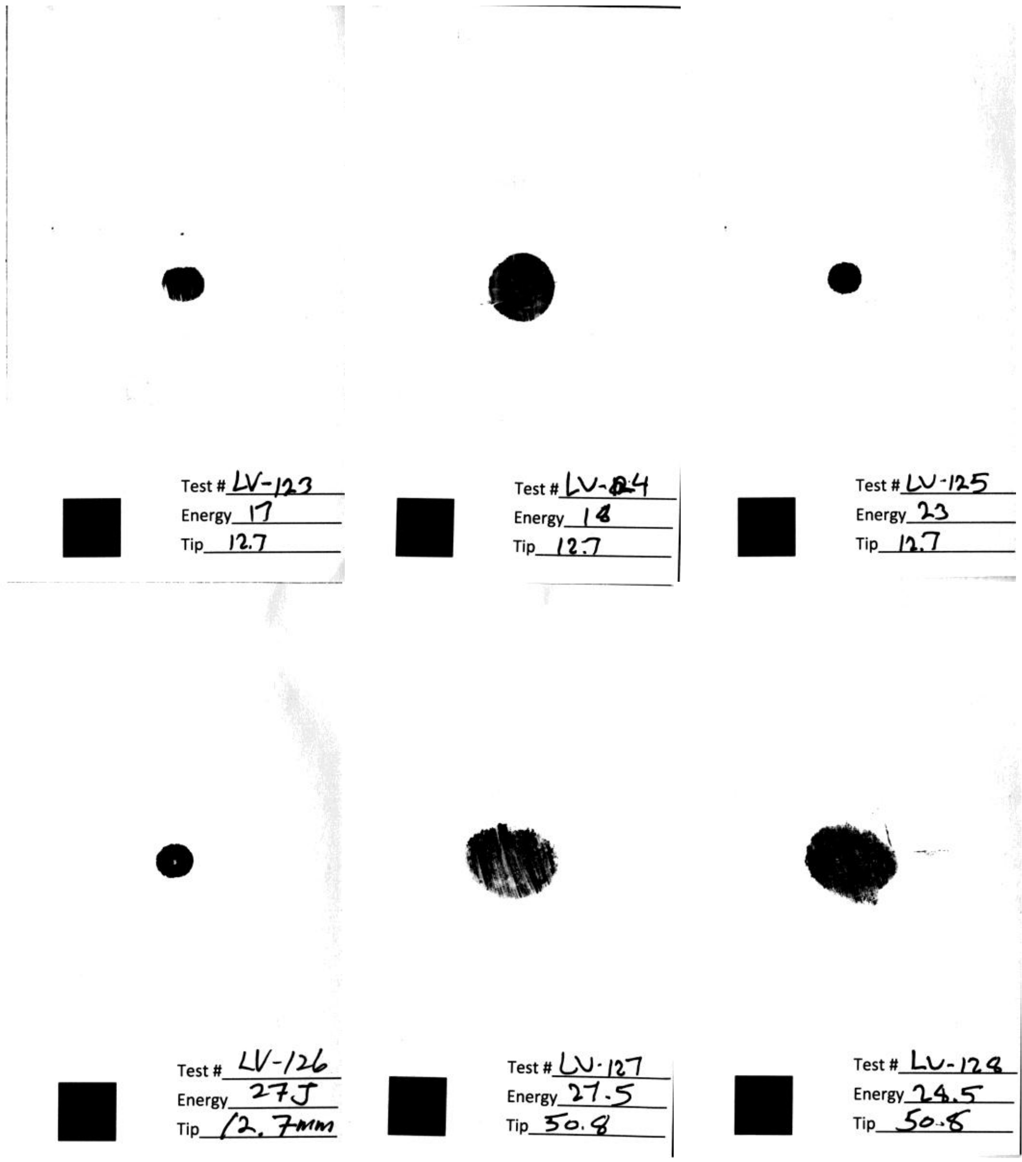
Test # LV-123
Energy 17
Tip 12.7
Test # LV-124
Energy 18
Tip 12.7
Test # LV-125
Energy 23
Tip 12.7
Test # LV-126
Energy 27J
Tip 12.7mm
Test # LV-127
Energy 27.5
Tip 50.8
Test # LV-128
Energy 24.5
Tip 50.8

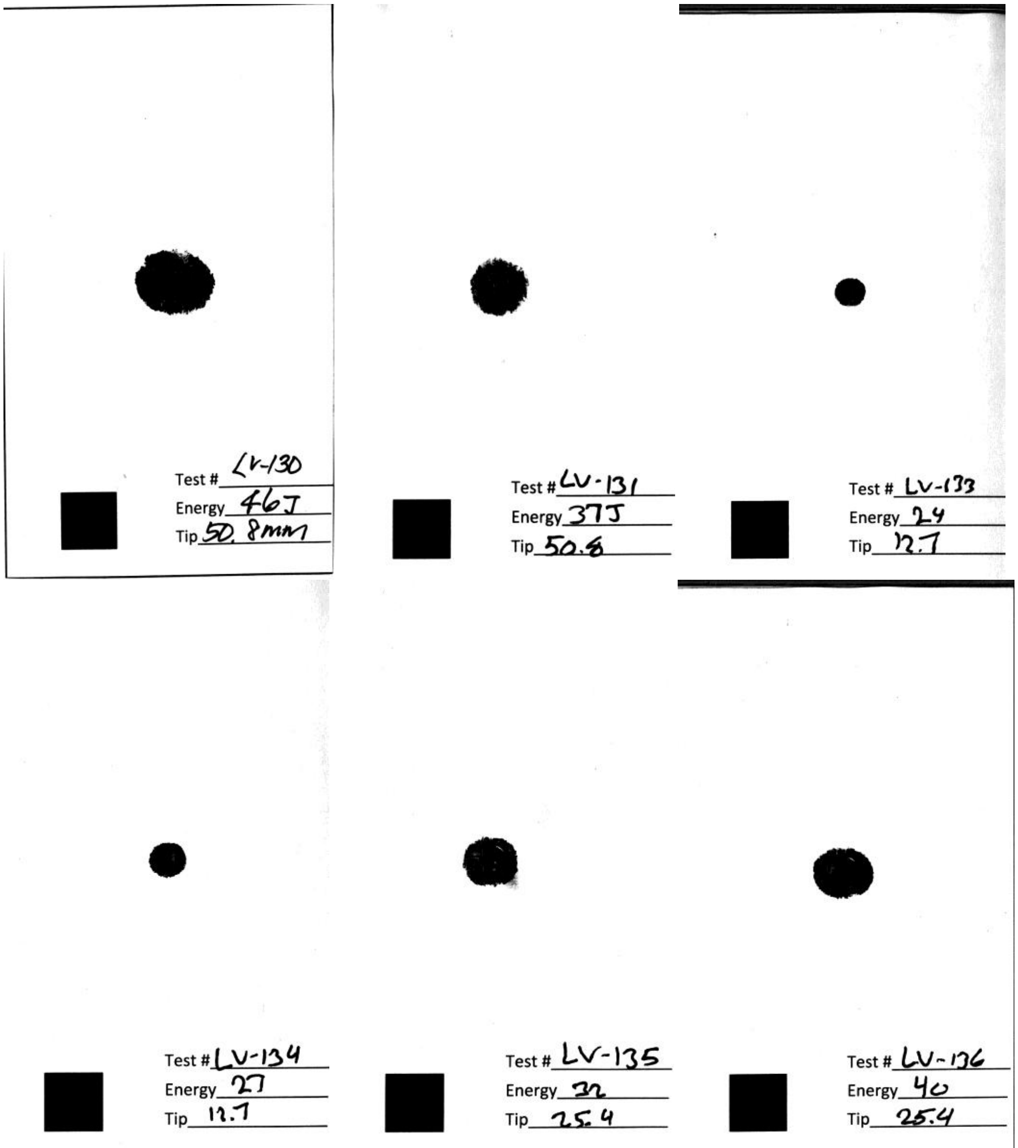
Test # LV-130
Energy 46J
Tip 50.8mm
Test # LV-131
Energy 37J
Tip 50.8
Test # LV-133
Energy 24
Tip 12.7
Test # LV-134
Energy 27
Tip 12.7
Test # LV-135
Energy 32
Tip 25.4
Test # LV-136
Energy 40
Tip 25.4

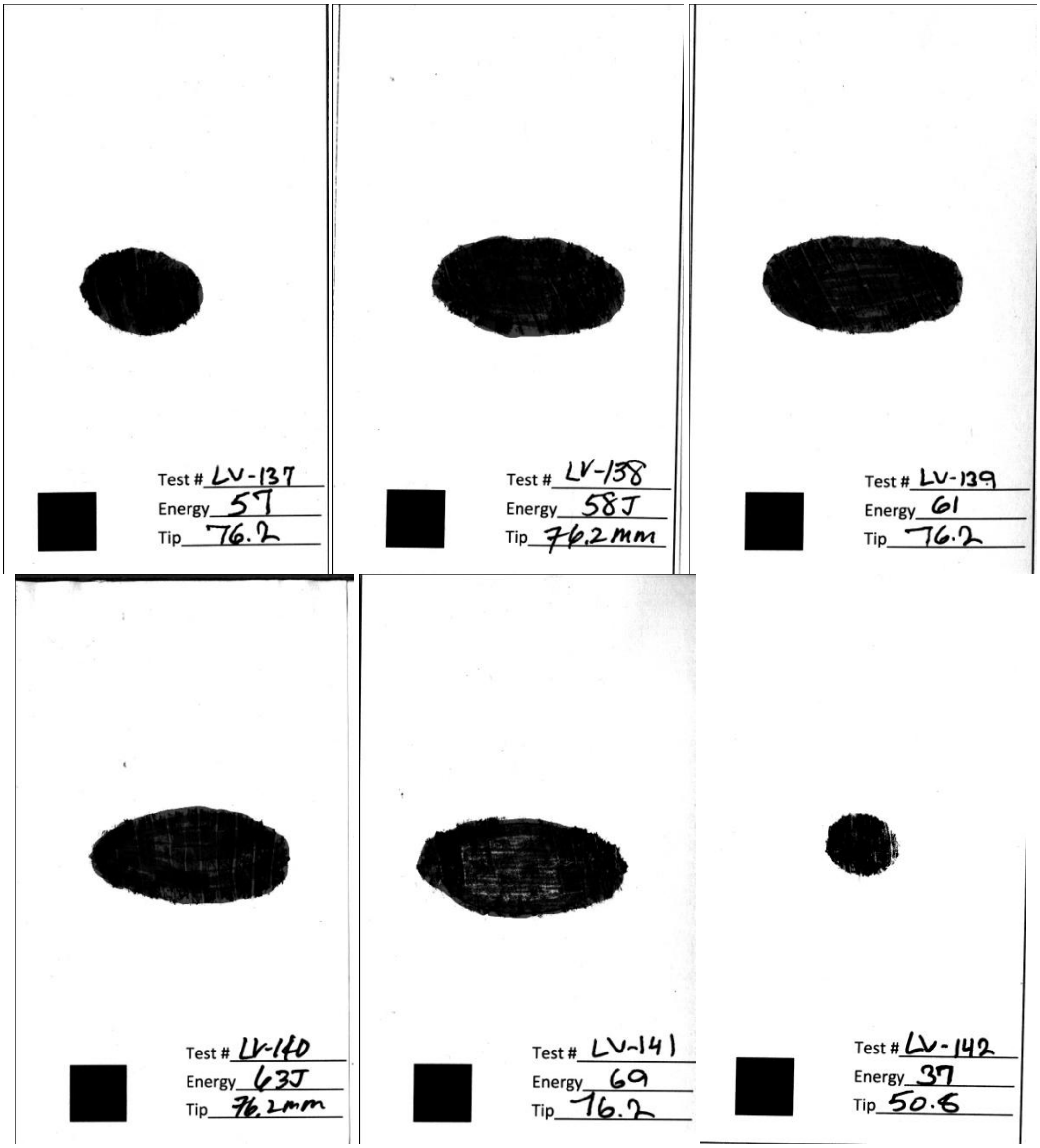

Test # LV-137
Energy 57
Tip 76.2
Test # LV-138
Energy 58J
Tip 76.2mm
Test # LV-139
Energy 61
Tip 76.2
Test # LV-140
Energy 63J
Tip 76.2mm
Test # LV-141
Energy 69
Tip 76.2
Test # LV-142
Energy 37
Tip 50.8

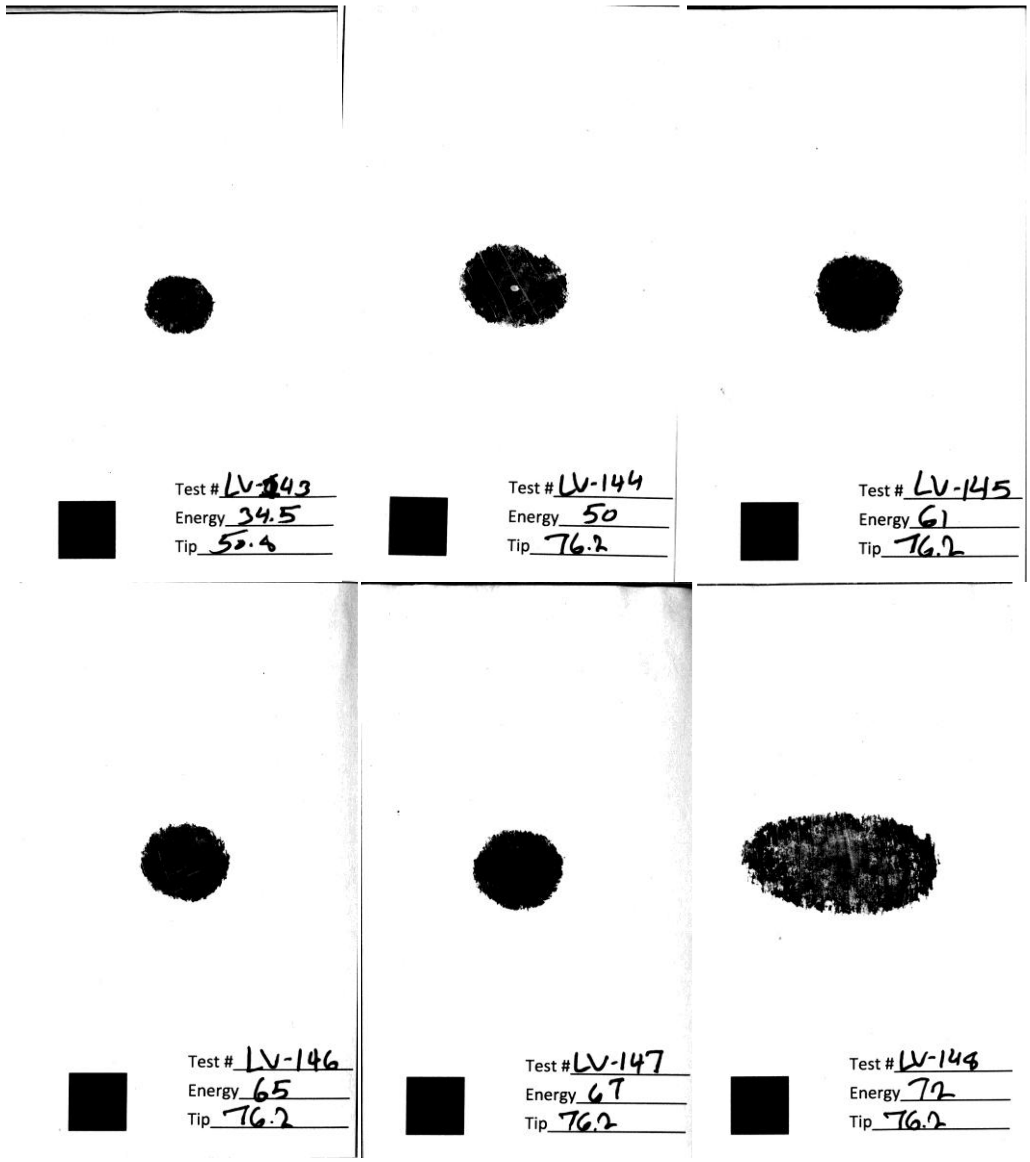

Test #
Energy 34.5
Tip
Test # LV-144
Energy 50
Tip 76.2
Test # LV-145
Energy 61
Tip 76.2
Test # LV-146
Energy 65
Tip 76.2
Test # LV-147
Energy 67
Tip 76.2
Test #
Energy 72
Tip 76.2

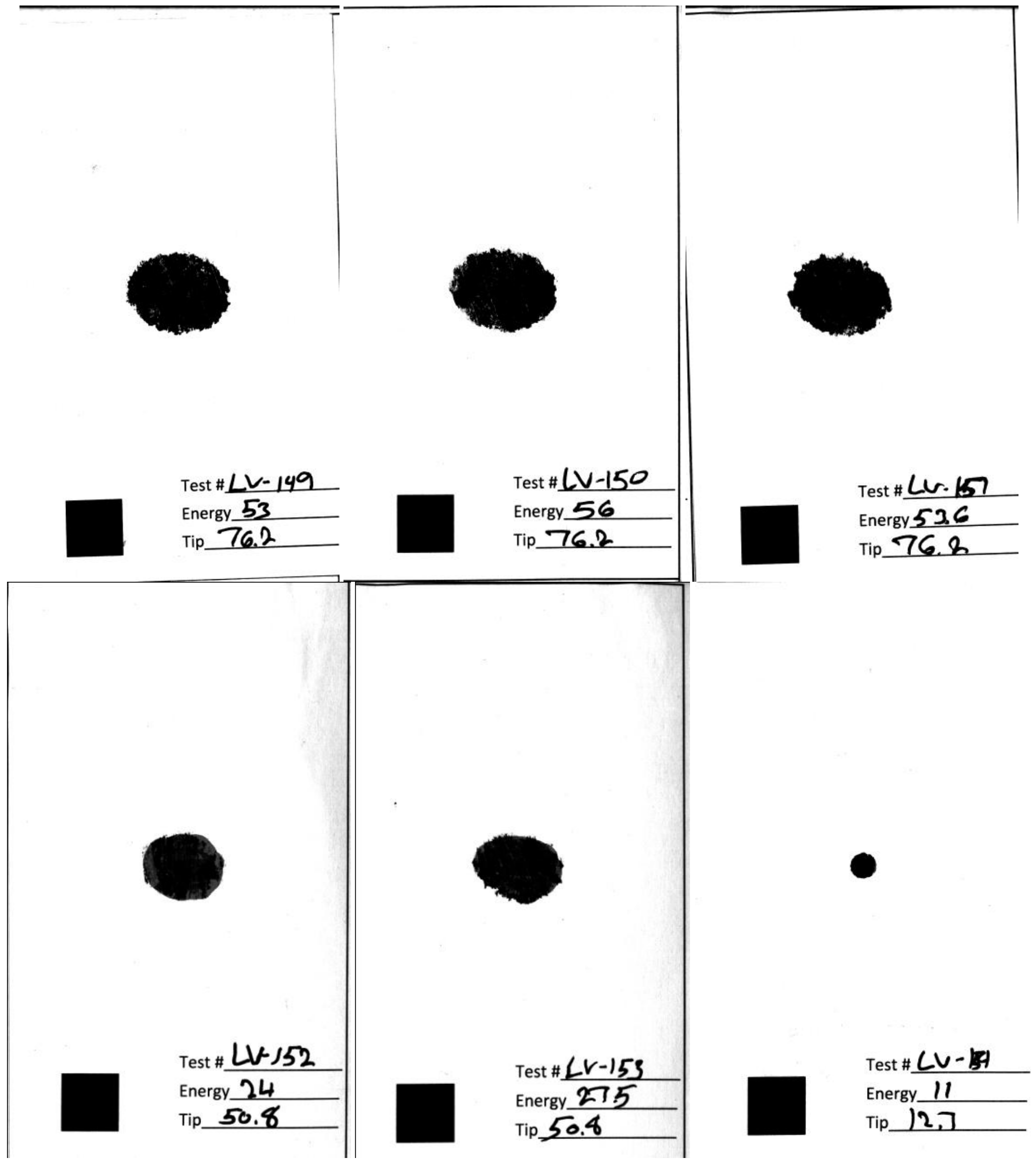
Test # LV-149
Energy 53
Tip 76.2
Test # LV-150
Energy 56
Tip 76.2
Test #
Energy
Tip 76.2
Test # LV-152
Energy 24
Tip 50.8
Test # LV-153
Energy
Tip 50.8
Test #
Energy 11
Tip 12.7

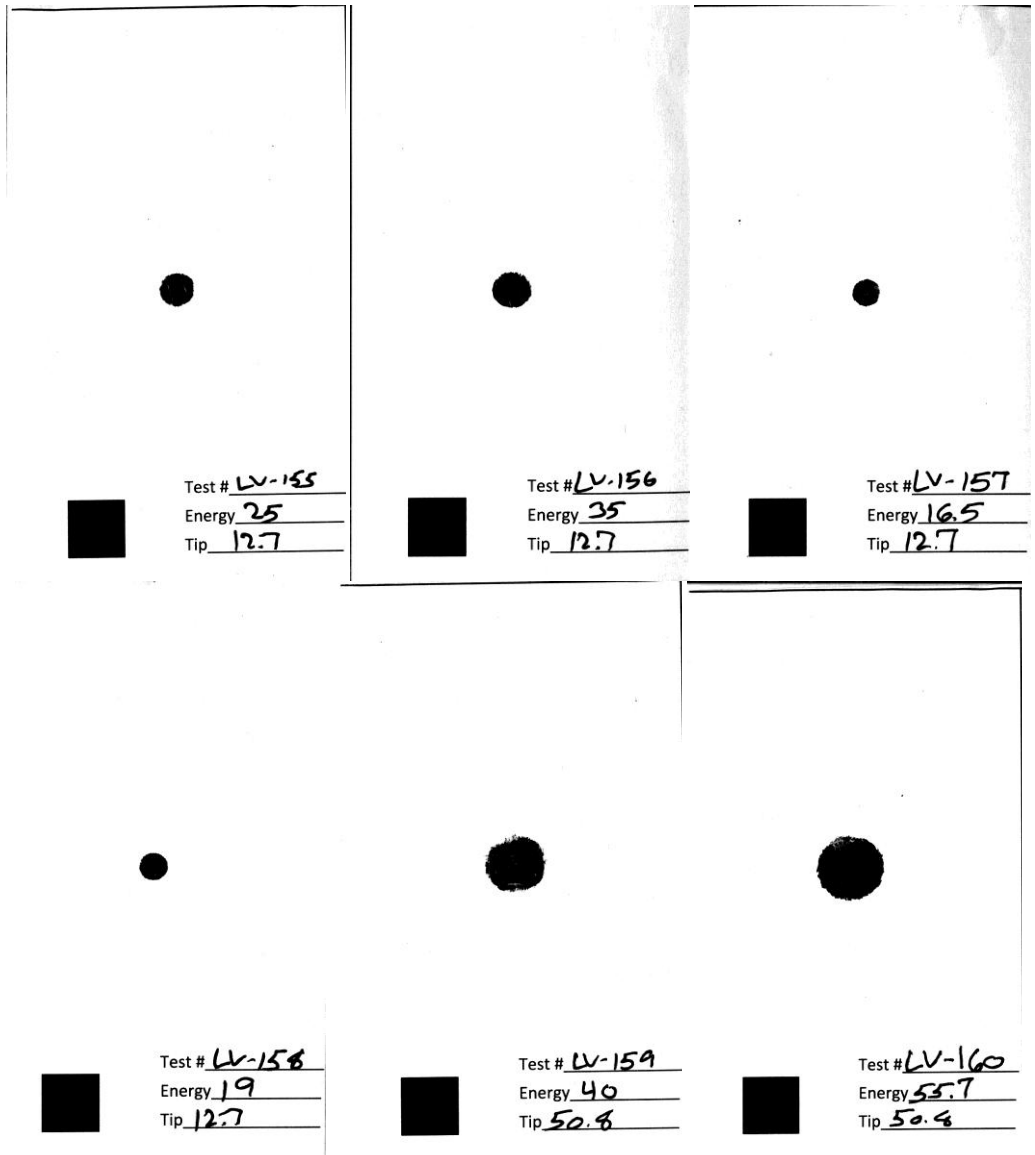
Test # LV-155
Energy 25
Tip 12.7
Test # LV-156
Energy 35
Tip 12.7
Test # LV-157
Energy 16.5
Tip 12.7
Test # LV-158
Energy 19
Tip 12.7
Test # LV-159
Energy 40
Tip 50.8
Test # LV-160
Energy 55.7
Tip 50.8

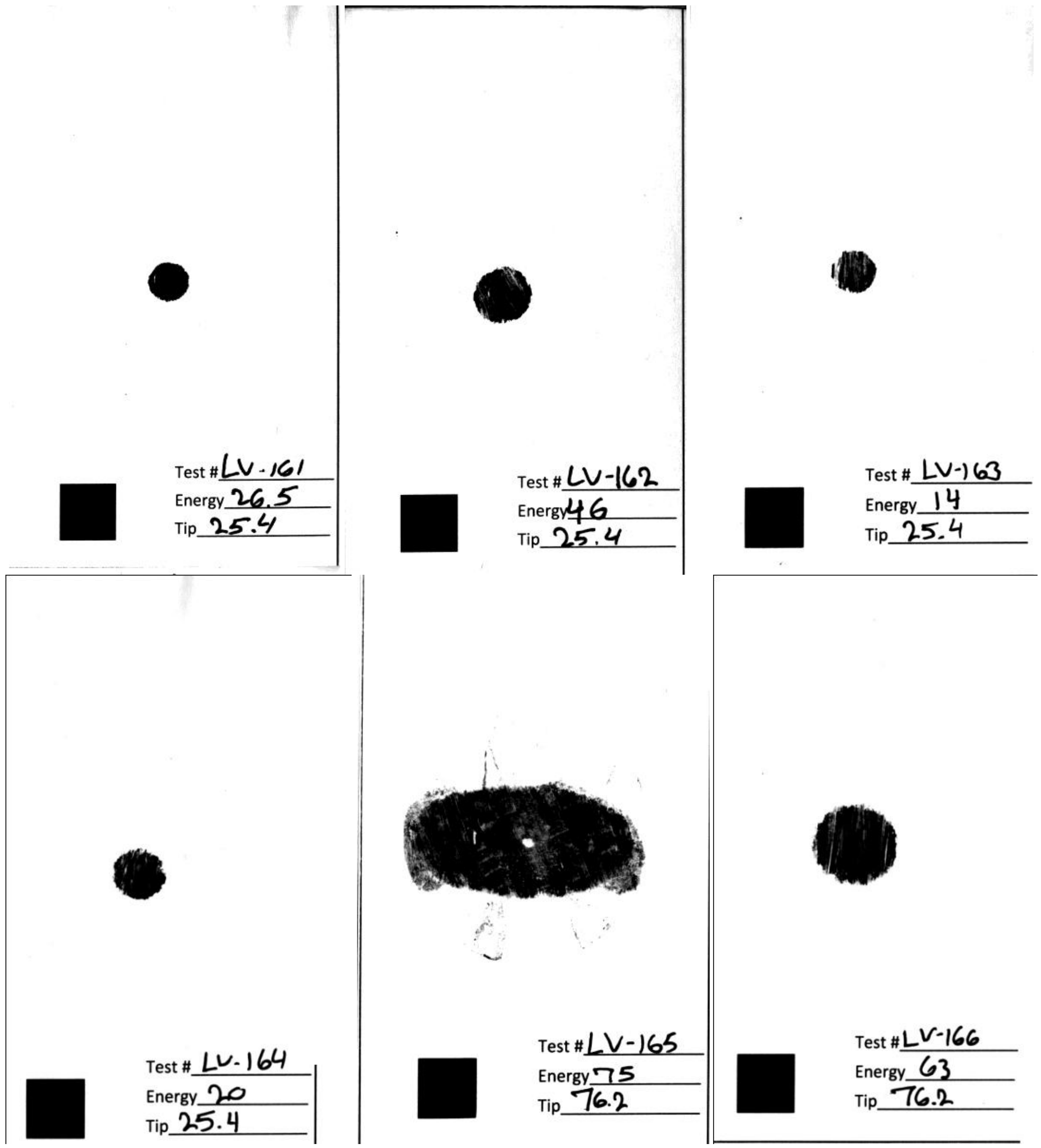
Test # LV-161
Energy 26.5
Tip 25.4
Test # LV-162
Energy 46
Tip 25.4
Test # LV-163
Energy 14
Tip 25.4
Test # LV-164
Energy 20
Tip 25.4
Test # LV-165
Energy 75
Tip 76.2
Test # LV-166
Energy 63
Tip 76.2

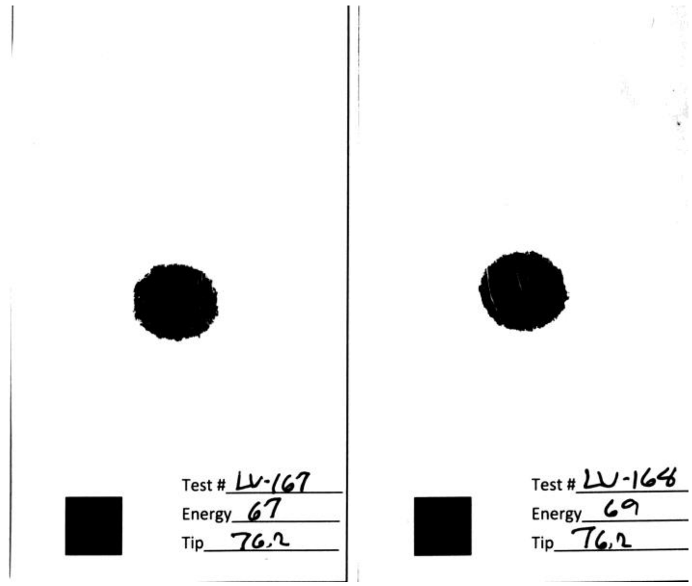
Test # LV-167
Energy 67
Tip 76.2
Test # LV-168
Energy 69
Tip 76.2

Appendix VI. Force and C-Scan Data

Plots are included here of the force vs. time history and C-Scans for each impact. When visually inspecting this data it was convenient to look at both the force curve and C-Scan data together for comparison, so they are paired for each impact here. They are organized by impact tip radius and panel thickness to facilitate the comparison of similar tests. Peak force and damage area for each test are reported in Appendix IV.

VIa. 12.7 mm tip, 8 ply panel

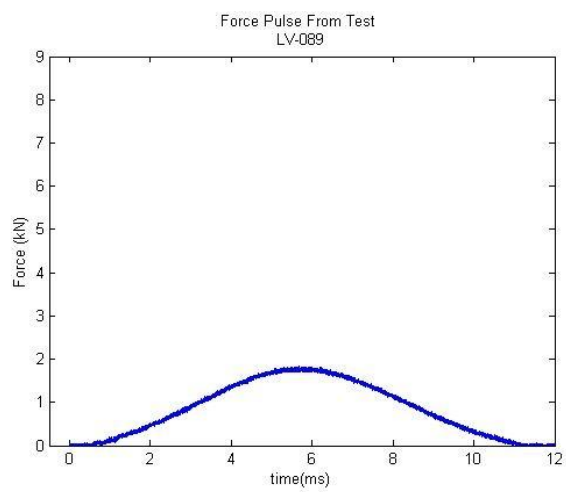

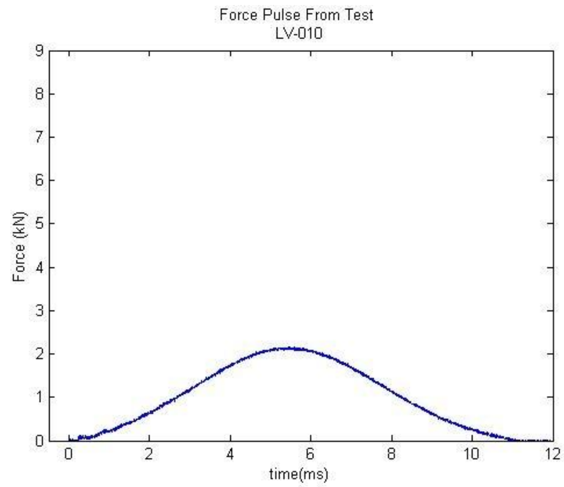
Force Pulse From Test
LV-010
Force (kN)
time(ms)
0
1
2
3
4
5
6
7
8
9
10
12

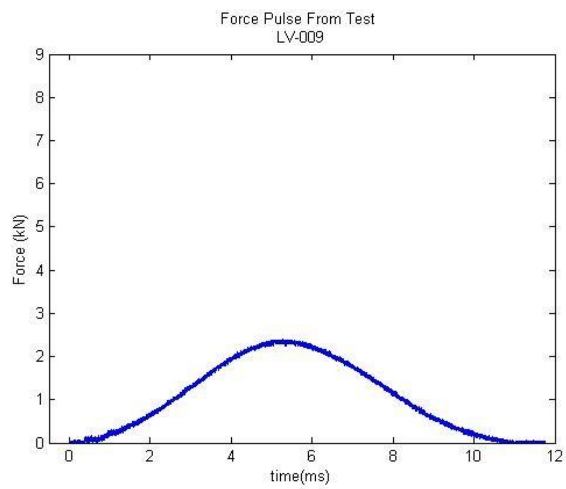
Force Pulse From Test
LV-009
Force (kN)
time(ms)
0
1
2
3
4
5
6
7
8
9
10
12

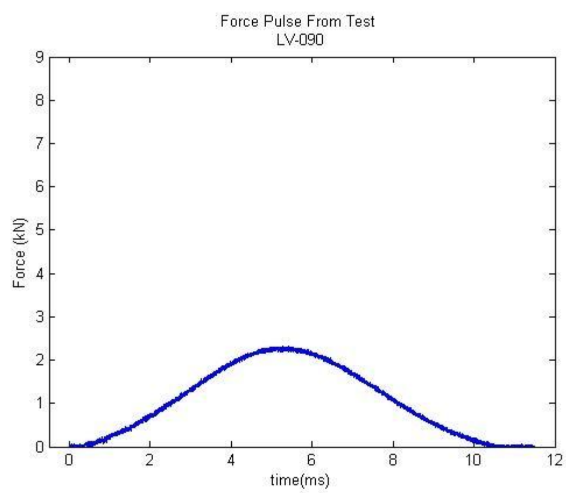
Force Pulse From Test
LV-090
Force (kN)
time(ms)
0
1
2
3
4
5
6
7
8
9
10
12

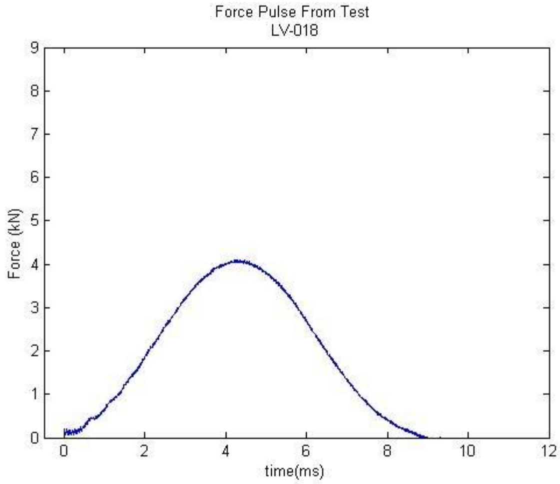
Force Pulse From Test
LV-018
Force (kN)
time(ms)
0 1 2 3 4 5 6 7 8 9
0 2 4 6 8 10 12

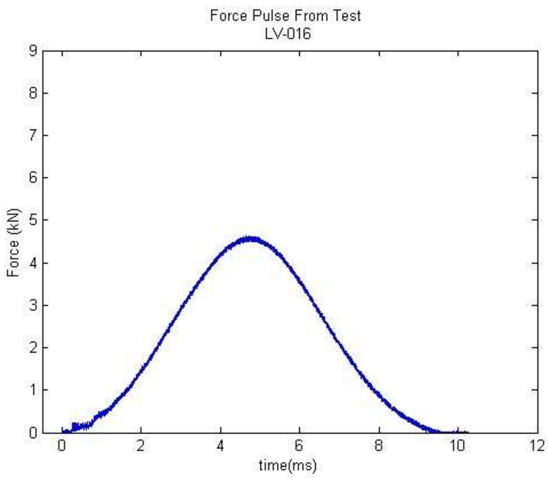
Force Pulse From Test
LV-016
Force (kN)
time(ms)
0 1 2 3 4 5 6 7 8 9
0 2 4 6 8 10 12

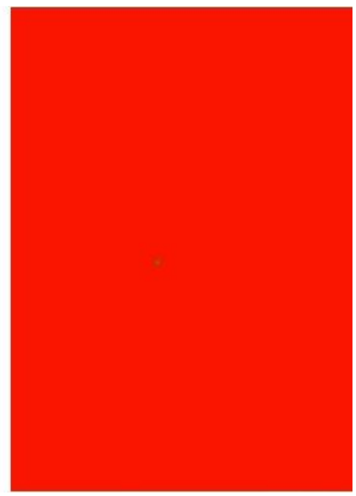

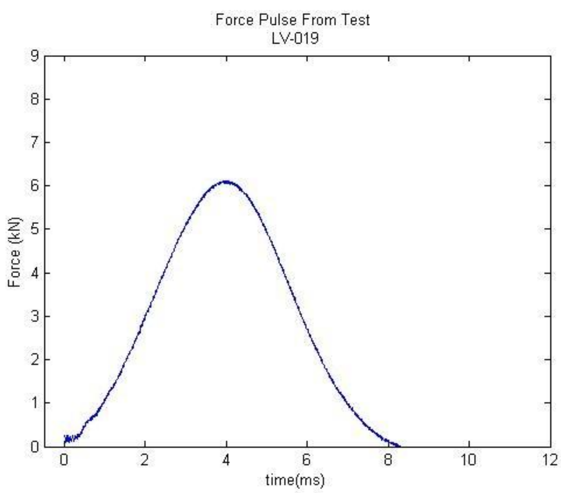
Force Pulse From Test
LV-019
Force (kN)
time(ms)
0 1 2 3 4 5 6 7 8 9
0 2 4 6 8 10 12

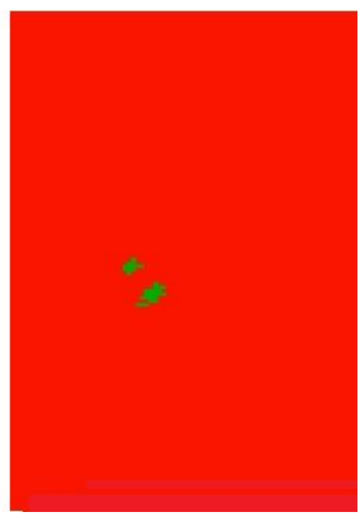

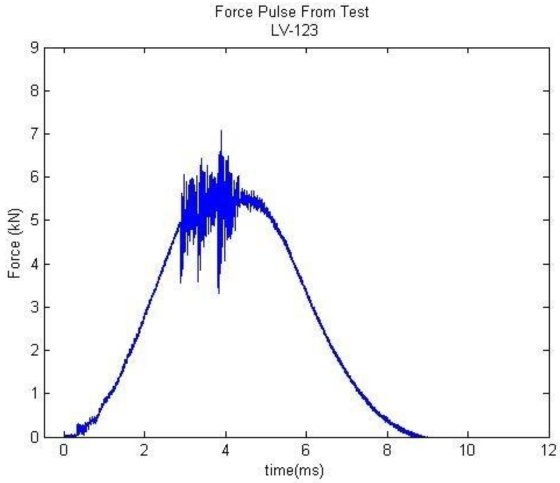

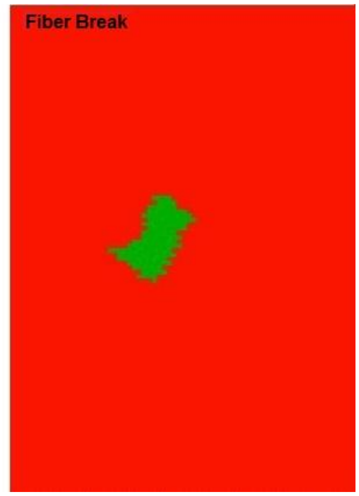

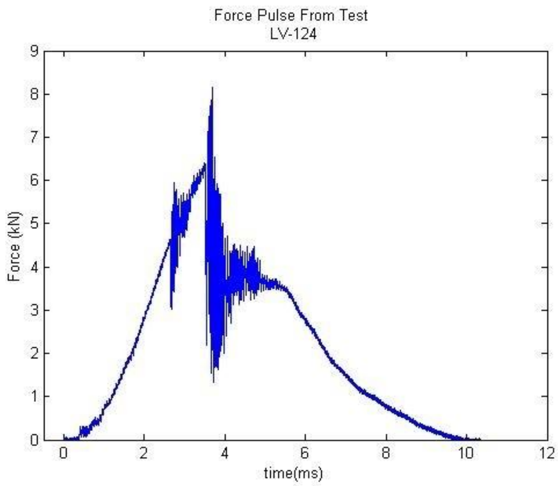

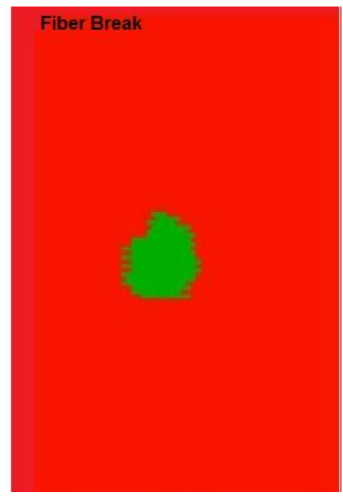

12.7 mm tip, 16 ply panel

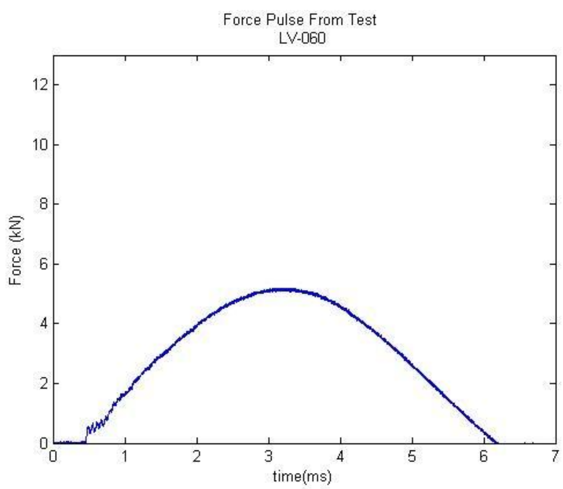

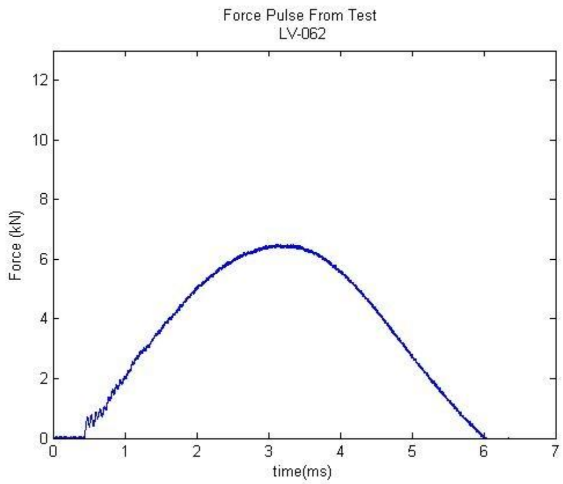
Force Pulse From Test
LV-062
Force (kN)
time(ms)

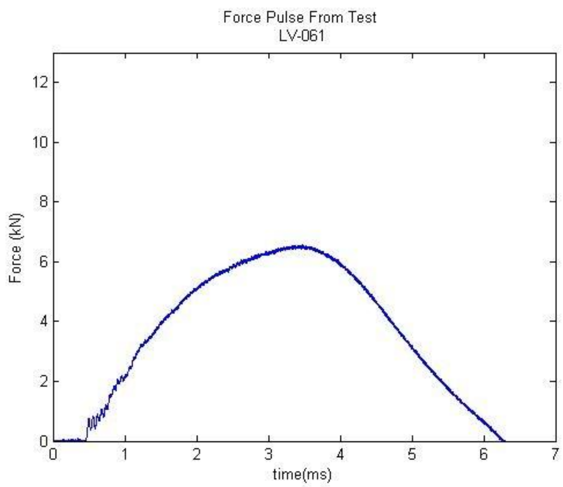
Force Pulse From Test
LV-061
Force (kN)
time(ms)

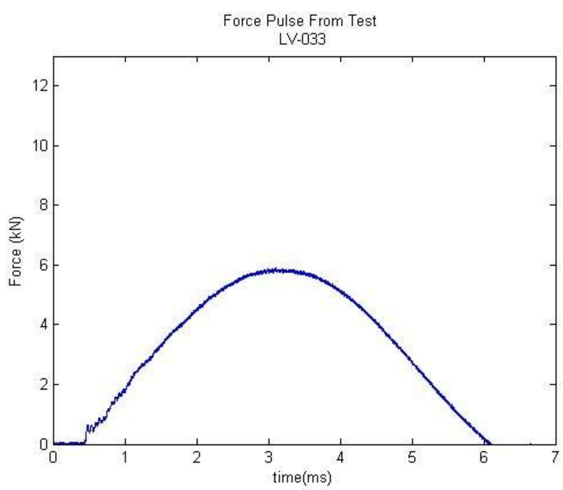
Force Pulse From Test
LV-033
Force (kN)
time(ms)

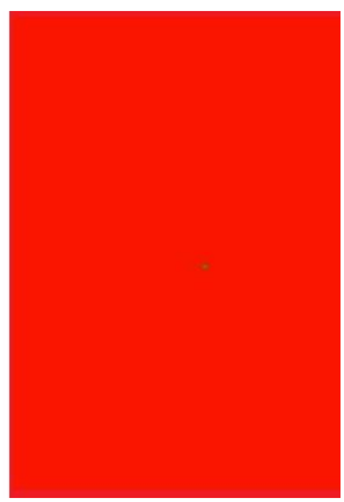

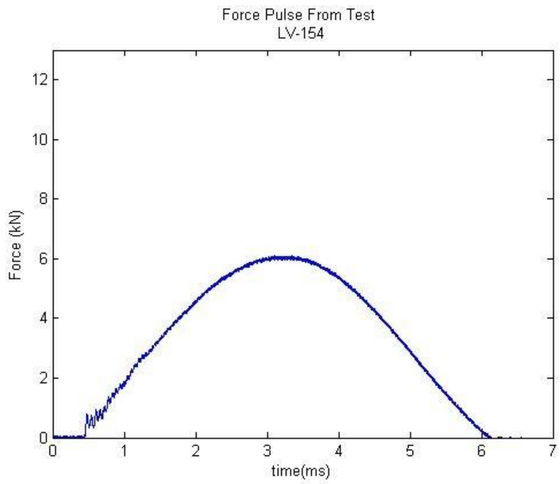
Force Pulse From Test
LV-154
Force (kN)
time(ms)
0
2
4
6
8
10
12
0
1
2
3
4
5
6
7

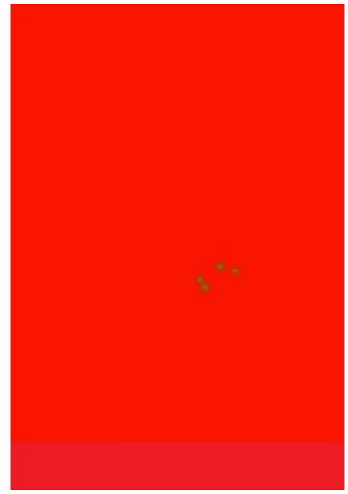

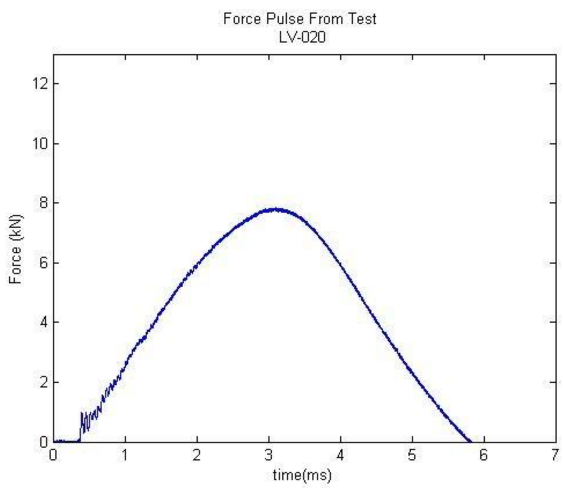
Force Pulse From Test
LV-020
Force (kN)
time(ms)
0
2
4
6
8
10
12
0
1
2
3
4
5
6
7

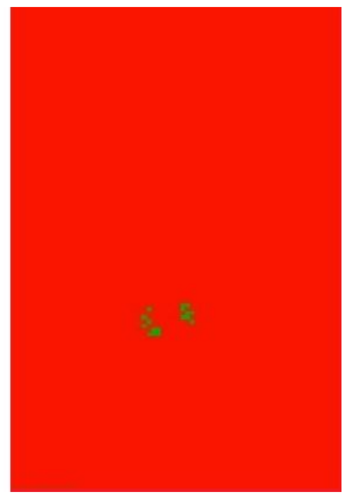

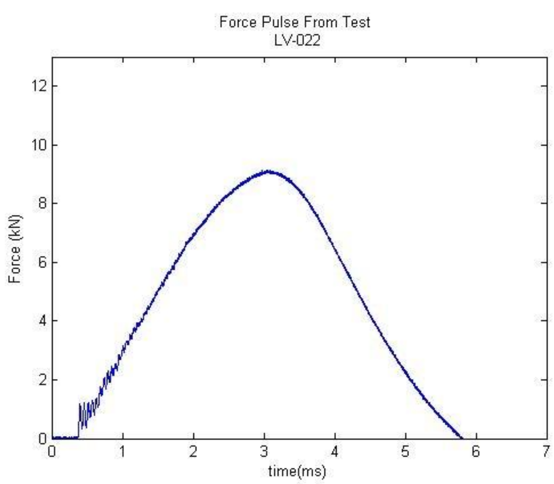
Force Pulse From Test
LV-022
Force (kN)
time(ms)
0
2
4
6
8
10
12
0
1
2
3
4
5
6
7

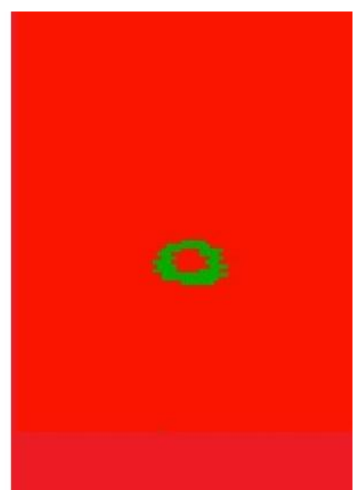

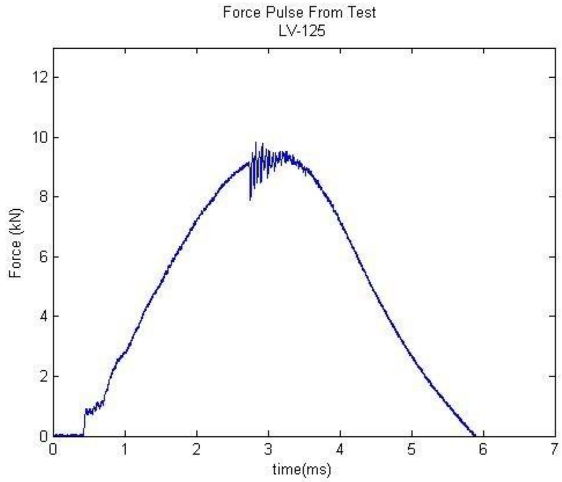
Force Pulse From Test
LV-125
Force (kN)
time(ms)

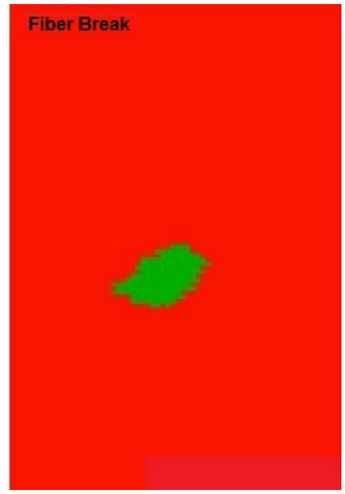
Fiber Break

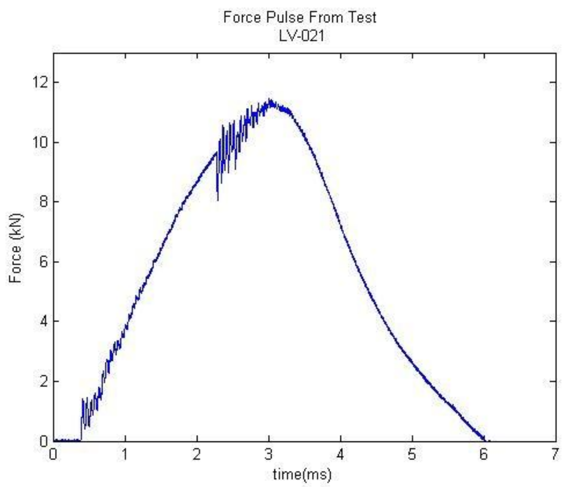
Force Pulse From Test
LV-021
Force (kN)
time(ms)

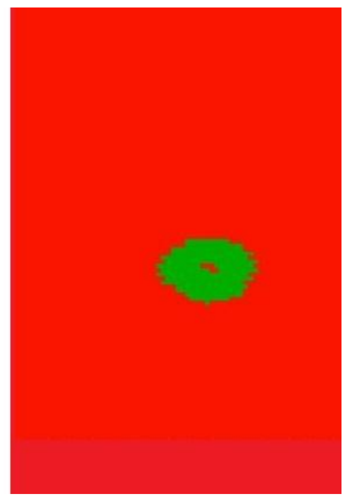

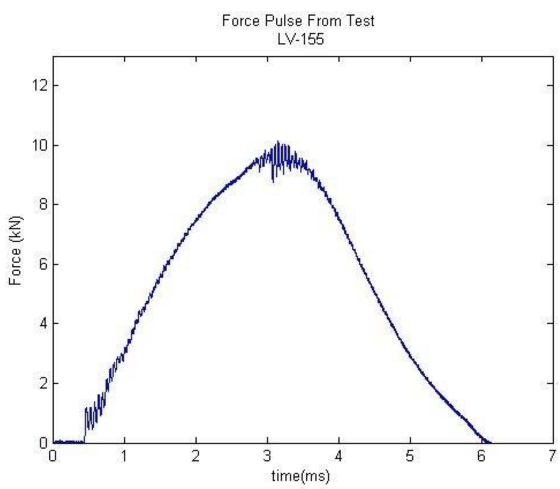
Force Pulse From Test
LV-155
Force (kN)
time(ms)

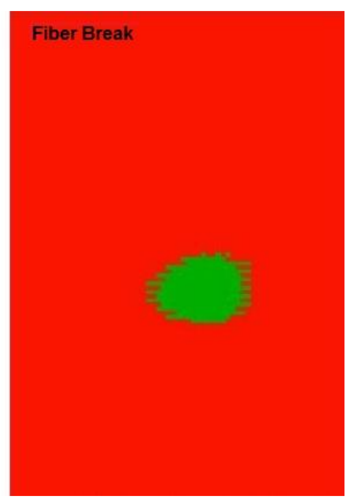
Fiber Break

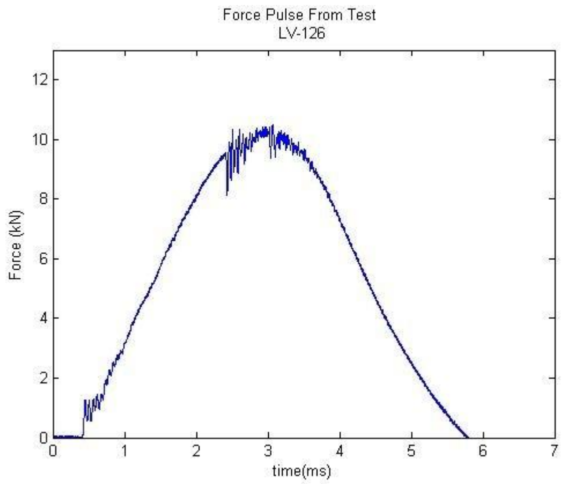

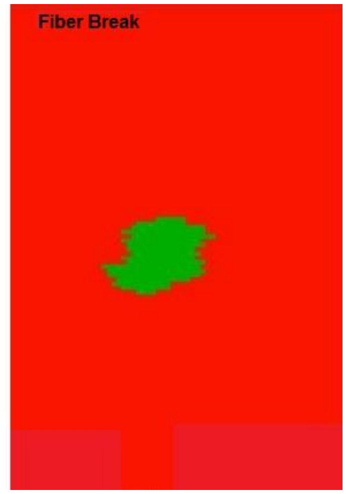

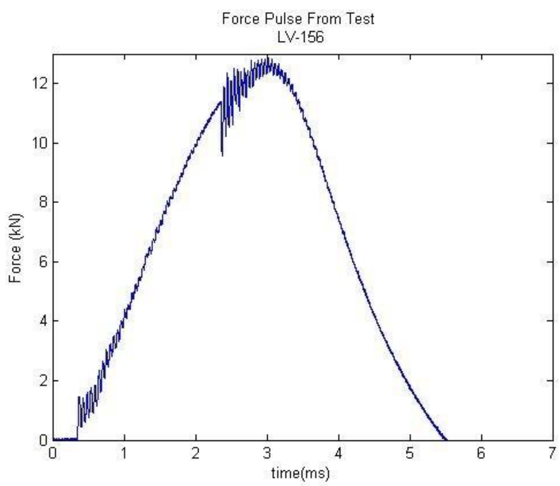

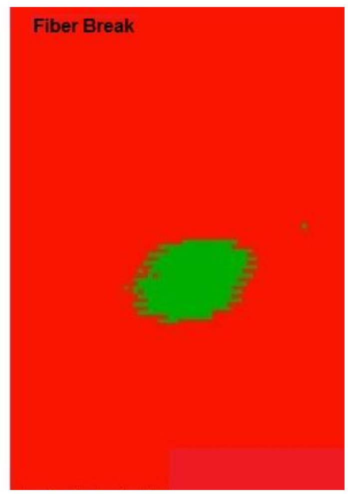

12.7 mm tip, 24 ply panel

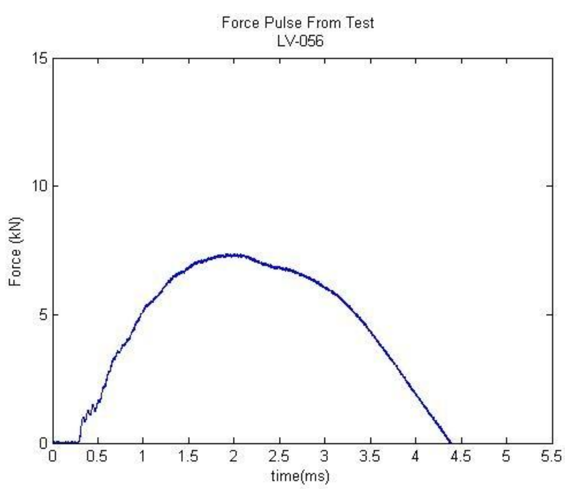

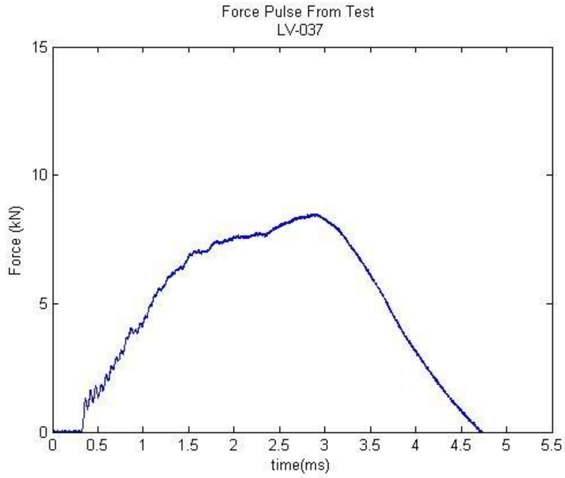
Force Pulse From Test
LV-037
Force (kN)
time(ms)
0
5
10
15
0
0.5
1
1.5
2
2.5
3
3.5
4
4.5
5
5.5

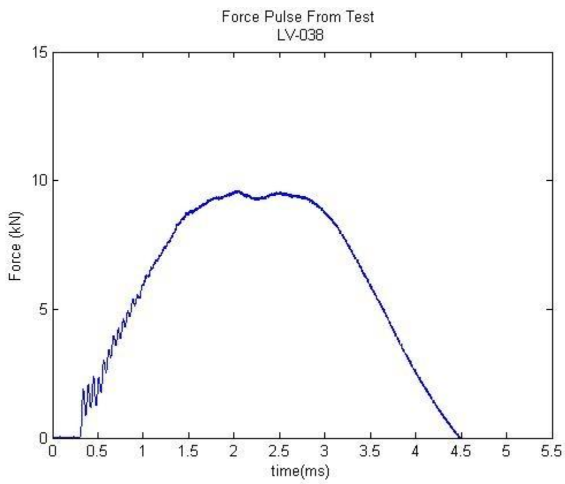
Force Pulse From Test
LV-038
Force (kN)
time(ms)
0
5
10
15
0
0.5
1
1.5
2
2.5
3
3.5
4
4.5
5
5.5

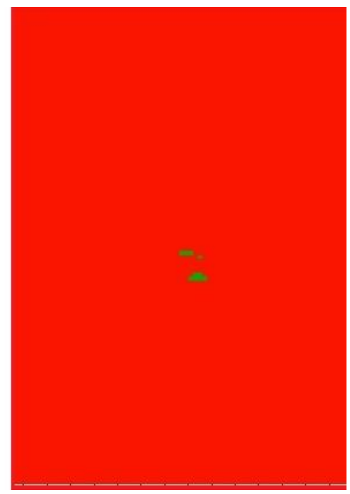

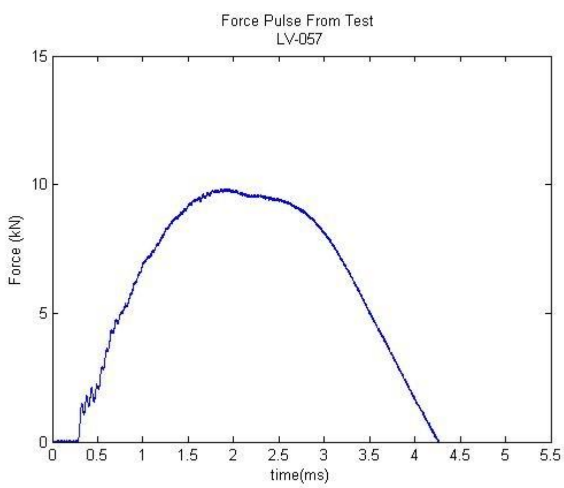
Force Pulse From Test
LV-057
Force (kN)
time(ms)
0
5
10
15
0
0.5
1
1.5
2
2.5
3
3.5
4
4.5
5
5.5

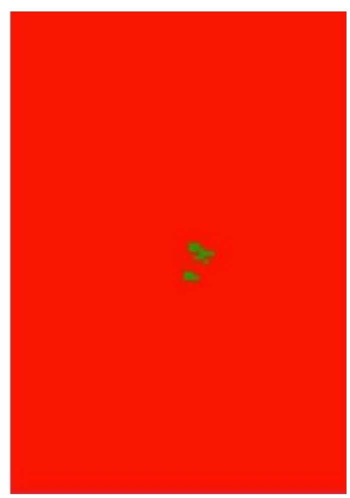

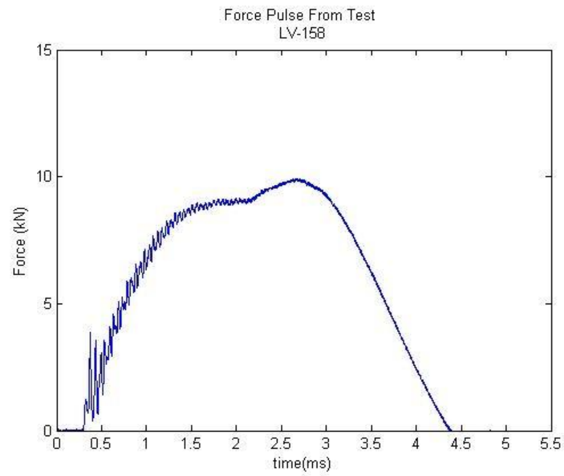
Force Pulse From Test
LV-158
Force (kN)
time(ms)
0
5
10
15
0
0.5
1
1.5
2
2.5
3
3.5
4
4.5
5
5.5

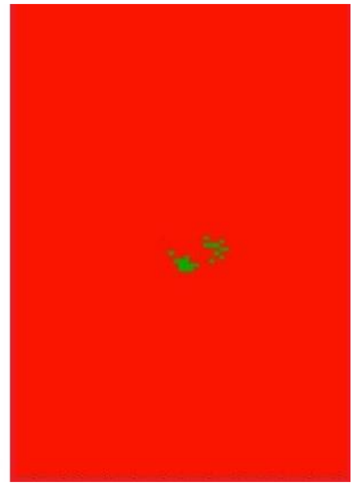

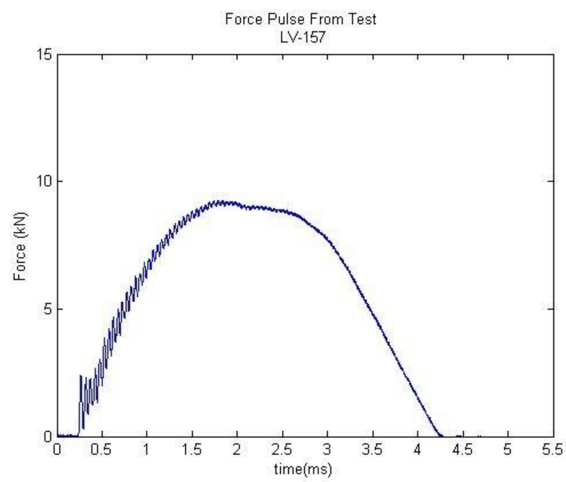
Force Pulse From Test
LV-157
Force (kN)
time(ms)
0
5
10
15
0
0.5
1
1.5
2
2.5
3
3.5
4
4.5
5
5.5

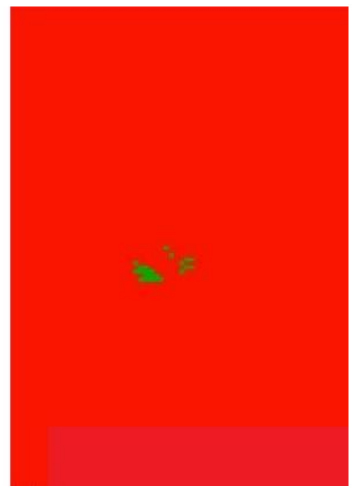

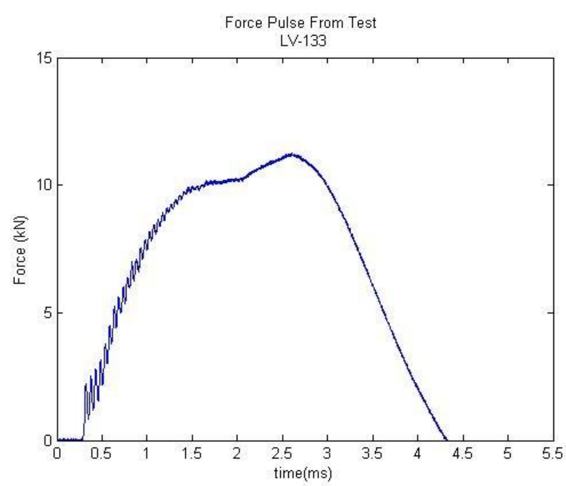
Force Pulse From Test
LV-133
Force (kN)
time(ms)
0
5
10
15
0
0.5
1
1.5
2
2.5
3
3.5
4
4.5
5
5.5

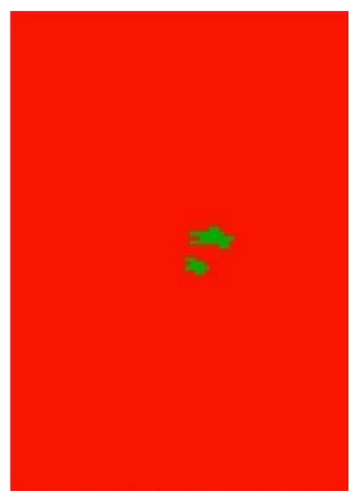

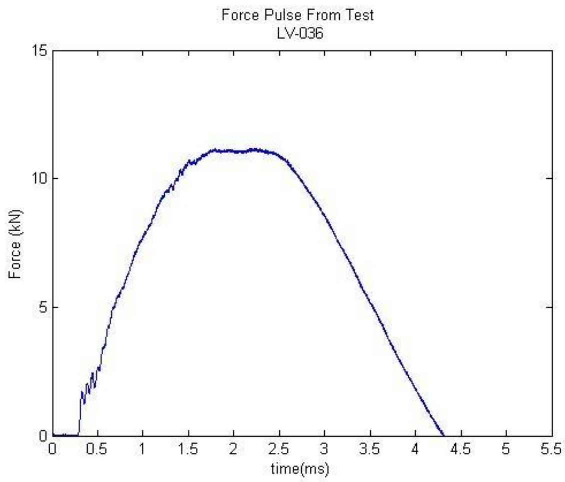
Force Pulse From Test
LV-036
Force (kN)
time(ms)
0
5
10
15
0.5
1
1.5
2
2.5
3
3.5
4
4.5
5
5.5

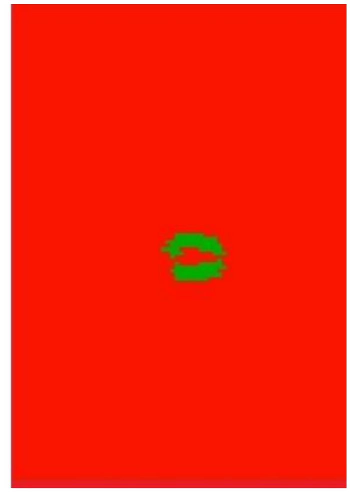

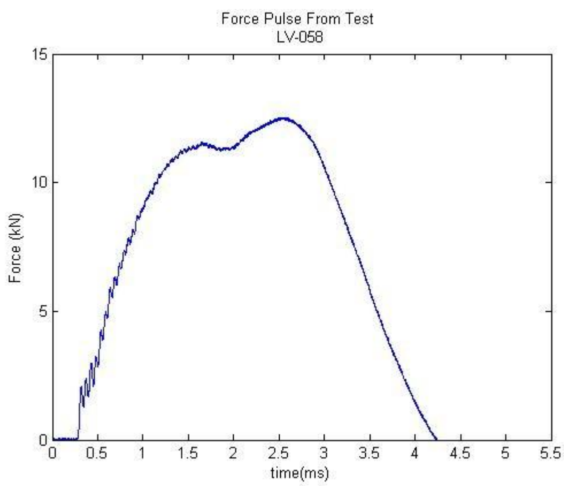
Force Pulse From Test
LV-058
Force (kN)
time(ms)
0
5
10
15
0.5
1
1.5
2
2.5
3
3.5
4
4.5
5
5.5

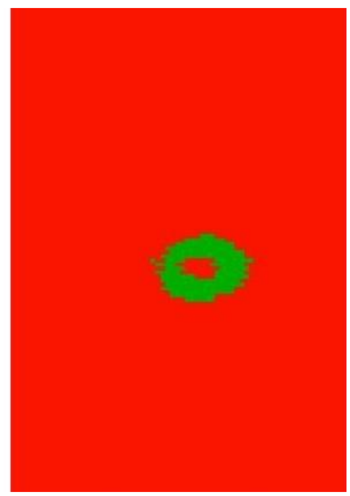

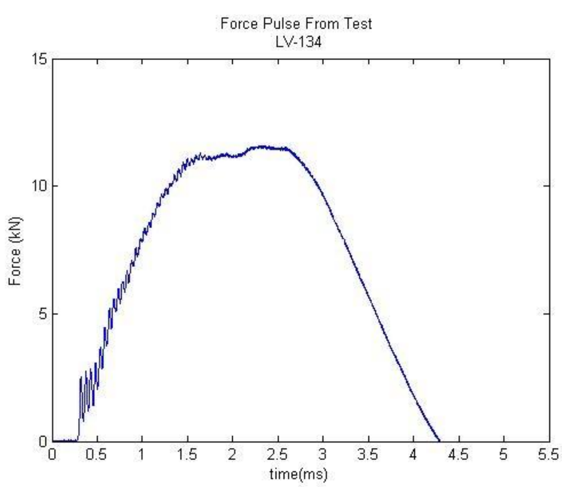
Force Pulse From Test
LV-134
Force (kN)
time(ms)
0
5
10
15
0.5
1
1.5
2
2.5
3
3.5
4
4.5
5
5.5

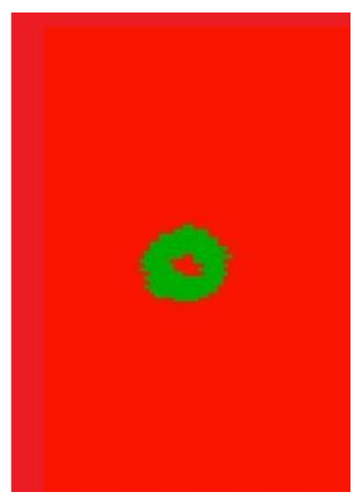

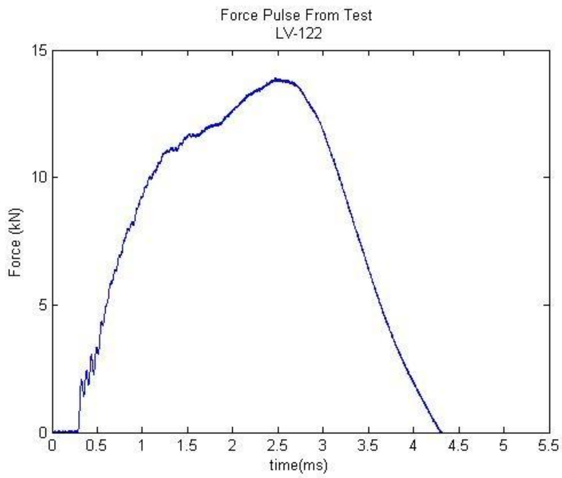
Force Pulse From Test
LV-122
Force (kN)
time(ms)
0
5
10
15
0
0.5
1
1.5
2
2.5
3
3.5
4
4.5
5
5.5

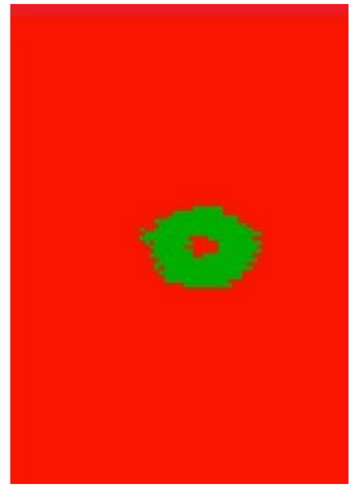

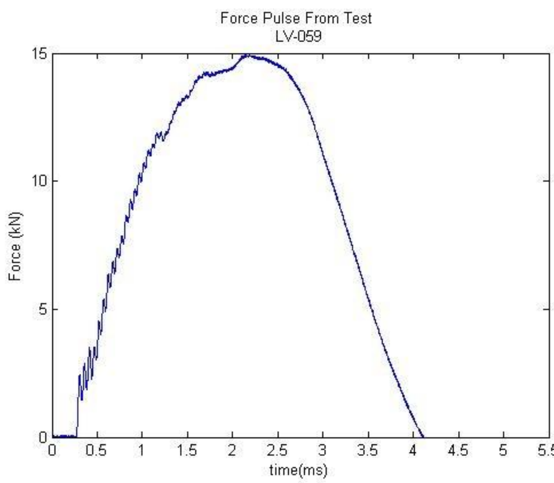
Force Pulse From Test
LV-059
Force (kN)
time(ms)
0
5
10
15
0
0.5
1
1.5
2
2.5
3
3.5
4
4.5
5
5.5

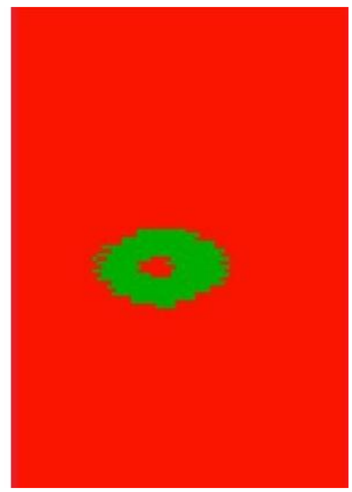

VIb. 25.4 mm tip,   8 ply panel

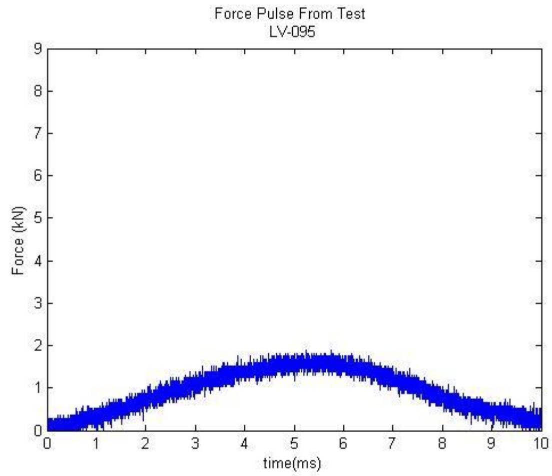

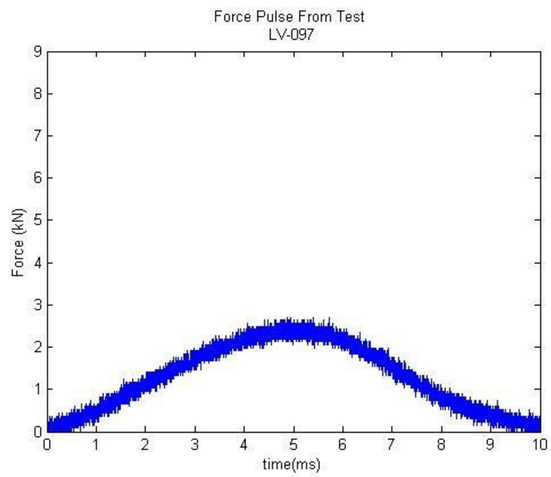

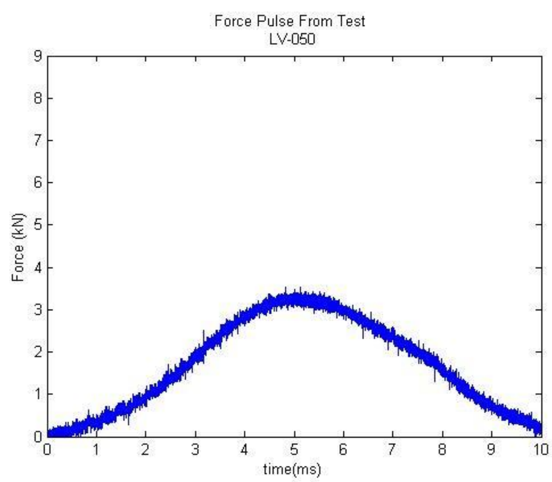

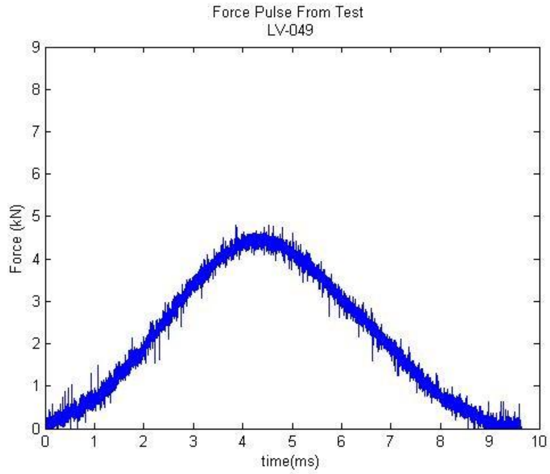
Force Pulse From Test
LV-049
Force (kN)
time(ms)

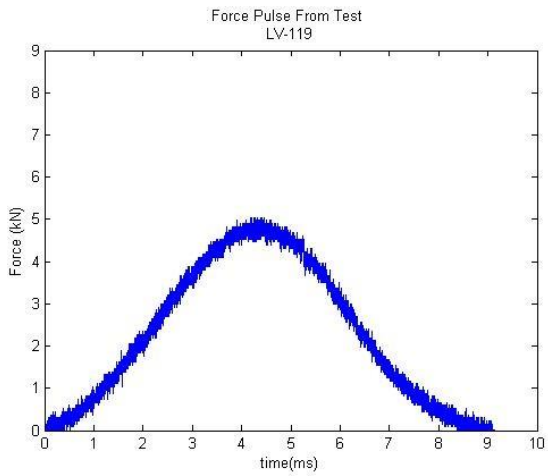
Force Pulse From Test
LV-119
Force (kN)
time(ms)

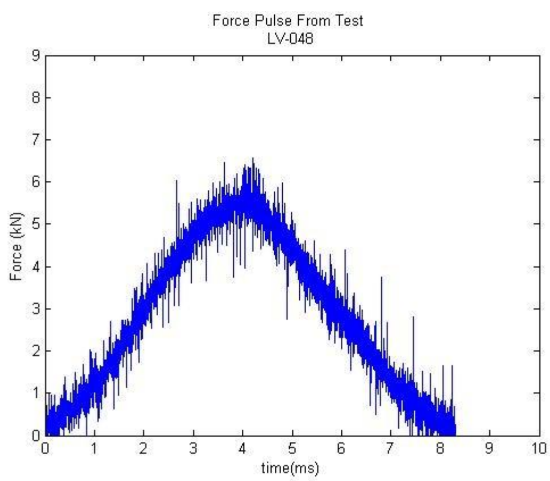
Force Pulse From Test
LV-048
Force (kN)
time(ms)

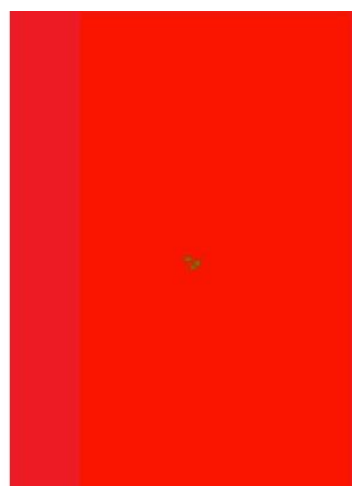

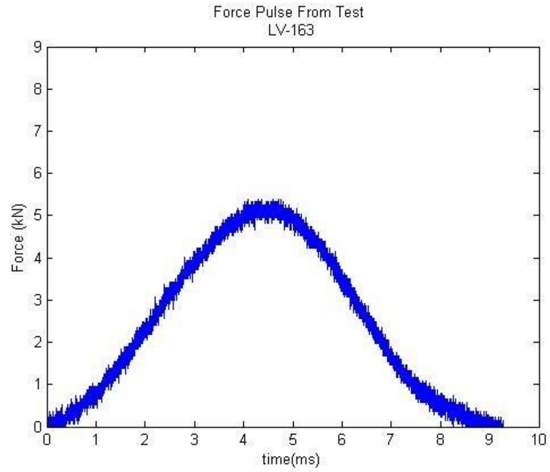
Force Pulse From Test
LV-163
Force (kN)
time(ms)

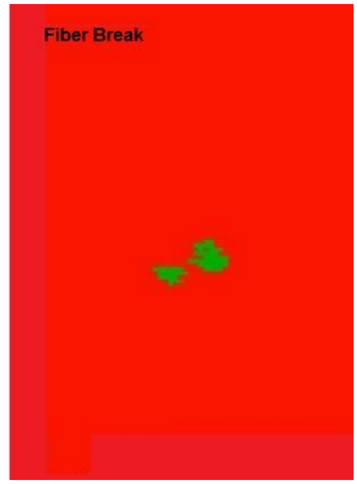
Fiber Break

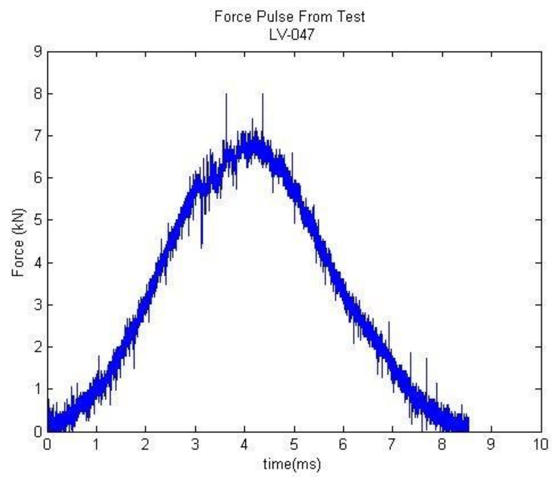
Force Pulse From Test
LV-047
Force (kN)
time(ms)

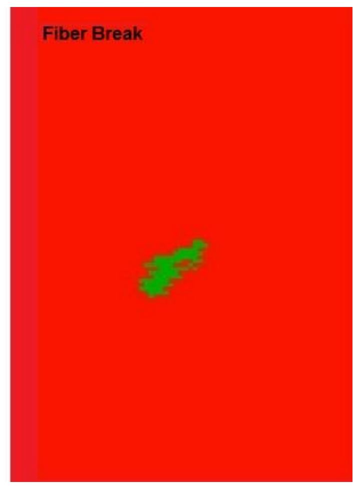
Fiber Break

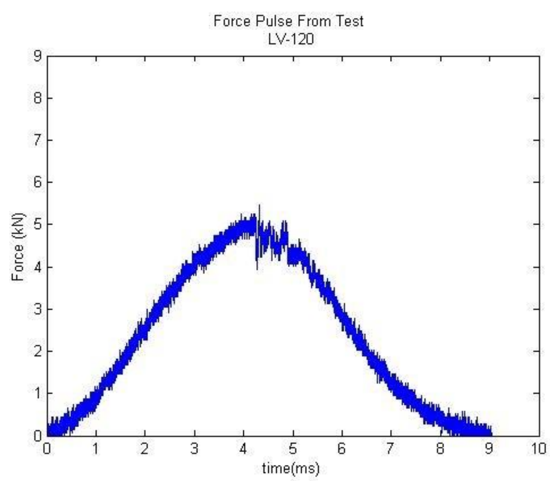
Force Pulse From Test
LV-120
Force (kN)
time(ms)

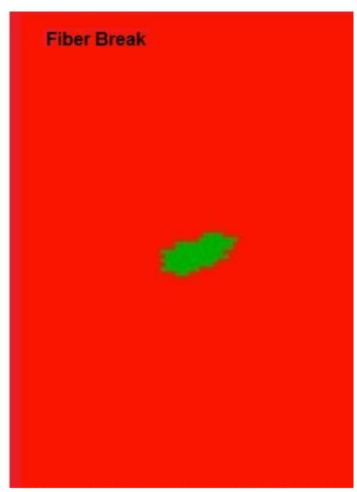
Fiber Break

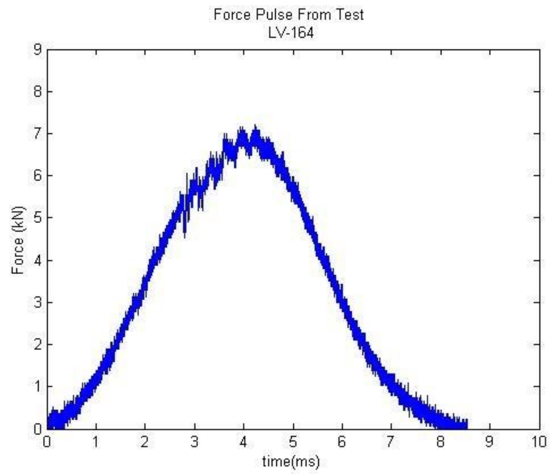
Force Pulse From Test
LV-164
Force (kN)
time(ms)
0 1 2 3 4 5 6 7 8 9 10
0 1 2 3 4 5 6 7 8 9

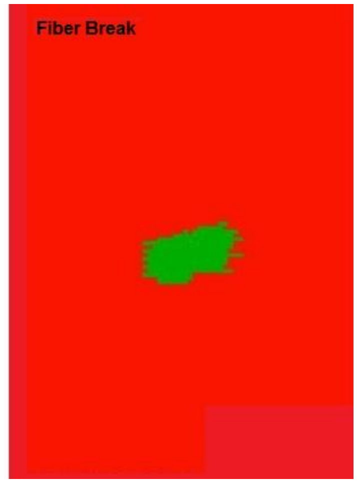
Fiber Break

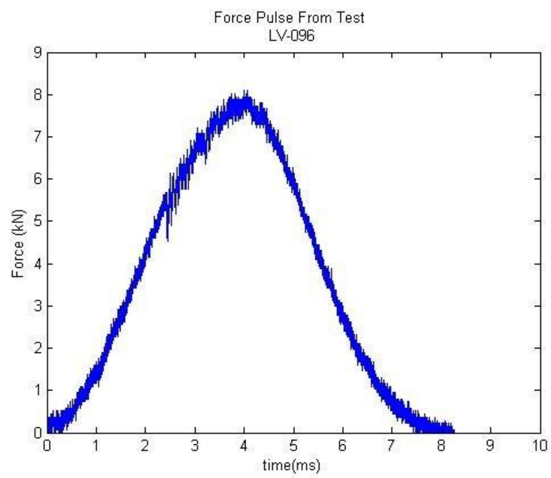
Force Pulse From Test
LV-096
Force (kN)
time(ms)
0 1 2 3 4 5 6 7 8 9 10
0 1 2 3 4 5 6 7 8 9

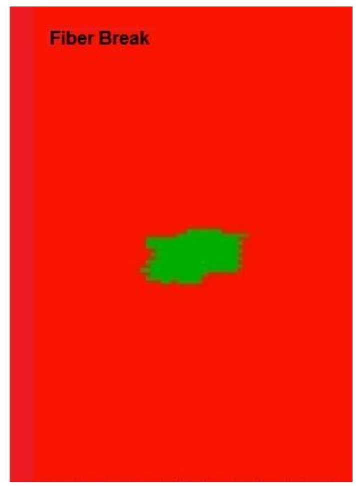
Fiber Break

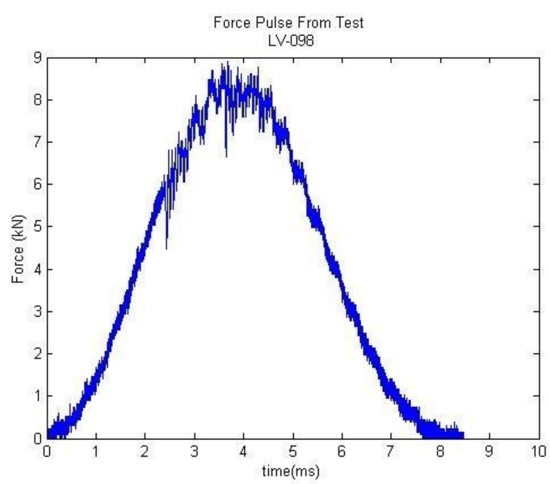
Force Pulse From Test
LV-098
Force (kN)
time(ms)
0 1 2 3 4 5 6 7 8 9 10
0 1 2 3 4 5 6 7 8 9

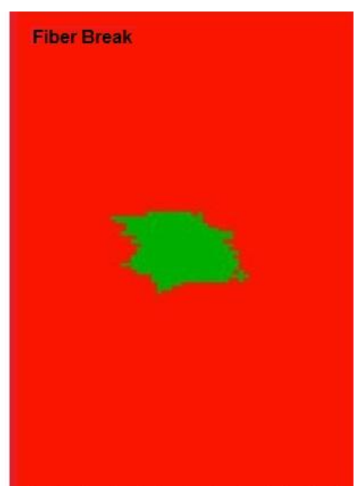
Fiber Break

25.4 mm tip, 16 ply panel

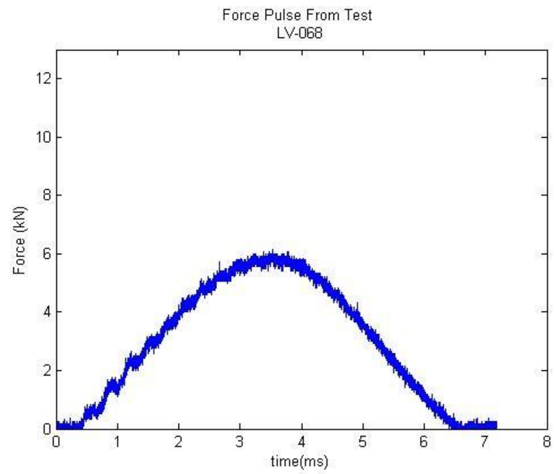

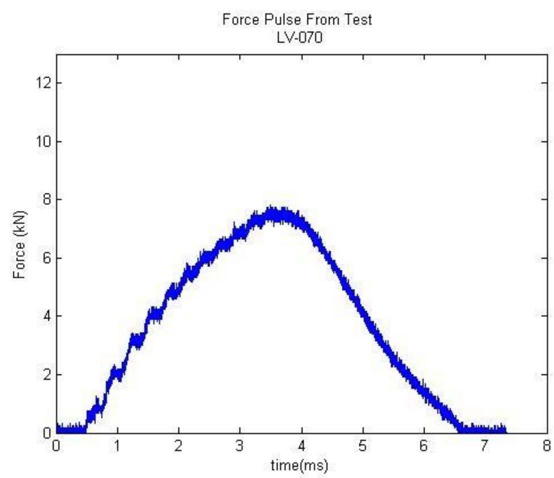

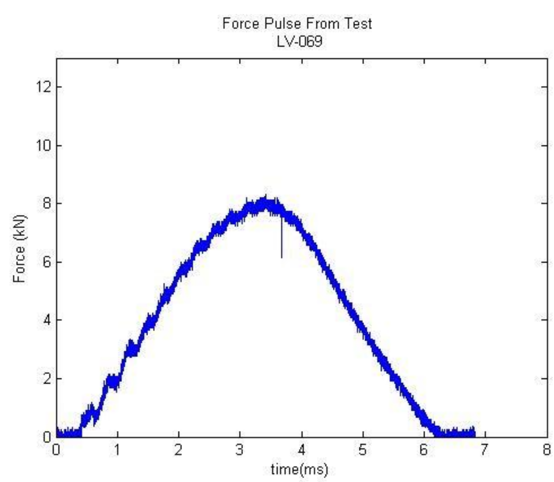

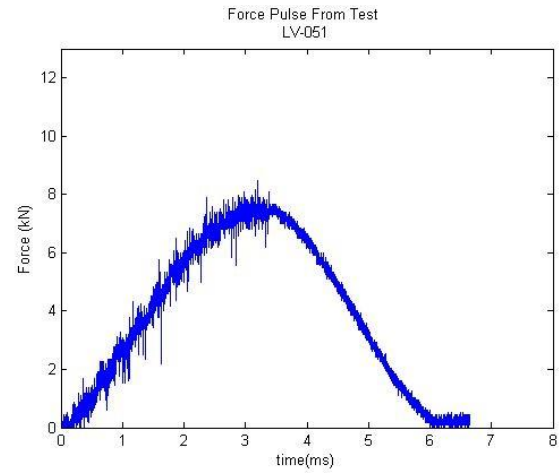
Force Pulse From Test
LV-051
Force (kN)
time(ms)

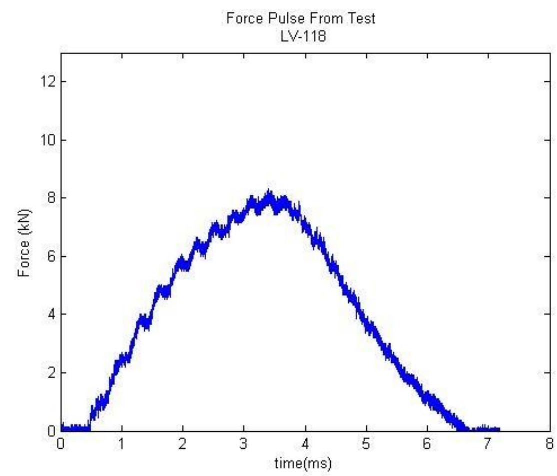
Force Pulse From Test
LV-118
Force (kN)
time(ms)

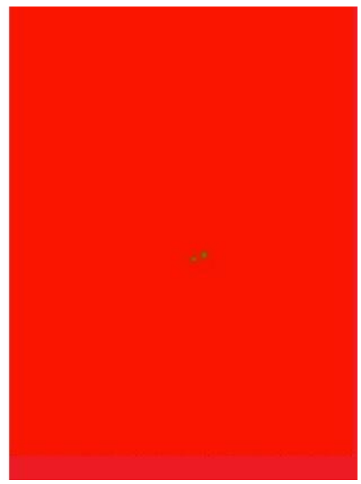

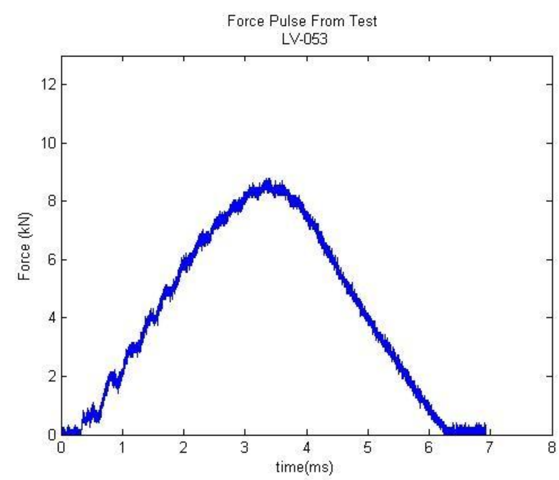
Force Pulse From Test
LV-053
Force (kN)
time(ms)

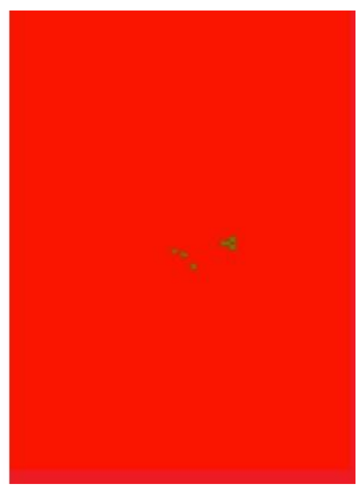

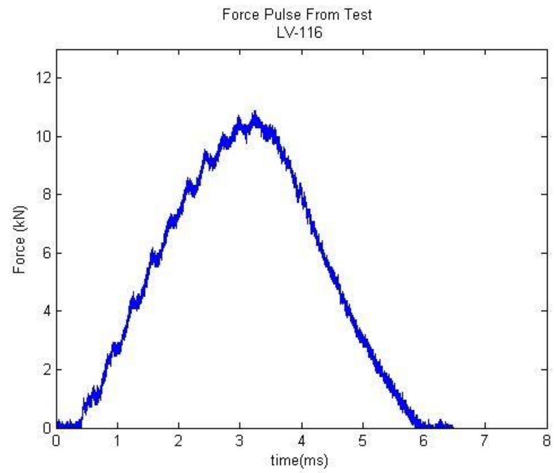
Force Pulse From Test
LV-116
Force (kN)
time(ms)

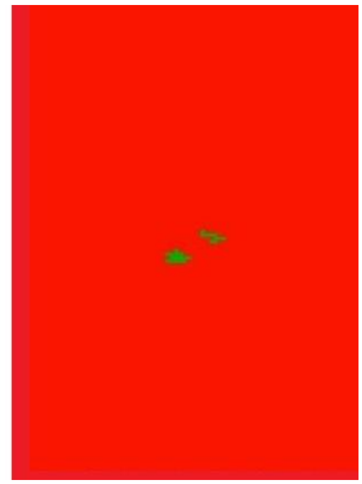

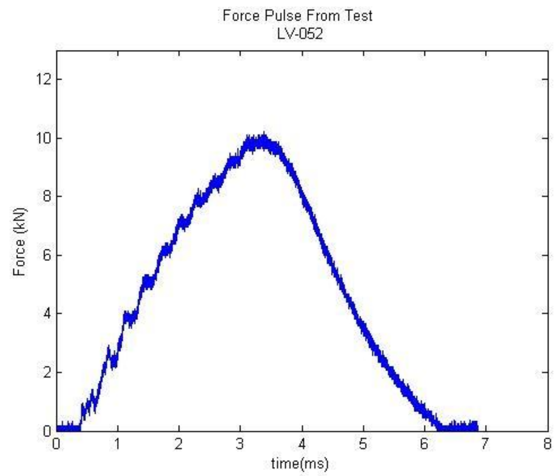
Force Pulse From Test
LV-052
Force (kN)
time(ms)

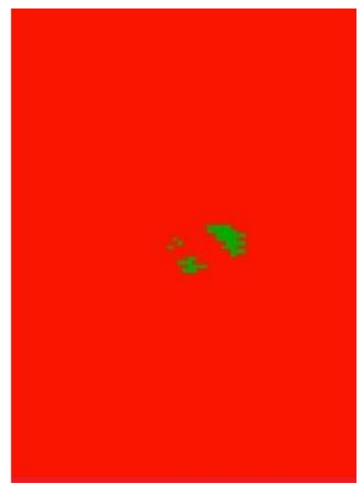

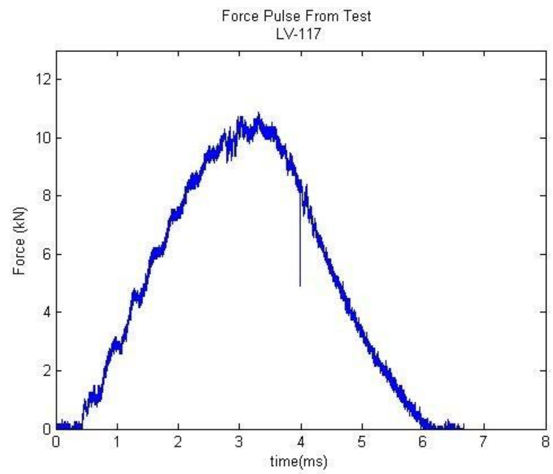
Force Pulse From Test
LV-117
Force (kN)
time(ms)

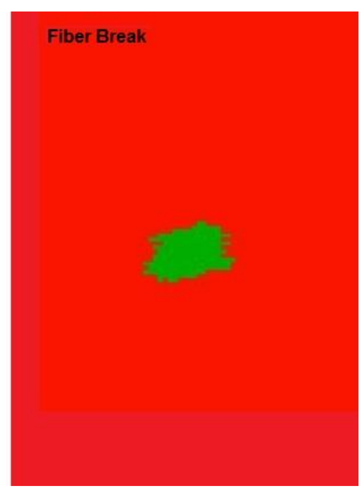
Fiber Break

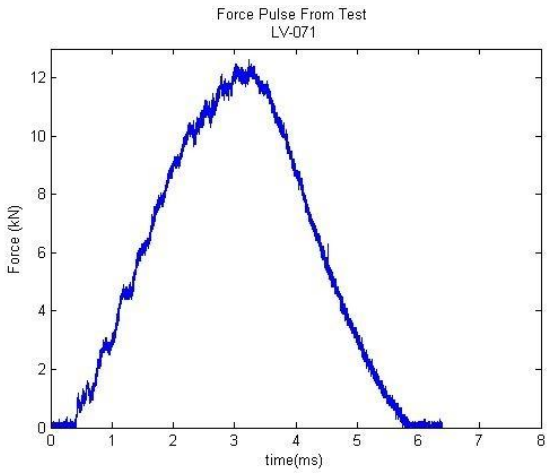
Force Pulse From Test
LV-071
Force (kN)
time(ms)
0
2
4
6
8
10
12
1
3
5
7

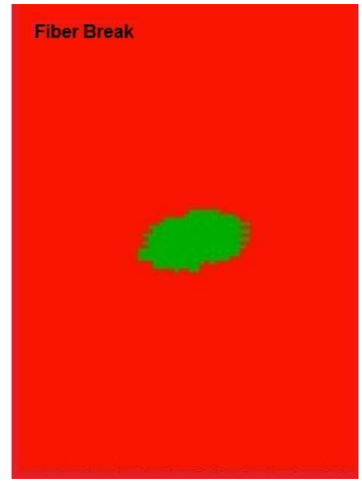
Fiber Break

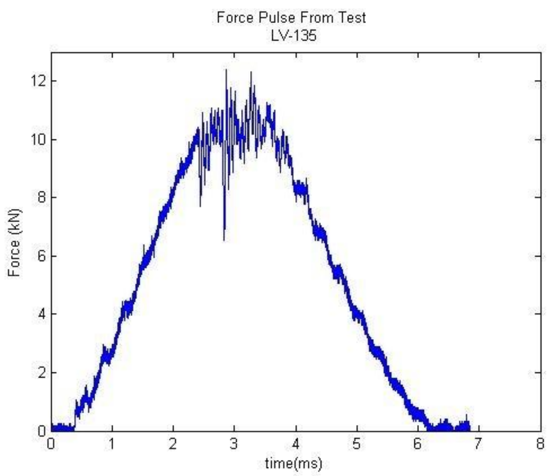
Force Pulse From Test
LV-135
Force (kN)
time(ms)

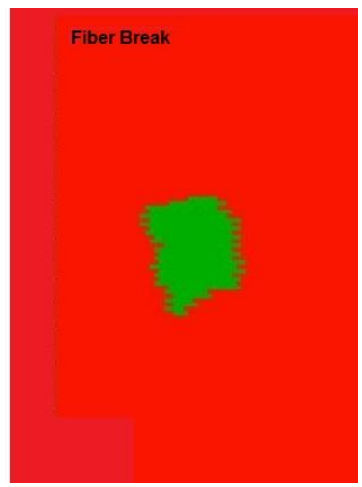
Fiber Break

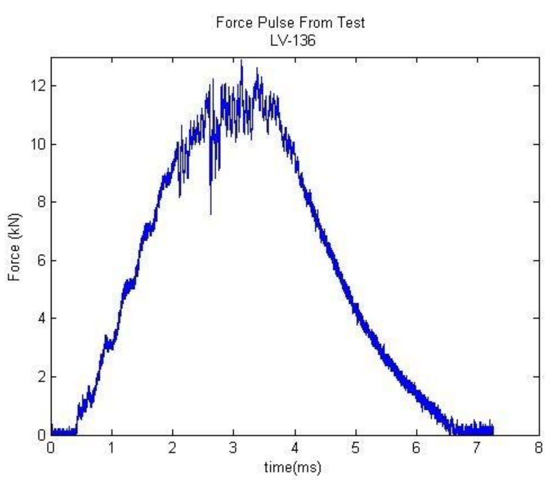
Force Pulse From Test
LV-136
Force (kN)
time(ms)

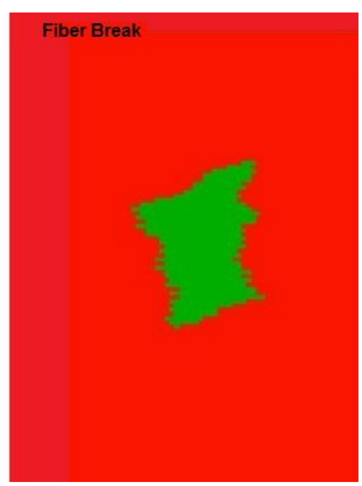
Fiber Break

25.4 mm tip, 24 ply panel

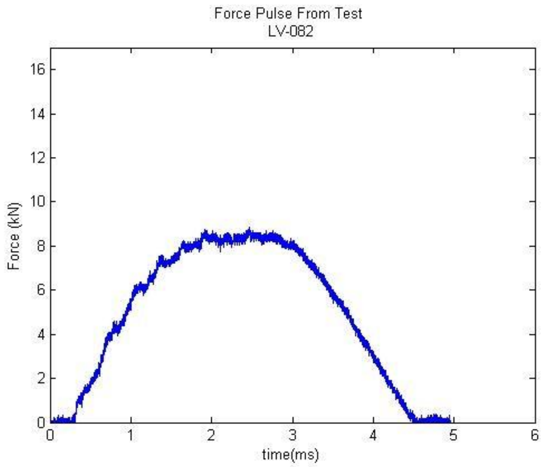

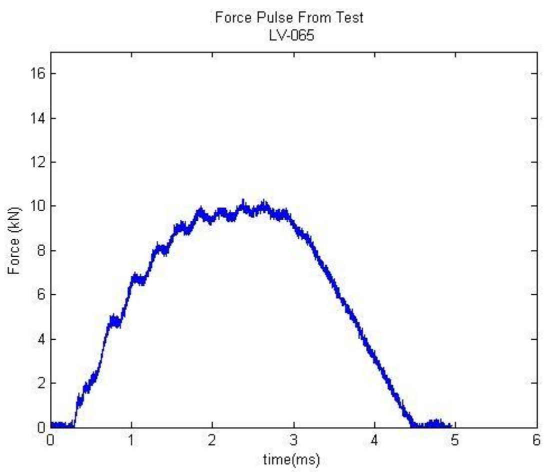

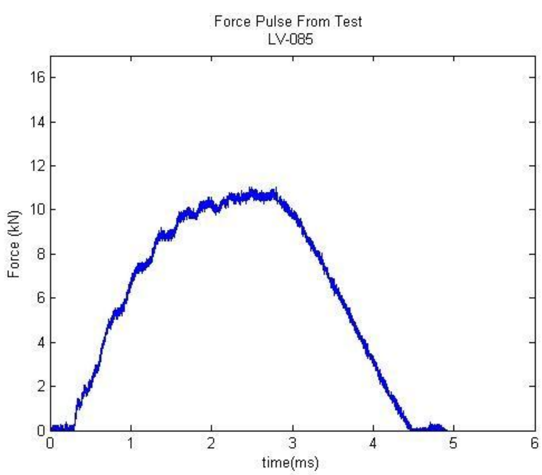

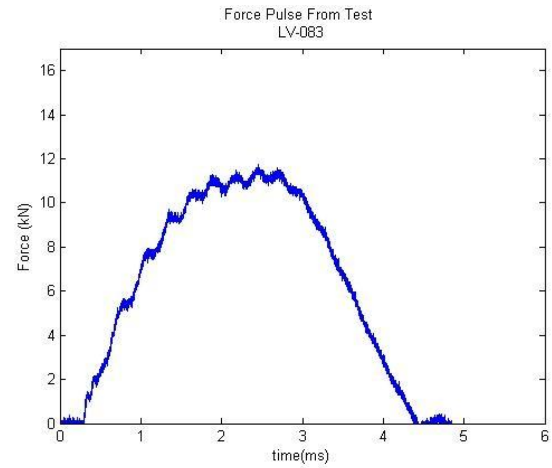
Force Pulse From Test
LV-083
Force (kN)
time(ms)

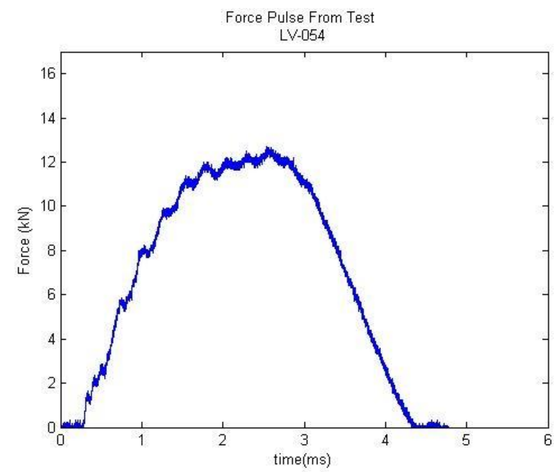
Force Pulse From Test
LV-054
Force (kN)
time(ms)

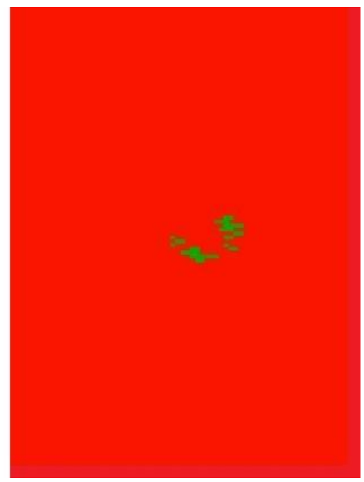

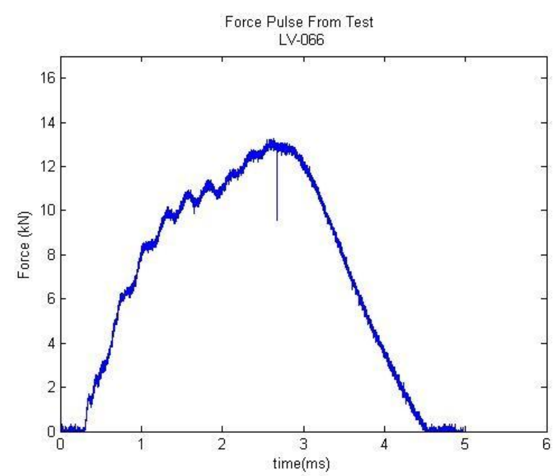
Force Pulse From Test
LV-066
Force (kN)
time(ms)

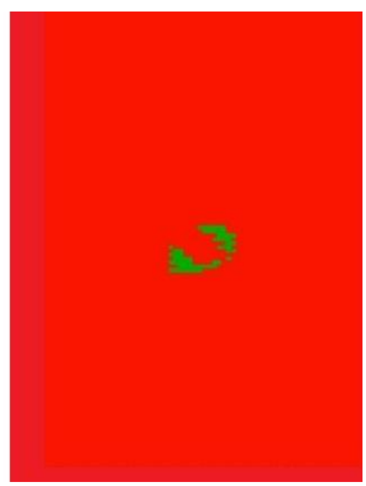

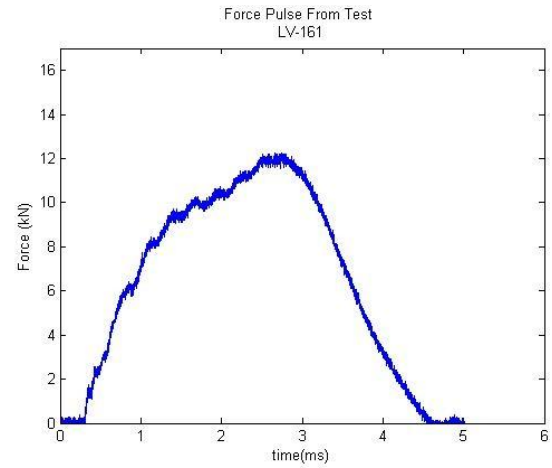
Force Pulse From Test
LV-161
Force (kN)
time(ms)
0
2
4
6
8
10
12
14
16
0
1
2
3
4
5
6

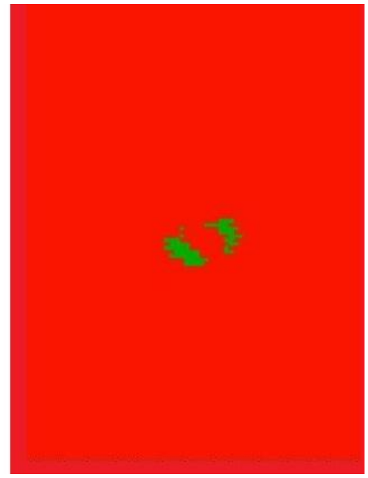

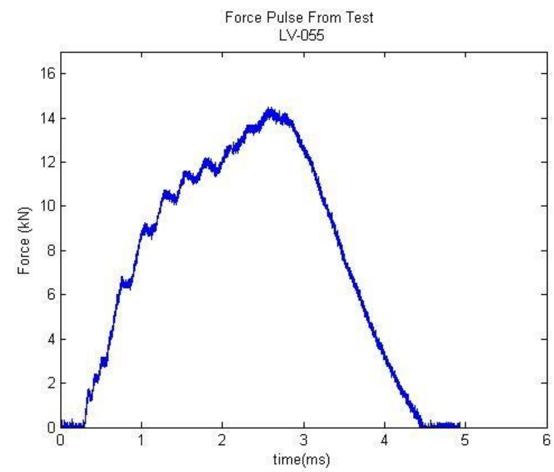
Force Pulse From Test
LV-055
Force (kN)
time(ms)
0
2
4
6
8
10
12
14
16
0
1
2
3
4
5
6

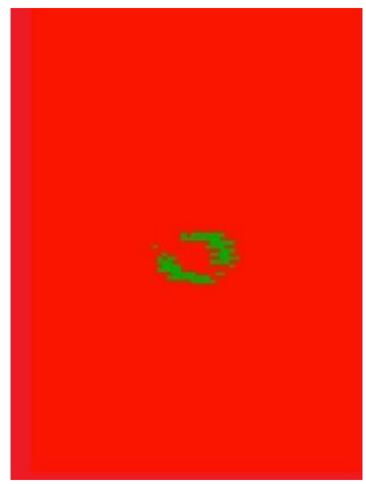

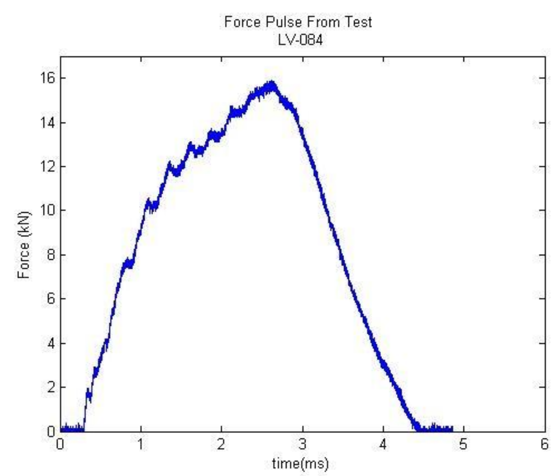
Force Pulse From Test
LV-084
Force (kN)
time(ms)
0
2
4
6
8
10
12
14
16
0
1
2
3
4
5
6

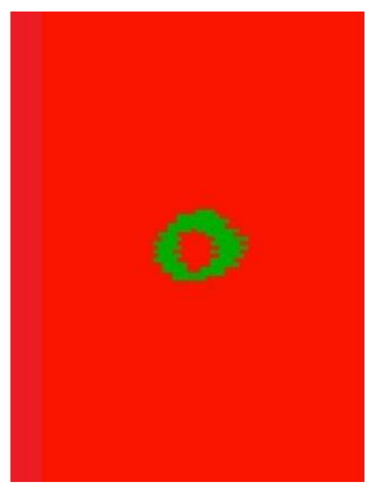

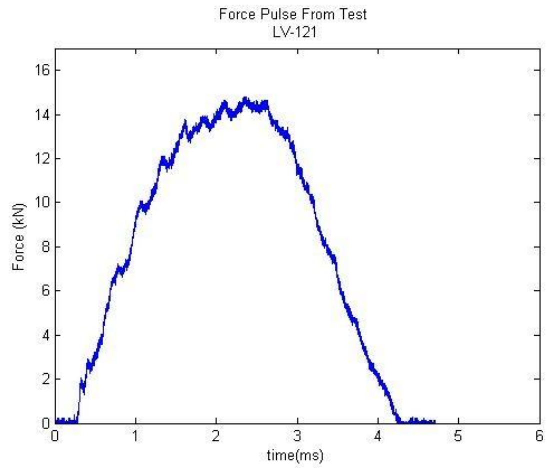
Force Pulse From Test
LV-121
Force (kN)
time(ms)
0
2
4
6
8
10
12
14
16
0
1
2
3
4
5
6

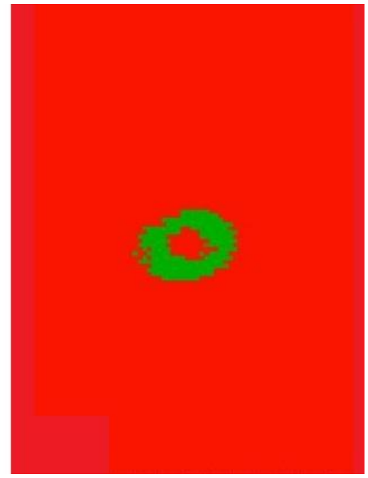

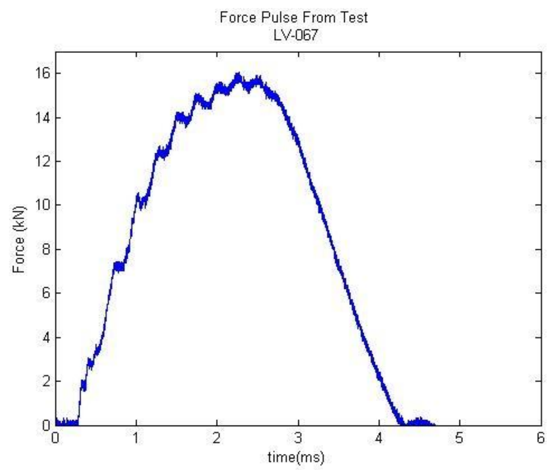
Force Pulse From Test
LV-067
Force (kN)
time(ms)
0
2
4
6
8
10
12
14
16
0
1
2
3
4
5
6

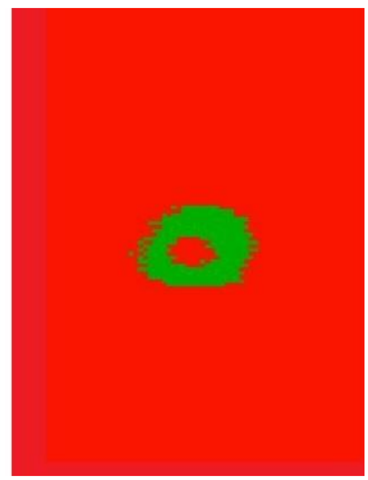

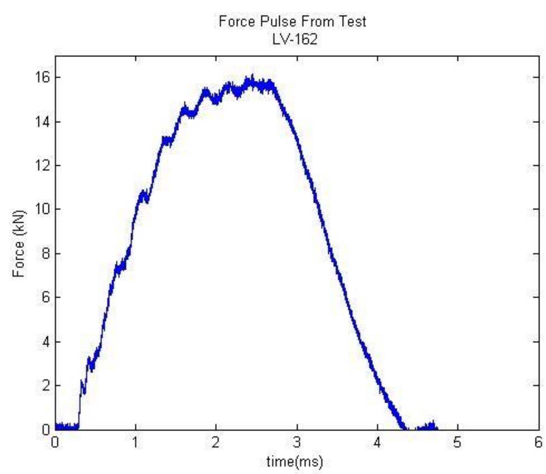
Force Pulse From Test
LV-162
Force (kN)
time(ms)
0
2
4
6
8
10
12
14
16
0
1
2
3
4
5
6

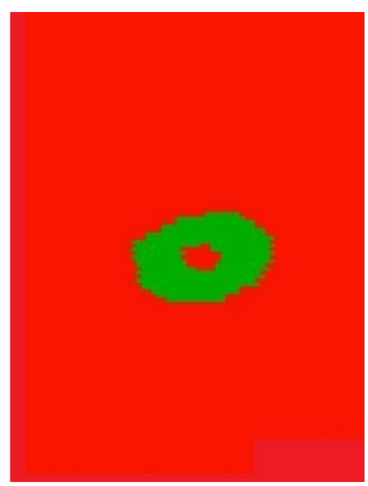

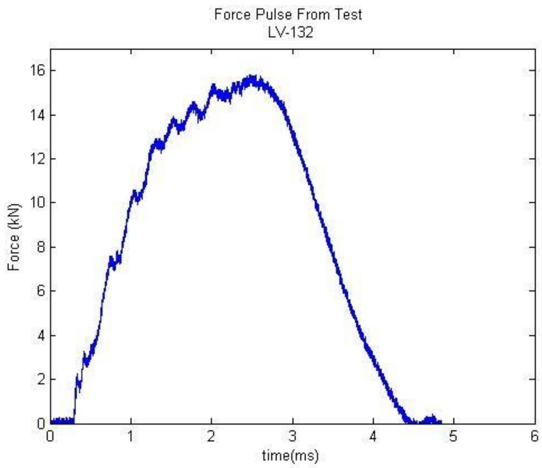
Force Pulse From Test
LV-132
Force (kN)
time(ms)
0
2
4
6
8
10
12
14
16
0
1
2
3
4
5
6

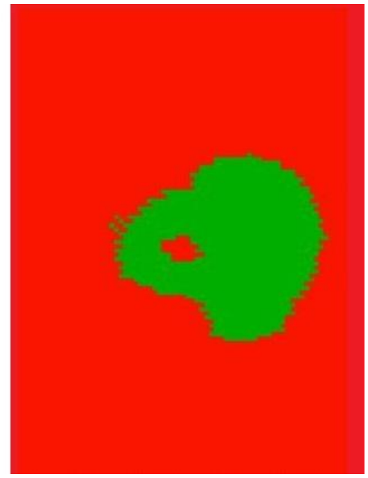

VIc. 50.8 mm tip, 8 ply panel

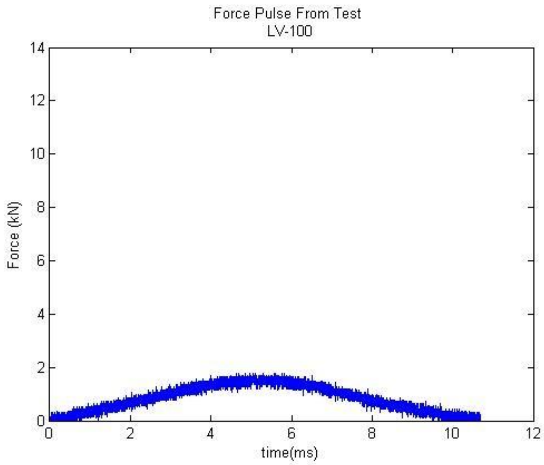

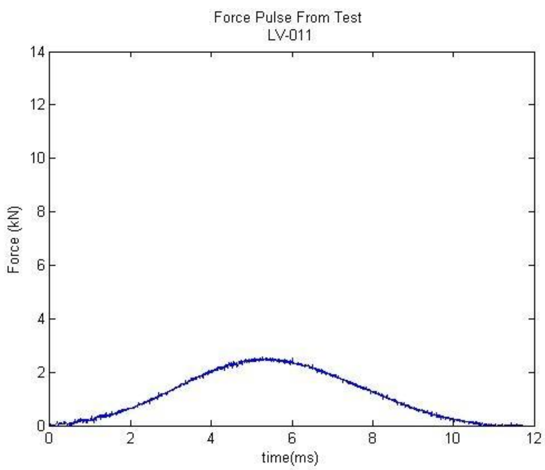

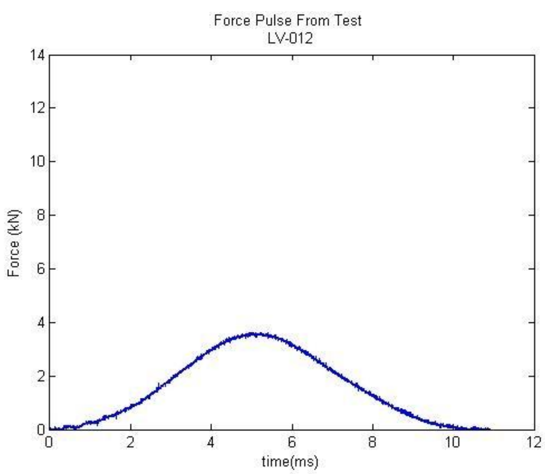

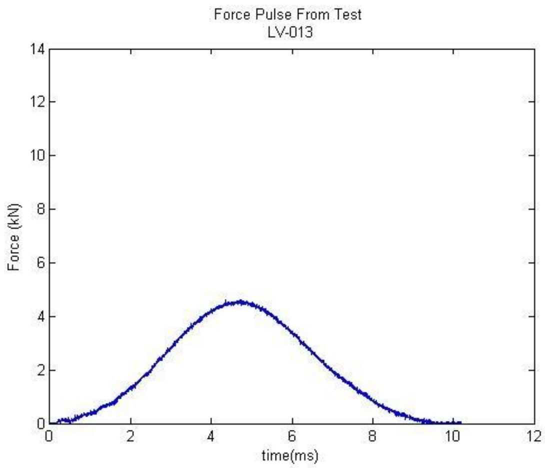
Force Pulse From Test
LV-013
Force (kN)
time(ms)
0
2
4
6
8
10
12
14

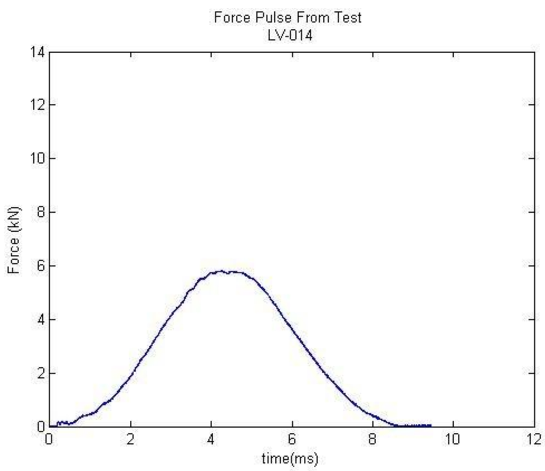
Force Pulse From Test
LV-014
Force (kN)
time(ms)
0
2
4
6
8
10
12
14

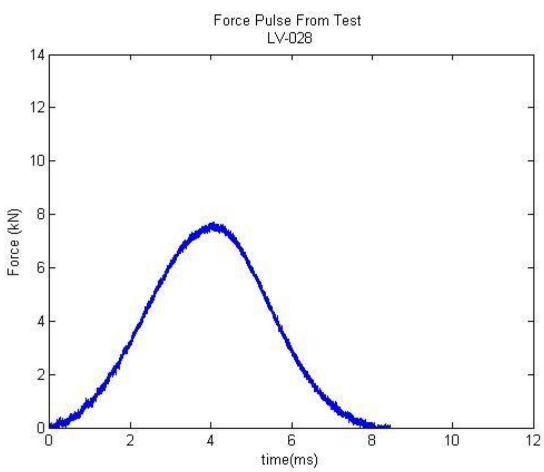
Force Pulse From Test
LV-028
Force (kN)
time(ms)
0
2
4
6
8
10
12
14

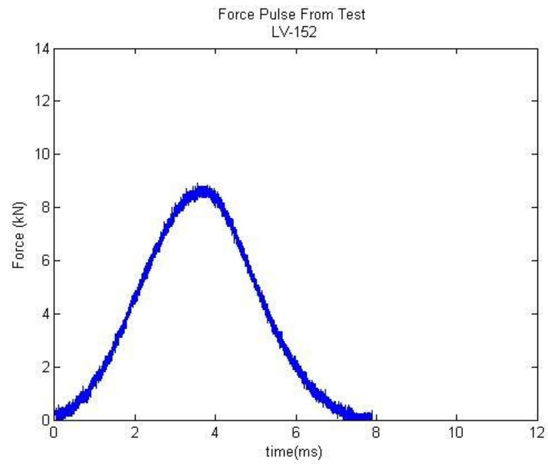
Force Pulse From Test
LV-152
Force (kN)
time(ms)
0
2
4
6
8
10
12
14

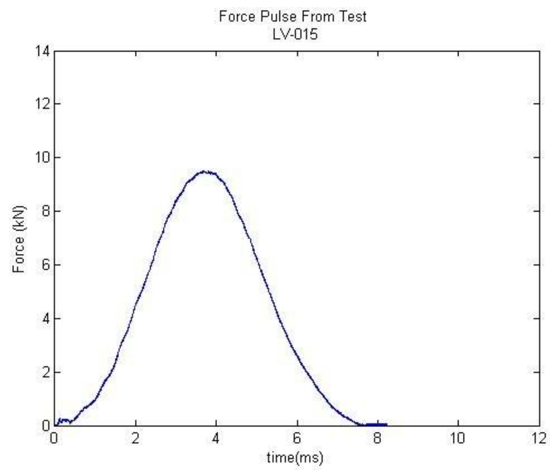
Force Pulse From Test
LV-015
Force (kN)
time(ms)
0
2
4
6
8
10
12
14

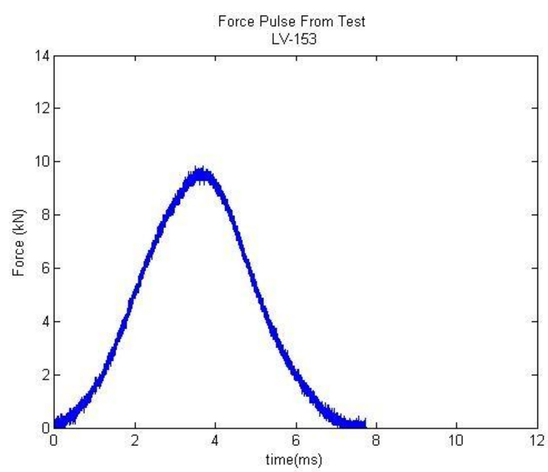
Force Pulse From Test
LV-153
Force (kN)
time(ms)
0
2
4
6
8
10
12
14

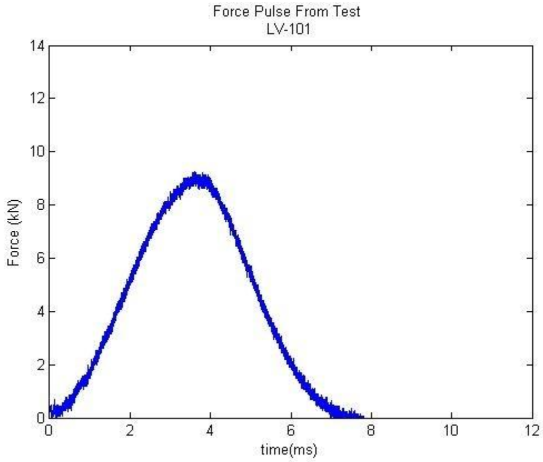
Force Pulse From Test
LV-101
Force (kN)
time(ms)
0
2
4
6
8
10
12
14

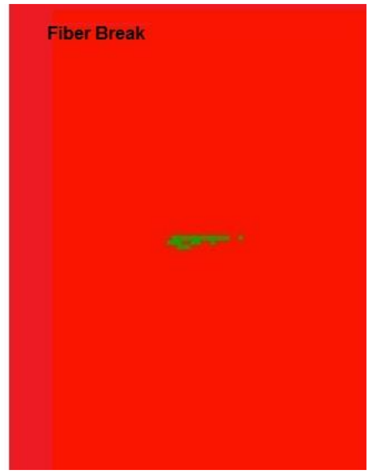
Fiber Break

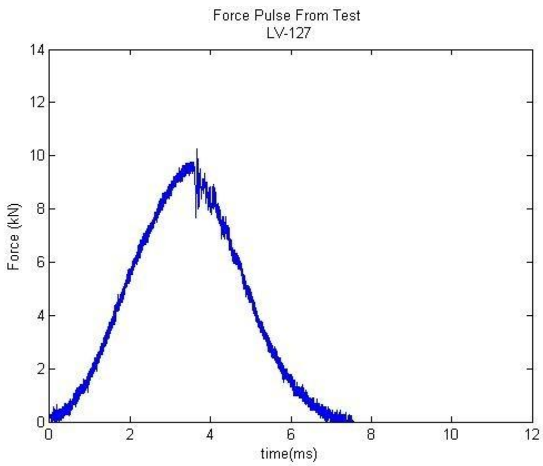
Force Pulse From Test
LV-127
Force (kN)
time(ms)
0
2
4
6
8
10
12
14

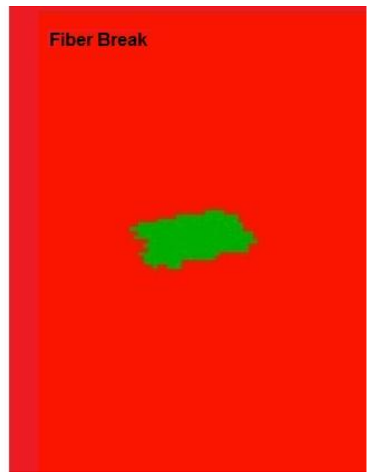
Fiber Break

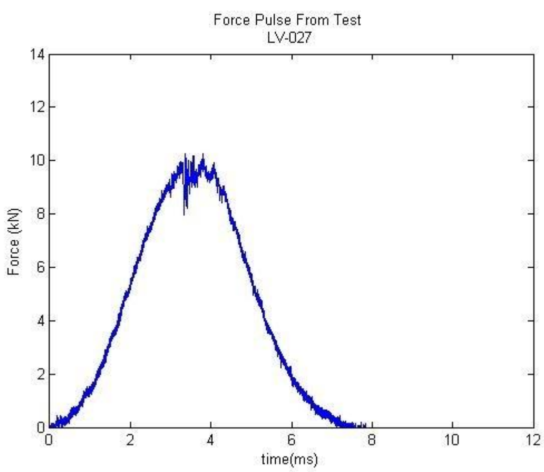
Force Pulse From Test
LV-027
Force (kN)
time(ms)
0
2
4
6
8
10
12
14

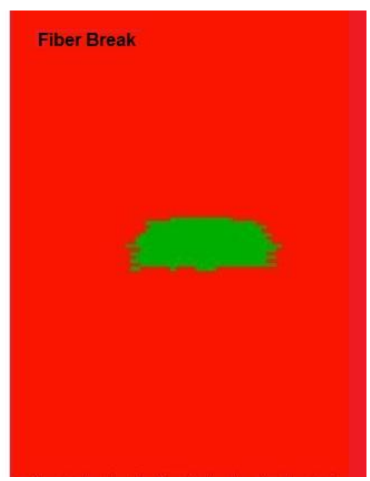
Fiber Break

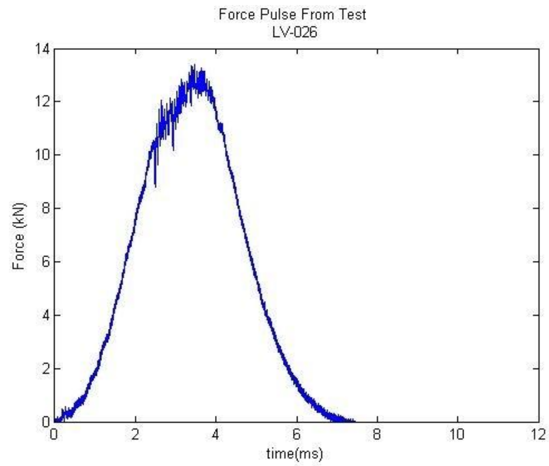

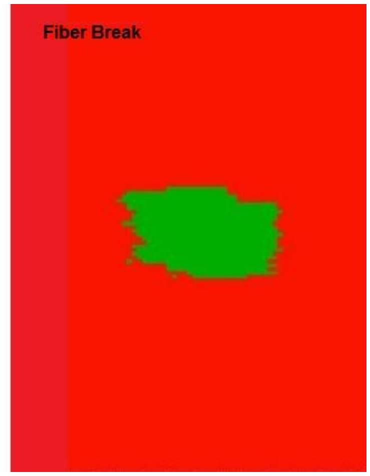

50.8 mm tip, 16 ply panel

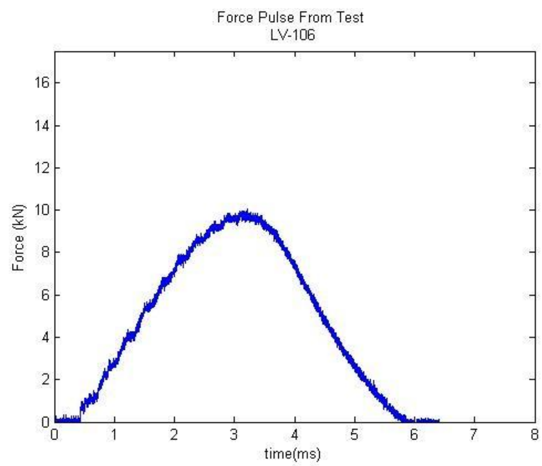

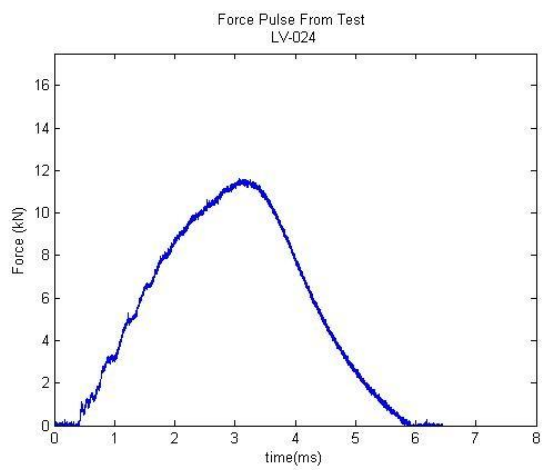

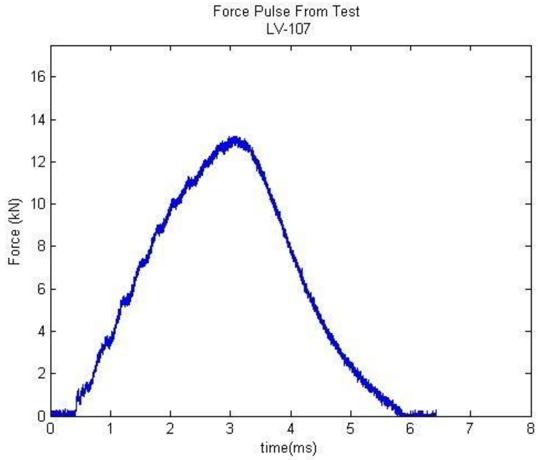
Force Pulse From Test
LV-107
Force (kN)
time(ms)

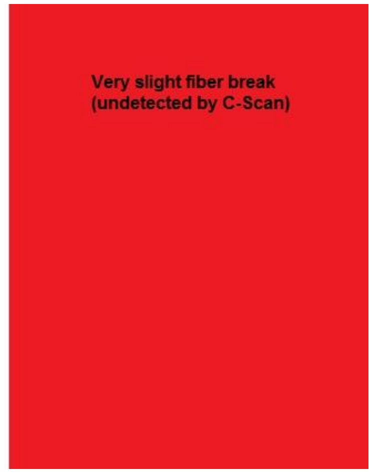
Very slight fiber break
(undetected by C-Scan)

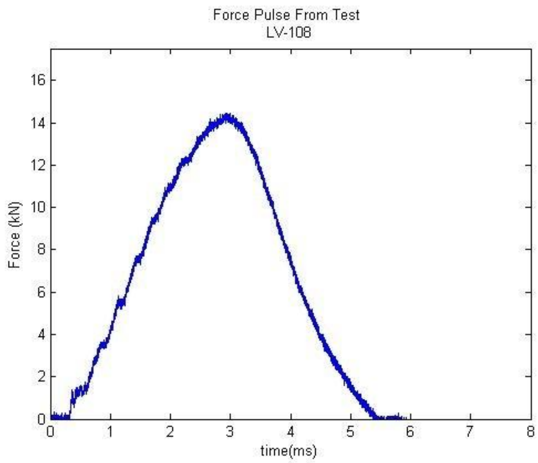
Force Pulse From Test
LV-108
Force (kN)
time(ms)

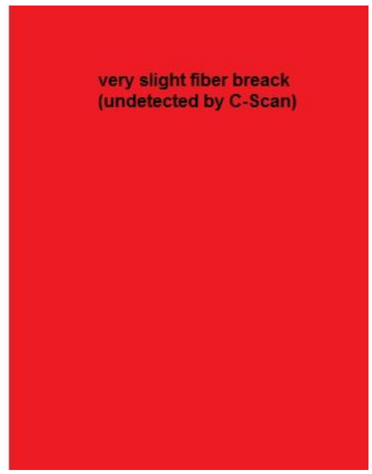
very slight fiber breack
(undetected by C-Scan)

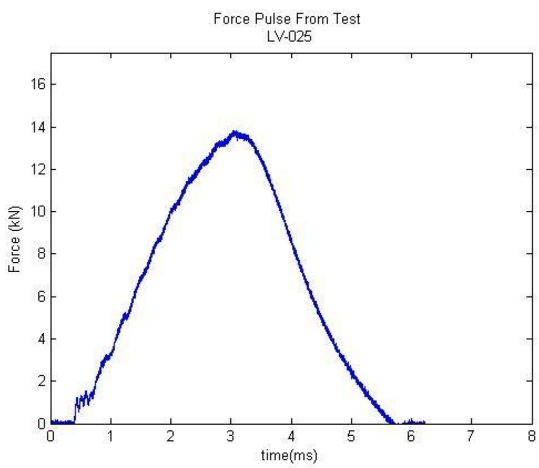
Force Pulse From Test
LV-025
Force (kN)
time(ms)

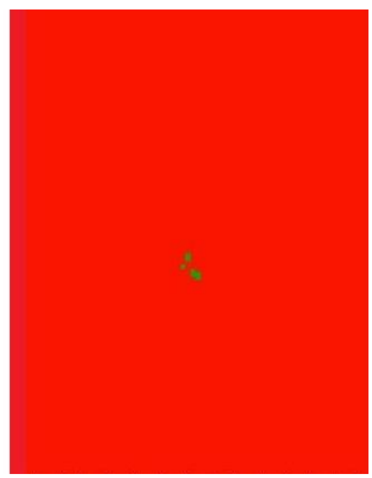

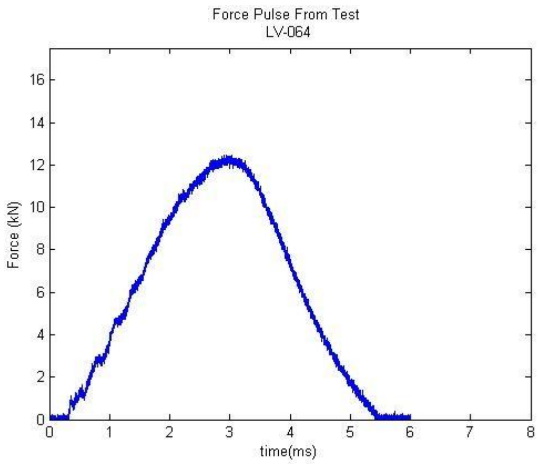
Force Pulse From Test
LV-064
Force (kN)
time(ms)

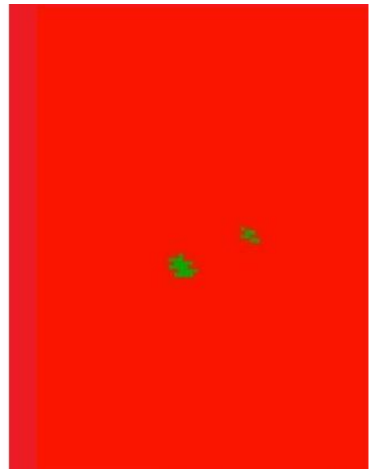

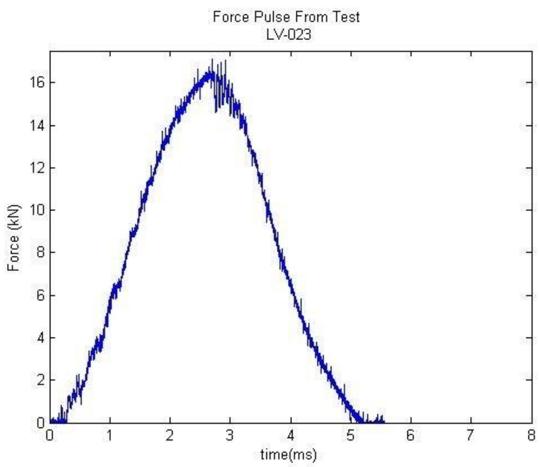
Force Pulse From Test
LV-023
Force (kN)
time(ms)

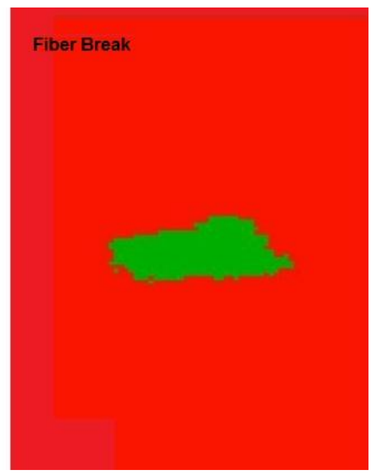
Fiber Break

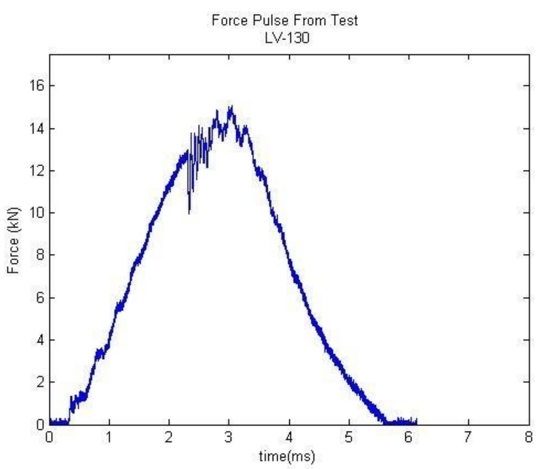
Force Pulse From Test
LV-130
Force (kN)
time(ms)

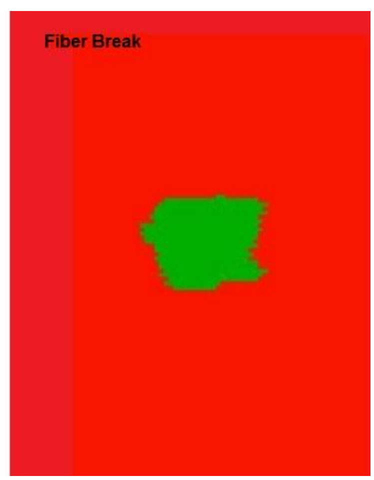
Fiber Break

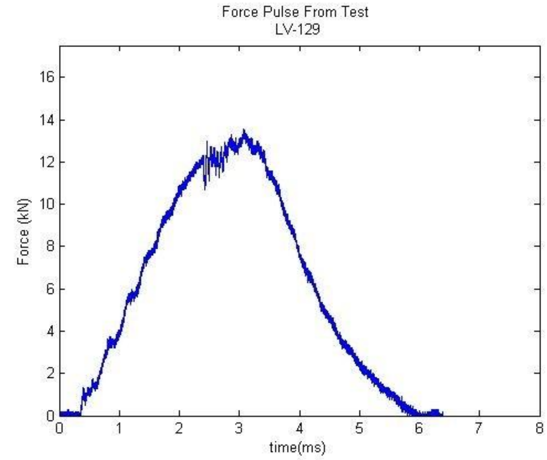
Force Pulse From Test
LV-129
Force (kN)
time(ms)

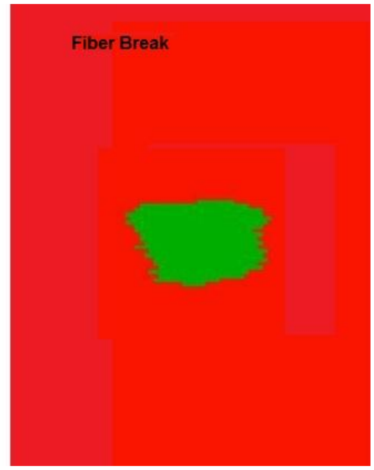
Fiber Break

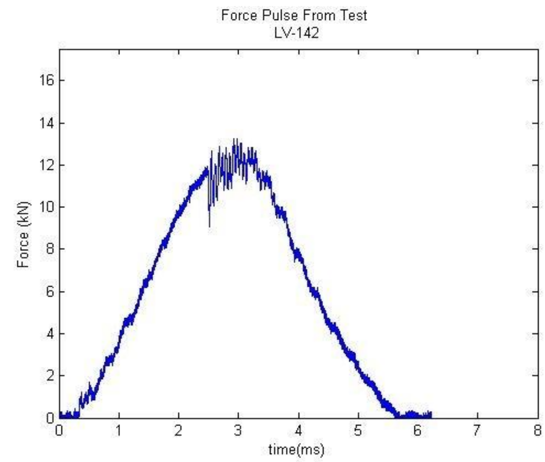
Force Pulse From Test
LV-142
Force (kN)
time(ms)

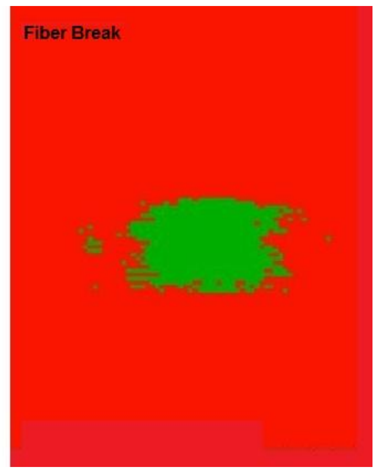
Fiber Break

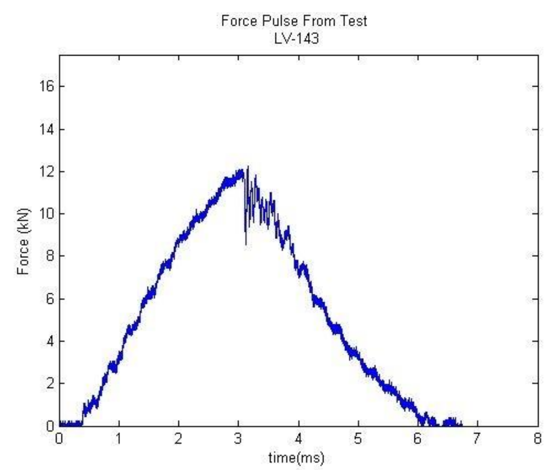
Force Pulse From Test
LV-143
Force (kN)
time(ms)

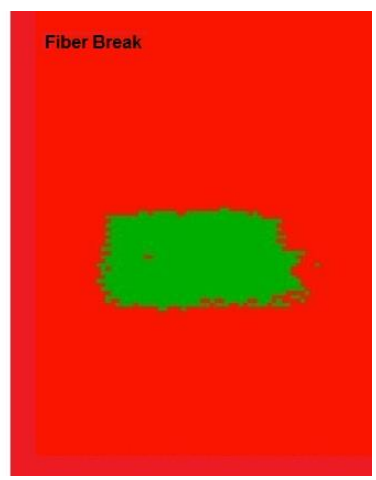
Fiber Break

50.8 mm tip, 24 ply panel

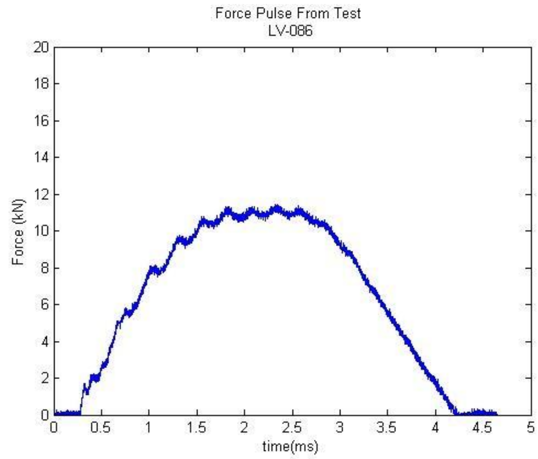

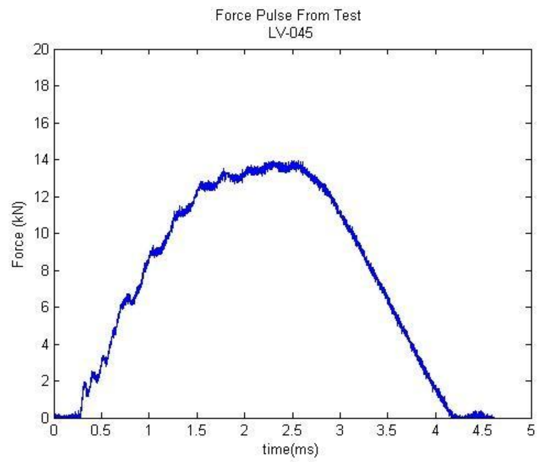

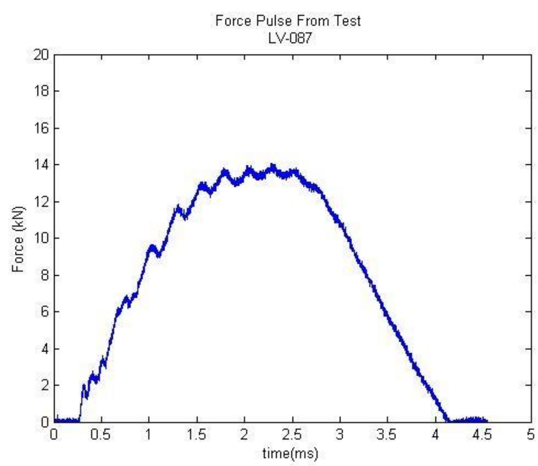

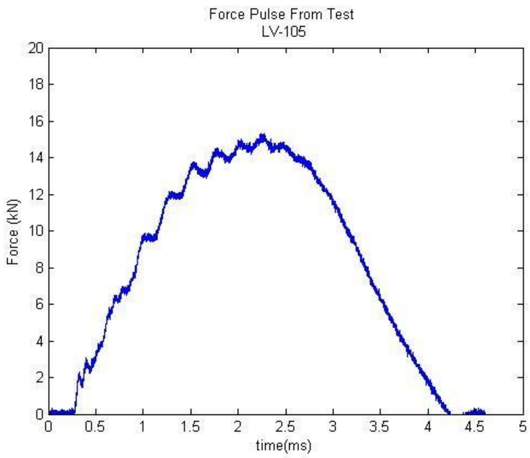
Force Pulse From Test
LV-105
Force (kN)
time(ms)
0 2 4 6 8 10 12 14 16 18 20
0 0.5 1 1.5 2 2.5 3 3.5 4 4.5 5

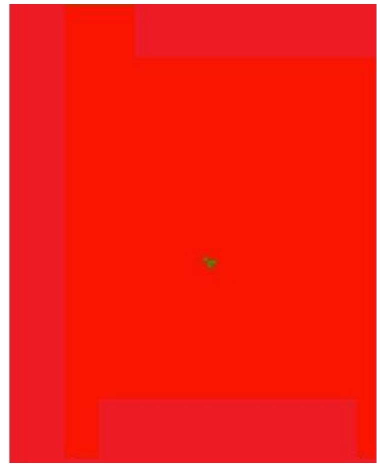

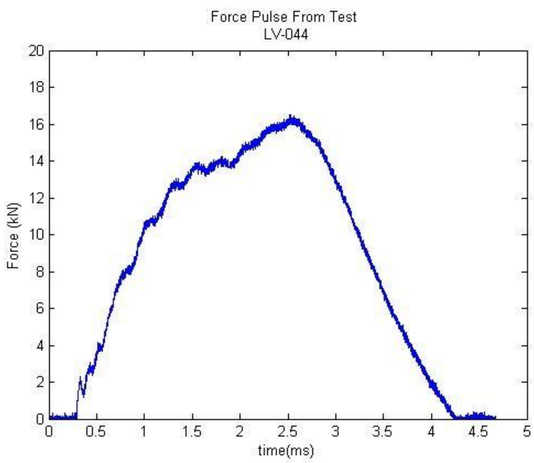
Force Pulse From Test
LV-044
Force (kN)
time(ms)
0 2 4 6 8 10 12 14 16 18 20
0 0.5 1 1.5 2 2.5 3 3.5 4 4.5 5

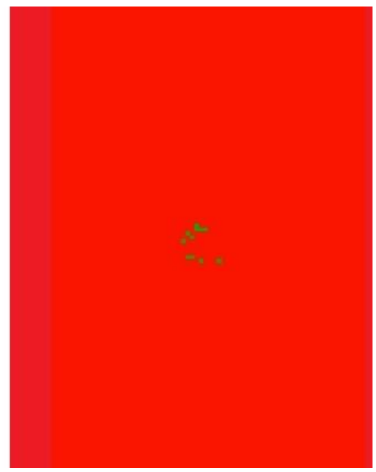

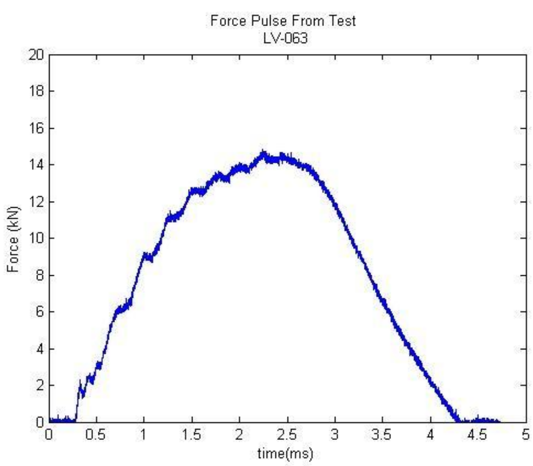
Force Pulse From Test
LV-063
Force (kN)
time(ms)
0 2 4 6 8 10 12 14 16 18 20
0 0.5 1 1.5 2 2.5 3 3.5 4 4.5 5

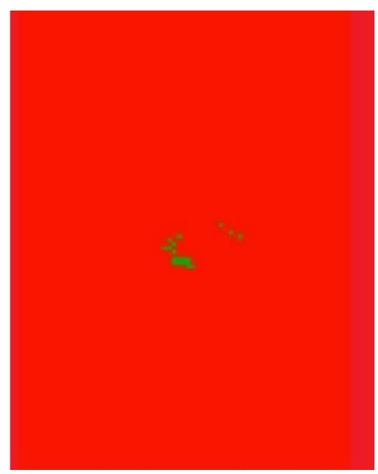

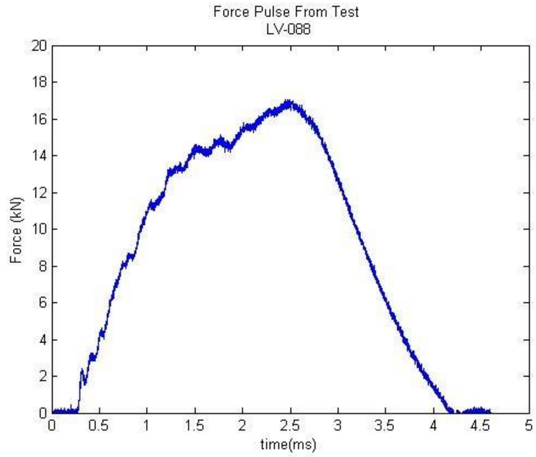
Force Pulse From Test
LV-088
Force (kN)
time(ms)

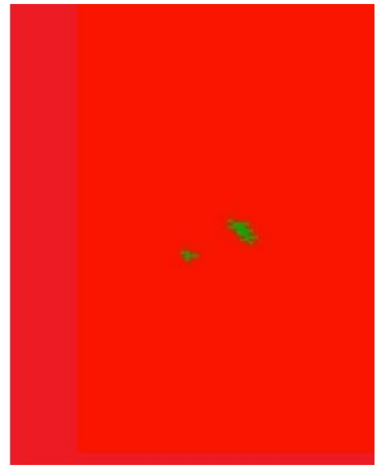

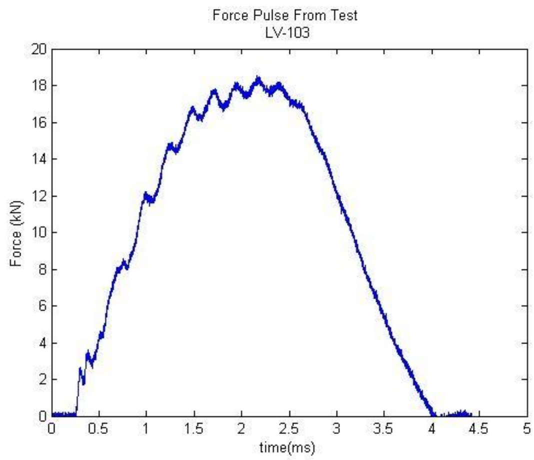
Force Pulse From Test
LV-103
Force (kN)
time(ms)

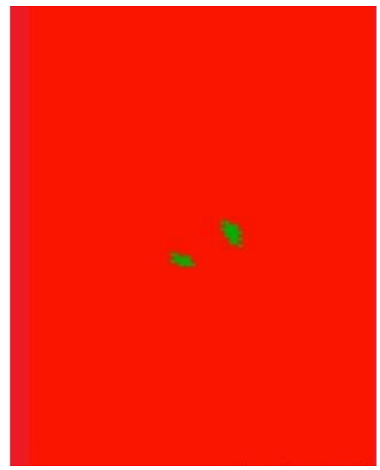

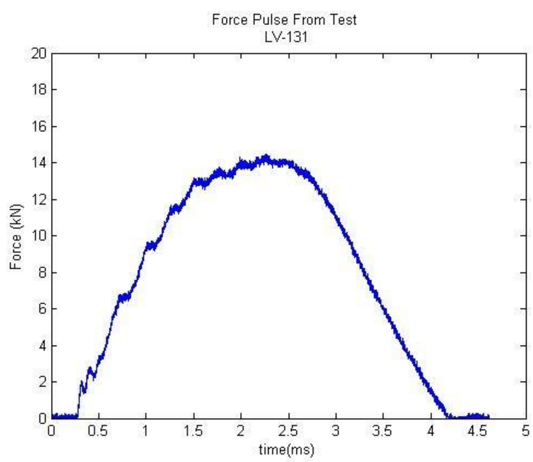
Force Pulse From Test
LV-131
Force (kN)
time(ms)

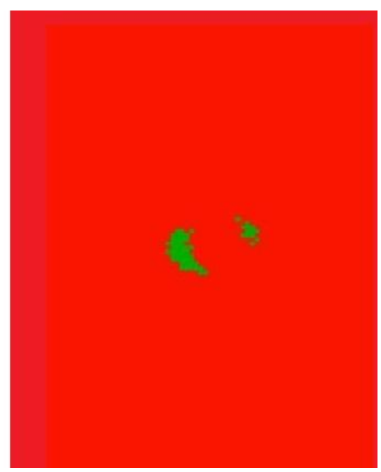

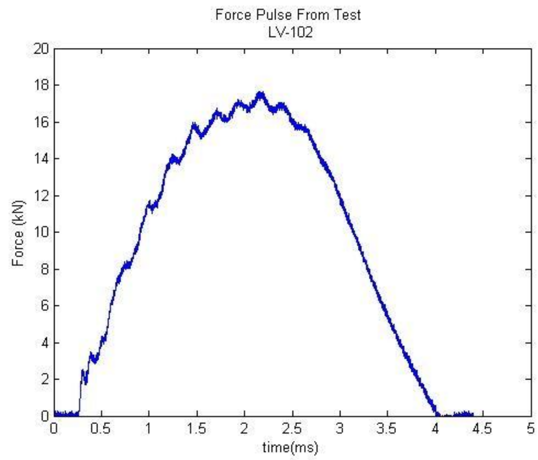
Force Pulse From Test
LV-102
Force (kN)
time(ms)
0
2
4
6
8
10
12
14
16
18
20
0.5
1
1.5
2
2.5
3
3.5
4
4.5
5

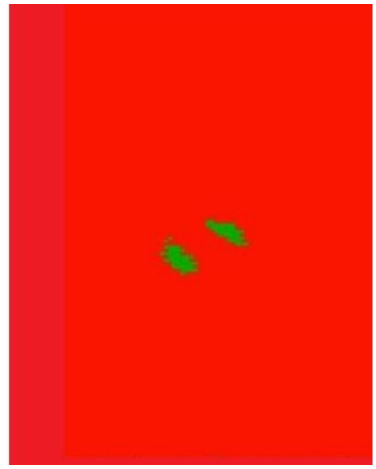

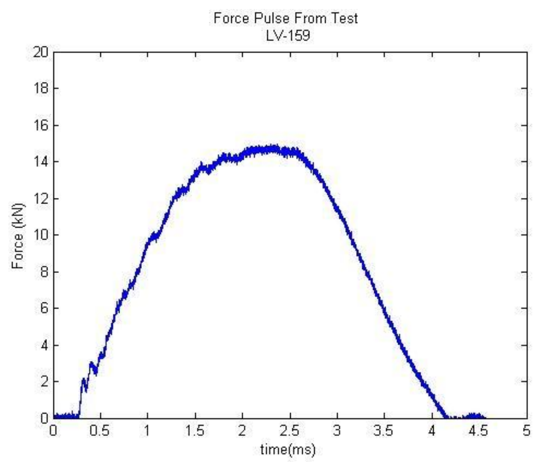
Force Pulse From Test
LV-159
Force (kN)
time(ms)
0
2
4
6
8
10
12
14
16
18
20
0.5
1
1.5
2
2.5
3
3.5
4
4.5
5

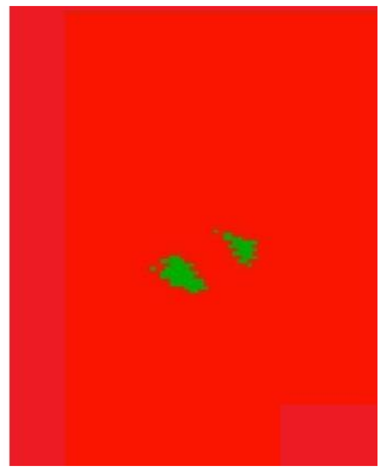

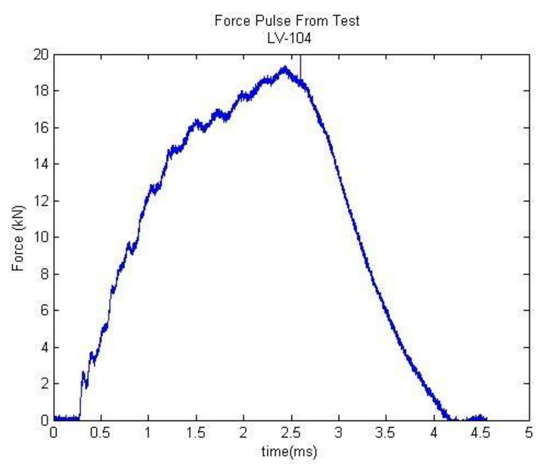
Force Pulse From Test
LV-104
Force (kN)
time(ms)
0
2
4
6
8
10
12
14
16
18
20
0.5
1
1.5
2
2.5
3
3.5
4
4.5
5

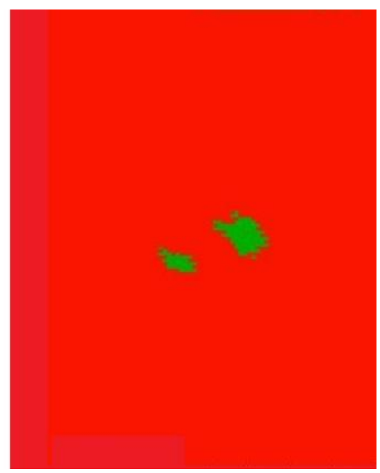

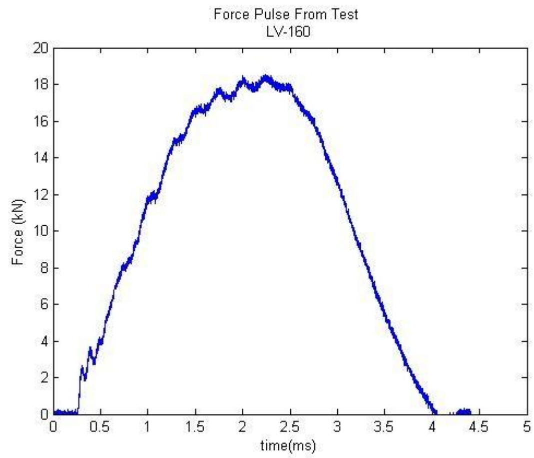

Force Pulse From Test
LV-160
Force (kN)
time(ms)
0
2
4
6
8
10
12
14
16
18
20
0.5
1
1.5
2
2.5
3
3.5
4
4.5
5

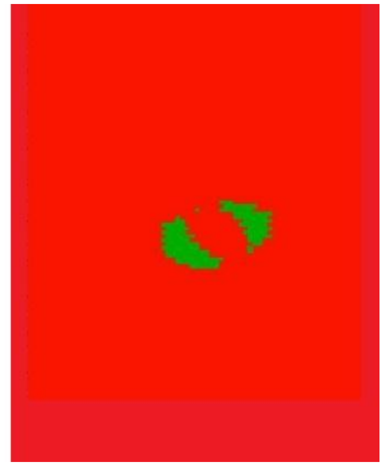

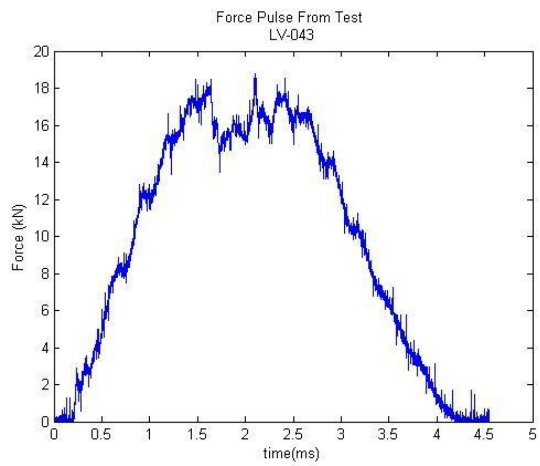

Force Pulse From Test
LV-043
Force (kN)
time(ms)
0
2
4
6
8
10
12
14
16
18
20
0.5
1
1.5
2
2.5
3
3.5
4
4.5
5

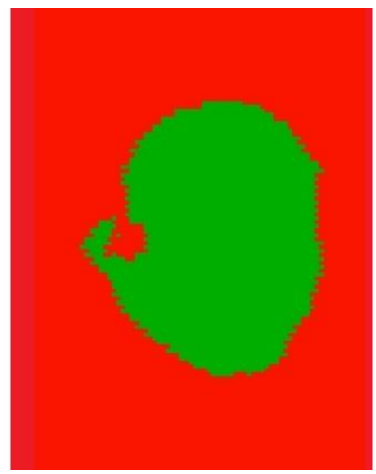

VId. 76.2 mm tip, 8 ply panel

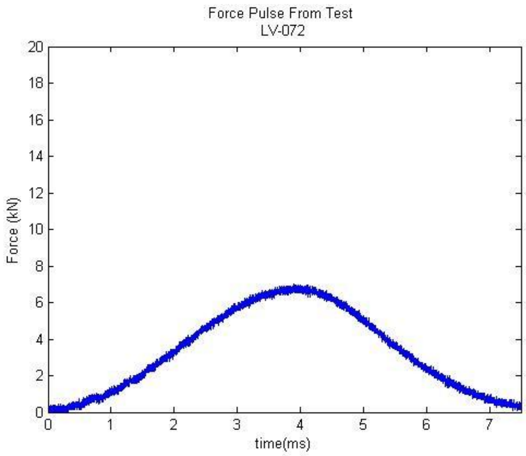

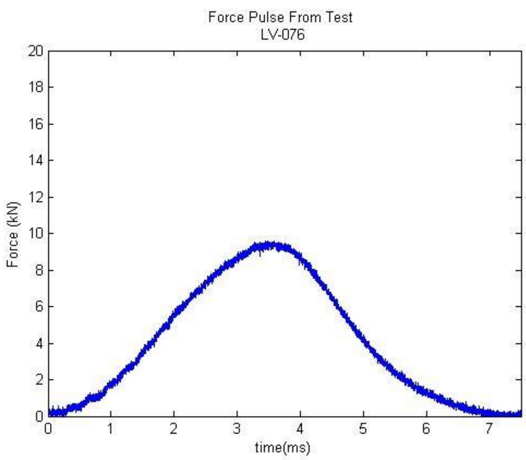

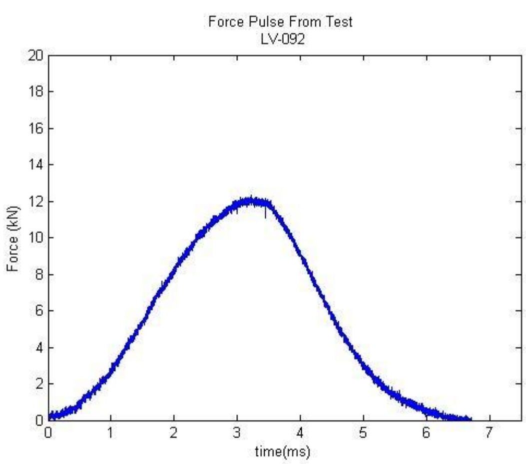

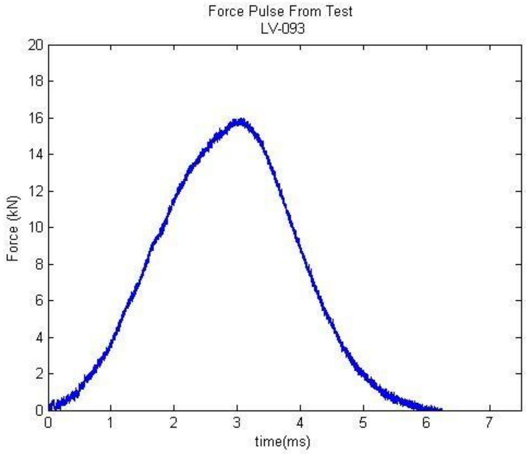
Force Pulse From Test
LV-093
Force (kN)
time(ms)
0
2
4
6
8
10
12
14
16
18
20
0
1
2
3
4
5
6
7

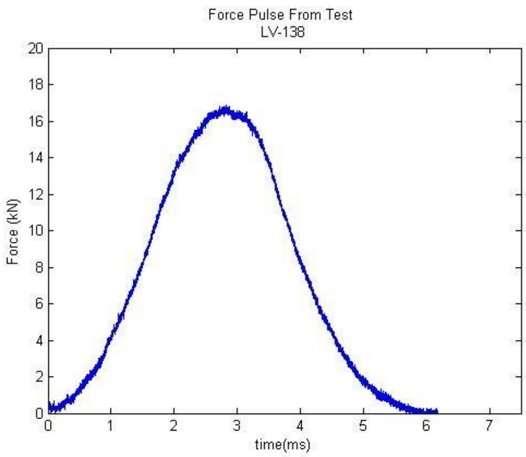
Force Pulse From Test
LV-138
Force (kN)
time(ms)
0
2
4
6
8
10
12
14
16
18
20
0
1
2
3
4
5
6
7

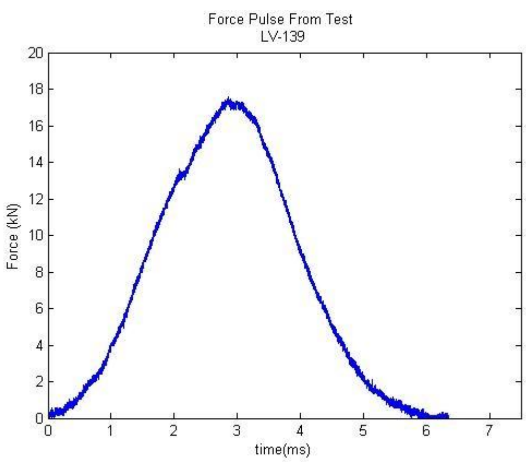
Force Pulse From Test
LV-139
Force (kN)
time(ms)
0
2
4
6
8
10
12
14
16
18
20
0
1
2
3
4
5
6
7

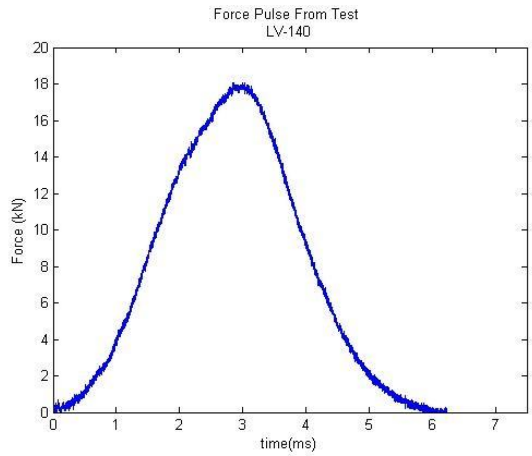
Force Pulse From Test
LV-140
Force (kN)
time(ms)

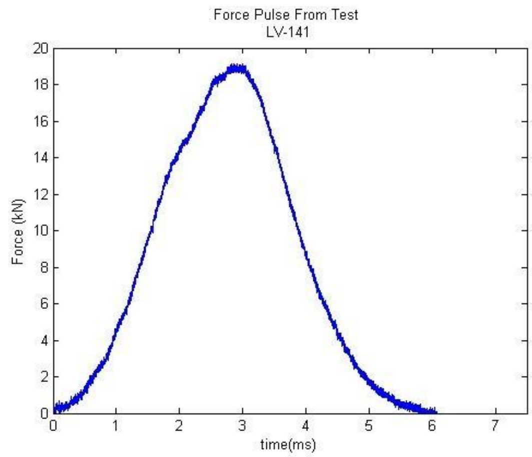
Force Pulse From Test
LV-141
Force (kN)
time(ms)

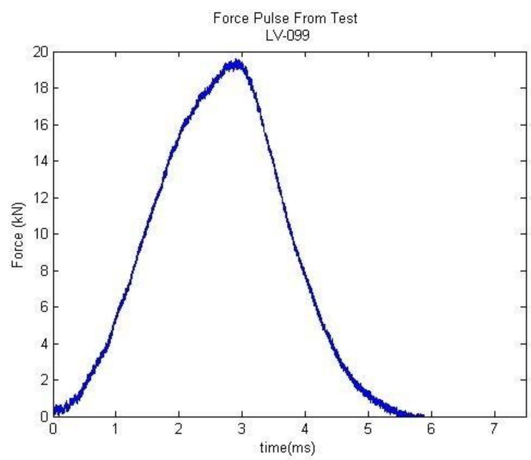
Force Pulse From Test
LV-099
Force (kN)
time(ms)

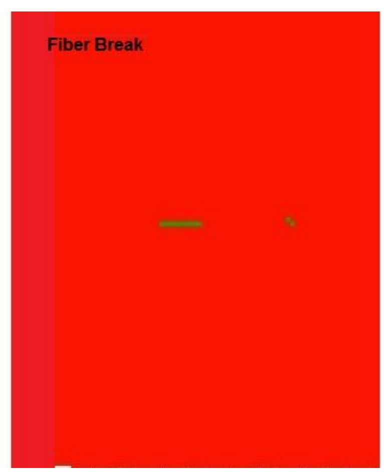
Fiber Break

76.2 mm tip, 16 ply panel

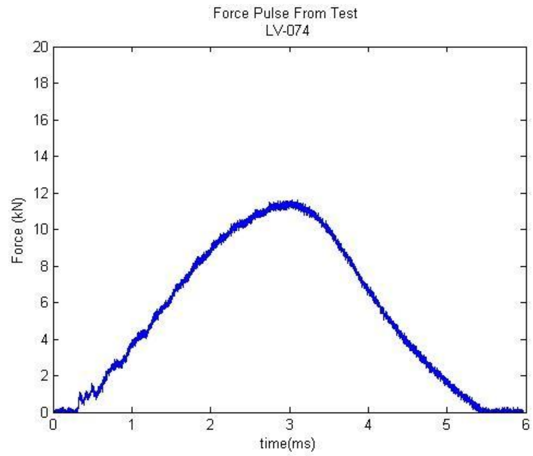

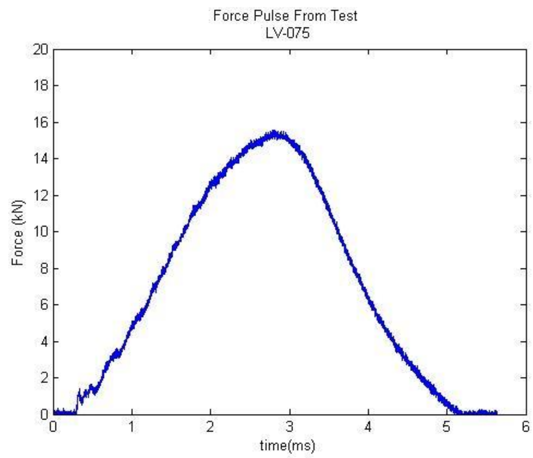

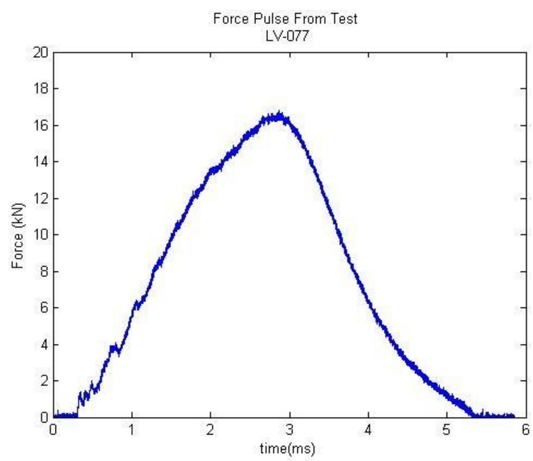

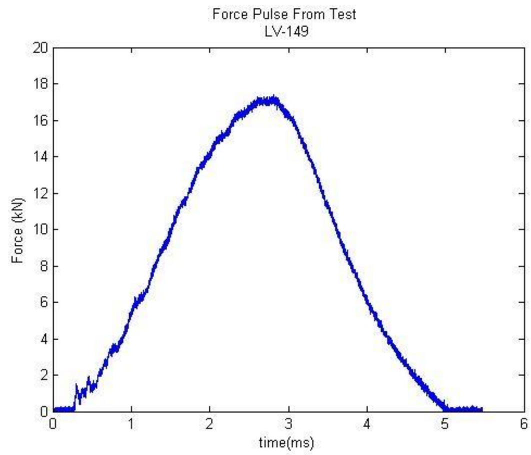
Force Pulse From Test
LV-149
Force (kN)
time(ms)

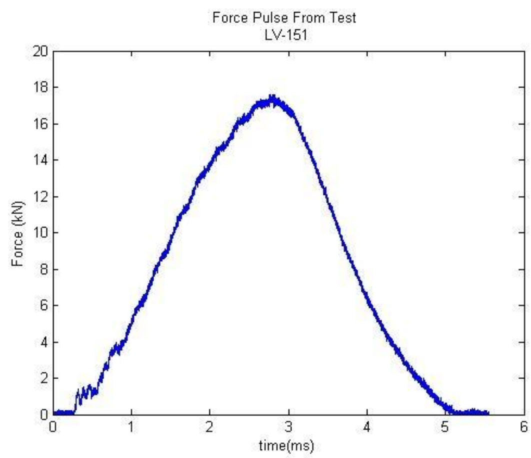
Force Pulse From Test
LV-151
Force (kN)
time(ms)

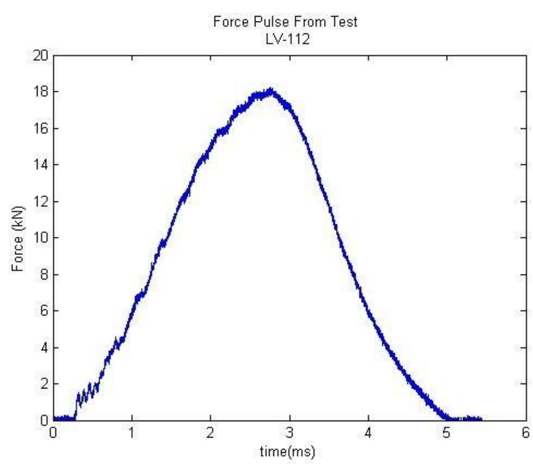
Force Pulse From Test
LV-112
Force (kN)
time(ms)

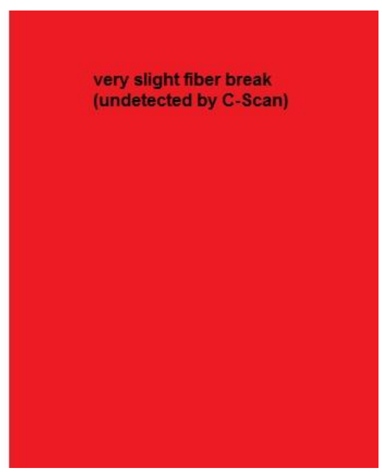
very slight fiber break
(undetected by C-Scan)

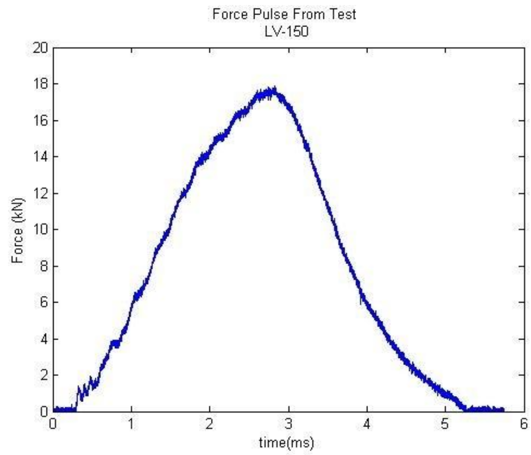
Force Pulse From Test
LV-150
Force (kN)
time(ms)

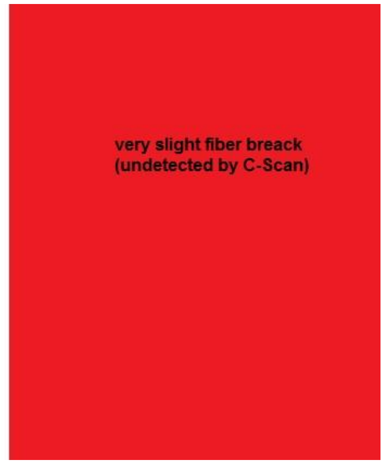
very slight fiber breack
(undetected by C-Scan)

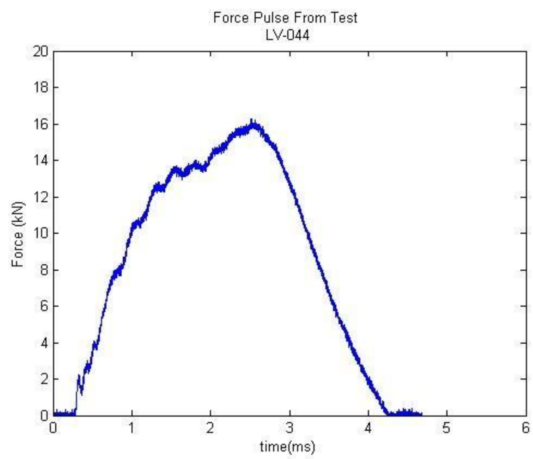
Force Pulse From Test
LV-044
Force (kN)
time(ms)

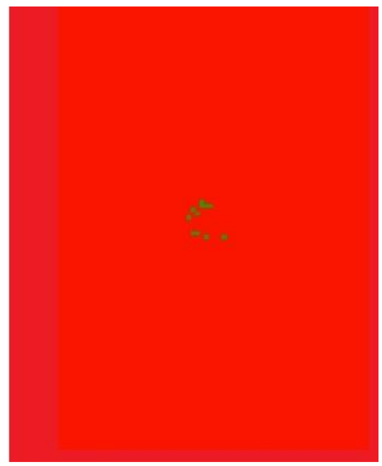

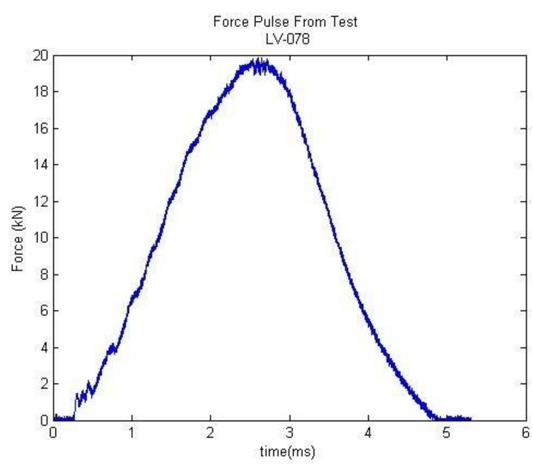
Force Pulse From Test
LV-078
Force (kN)
time(ms)

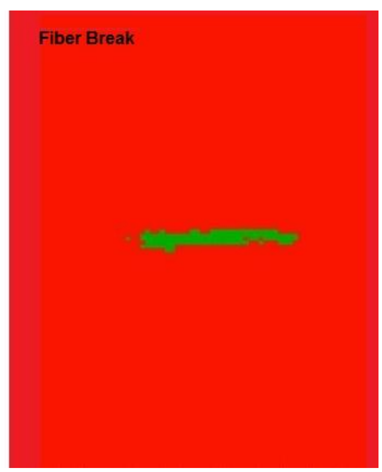
Fiber Break

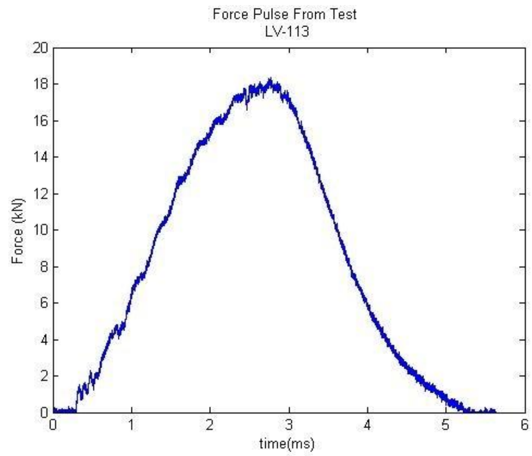

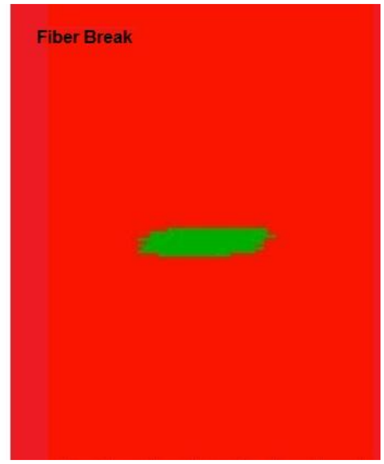

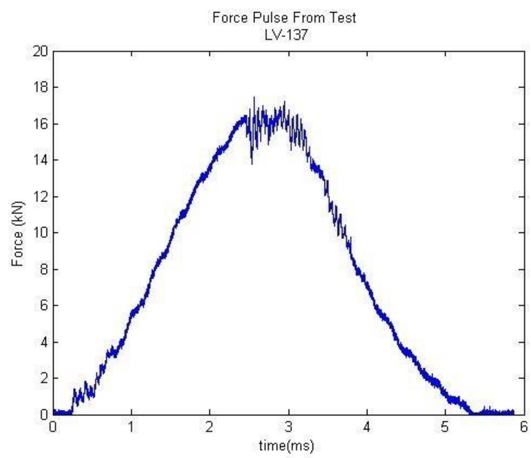

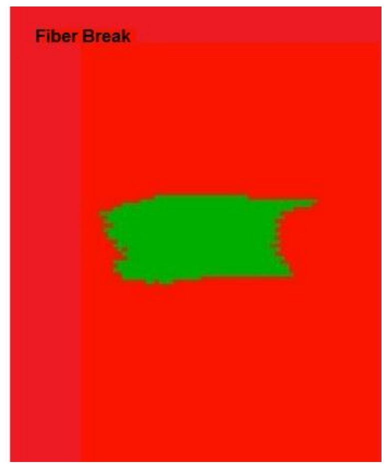

76.2 mm tip, 24 ply panel

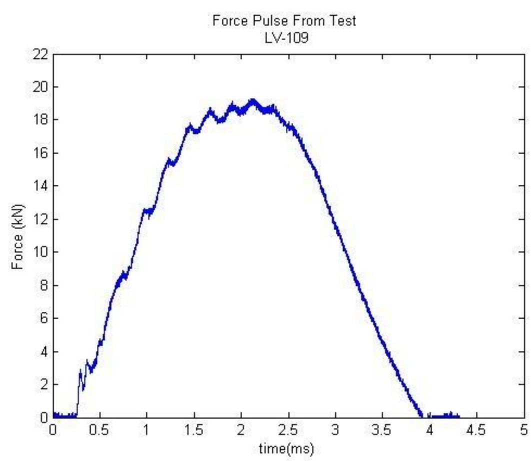

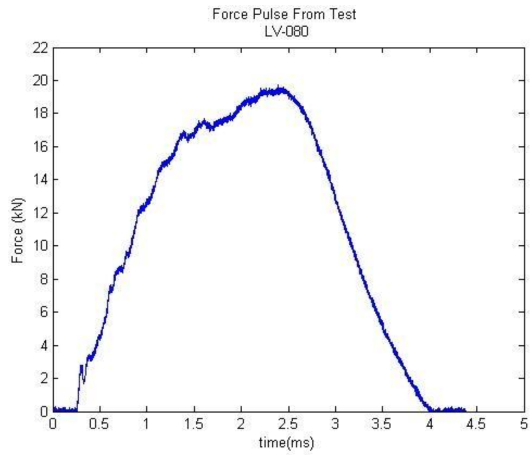
Force Pulse From Test
LV-080
Force (kN)
time(ms)
0 2 4 6 8 10 12 14 16 18 20 22
0 0.5 1 1.5 2 2.5 3 3.5 4 4.5 5

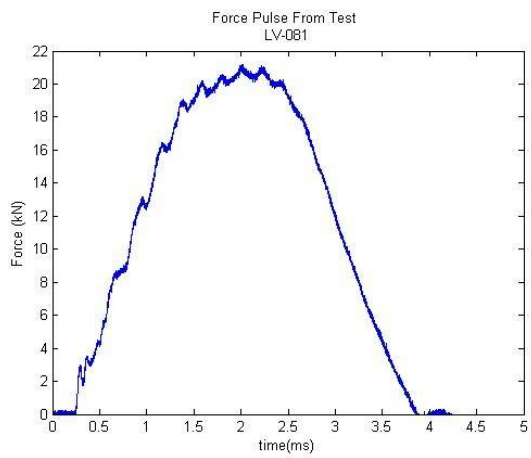
Force Pulse From Test
LV-081
Force (kN)
time(ms)
0 2 4 6 8 10 12 14 16 18 20 22
0 0.5 1 1.5 2 2.5 3 3.5 4 4.5 5

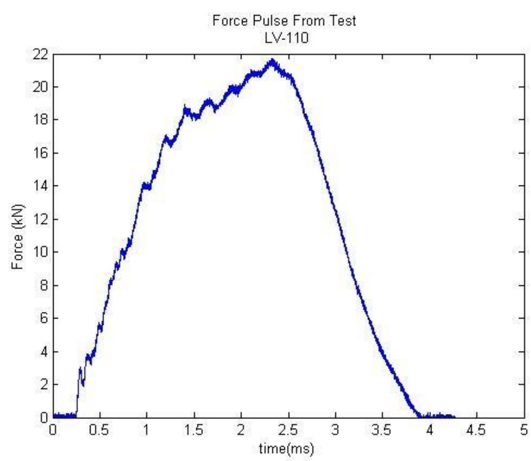
Force Pulse From Test
LV-110
Force (kN)
time(ms)
0 2 4 6 8 10 12 14 16 18 20 22
0 0.5 1 1.5 2 2.5 3 3.5 4 4.5 5

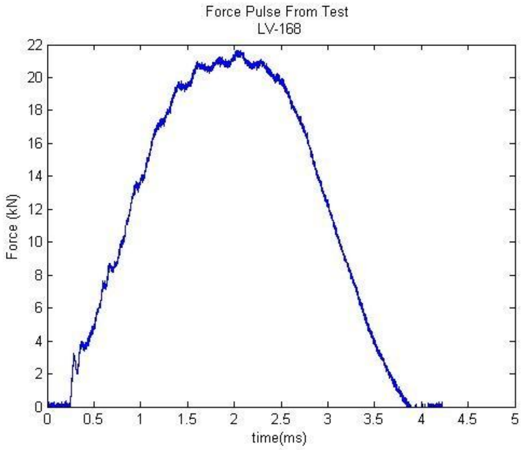
Force Pulse From Test
LV-168
Force (kN)
time(ms)

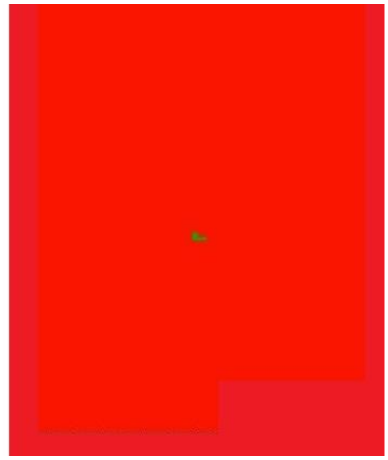

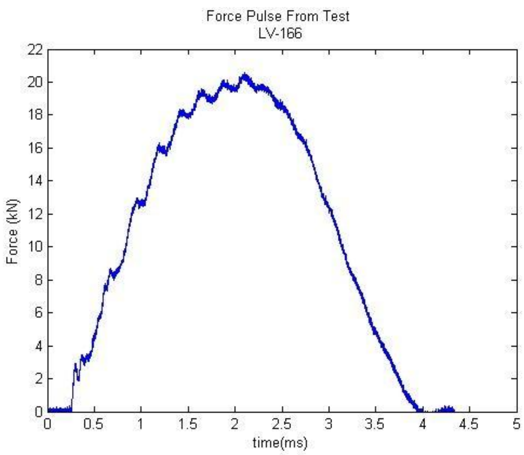
Force Pulse From Test
LV-166
Force (kN)
time(ms)

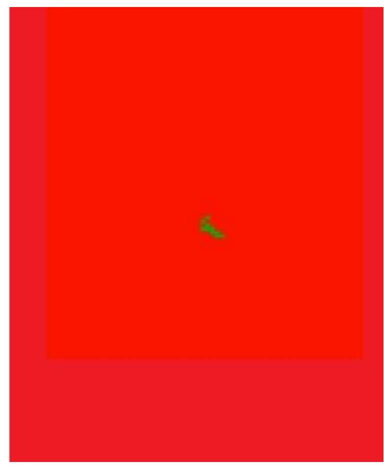

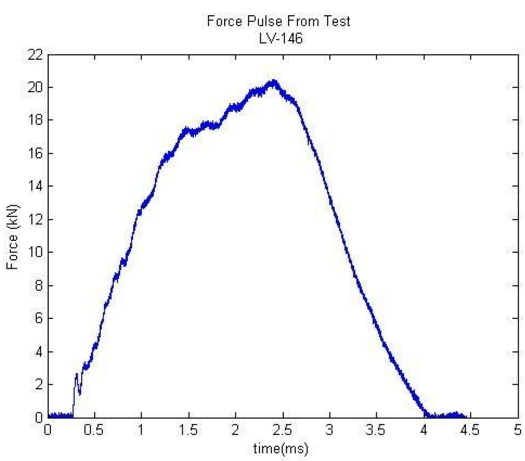
Force Pulse From Test
LV-146
Force (kN)
time(ms)

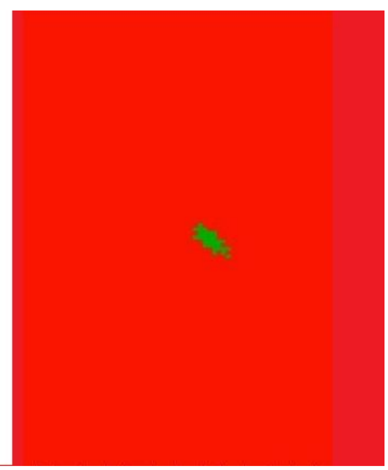

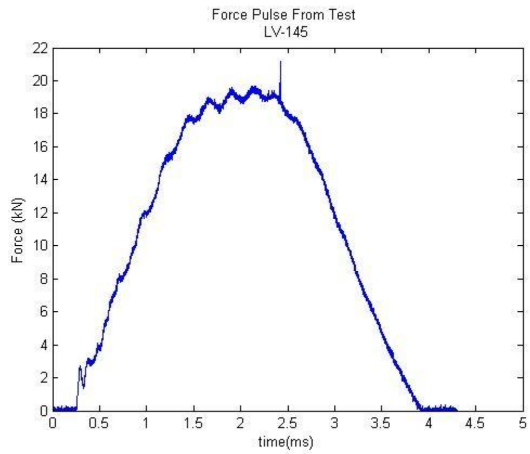
Force Pulse From Test
LV-145
Force (kN)
time(ms)
0 2 4 6 8 10 12 14 16 18 20 22
0 0.5 1 1.5 2 2.5 3 3.5 4 4.5 5

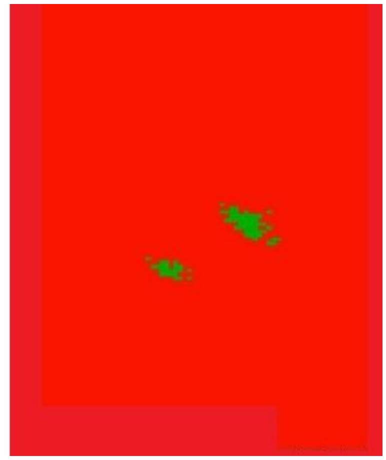

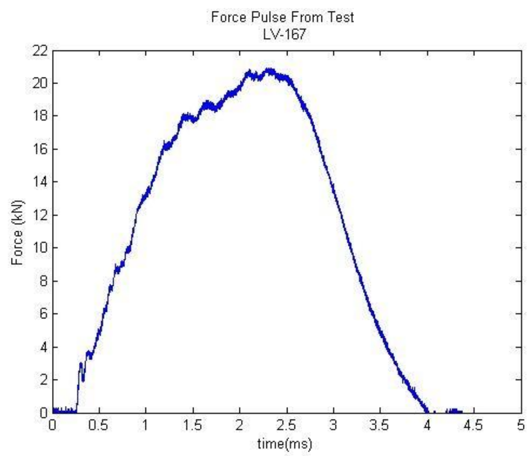
Force Pulse From Test
LV-167
Force (kN)
time(ms)
0 2 4 6 8 10 12 14 16 18 20 22
0 0.5 1 1.5 2 2.5 3 3.5 4 4.5 5

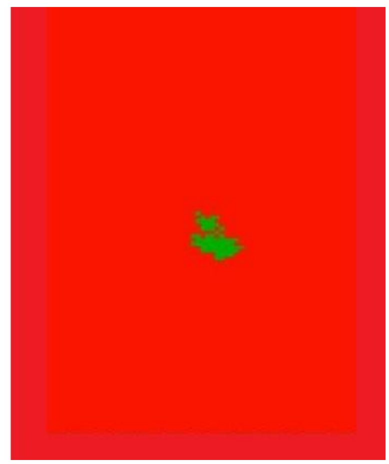

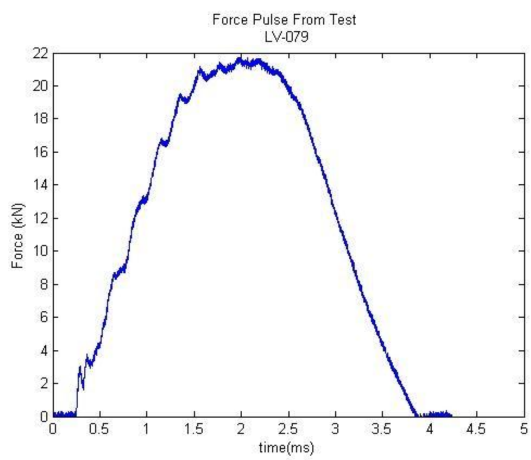
Force Pulse From Test
LV-079
Force (kN)
time(ms)
0 2 4 6 8 10 12 14 16 18 20 22
0 0.5 1 1.5 2 2.5 3 3.5 4 4.5 5

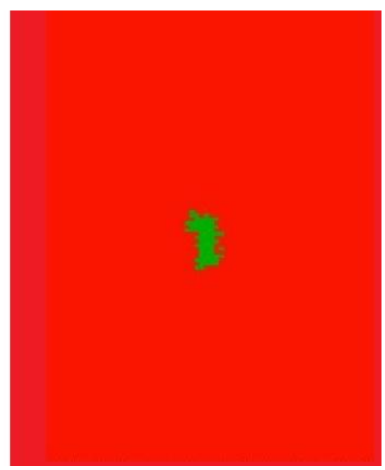

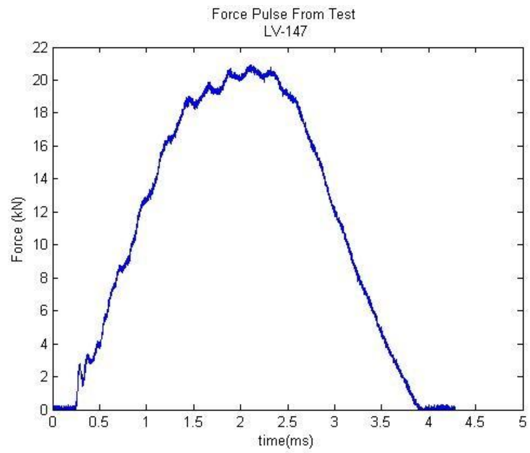
Force Pulse From Test
LV-147
Force (kN)
time(ms)
0 2 4 6 8 10 12 14 16 18 20 22
0 0.5 1 1.5 2 2.5 3 3.5 4 4.5 5

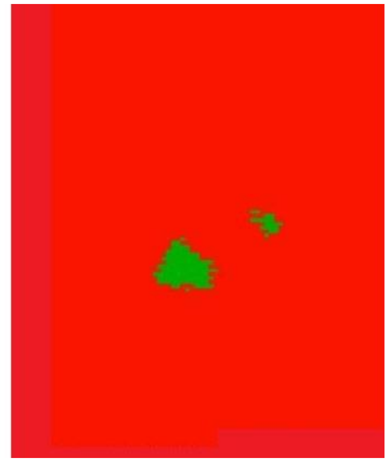

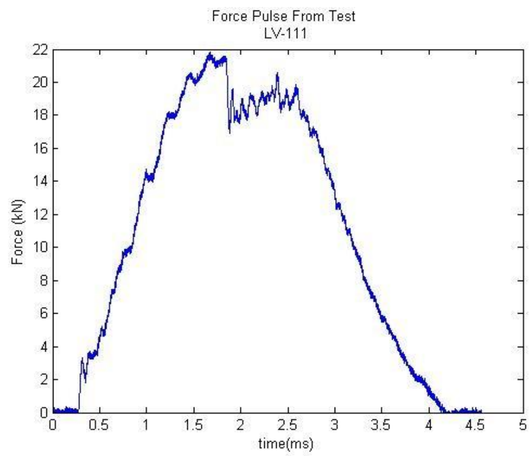
Force Pulse From Test
LV-111
Force (kN)
time(ms)
0 2 4 6 8 10 12 14 16 18 20 22
0 0.5 1 1.5 2 2.5 3 3.5 4 4.5 5

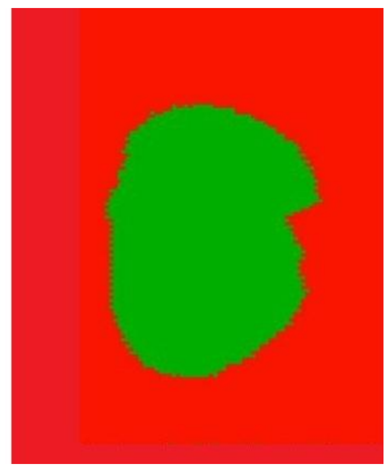

Appendix VII. Contact Area Processing

In order to calculate the contact area between the pendulum impactor and the panel, the tip of the impactor was lightly coated with Dry Erase ink using a marker and during the impact the ink would transfer onto a sheet of paper placed on the surface of the panel. This sheet of paper included a reference square of known area printed out on it. The contact sheet would be scanned and processed using image processing software to remove any stray marks and darken the occasional area that did not transfer properly. This processing was minimal and did not alter the shape or area of the mark left by the impactor, it was only to facilitate the process of calculating the area of the mark. An example of a typical unprocessed and processed contact sheet is seen in Figure 43:

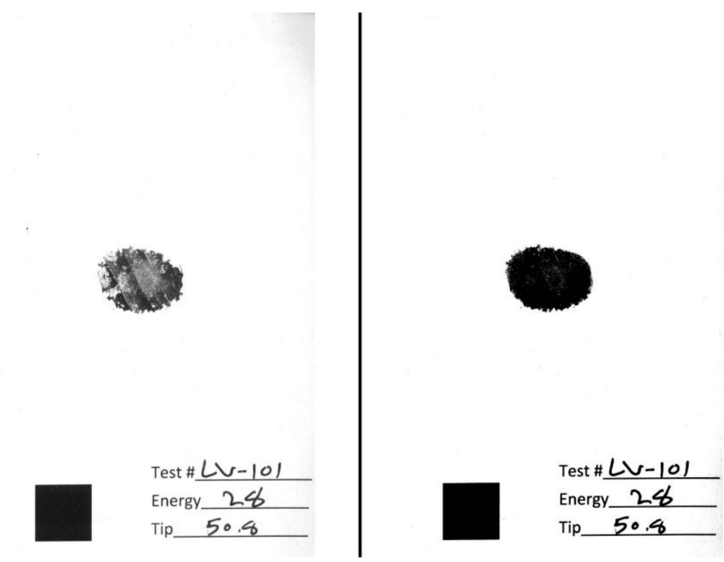

Figure 43. Unprocessed contact sheet image (left) vs. processed image (right)

In order to measure the area of the mark, the image was processed using a MATLAB function. The function would first scan the area of the image containing the reference square and record how many pixels the square contained. Then it would scan the area of the sheet with the contact mark in it, record how many pixels the mark contained. This value was then compared to the pixels in the reference square to calculate the area of the mark. In order to verify that the correct areas were scanned, and that no part of the reference square or mark was left out, the function produced an image that indicated the areas scanned and what counted as the reference square and mark. For example, the image produced after analyzing the image from Figure 30 would look like this:

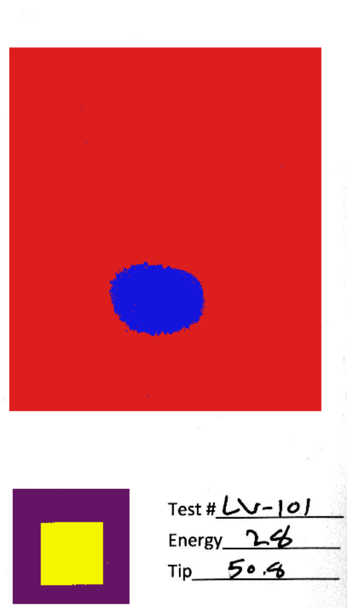

Figure 44. Image produced by MATLAB function to verify that the contact area was properly measured

Figure 44 verifies that the entire reference square and contact mark were included in the scans, and that no stray marks were included in the determination of either area. Since each image is a fairly large file, the function takes about 45 seconds to run each time. To expedite the process of analyzing many files at a time, a loop was incorporated in the function so that it would run as many files as needed at once. The code for this process is as follows:

```
clear all

files=input('Number of Files: ');
H1=zeros(files,1);

for q=1:files
    fprintf('File%4.0f',q)
    A{q}=input(':');
end

tic
for z=1:files
a=imread(A{z});
AREA=12.33^2; %area of reference square, mm^2
REF=0;
HIT1=0;
c=a;
s=size(a);
for j=floor(0.08*s(2)):ceil(0.40*s(2))
    for i=floor(0.80*s(1)):ceil(0.99*s(1))
        m=mean(a(i,j,:));
        if m<200
            REF=REF+1;
            c(i,j,3)=0;
            c(i,j,2)=245;
            c(i,j,1)=245;
        else
            c(i,j,3)=100;
            c(i,j,2)=20;
            c(i,j,1)=100;
        end
    end
end
for j=floor(0.07*s(2)):ceil(0.93*s(2))
    for i=floor(0.07*s(1)):ceil(0.67*s(1))
        m=mean(a(i,j,:));
        if m<210
            HIT1=HIT1+1;
            c(i,j,3)=220;
            c(i,j,2)=20;
            c(i,j,1)=20;
        else
            c(i,j,3)=30;
            c(i,j,2)=30;
            c(i,j,1)=220;
        end
    end
end
```

```
figure
imshow(c)
Y=REF/AREA;
H1(z,1)=HIT1/Y;
clc
end
for k=1:files
    fprintf(A{k})
    fprintf('\nArea = %4.4f mm^2\n',H1(k))
end
fprintf('\n')
toc
```

Appendix VIII. Binomial Regressions using MATLAB

In order to determine the failure thresholds using MATLAB, the glmfit, or generalized linear model regression was used. Since the failure thresholds were constantly being refined during the course of testing, a function was written that would compile the data from a spreadsheet and determine either the FTEs or FTFs of any panel thickness or all of them together. The function that would calculate the thresholds and plot the binomial regressions is as follows:

```
function [thresh12, thresh25, thresh50, thresh76, test12, test25,
test50, test76]=FTE16Ply(m)
if m==3
    x=linspace(0,25,300);
else
    x=linspace(0,80,300);
end
y12=zeros(length(x));
y25=zeros(length(x));
y50=zeros(length(x));
y76=zeros(length(x));

[dat,~,~]=xlsread('Datasheet','8 Ply','D1:N75');
ply8=[dat(:,m),zeros(length(dat),1)];
i=1;
while dat(i,1)==12.7
    if dat(i,11)>0
        ply8(i,2)=1;
    end
    ply812(i,1)=ply8(i,1);
    ply812(i,2)=ply8(i,2);
    i=i+1;
end
test12=i;
n=ones(length(ply812),1);
ply812=sortrows(ply812);
fit812=glmfit(ply812(:,1), [ply812(:,2) n],'binomial','link','logit');
a12=fit812(1); b12=fit812(2);
yfit812=glmval(fit812, ply812(:,1),'logit','size', n);
thresh12=threshcalc(yfit812,ply812(:,1));
j=1;
for k=1:length(x)
    y12(k)=1/(1+exp(-(a12+b12*x(k))));
end
while dat(i,1)==25.4
    if dat(i,11)>0
```

```
            ply8(i,2)=1;
         end
        ply825(j,1)=ply8(i,1);
        ply825(j,2)=ply8(i,2);
        i=i+1;
        j=j+1;
    end
    test25=j;
    n=ones(length(ply825),1);
    ply825=sortrows(ply825);
    fit825=glmfit(ply825(:,1), [ply825(:,2) n],'binomial','link','logit');
    a25=fit825(1); b25=fit825(2);
    yfit825=glmval(fit825, ply825(:,1),'logit','size', n);
    thresh25=threshcalc(yfit825,ply825(:,1));
    j=1;
    for k=1:length(x)
        y25(k)=1/(1+exp(-(a25+b25*x(k))));
    end
    while dat(i,1)==50.8
        if dat(i,11)>0
            ply8(i,2)=1;
        end
        ply850(j,1)=ply8(i,1);
        ply850(j,2)=ply8(i,2);
        i=i+1;
        j=j+1;
    end
    test50=j;
    n=ones(length(ply850),1);
    ply850=sortrows(ply850);
    fit850=glmfit(ply850(:,1), [ply850(:,2) n],'binomial','link','logit');
    a50=fit850(1); b50=fit850(2);
    yfit850=glmval(fit850, ply850(:,1),'logit','size', n);
    thresh50=threshcalc(yfit850,ply850(:,1));
    j=1;
    for k=1:length(x)
        y50(k)=1/(1+exp(-(a50+b50*x(k))));
    end
    while i<=length(dat(:,1))
        if dat(i,11)>0
            ply8(i,2)=1;
        end
        ply876(j,1)=ply8(i,1);
        ply876(j,2)=ply8(i,2);
        i=i+1;
        j=j+1;
    end
    test76=j;
    n=ones(length(ply876),1);
    ply876=sortrows(ply876);
    fit876=glmfit(ply876(:,1), [ply876(:,2) n],'binomial','link','logit');
    a76=fit876(1); b76=fit876(2);
    yfit876=glmval(fit876, ply876(:,1),'logit','size', n);
    thresh76=threshcalc(yfit876,ply876(:,1));
    for k=1:length(x)
```

```
    y76(k)=1/(1+exp(-(a76+b76*x(k))));
end
figure
hold on
p1=plot(ply812(:,1),ply812(:,2),'rs','LineWidth',2,'MarkerSize',9);
plot(x,y12,'r-')
p2=plot(ply825(:,1),ply825(:,2),'b^','LineWidth',2,'MarkerSize',9);
plot(x,y25,'b-')
p3=plot(ply850(:,1),ply850(:,2),'ko','LineWidth',2,'MarkerSize',9);
plot(x,y50,'k-')
p4=plot(ply876(:,1),ply876(:,2),'g>','LineWidth',2,'MarkerSize',9);
plot(x,y76,'g-')
%title('16 Ply')
if m==2
    xlabel('Impact Energy (J)')
    axis([0 80 0 1])
elseif m==3
    xlabel('Peak Contact Force (kN)')
    axis([0 23 0 1])
else
end
ylabel('Damage')
h=[p1(1) p2(1) p3(1) p4(1)];
legend(h, '12.7 mm', '25.4 mm', '50.8 mm','76.2 mm');
box on

end
```

This function was only used to determine the thresholds for the 8 ply panel. Two other similar functions would call the data for the 16 and 24 ply panels. A script was written in order to easily calculate the failure thresholds in terms of whichever parameter was needed. This function would also display the calculated thresholds and plot the threshold vs. tip radius for each panel thickness.

```
met=input('Force or Energy Thresholds (1/2):');
if met==1
    m=3;
elseif met==2
    m=2;
else
    m=input('Threshold Parameter:');
end
ply=input('Panel Thickness:');
 if ply==8
    [t8(1),t8(2),t8(3),t8(4),p8(1),p8(2),p8(3),p8(4)]=FTE8Ply(m);
    fprintf('Failure Threshold Energies: 8 Ply\n\n')
    fprintf('12.7 mm: %4.4f, %2.0f tests\n',t8(1),p8(1))
```

```
    fprintf('25.4 mm: %4.4f, %2.0f tests\n',t8(2),p8(2))
    fprintf('50.8 mm: %4.4f, %2.0f tests\n',t8(3),p8(3))
    fprintf('76.2 mm: %4.4f, %2.0f tests\n',t8(4),p8(4))
elseif ply==16
    [t16(1),t16(2),t16(3),t16(4),p16(1),p16(2),p16(3),p16(4)]=FTE16Ply(m);
    fprintf('Failure Threshold Energies: 16 Ply\n\n')
    fprintf('12.7 mm: %4.4f, %2.0f tests\n',t16(1),p16(1))
    fprintf('25.4 mm: %4.4f, %2.0f tests\n',t16(2),p16(2))
    fprintf('50.8 mm: %4.4f, %2.0f tests\n',t16(3),p16(3))
    fprintf('76.2 mm: %4.4f, %2.0f tests\n',t16(4),p16(4))
elseif ply==24
    [t24(1),t24(2),t24(3),t24(4),p24(1),p24(2),p24(3),p24(4)]=FTE24ply(m);
    fprintf('Failure Threshold Energies: 24 Ply\n\n')
    fprintf('12.7 mm: %4.4f, %2.0f tests\n',t24(1),p24(1))
    fprintf('25.4 mm: %4.4f, %2.0f tests\n',t24(2),p24(2))
    fprintf('50.8 mm: %4.4f, %2.0f tests\n',t24(3),p24(3))
    fprintf('76.2 mm: %4.4f, %2.0f tests\n',t24(4),p24(4))
else
    [t8(1),t8(2),t8(3),t8(4),p8(1),p8(2),p8(3),p8(4)]=FTE8Ply(m);
    [t16(1),t16(2),t16(3),t16(4),p16(1),p16(2),p16(3),p16(4)]=FTE16Ply(m);
    [t24(1),t24(2),t24(3),t24(4),p24(1),p24(2),p24(3),p24(4)]=FTE24ply(m);
    fprintf('Failure Threshold Energies: 8 Ply\n\n')
    fprintf('12.7 mm: %4.4f, %2.0f tests\n',t8(1),p8(1))
    fprintf('25.4 mm: %4.4f, %2.0f tests\n',t8(2),p8(2))
    fprintf('50.8 mm: %4.4f, %2.0f tests\n',t8(3),p8(3))
    fprintf('76.2 mm: %4.4f, %2.0f tests\n\n',t8(4),p8(4))
    fprintf('Failure Threshold Energies: 16 Ply\n\n')
    fprintf('12.7 mm: %4.4f, %2.0f tests\n',t16(1),p16(1))
    fprintf('25.4 mm: %4.4f, %2.0f tests\n',t16(2),p16(2))
    fprintf('50.8 mm: %4.4f, %2.0f tests\n',t16(3),p16(3))
    fprintf('76.2 mm: %4.4f, %2.0f tests\n\n',t16(4),p16(4))
    fprintf('Failure Threshold Energies: 24 Ply\n\n')
    fprintf('12.7 mm: %4.4f, %2.0f tests\n',t24(1),p24(1))
    fprintf('25.4 mm: %4.4f, %2.0f tests\n',t24(2),p24(2))
    fprintf('50.8 mm: %4.4f, %2.0f tests\n',t24(3),p24(3))
    fprintf('76.2 mm: %4.4f, %2.0f tests\n',t24(4),p24(4))
    figure
    hold on
    tip=[12.7 25.4 50.8 76.2];
    plot(tip,t8,'bd','MarkerSize',9,'MarkerFaceColor','b')
    plot(tip,t16,'rs','MarkerSize',9,'MarkerFaceColor','r')
    plot(tip,t24,'g^','MarkerSize',9,'MarkerFaceColor',[0 0.7 0],'Color',[0 0.7
0])
    legend('8 Ply','16 Ply','24 Ply')
    xlabel('Impact Tip Radius (mm)')
    box on
    if m==3
        ylabel('Failure Threshold Force (kN)')
        axis([0 80 0 23])
    else
        ylabel('Failure Threshold Energy (J)')
        axis([0 80 0 80])
    end
end
```